A THESIS

entitled

THERMODYNAMICS OF PROTON TRANSFER REACTIONS IN THE GAS PHASE

by

M. TEREZA N. FERNANDEZ

Submitted to the University of Warwick
in fulfilment of the requirements for
the award of the degree of
Doctor of Philosophy.

December 1986

To my parents

CONTENTS

Acknowledgements

I must express my gratitude to my supervisor Professor K. R. Jennings for his untiring support, and invaluable discussions throughout this work. I wish to thank Dr R. S. Mason from whom I also acquired knowledge and the skills to deal with ions and molecules in the gas phase.

My thanks are extended to the technical staff in the workshop, the electronic workshop and the glass blowing workshop for their willing help. In the Computer Unit I must thank Bal Dhesi and Neil Coveney for their assistance. I would like to thank all my colleagues in my group and Inder Katyal for their help; particularly Dr. Steve Kelly for helpful discussions and Richard Gallagher for his support throughout the bad and good moments of sharing the MS9. The experiments on toluene/metafluorotoluene system were carried out jointly with Annabel Lloyd as part of her undergraduate research project and my postgraduate research project – my thanks to her.

I wish to express my gratitude to Dr. Rachel Parkins and David Wright for their human support and help with computers; in particular to Rachel who corrected most of the English of the manuscript and was the mentor of the typing of this thesis and herself typed tables and equations.

My thanks are extended to Gill Buxton for typing most of the manuscript, to Linda Hodierne and Henrique Nuno for drawing most of the diagrams.

I thank Gulbenkian Foundation for the financial support for 15 months and the Instituto Nacional de Investigação Cientifica for a two years grant.

I would like to thank Professor Maria Alzira A. M. Ferreira for her support throughout these years. My thanks are also due to Prof. Maria Helena Florêncio for her help back in Portugal and to Dr Maria de Lourdes S. L. Costa for encouraging me to come to Warwick.

I also wish to express my gratitude to my colleagues Maria do Rosário de Jesus, Maria da Piedade de Sá and Maria Filomena Duarte who did my teaching in Portugal over the period November 83 to February 84.

Finally I would like to remember Professor Maria Tereza Robert Lopes with whom I first started to learn the art of Mass Spectrometry.

DECLARATION

Parts of the work described in this thesis have been accepted for publication in the following scientific literature with the following references:

M.T. Fernandez, K.R. Jennings and R.S. Mason, J. Chem. Soc. Faraday Trans. 1, in press (1987)

R.S. Mason, M.T. Fernandez and K.R. Jennings, J. Chem. Soc. Faraday Trans. 1, in press (1987)

Parts of this work have also been presented at the 32th Annual Conference on Mass Spectrometry and Allied Topics at San Antonio, U.S.A. in 1984; the Annual Conference of the Portuguese Society of Chemistry at Lisbon, Portugal, in 1984; the 33th Annual Conference on Mass Spectrometry and Allied Topics at San Diego, U.S.A. in 1985; the 10th International Mass Spectrometry Conference at Swansea, U.K. in 1985; the 14th Meeting of British Mass Spectrometry Society at Sussex, U.K. in 1986. The extent of work carried out jointly with Dr.R.S. Mason and Prof.K.R. Jennings is as published.

List of Abbreviations

PTR	- Proton transfer reactions
HPPS	- High pressure pulsed electron beam source technique
FA	- Flowing afterglow technique
ICR	- Ion cyclotron resonance
LFER	- Linear free energy relationship
NMR	- Nuclear magnetic resonance
PA	- Proton affinity
IMR	- Ion molecule reactions
GB	- Gas phase basicity
GA	- Gas phase acidity
AE	- Appearance energy
IP	- Ionisation potential
PT	- Proton transfer
ADO	- Average dipole orientation theory
SIFT	- Selected ion flow tube technique
EI	- Electron impact
CID	- Collision induced dissociation
CI	- Chemical ionisation
MCA	- Multi-channel analyser
S'_A	- Entropy of protonation of species A
ΔS_{mix}	- Mixing entropy change
ΔS_{exp}	- Entropy change measured experimentally
DME	- Dimethyl ether
HF SCF	- Hartree Fock self consistent field method
LCAO	- Linear combination of atomic orbitals
STO	- Slater type orbital

GTO - Gaussian type orbital

MIKE - Mass analysed ion kinetic energy

ncr - Concentration ratio of neutral species

List of Figures

List of Tables

SUMMARY

This work is a study of proton transfer equilibria, with temperature dependence, in binary mixtures containing benzene, mono and disubstituted benzenes, using High Pressure Pulsed Electron Beam Source Mass Spectrometry.

The measurements of equilibrium constants with temperature variation led to the determination of thermodynamic properties such as relative proton affinities (PAs), gas phase basicities (GBs) and entropy changes. It was also intended to infer the sites for proton attachment in the species under study through the entropy changes. For Proton Transfer Reactions it is generally accepted that the main contribution to the entropy changes arises from rotational symmetry changes which depend upon the protonation site. They are, therefore, usually very small. The existence of isomeric species can give rise to another entropy contribution designated as entropy of mixing which is, in most cases in proton transfer reactions, also very small.

The sum of both contributions for the systems under study was in general expected to be less than 13 $Jmol^{-1}K^{-1}$. The ΔS° experimentally determined were found to be, for some systems, much higher ($60Jmol^{-1}K^{-1}$) than expected on the grounds of the classical contributions.

Confirmation for these values was sought from *ab initio* calculations which were carried out at 4-31G basis set level.

The conclusions drawn from this study indicate that a novel contribution to entropy changes must be taken into account in aromatics protonating on the ring if various adjacent sites are equally favoured for proton attachment. This is considered to be an internal translational contribution due to proton migration which is supposed to produce a dynamic structure for those protonated compounds. Substituted benzenes where, this contribution does not occur, seem to have a structure similar to the benzenium ion.

CHAPTER 1: INTRODUCTION

1.1 Introduction

Proton Transfer Reactions (PTR) are amongst the most widely studied group of reactions. During the last fifteen years, studies in the gas phase have enlarged considerably the already vast knowledge obtained in solution.

These reactions cannot be dissociated from the acid-base definition of Brönsted.[11] Any species able to donate a proton is regarded as an acid and any species able to accept a proton is designated a base. In the Lewis concept an acid is an acceptor of a pair of electrons and a base is a donor of a pair of electrons. Although the Lewis definition encompasses the Brönsted definition, the latter shows by no means less generality if carefully considered.

The strengths of Lewis acids depend upon the bases chosen to measure them. General scales in solution are not available.[12] On the contrary all proton acids generate solvated protons. In a given solvent a scale of acidities can be built up on the basis of the concentration of the solvated proton without relating directly to the basis available in solution for proton transfer. Basicity scales can be built in the same way. The generality of these scales can further be improved by measurements in the gas phase where solvent is not present and absolute scales may be drawn up (see Section 2.2.2.1).

Because this work is concerned with PTR the Lewis definition will not be mentioned again, except to note that studies on the subject have been carried out in the gas phase.[13,14]

Proton Transfer Reactions are usually fast and easily reversible[12] both in solution ($k=10^{-11} cm^3 molec^{-1} s^{-1}$) and in gas phase ($k=10^{-9} cm^3 molec^{-1} s^{-1}$),

although they are much faster in the gas phase. Their particular behaviour can be ascribed to their common element, the proton. The proton itself has unique features. The absence of electrons around its nucleus leads to a very small radius (10^{-13}cm) when compared with other singly charged ions (10^{-8}cm), this results in a large polarising power. The lack of electrons means also that in PTR important changes between bonding or non-bonding electrons do not occur.

Still, the absence of electrons facilitates the hydrogen bond formation, promoting a link between two atoms which is often regarded as an intermediate in PTR.

Its light mass is responsible for important isotopic and tunnel effects[1-3].

The importance of these reactions is not restricted to the establishment of acidity or basicity scales. The understanding of their mechanism and rates is fundamental in studies of chemical and biochemical systems.

In solution diverse fields have been studied, such as ionisation constants, behaviour of electrolyte solutions, substituent effects in organic molecules. Their investigation in the gas phase should give more accurate results because any studies would be free of solvent interference. Moreover the versatility of gas phase techniques allow one to reproduce solvation conditions[1-5] and so a link can be established between the condensed and the gas phase. An example is given below.

$$H_3O^+.(H_2O)_n + B \rightleftharpoons BH^+(H_2O)_m + (n-m+1)H_2O \qquad (1.1)$$

$$CH_3O^-.(CH_3OH)_n + HA \rightleftharpoons A^-.(CH_3OH)_m + (n-m+1)CH_3OH \qquad (1.2)$$

The development of the study of gas phase ion-molecule reactions was postponed until improved techniques in the mass spectrometry field were made available. A main problem to overcome was the rapid loss of ions by discharge to the walls of the instrument or by collision with ions carrying an opposite charge. The use of higher pressures (up to 8Torr[1-6]) inside reactors (High Pressure Source Mass Spectrometry) made it possible to slow down the discharge of ions. Ion recombination was also minimised by using low ion densities, while if high concentration of

neutrals are present high rates of ion-molecule reactions will arise when compared with other competing reaction channels.

In very first experiments of PTR in gas phase measurements of ion-molecule equilibria were not made directly. Relative basicities or acidities were determined by a qualitative technique known as Bracketing Technique[17]. Conclusions were drawn from the sign of ΔG°.

At that time it was accepted that the rates of PTR were always close to the collision rate ($k_c = 10^{-9} cm^3 molec^{-1} s^{-1}$) and that activation energy barriers were not present. It was assumed that any reaction occurring was certainly exothermic. Hence if reaction (1.3) was taking place but

$$AH^+ + B \rightarrow A + BH^+ \qquad (1.3)$$

$$CH^+ + B \quad . \qquad (1.4)$$

reaction (1.4) could not proceed, this would mean that

$$GB(C) > GB(B) > GB(A)$$

This technique is still useful when proton transfer equilibria measurements are difficult to perform.

The first quantitative measurement of an equilibrium constant was performed in a double resonance experiment with an ion cyclotron resonance spectrometer by Bowers et al.[18] They observed that equilibrium was being reached in the proton-transfer between pyrrolidine and azetidine during the performance of a qualitative experiment to determine in what direction the reaction proceeded. The ratio of both ionic species was found to reach a constant value above 10^{-4} Torr of total pressure. Since then extensive basicity and acidity scales have been established.[1,9,10]

Proton Transfer Reactions have been studied by Kebarle et al.[11] and by Böhme et al,[16] under thermal conditions using High Pressure Pulsed Electron Beam Source Technique (HPPS), by Böhme et al[12] using Flowing Afterglow Technique (FA), and by many other authors using the three techniques mentioned

above, ICR, HPPS and FA. In addition a great number of equilibrium constants for ion molecule transfer reactions other than PTR have been measured in the gas phase. Some examples are shown below[1 13].

Charge Transfer

$$C_2F_4^- + C_2HF_3 \rightleftharpoons C_2F_4 + C_2HF_3^- \quad (1.6)$$

$$NO_2^- + Cl_2 \rightleftharpoons NO_2 + Cl_2^- \quad (1.7)$$

Hydride ion transfer

$$t\text{-}C_4H_9^- + i\text{-}C_5H_{12} \rightleftharpoons C_5H_{11}^- + i\text{-}C_4H_{10} \quad (1.8)$$

Halide ion transfer

$$R_1^- + R_2X \rightleftharpoons R_1X + R_2^- \quad (1.9)$$

Clustering adduct formation

$$O_2^+ + O_2 \rightleftharpoons O_4^+ \quad (1.10)$$

$$Cl^-(CH_3OH)_{n-1} + CH_3OH \rightleftharpoons Cl^-(CH_3OH)_n \quad (1.11)$$

$$H^+(H_2O)_{n-1} + H_2O \rightleftharpoons H^+(H_2O)_n \quad (1.12)$$

From these studies, the already recognised importance of structure on determining reactivity was confirmed for both negative[1 10] and positive[1 9] species. In this work the following convention will be used, a neutral proton acceptor will be designated base B according to reation (1.3), and a neutral proton donor will be designated acid HA.

$$AH + B^- \rightleftharpoons A^- + BH \quad (1.13)$$

The effect of substituents on equilibria and rates in reactions involving aromatic compounds has been expressed by linear free energy relationships (LFER). They have been extensively studied in solution.[1 14] The PTR are included in these studies as a subgroup and their study from the same point of view but in gas phase has been proposed by Kebarle et al[1 15] also (see figure 1.1). They investigated PTR between benzene and a group of monosubstituted benzenes. They produced a plot of ΔH_{exp} and ΔE_{calc} vs. σ_p^+ for substituents.

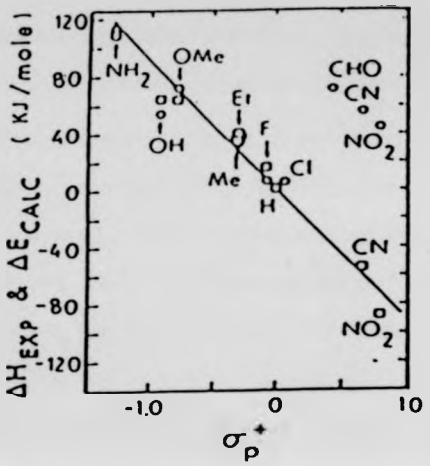

FIG.1.1. COMPARISON BETWEEN ΔH_0 AND ΔE_0 IN A σ_p^+ PLOT

The gas phase studies allow separation of the electronic effects of substituents from solvation effects. The site for protonation is closely related to the charge distribution in the ring so the establishment of the structure of the ionic species involved in PTR is proved to be important.

In solution NMR[1.16] has been found to be a very good technique for structure elucidation but again solvation cannot be avoided. Although gas phase techniques are advantageous in that they are solvent free, the assignment of the ions is based on their masses not on their structure. Hence further experimental information is sometimes sought from isotopic-labelling of species and assumed structures are the subject of theoretical calculations. Moreover in favourable cases the entropy changes for PTR may supply evidence for certain structures.

The proton transfer reaction between benzene and halobenzenes was first studied by Kebarle et al[1.15] in the gas phase with temperature dependence.

$$C_6H_7^+ + C_6H_5X \rightleftharpoons C_6H_6 + C_6H_5X.H^+ \qquad (1.14)$$

X=F, Cl

The experimental ΔS° obtained from the van't Hoff Plots was in both cases -14.6 J $mol^{-1}K^{-1}$. It has been customary to assume[117] that for PTR the main contribution to ΔS arises from the rotational entropy change. (Section 2.2.4), which is well approximated by equation (1.15).

$$\Delta S_{rot} = R\ln\frac{\sigma_{AH^+}\sigma_B}{\sigma_{BH^+}\sigma_A} \qquad (1.15)$$

where σ are symmetry numbers of species from reaction (1.3).

The calculated ΔS_{rot} from equation (1.15) is 14.9 J $mol^{-1}K^{-1}$ for Kebarle's systems when para protonation is assumed for both halobenzenes. The agreement is very good between the experimental value for ΔS° and that calculated from statistical thermodynamics. This also accords with the classification of halogen substituents as π electron donors by mesomeric effect, directing electrophilic attacks firstly towards the para position and secondly the ortho position to the substituents.

These results were partially confirmed by experiments performed by Böhme et al[116] on the same systems (temperature range 300-600K). The proton transfer equilibrium measurement in the benzene/fluorobenzene system led to $\Delta S^\circ = 15$ J $mol^{-1}K^{-1}$ in good agreement with the previous data, but for benzene/chlorobenzene system a smaller entropy change was found (11J$mol^{-1}K^{-1}$). This seemed to point to the possibility of ortho protonation occurring to some extent.

When either ion exists in more than one isomeric form another entropy term must be considered and it is designated the entropy of mixing.

Complementary publications on the PTR of systems above appeared in the literature such as theoretical calculations and experimental measurements[118] of equilibria for reaction (1.14) when X = alkyl group.

More experiments were carried out for these systems by Lias et al[119] using

ICR (temperature range 300-400K). The ΔS° for benzene/fluorobenzene and benzene/chlorobenzene were found to be 11.3 $Jmol^{-1}K^{-1}$ and 9.2 $J\ mol^{-1}K^{-1}$ respectively. It is believed that these results show poorer agreement with previous ones because ICR is likely to suffer from two limitations. First of all the temperature of the experiment may not be well defined and secondly experiments were performed over a narrow temperature range. A natural further step to take was the investigation of the effect of two substituents on the protonation of benzene.

Lias et al[119] performed some proton transfer equilibria measurements in the *meta*difluorobenzene/fluorobenzene system but they are probably affected by the limitations just mentioned. Their gas phase basicities at 373K for difluorobenzenes showed the following trend.

$$GB(1,3C_6H_4F_2) > GB(1,2C_6H_4F_2) > GB(1,4C_6H_4F_2)$$

Furthermore it was observed that the introduction of one fluorine atom increase the PA compared to C_6H_6 and two fluorine atoms reverse the effect by decreasing the PA.

Measurements of relative gas phase basicities for toluene and halogenotoluenes, at 369K, using HPPS have been reported by Mason et al.[120] From these data emerges a trend similar to the one observed for difluorobenzene by Lias et al.[119]

$$GB(1,3CH_3C_6H_4X) > GB(1,2CH_3C_6H_4X) > GB(1,4CH_3C_6H_4X)$$

where X = F, Cl, Br, I

This trend was rationalised in terms of the combined ortho-para directing effects of both substituents (methyl group and halogen) on the electronic charge distribution in the ring (Section 4.6.3).

Semi-empirical CNDO/2 calculations[121] have indicated the carbon atom bearing the methyl group as a potential site for protonation in ortho and para fluorotoluenes. This is known as ipsoprotonation.

Evidence for ipsoprotonation has also been found for ortho and para xylenes by Devlin et al[1,22] from *ab initio* calculations.

The information gathered from experiments on the influence of one and two substituents on the relative affinities towards the proton of mono and disubstituted benzenes is summarised in figure (1.2).

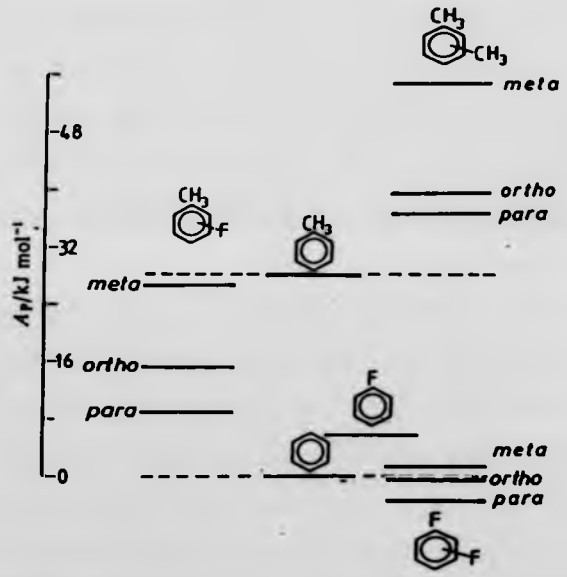

FIG.1.2.—Relative proton-affinity ladder for benzene, toluene, the xylenes, the difluorobenzenes, the fluorotoluenes and fluorobenzene.

This stage was the starting point for the work here reported. The aim was to obtain structural information for the ionic species present in the PTR between halogenotoluenes. The measurement of equilibrium constants for PTR between halogenotoluenes with temperature dependence would lead to real experimental relative PAs for these compounds. On the other hand the determination of $\Delta H°$ and $\Delta S°$ for the reactions would clarify whether or not the different GBs measured for the isomeric forms were due to $\Delta H°$ or $\Delta S°$ variation. Finally $\Delta S°$ could eventually provide information about the site of protonation. Thus in Chapter 4 the determination of thermodynamic properties for PTR in mixtures of

halogenotoluenes is outlined. The structural implications of this study are also discussed.

Surprisingly, the experiments carried out for halogenotoluenes produced, for some systems, large entropy changes compared with the classical rotational and mixing contributions mentioned above.

This situation created the need for confirmation of the observed effect in other systems. Hence the experiments were extended to the xylenes which are reported in Chapter 5. Chapter 6 gives an account of a similar study carried out with systems involving benzene and substituted benzenes associated either with aliphatic compounds or disubstituted benzenes.

Although the qualitative model proposed in Chapter 4 to interpret the data has received support from studies both in solution[123] and in the gas phase[124], additional evidence was sought from *ab initio* calculations. Molecular orbital calculations can predict protonation sites on a quantitative basis rather than the qualitative mechanistic predictions (Section 4.6.3). In Chapter 7 very simple concepts for the understanding of molecular orbital calculations are presented and followed by a description of the ab initio calculations carried out for fluorotoluenes. Neutral species (M) and ionic species $(M+1)^+$ were dealt with.

An attempt to put together all the conclusions of previous chapters is made in Chapter 8, as well as the suggestion of some lines of research for future work.

Chapter 3 gives a description of the technique, High Pressure Pulsed Electron Beam Source, which was used to perform the experiments throughout this work and also the foundations of the method for studying ion-molecule equilibria in gas phase.

Chapter 2 contains a summary survey of different areas of interest in the study of PTR in the gas phase.

1.2 References

1.1 R.J. Gillespie, in "Proton Transfer Reactions", (1975), 1, (ed. E. Caldin and V. Gold), Chapman and Hall.

1.2 R.P. Bell, "The Proton in Chemistry", (1973), Chapman and Hall.

1.3 R.R. Corderman and J.L. Beauchamp, J. Am. Chem. Soc., (1976), **98**, 3998.

1.4 a) J.S. Uppal and R.H. Staley, J. Am. Chem. Soc., (1982), **104**, 1235

b) J.S. Uppal and R.H. Staley, J. Am. Chem. Soc., (1982), **104**, 1238

1.5 R.W. Taft, in "Proton Transfer Reactions", (1975), 31, (E. Caldin and V. Gold), Chapman and Hall.

1.6 D.K. Bŏhme, J.A. Stone, R.S. Mason, R.S. Stradling and K.R. Jennings, Int. J. Mass Spectrom. Ion Phys., (1981), **37**, 283

1.7 J.L. Beauchamp, Ann. Rev. Phys. Chem., (1971), **22**, 527

1.8 M.T. Bowers, D.H. Aue, H.M. Webb and R.T. McIver, J. Am. Chem. Soc. (1971), **93**, 4314

1.9 D.H. Aue and M.T. Bowers, in "Gas Phase Ion Chemistry", 1979, vol.2, 2, ed. M.T. Bowers, Academic Pres.

1.10 J.E. Bartmess and R.T. McIver, Jr., in "Gas Phase Ion Chemistry", 1979, vol.2, ed. M.T. Bowers, Academic Press

1.11 J.P. Briggs, R. Yamdagni and P. Kebarle, J. Am. Chem. Soc. (1972), **94**, 5138

1.12 a) D.K. Bŏhme, E. Lee-Ruff, L.B. Young, J. Am. Chem. Soc., (1971), **93**, 4608

b) D.K. Bŏhme, P. Fennelly, R.S. Hemsworth, H.I. Schiff, J. Am. Chem. Soc, (1973), **95**, 7512

c) D.K. Bŏhme, R.S. Hemsworth, H.W. Rundle and H.I. Schiff, J. Chem. Phys., (1973), **58**, 3504

1.13 P. Kebarle, in "Interaction between Ions and Molecules", Nato Advanced Study Institutes Series B, 1975, vol.6, 459, (ed. P. Ausloos), Plenum Press.

1.14 J. Hine, "Structural Effects on Equilibria in Organic Chemistry", (1975), J. Wiley and Sons.

1.15 J.K. Lau and P. Kebarle, J.Am. Chem. Soc. (1976), 98, 7452.

1.16 G. Olah and Y.K. Mo, Adv. Fluorine Chem., 1973, 7, 69

1.17 S.G. Lias, in "Kinetics of Ion Molecule Reactions", Nato Advanced Study Institutes, series B, 1979, vol. 40, 223. (ed. P. Ausloos), Plenum Press.

1.18 W.J. Hehre, R.T. McIver, J.A. Pople and P.v.R. Schleyer, J. Am. Chem. Soc., 1974, 96, 7162

1.19 K.G. Hartman and S.G. Lias, Int. J. Mass Spetrom. Ion Phys., (1978) 28, 213.

1.20 R.S. Mason, D.K. Böhme and K.R. Jennings, J. Chem. Soc., Faraday Trans. I., (1972), 78, 1943

1.21 J. Burdon, personal communication (University of Birmingham, Chemistry Department).

1.22 J.L. Devlin, J.F. Wolf, R.W. Taft and W.J. Hehre, J. Am. Chem. Soc., (1976), 98, 1990

1.23 G.A. Olah, R.H. Schlosberg, R.D. Porter, Y.K. Mo, D.P. Kelly and G. Mateescu, J.Am. Chem. Soc. (1972), 94, 2034

1.24 A.P. Bruins and N.M.M. Nibbering, Org. Mass Spectrom., (1976), 11, 950.

CHAPTER 2: PROTON TRANSFER REACTIONS IN THE GAS PHASE

2.1 Introduction

The first observation of ion-molecule reactions was as long ago as 1916 when Dempster[21] identified an ion of m/z=3 as being H_3^+. The occurence of this ion was confirmed later in 1925 by Hogness and Lunn[22] through reaction (2.1).

$$H_2^+ + H_2 \rightarrow H_3^+ + H \qquad (2.1)$$

During the late 1920's, other ion-molecule reactions (IMR) were observed such as the formation of I_3^+ and I_3^- from iodine vapour under electron impact by Hogness and Harkness.

During the period of time between the 1930's and the 1950's the improvement in instrumentation and vacuum technology led to the study of primary processes being the major interest in gas-phase ion chemistry. Only in the late 1950's did the simultaneous discovery of the ion CH_5^+ by Tal'roze and Lyubimova in the U.S.S.R. and Stevenson et al in the U.S.A. by reaction (2.2)

$$CH_4^+ + CH_4 \rightarrow CH_5^+ + CH_3 \qquad (2.2)$$

trigger a renewed interest of chemists in IMR. Thereafter, the study of IMR expanded rapidily as new equipment became available for work on them. The study of Proton Transfer Reactions as a subgroup of IMR developed simultaneously. Their importance does not need justification since they have been perhaps the most extensively studied reactions in condensed phase because the acid-base concepts are among the most fundamental in chemistry.

Thus the possibility of looking at their behaviour in the gas phase was most welcome because it was the first opportunity of studying them without solvent

interference. Since ions and molecules in the gas phase are not usually surrounded by solvent molecules, gas phase proton transfer reactions reveal the intrinsic molecular properties determining acidity and basicity. Therefore the data generated in the gas phase are more reliable in absolute terms than those obtained in solution.

Some experimental techniques[2,3] which will be mentioned in this chapter have given rise to considerable progress in the investigation of IMR leading to the study of thermal rate constants, ion-molecule equilibria and consequently more accurate thermodynamic data.

Attention will be paid to these subjects in this chapter.

2.2 Thermochemical Data

2.2.1 Gas Phase Basicities and Acidities

The Brönsted concepts of a base as a proton acceptor and an acid as a proton donor, though old, have not lost their importance in reactivity terms.

The absolute gas phase basicity (GB) of neutral species A is defined as the standard energy change for processes[2,4,5] (2.3)

$$AH^+ \rightarrow A + H^+ \qquad (2.3)$$

$\Delta G^\circ = GB(A)$

$\Delta H^\circ = PA(A)$

On the other hand the standard enthalpy change ΔH^0 for reaction (2.3) is the absolute proton affinity (PA) of the neutral species A. This absolute PA is a measure of the energy required to remove a proton from AH^+. For negative ions it is possible to define an absolute gas phase acidity which is considered to be ΔG° for reaction (2.4).

$$AH \rightarrow A^- + H^+ \qquad (2.4)$$

$\Delta G^\circ = GA(HA)$

$\Delta H^\circ = \Delta H^\circ_{ac}(HA)$

The standard enthalpy change is identified as the heterolytic bond dissociation energy and gives a measure of the acidity of the neutral species, HA.

Processes (2.3) and (2.4) to be spontaneous require more energy than is available under thermal conditions; therefore under these conditions, measurements require the establishment of proton transfer equilibria[25,26] reactions (2.5) and (2.6) between pairs of species.

$$AH^+ + B \rightleftharpoons BH^+ + A \qquad (2.5)$$

$\Delta H^\circ = PA(A) - PA(B)$

$\Delta G^\circ = GB(A) - GB(B)$

$$HA + B^- \rightleftharpoons A^- + HB \qquad (2.6)$$

$\Delta H^\circ = \Delta H^\circ_{ac}(HA) - \Delta H^\circ_{ac}(HB)$

$\Delta G^\circ = GA(HA) - GA(HB)$

With the advent of the equilibrium methods[25,27,28] the measurements of gas phase equilibrium constants became relatively straightforward. Let us take reaction (2.5) as an example. K is given by expression (2.7.)

$$K = \frac{[BH^+]}{[AH^+]} \times \frac{[A]}{[B]} \approx \frac{[A]}{[B]} \propto \frac{I_{BH^+}}{I_{AH^+}} \qquad (2.7)$$

I_{BH^+}, I_{AH^+} - relative intensities of ions BH^+ and AH^+ at equilibrium.

Should the relative intensities of ions BH^+ and AH^+ be measurable at equilibrium, then since the concentration ratio of neutrals A and B are accurately known, the evaluation of K is straightforward.

The relationships (2.8) and (2.9)

$$\Delta G^\circ = -RT\ln K^\circ \qquad (2.8)$$

$$\Delta G^\circ = \Delta H^\circ - T\Delta S^\circ \qquad (2.9)$$

show that from equilibrium constant measurements one may determine either relative gas phase basicities or relative proton affinities and entropy changes depending upon whether the experiments are done at a single temperature or over a range

of temperatures respectively.

In the latter case, from a van't Hoff plot, ΔH° and ΔS° may be determined from slope and intercept respectively provided the temperature may be accurately measured, and equilibrium established.

2.2.2 Absolute Proton Affinities

The last section described how relative values of different thermodynamic properties such as proton affinities could be measured. This section describes how to determine absolute proton affinities (PAs).

One must be aware that the proton transfer equilibria leading to relative values of PAs are performed at varying temperatures and unlike "electron affinity", "proton affinity" does not imply a threshold measurement. It has been suggested[2 9] that "enthalpy of protonation" would be a better designation and that "proton affinity" should be reserved for threshold values.

The absolute threshold value for proton affinity of species A in reaction (2.3) is defined by equation (2.10)

$$\Delta H_o = \Delta H_{f_o}(A) + \Delta H_{f_o}(H^+) - \Delta H_{f_o}(AH^+) = PA_o(A) \qquad (2.10)$$

At first sight the only values required appear to be the heats of formation of neutral species (A), ionic species (AH^+) and of the proton. The heats of formation of neutral species are available from the literature. The heat of formation of the proton at zero Kelvin is known from spectroscopic measurements[2 10] and is 1528 kJ mol^{-1}.

Although the heats of formation of neutral species are frequently a source of uncertainty in these calculations, the major difficulty is to obtain accurate heats of formation for the ionic species. The main problems are:

1) to find species whose ionisation or fragmentation produce AH^+ species.

2) to convert the threshold values PA obtained in equation (2.10), into values at

the experimental temperature. A knowledge of the heat capacities is needed.

3) to decide which heat capacity to use for the electron for which two conventions are available.

The heat of formation of ion AH^- may be obtainable from either Appearance Energy (AE) or Ionisation Potential (IP) measurements. AE measurements for process (2.11) and IP measurement for reaction (2.12) may give energies at zero degrees Kelvin depending on the chemistry of the process, the standard state of neutral species and the energy of formation of the electron.

$$MAH \rightarrow M + AH^- + e^- \qquad (2.11)$$

$$X \rightarrow X^- + e^- \qquad (2.12)$$

$$AE = \Delta H_o = \Delta H_{f_o}(M) + \Delta H_{f_o}(AH^-) + \Delta H_{f_o}(e^-) - \Delta H_{f_o}(MAH) \qquad (2.13)$$

$$IP = \Delta H_o = \Delta H_{f_o}(X^+) + \Delta H_{f_o}(e^-) - \Delta H_{f_o}(X) \qquad (2.14)$$

In order to set up an absolute scale of PAs where absolute values arising from equation (2.10) could be compared with experimental values measured at temperature T, the former ones have to be estimated at temperature T by means of equation (2.15) where heat capacities of various species must be known.

$$\Delta H_T = \Delta H_o + \int_0^T (C_{P_{products}} - C_{P_{reactants}})dT \qquad (2.15)$$

As a simple example let us consider the application of the general equation (2.15) to the process (2.12). Its heat of reaction at temperature T is an ionisation energy related to IP by equation (2.16).

$$IE = IP + \int_0^T [C_p(X^+) + C_p(e^-) - C_p(X)]dT \qquad (2.16)$$

Therefore the heat of formation of ion X^+ at temperature T is given by equation (2.17).

$$\Delta H_{f_T}(X^+) = IP - \Delta H_{f_T}(e^-) + \Delta H_{f_T}(X) + \int_0^T [C_p(X^+) + C_p(e^-) - C_p(X)]dT \qquad (2.17)$$

At this stage one has to take into account two different conventions[2,11] regarding the electron. The first one, the thermal electron convention, treats the electron as

a conventional chemical element whose standard enthalpy of formation is zero at all temperatures. Further it is assumed that the electron is an ideal gas at all temperatures therefore its heat capacity is 5/2R. The second one, the stationary electron convention, assumes that the electron is at rest at all temperatures and consequently its heat capacity is zero at any temperature. One has to be careful not to mix in the same expression thermochemical values calculated on the basis of different conventions.

It is a general practice for threshold measurements to adopt the second convention. Thus equation (2.17) is simplified to equation (2.18).

$$\Delta H_{f_T}(X^+) = IP + \Delta H_{f_T}(X) + \int_0^T [C_p(X^+) - C_p(X)]dT \qquad (2.18)$$

It is generally assumed that $C_p(X^+)-C_p(X)$ is close to zero. The actual C_p is a sum of different contributions

$$\Delta C_p = \Delta C_p(\text{trans}) + \Delta C_p(\text{rot}) + \Delta C_p(\text{elect}) + \Delta C_p(\text{vib}) \qquad (2.19)$$

In fact the change in mass is in most cases negligible hence $\Delta C_p(\text{trans})=0$. The $\Delta C_p(\text{rot})$ will be close to zero unless there is a considerable change in symmetry. The maximum contribution from $\Delta C_p(\text{elect})$[2.11] is 0.9 kJ mol^{-1} in the temperature range 0-400K as a consequence of the splitting of the energies of degenerate states as most ions have a doublet ground electronic state and neutral molecules a singlet ground electronic state.

The $\Delta C_p(\text{vib})$ is the major contributor, due to changes in vibrational frequencies of bonds associated with chemical changes. The removal of an electron from a π-bond in an alkene produces a lowering of stretching and twisting frequencies of the bond hence a $\Delta C_p(\text{vib})$ contribution of 1 kJ mol^{-1} arises in the temperature range 0-400 K. Nevertheless in many cases the contribution is negligible.

On the reasonable assumption of $C_p(X^+)\approx C_p(X)$ the equation (2.18) becomes (2.20).

$$\Delta H_{f_{298}}(X^-) = IP + \Delta H_{f_{298}}(X) \quad (2.20)$$

From the above considerations[29], it may readily be proved that the two different arbitrary ways of treating the electron lead to

$$\Delta H_{f_{298}}(X^-) - \Delta H_{f_{298}}(X) = IP + 6.2 kJmol^{-1} \quad (2.21)$$

$$\Delta H_{f_{298}}(X^+) - \Delta H_{f_{298}}(X) = IP \quad (2.22)$$

Neither of these conventions seem to be absolutely appropriate to describe the electron.

2.2.2.1 Reference Standards for Absolute Proton Affinities

Accurate values of IP and AP for ions of general form AH^+ are scarce so quite a few absolute proton affinities can be calculated as in 2.2.2. Not many, however, are needed as reference standards to anchor the relative values and set up an absolute scale, provided those values are accurate.

Different reference standards have been used such as ammonia, isobutene, propene, ethene, etc.

As mentioned above, the absolute proton affinities carry the uncertainty of enthalpy of formation of the neutral species plus the uncertainty of the arbitrary conventions, and none is likely to be absolutely correct. On the other hand the threshold measurements from different laboratories are not always consistent.

Rosenstock[212] suggested propene as a good reference since an accurate measurement by threshold Photo Ion-Photoelectron Coincidence had been made for the process (2.23).

$$(CH_3)_2CH - X \rightarrow (CH_3)_2CH^+ + X + e^- \quad (2.23)$$

where X = halogen

$$AE[C_3H_7^+,(CH_3)_2CH-X] = \Delta H_f(C_3H_7^+) + \Delta H_f(e^-) - \Delta H_f[(CH_3)_2CHX] + \Delta H_f(X) \quad (2.24)$$

giving

$$\Delta H_{f_{298}}(C_3H_7^+) = 798.8 \pm 2 kJmol^{-1}$$

This is a reliable standard as most of the data available in the literature for these

calculations are consistent.

The absolute PA for propene is now available at 298K.

$$PA_{298}(\text{propene}) = \Delta H_{f_{298}}(\text{propene}) + \Delta H_{f_{298}}(H^+) - \Delta H_{f_{298}}(C_3H_7^+) \quad (2.25)$$

An absolute scale. Figure 2.1[2 13] is still no more precise than $+8 kJmol^{-1}$.

2.2.3 Absolute Acidities

The absolute gas phase acidity was defined by reaction 2.4 which can be split in two steps.

$$AH \rightarrow A + H \quad (2.26)$$

$$A + H \rightarrow A^- + H^+ \quad (2.27)$$

$\Delta H^\circ_{298} = DH^\circ(A-H)$

$\Delta H^\circ_{298} \approx \Delta H^\circ_0 = IP(H) - EA(A)$

$$\Delta H^\circ_{ac} \approx DH^\circ(A-H) + IP(H) - EA(A) \quad (2.28)$$

Although ΔH°_{ac} is not designated as the gas phase acidity of AH it gives a measure of the acidity of AH.

For most species in gas phase, reaction (2.4) is endothermic therefore in acidity scales the acidity increases as ΔH°_{ac} decrease.

The calibration of relative values of acidities is easier and more accurate than for PA because some acids such as HCl[2 5 2 8] possess a well defined ΔH°_{ac} and are therefore reliable standard reference compounds.

$$\Delta H^\circ_{ac} = DH^\circ(HCl) + IP(H) - EA(Cl) \quad (2.29)$$

The three quantities on the right side of the equation (2.29) are accurately known from spectroscopic data.

The IP(H)[2 14] is 1312 kJ mol^{-1} and it is a constant for all acids therefore the enthalpy of reaction (2.4) is ruled by the bond strength DH(A-H) and the electron affinity of radical A, EA(A).

The main sources of error in these calculations are some disparate values of

FIG.2.1. BASICITY SCALE

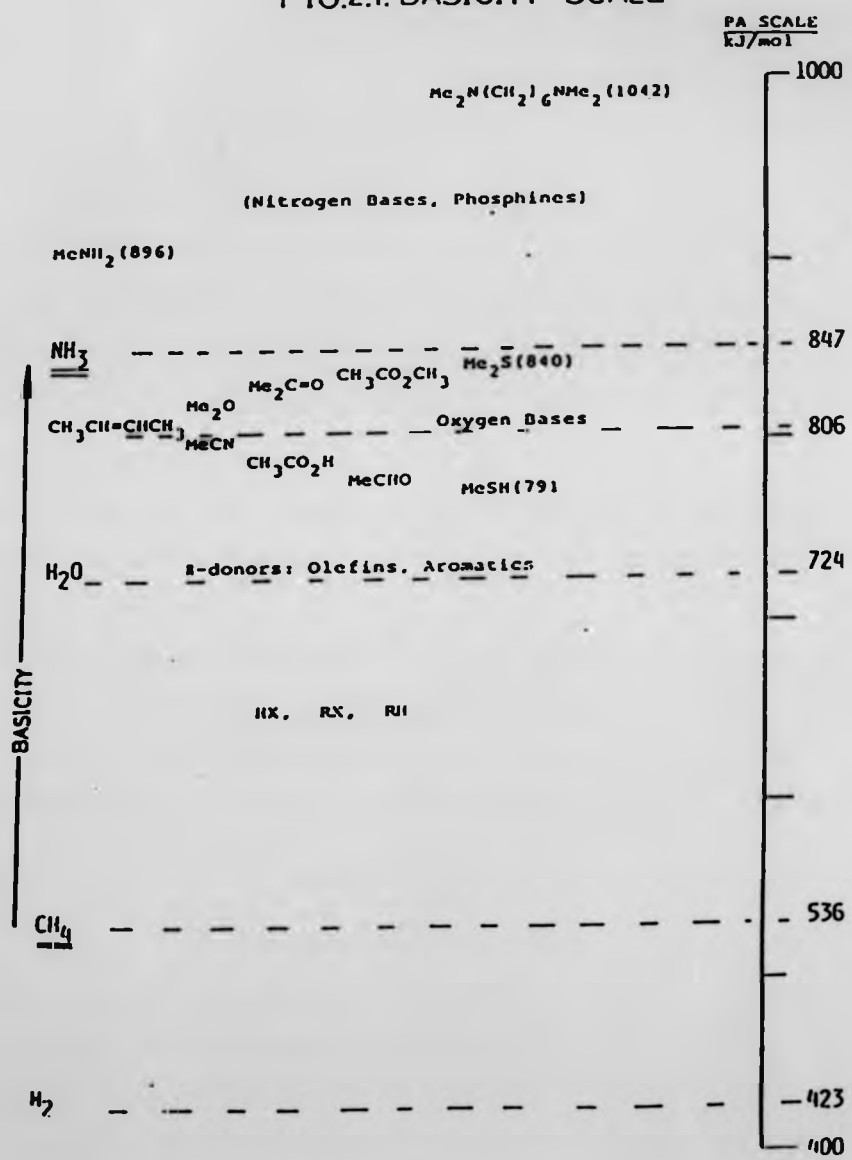

DH(A-H) and EA from different laboratories. The more trustworthy values of EA are obtained by Electron Photodetachment and Photoelectron Spectroscopy PES; however, not many are reliable which is a limitation. On the other hand bond dissociation energies are usually reported at 298K whilst electron affinities are measured at 0K. Nevertheless it is usually assumed that $IP_T(H^-) \approx IP_o(H^-)$ and $EA_T(A^-) \approx EA_o(A^-)$ because H^+/H and A^-/A are similar in structure. An acidity scale[2 13] is shown in fig 2.2.

2.2.4 Estimation of Entropy Changes

Gas phase equilibrium measurements as a function of temperature are an experimental way of evaluating entropy changes as can be seen from equation (2.30).

$$\ln K = -\frac{\Delta H}{RT} + \frac{\Delta S}{R} \qquad (2.30)$$

Nevertheless, most of the experimental work already carried out for PTR has been done at a single temperature leading to the determination of the free energy change for the reaction under study, i.e. the gas phase basicity difference between the two species involved.

It has been generally assumed[2 11,2 15,2 16] that for PTR the ΔG° measured is very close to ΔH° since $T\Delta S^\circ$ is either taken as approximately zero or equated to ΔS°_{rot}, calculated using statistical mechanics. Bearing in mind the reaction (2.5), the different contributions to the partition functions ΔS will become

$$\Delta S = R \ln \frac{Q_{BH^+} \cdot Q_A}{Q_{AH^+} \cdot Q_B} \qquad (2.31)$$

$$\Delta S^\circ = \Delta S^\circ_{trans} + \Delta S^\circ_{rot} + \Delta S^\circ_{vib} + \Delta S^\circ_{elect} \qquad (2.32)$$

For many reactions, this is close to zero. For PTR ΔS_{trans} is ignored unless there is a very large change in reduced mass between reactants and products. In thermal conditions one does not expect any electronic excited states, that is to say ΔS_{elect} is zero. The ΔS_{vib} is also close to zero. Apart from a cancellation effect the $(X-H)^+$ bond is a strong one (750 $kJmol^{-1}$) and possible vibrational contributions

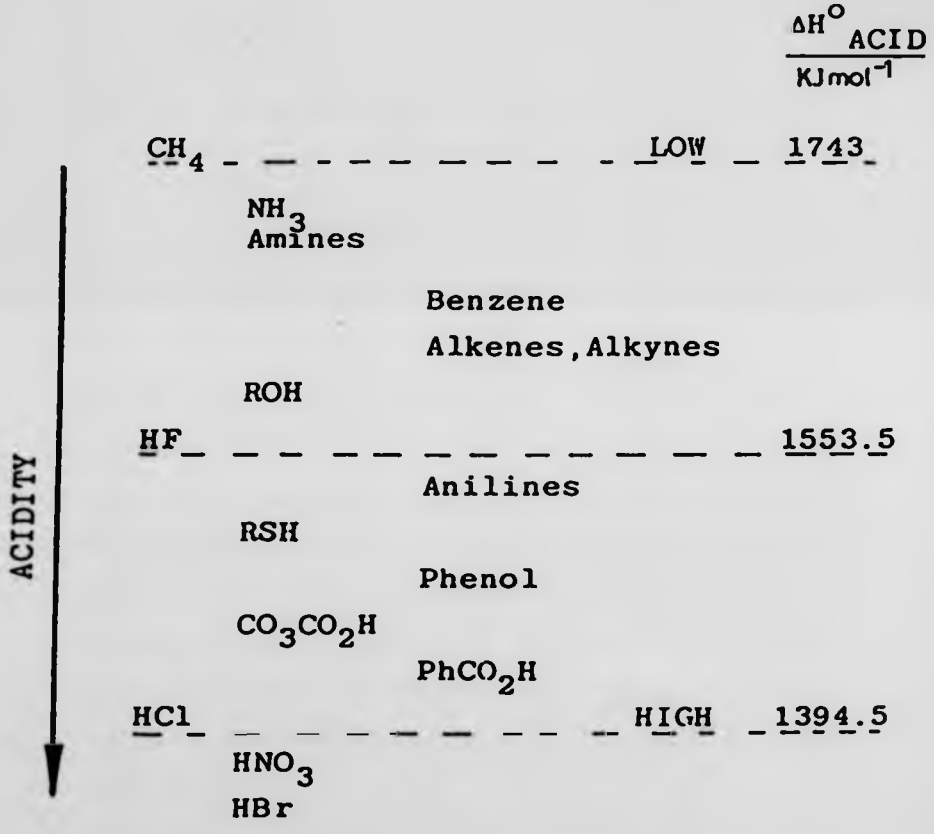

FIG.2.2 ACIDITY SCALE

are certainly very small. Hence it is common to consider that the only significant contribution arises from changes in rotational symmetry[2 11] in equation (2.33).

$$\Delta S^{\circ}_{rot} = R\ln\left(\frac{I_{BH}\cdot I_A}{I_{AH}\cdot I_B}\right)^{\frac{1}{2}}\frac{\sigma_{AH}\cdot\sigma_B}{\sigma_{BH}\cdot\sigma_A} \qquad (2.33)$$

where I_x - Inertia moment

σ_x - Symmetry number

For PTR the ratio of moments of inertia is close to 1. Then equation (2.31) becomes

$$\Delta S^{\circ} \approx \Delta S^{\circ}_{rot} = R\ln\frac{\sigma_{AH}\cdot\sigma_B}{\sigma_{BH}\cdot\sigma_A} \qquad (2.34)$$

When small changes in symmetry take place, and this is often the case, ΔS°_{rot} is obviously small but is the main contribution to ΔS°.

This has been in fact verified for very many PTR[2 15,2 16,2 17,2 18,2 19 2 20].

In order to estimate ΔS° it is necessary to know the symmetry of neutral and protonated species; in the latter case, this may vary with the site of protonation. In spite of this requirement, ΔS° is often able to give information on the structures of protonated species. A prediction about a likely site of protonation can be made and, based on this assumption, ΔS_{rot} can be calculated from statistical mechanics and comparison with experimental values may help in establishing the site of protonation. Experimental values may also be compared with theoretical predictions from *ab initio* calculations.

The fluorobenzene-*meta*difluorobenzene system[2 21] illustrates not only a small ΔS° value but also how it may confirm the assumed position of protonation.

From classical mechanistic arguments the following sites of protonation were assumed.

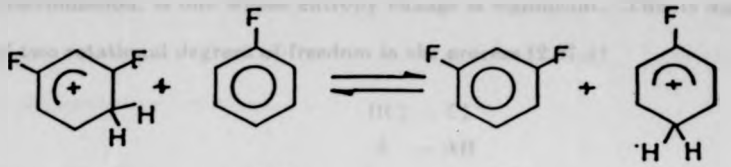

(2.35)

$$\Delta S^{\circ}_{rot,st.} = R\ln\frac{1\times 2}{2\times 2} = -5.8 J mol^{-1}K^{-1}$$

$$\Delta S^{\circ}_{exp} = -5.2 \pm 2.1 J mol^{-1}K^{-1}$$

The agreement is good as is also the case for another proton transfer reaction that between benzene and fluorobenzene[2,18].

There is evidence[2,22] that in fluorobenzene the proton is attached to a carbon atom of the ring which exhibits tetrahedral sp^3 valence. It was also assumed that protonation occurs at para position.

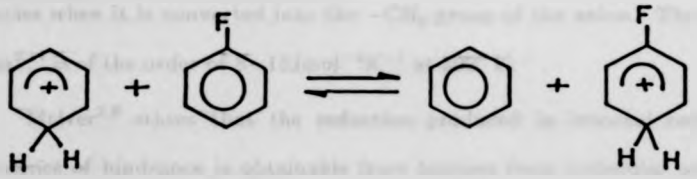

(2.36)

$$\Delta S^{\circ}_{rot,st.} = R\ln\frac{2\times 2}{12\times 2} = -14.9 J mol^{-1}K^{-1}$$

$$\Delta S^{\circ}_{exp} = -15.0 \pm 2 J mol^{-1}K^{-1}$$

This system exhibits a larger ΔS_{rot} but it is calculable from statistical mechanics and again the agreement between ΔS_{rot} calculated and ΔS_{exp} confirms the suggested para protonation.

The assumptions previously made that the various contributions for ΔS° in equation (2.32) are close to zero, apart from ΔS_{rot}, still hold in the evaluation of entropy changes in PTR for anions. However the loss of hindrance of internal rotations can also give important contribution to ΔS°_{sc}.

The normal equilibrium (2.37)[2 13], where HCl is the standard for acidity determination, is one whose entropy change is significant. This is due to the loss of two rotational degrees of freedom in the process (2.37.1)

$$HCl \rightarrow Cl^- \qquad (2.37.1)$$

$$A^- \rightarrow AH \qquad (2.37.2)$$

The reverse process (2.37.2) can only partially compensate that loss by creation of just one internal rotation in favourable cases where AH is, for instance, a phenol or a carboxylic acid. This rotational contribution[2 13, 2 14] is of the order of $20 J mol^{-1} K^{-1}$ at 300K.

Another type of contribution which must be accounted for is the decrease in internal rotation due to hindrance in species AH. A good example is the reaction (2.38).

$$CH_3COCH_3 - CH_3COCH_2^- \qquad (2.38)$$

A barrier is formed to the free internal rotation of the methyl group in the neutral species when it is converted into the $-CH_2$ group of the anion. The ΔS contribution[2 14] is of the order of $8-13 J mol^{-1} K^{-1}$ at 300° K.

McIver[2 8] states that the reduction produced in internal rotation by the existence of hindrance is obtainable from barriers from molecular orbital calculations, microwave spectra.

When determination of entropy changes by measurements of PT equilibria fail or are inconclusive the entropy change may be evaluated by the standard statistical mechanics equation (2.31). On the other hand ΔS°_{ac} for reaction (2.4) has been calculated through equation (2.39).

$$\Delta S^\circ_{ac} = S^\circ(H^+) + S^\circ(A^-) - S^\circ(AH) \qquad (2.39)$$

The entropy of the neutrals is estimated usually by Group Additivity[2 23] if not available in the literature. The entropy of the proton is known and published in tables[2 24] and for negative ions is common practice to assume that their entropies are equal to the entropies of isoelectronic neutrals, i.e. $S^\circ_{HCO^-} = S^\circ_{HCN}$.

Very good agreement was found[2 8] between ΔS° calculated by the isoelectronic method and that given by statistical mechanical methods. Some experiments lead to ΔS° values with a deviation of $0.42 JK^{-1}mol^{-1}$ from the predictions of the isoelectronic method.

2.2.5 The Theoretical Approach

The development of gas phase equilibria measurements and the consequent huge number of thermochemical data there available became a challenge for theoreticians, supplying them with a reliable data base, free from solvent interactions, against which to compare their calculations.

PTR are particularly suitable for these tests because they are isodesmic processes, and potential errors in calculations are therefore expected to cancel.

The *ab initio* methods[2 22] have largely spread and improved by the use of larger basis sets, polarised functions and perturbation theory[2 25] to the extent that they can be considered as a parallel method of determining PAs. Furthermore, semi-empirical methods have had an improtant role[2 26].

The figure 2.3 shows the good agreement between experimental PAs and theoretical PAs for a considerable number of first and second row bases[2 27].

The experimental values are from the same sources wherever possible. The theoretical PAs are 0-40 kJ mol^{-1} above experimental values. The deviation is assumed to arise from zero point vibrational energy not taken into account plus a neglected correction of the discrepancy in temperature between both sets of data.

The zero point vibrational energy correction was found to be up to $40kJmol^{-1}$ and positive; it will therefore lower the calculated PAs.

Theoretical calculations can provide information about the protonation site by providing estimates of the different PAs at the various basic sites borne by the same molecule when experimental data are inconclusive.

The study of substituent effects[2 28,2 29,2 30] on protonation, stability for protonated structures, and potential energy surfaces[2 31] has also been investigated by theoretical means.

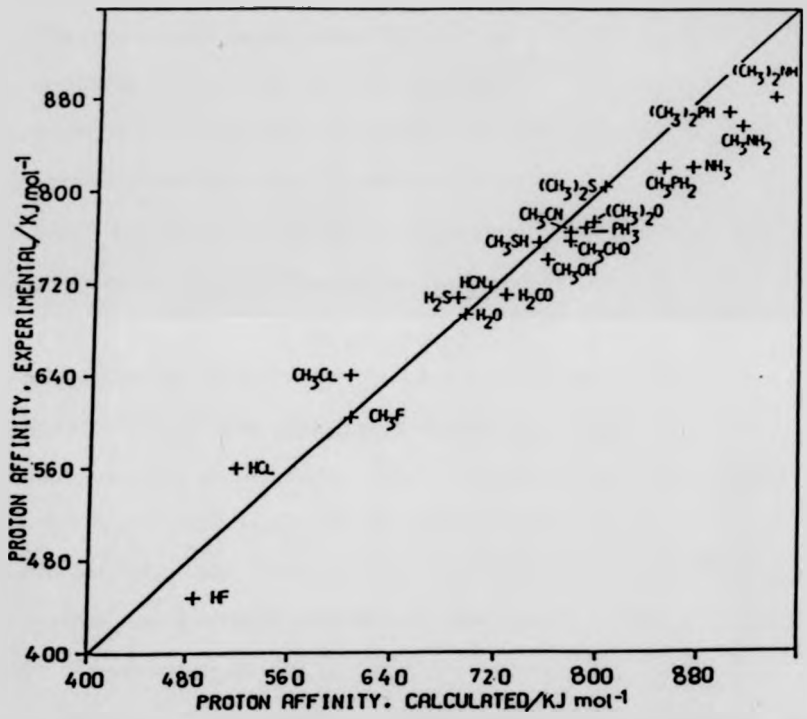

Figure.23. Calculated (6-31G*) vs. experimental proton affinities. The straight line corresponds to a line of unit slope.

2.2.6 A Correlation between PAs and Core-Electron Ionisation Potentials

It is important to mention studies which provide a different approach to predict PAs as well as sites of protonation derived from the predicted PAs. This method is very useful when experimental PAs are difficult to measure.

A linear relationship between PAs and 1s orbital energies for compounds

whose heteroatom was either N or O was observed by Thomas and al[2 32]. The effect looked understandable on the grounds of the electrical equivalency of a core-electron removal from the heteroatom and the addition of a proton to the same site. In both processes a highly localised positive charge has to be accommodated on the heteroatom.

The correlation holds for various homologous series of compounds where the heteroatoms O, N have been extended to P and S[2 34]. It breaks down when the protonation does not take place on the heteroatom which is the site of ionisation or if protonation provokes important geometry changes.

Martin and Shirley[2 34] and independently Davis and Rabelais[2 35] proposed an equation based on a theoretical model for the suggested relationship.

$$PA = -IE(X_{1s}) + c \qquad (2.40)$$

where $IE(X_{1s})$ is the ionisation energy for the 1S electron (X=O or N). More recent studies[2 36] have shown that a multivariate linear correlation may be used to make the same type of predictions. This multivariate relationship correlates PAs (exp) with inner shell ionisation energies and first ionisation potentials as a linear function (see figure 2.4). These workers believe that is the combination of those two energies that is actually equivalent to the protonation process. Martin and Shirley[2 33] suggested an analogy between these processes.

$$MOH \rightarrow MO^{+}H + e^{-} \qquad (2.41)$$

$\Delta H^{\circ}=E_B(1s)$

$$MOH + H^{+} \rightarrow MOH_2^{+} \qquad (2.42)$$

$\Delta H^{\circ}=-PA$

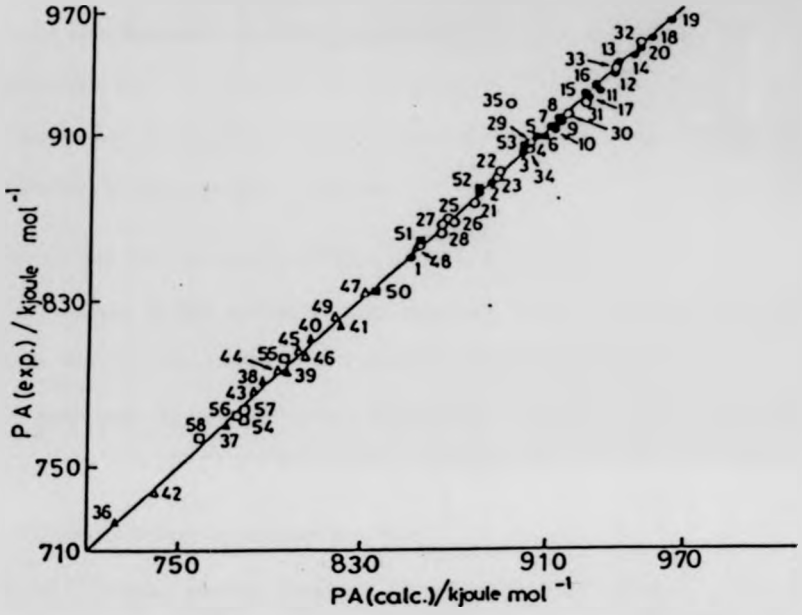

FIGURE 2.4. EXPERIMENTAL PAs vs. CALCULATED PAs BY A MULTIVARIATE CORRELATION

However the first one is a vertical process and the second an adiabatic one.

The protonation process is proposed by Catalán et al[2,36] as being described rather as two steps:

1) the positive charge localisation on an oxygen atom (analogy with 2.41)

2) the new ion suffers a redistribution of its charge

The first step shows a local character (accommodation of postive charge in basic site equivalence to 1s orbital energy),

The second step shows a molecular character (transfer of charge from base to proton equivalence to ionisation potential).

In fact this multivariate correlation is satisfactory for various homologous series and even molecules not fitting relationship (2.40) very well adjust well to the Catalán proposal.

Apparently, the multivariate correlation combines two factors which determine the basicity of a particular molecule.

2.3 Structural Effects on Gas-Phase Acidity-Basicity

It is not the aim of this section to treat exhaustively the influence of structural effects on reactivity but rather to refer to some of them as examples.

A systematic analysis of these effects requires one to apply extreme care because of the various effects which may be superimposed.

2.3.1 Intramolecular Hydrogen Bonding

Aue et al[2.37] pointed out the formation of intramolecular hydrogen bonding in diaminoalkanes.

Kebarle[2.19] et al made a comparative study of PTR as a function of temperature between two series of amines. The first series was treated as a PTR between a base B and alkylamines.

$$BH^+ + CH_3(CH_2)_nNH_2 \rightleftharpoons B + CH_3(CH_2)_nNH_3^+ \qquad (2.43)$$

The second series dealt with base B and α, ω diamino-alkanes.

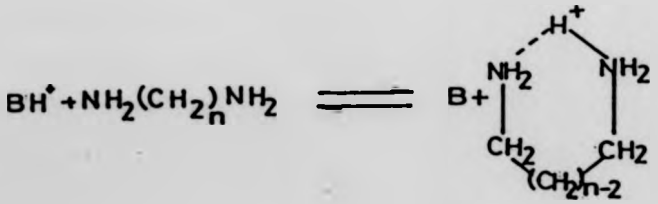

(2.44)

As a matter of fact these experiments confirmed Aue's findings. If an intramolecular hydrogen bonding occurs producing cyclisation, these PAs for

diamines should be larger than for monoamines due to stabilisation of the ammonium ion produced by the additional bond.

On the other hand the entropy changes for reaction (2.44) should be much larger than for reaction (2.43) as the cyclisation produces loss of freedom and symmetry gain.

Both situations do actually occur. The PAs of diamines are approximately 84 kJ mol^{-1} higher than the PAs for monoamines and ΔS° for reactions of diamines are as big as 86 J $mol^{-1}K^{-1}$ unlike ΔS for monoamine reactions for which ΔS° was estimated to be $\approx$ 12 $Jmol^{-1}K^{-1}$.

Another interesting point is that PAs and ΔS° values for diamines proton transfer show a sudden increase when $n>2$. The ring strain on the cyclic cation was assumed to be given by $\Delta H_p - \Delta H_c$ where ΔH_p is the enthalpy change of reaction (2.45).

$$C_kH_{2k+1}NH_3^+ + C_kH_{2k+1}NH_2 \rightleftharpoons (C_kH_{2k+1}NH_2)_2H^+ \qquad (2.45)$$

and ΔH_C the enthalpy change of reaction (2.44). The ΔH_p gives a measure of hydrogen bridge energy when a proton bound dimer is formed. The ring strain was found to be minimum at $n=3$.

The same effect on PAs and ΔS governed by an intramolecular hydrogen bond was detected in tertiary diamines, diols and diketones[2.5].

2.3.2 Alkyl Group Effect

This effect on basicity and acidity has been studied[2.5,2.8] for alkyalmines, alkoxide ions and other compounds. A mechanism of charge-induced dipole interaction is established between the charge centre of the ion and the alkyl group. The interaction is given by equation (2.46).

$$E = -\frac{\alpha q^2}{2\epsilon r^4} \qquad (2.46)$$

where

r - distance of separation

E - interaction energy

α - group polarizability

q - charge of the ion

ϵ - dielectric constant

As a consequence the ion structure gains stabilisation with an immediate increase of PAs where an alkyl group is added, i.e. $PA(NH_3)=838.1kJmol^{-1}$ and $PA(MeNH_2)=894.9kJmol^{-1}$.

The energy of interaction is dependent on $1/r^4$ so as the chain lengthens the stabilisation effect would be expected to attenuate. However the expected attenuation is not observed; instead, a constant small increase is observed up to decylamine. This appears to arise from a geometry change of the chain whereby the polarisable alkyl group is brought close to the charge centre.

2.3.3 Inductive Effects

According to Staley[2 38] et al the polarizability of certain halogenated amines and alcohols would account for larger PA's than those they actually display. Apparently the discrepancy can be explained by an electron withdrawal by the inductive effect of the halogen substituent desestabilising the cation.

As would be expected from the above considerations, the PA values decrease in the amines series as the number of halogen atoms increase. On the other hand PAs increase as the chain length increases for a given number of halogen atoms.

It is not clear if the inductive effect acts by either a through-bond inductive mechanism or a through-space field mechanism. In the latter case the effect is ruled by equation (2.47).

$$E = \frac{q\mu\cos\theta}{\epsilon r^2} \qquad (2.47)$$

where

q - charge

r - distance of separation

μ - dipole moment

ϵ - dielectric constant

θ - angle of the dipole

2.3.4 Acidity and Periodic Table

The acidity of hydrides varies as shown[28]

CH_4	<	NH_3	<	H_2O	<	HF
416.6±1		403.6±1		390.8±0.4		371.5±0.7
SiH_4	<	PH_3	<	H_2S	<	HCl
371.5±2		370.4±2		353.4±2		333±0.3
GeH_4	≈	AsH_3	<	H_2Se	<	HBr
360.7±3		359±7		339±5		323.6±0.3
						HI
						316.3±2

increasing along rows from left to right and along columns from top to bottom. The $\Delta H°_{ac}$ values, in kJ/mol. in the scheme vary in the opposite way.

As was stated in 2.2.3 and recalling equation (2.25), $\Delta H°_{ac}$ is determined by DH (A-H) and EA (A).

The electronegativity in the periodic table increases along rows and this affects the electron affinity of the hydrides in fig 2.5 in the same way. As the electron affinity increases, the acidity increases also which is actually verified for these hydrides. In the scheme presented the acidity is governed along rows by EA.

Although in the periodic table the electronegativity increases from bottom to top of the columns, in the columns of the scheme above the acidity increases in the opposite way. This is due to smaller variation of EA than DH (A-H) which determines the acidity along the columns of this scheme.

2.4 Kinetics and Energetics

2.4.1 Introduction

Although the thermodynamic properties of the species involved in the equilibrium provide information about the composition of the final state and the energetics of the system, they cannot give information about the time needed to achieve equilibrium and behaviour during the transformation. This information is given by the kinetics of the approach to equilibrium.

A summary account will be given below of the kinetics of PTR and how it may be influenced by thermodynamic properties.

2.4.2 The Fast Proton Transfer Reactions

Typically PTR proceed through intermediate complexes whose potential energy is lower than for reactant species and product species. This is easily understood in terms of long range forces between ions and dipoles, either induced or permanent.

Additional stability is conferred on the intermediate complex in PTR by hydrogen bond formation.

This feature gives rise to the potential energy surface[2.39] of the type below (figure 2.5).

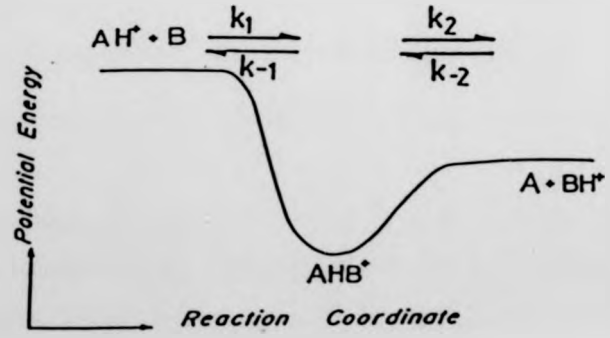

FIG. 2.5 POTENTIAL ENERGY DIAGRAM FOR P.T.REACTIONS

Using a steady state treatment for the activated complex AHB^* the rate constant (k_f)for the reaction in figure 2.5 is the product of the collision rate k_1 and the efficiency ratio for dissociation of the complex

$$k_f = k_1 \times \frac{k_2}{k_{-1}+k_2} \qquad (2.48)$$

As the branching ratio approaches unity, k_f tends towards the collision rate constant k_1.

In fact most of the exothermic PTR studied are very fast at thermal energies $k_{300} = 10^{-9} cm^3 molec^{-1} s^{-1}$ which is close to collision rate[2,40,24]. Thus these reactions must be one type of IMR which is suitable for checking the classical ion-molecule collision theory.

For systems[2,40] having a Boltzmann distribution the classical ion-molecule collision theory predicts a collision rate coefficient given by equation (2.49).

$$k_c = \frac{2\pi q}{\mu^{\frac{1}{2}}} \left[\alpha^{\frac{1}{2}} + c\mu_D \left(\frac{2}{\pi kT} \right)^{\frac{1}{2}} \right] \qquad (2.49)$$

where

q - charge of ion

μ - reduced mass of the colliding species

α - polarizability of the neutral species

μ_D - permanent dipole moment of the neutral molecule

c - constant depending on α and μ (tabulated by Su and Bowers).

Equation (2.49) can account for three different situations of the ion-molecule interaction.

If c=0 the equation is identical to that of the Langevin theory applied to IMR where neutrals are non-polar. It is assumed both partners are point particles with no internal energy and the interaction between them arises solely from ion-induced dipole forces.

If c=1 the equation is identical to that of the "Locked Dipole" Approximation for IMR with polar molecules. The permanent dipole is treated as having a maximum effect on ion-molecule capture cross section, considering the angle θ between dipole and the line of centres of collision as zero.

The Average Dipole Orientation (ADO) theory considers that the permanent dipole has a smaller effect than predicted by the "Locked Dipole" Approximation, in that case c is a measure of the locking of the dipole. The average angle θ is calculated and c is a function of $\mu_D/\alpha^{1/2}$.

Böhme[241] report a sequence of PTR used to test the theories above (2.50).

$$XH^+ + NH_3 \rightarrow NH_4^+ + X \qquad (2.50)$$

The experimental rate constant measured at 300°K is plotted in figure 2.6 versus $\mu^{-1/2}$. These straight lines show the predictions for the behaviour of capture rate coefficients in terms of the three versions of collision theory:

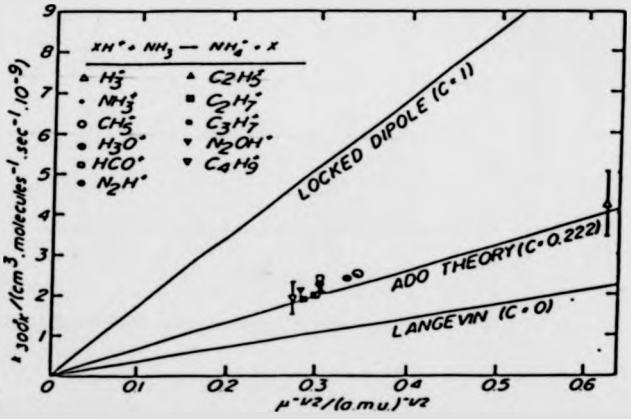

FIG. 2.6. A comparison of experimental reaction rate coefficients for P.T. with NH_3 (the solid bars represent an estimated accuracy of ±25%) with collision rate coefficients predicted by classical theories.

The experimental rate coefficients for proton transfer to NH_3 (α=2.16Å^3, μ_D=1.47D) are in good agreement with the prediction based on by ADO Theory.

The "Locked Dipole" Approximation clearly overestimates the rate coefficients.

Harrison[24] found good agreement for experimental rate constants for systems having non polar molecules and the calculated rate constants from Langevin theory.

Another interesting observation made by Böhme is displayed in figure 2.7.

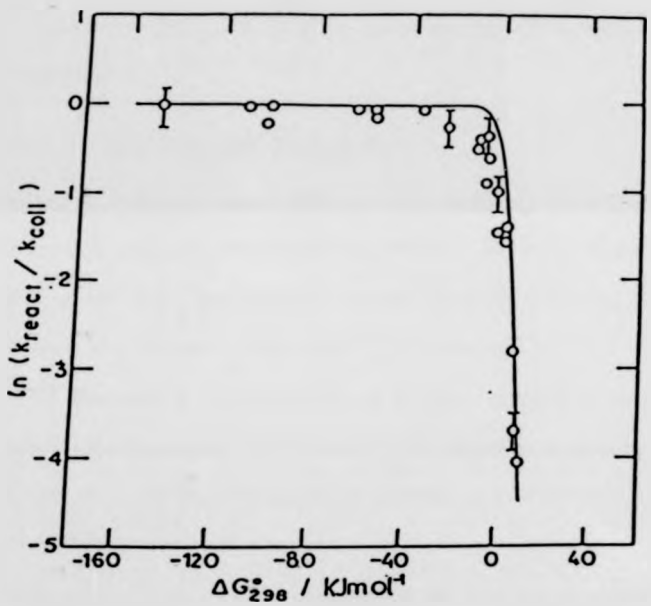

FIGURE 2.7. Efficiency of proton transfer as a function of ΔG°

A high reaction efficiency was observed for Brönsted acids for exoergic reactions. As the reaction becomes thermoneutral the efficiency drops dramatically.

Apparently a great number of PTR do occur on every collision provided the reaction is not thermoneutral or endoergic ($\Delta G^\circ < -20 kJmol^{-1}$).

Given the fairly good agreement between experimental rate coefficients and classical collision theory predictions one would expect the rate constants not to

show any temperature dependence in systems having non polar molecules. For systems containing polar molecules the rate constants would probably show a weak negative temperature dependence.

Böhme[2 41] observed that the PTR (2.51)

$$N_2OH^+ + CO \rightleftharpoons HCO^+ + N_2O \qquad (2.51)$$

takes place at 60% of the Langevin collision rate and has Langevin behaviour as far as temperature is concerned. In other words the reaction is temperature independent in the range 280 - 500 K. (The correction for CO permanent dipole was considered negligible.)

2.4.3 The Slow Proton Transfer Reactions

As was mentioned in 2.42 very many PTR are very rapid. However some others were found to proceed at slower rates than the collision rate, even though some of them are slighly exothermic. Two typical examples are PTR involving delocalized anions[2 42] and those in which steric hindrance[2 43] is important.

Brauman[2 39] proposed a potential energy surface, figure 2.8, with double minima to explain simultaneously low efficiency and negative temperature dependence. These slow reactions are assumed to be thermal, to involve long lived complexes and to be ruled by statistical theory.

The reactants form a long lived complex $(AH..B)^+$ at collision rate, k_1, the complex may break either into products at a rate k_2 or back into reactants at a rate k_{-1}. $(AH..B)^+$ is internally excited by the exothermicity of the reaction leading to its formation.

The complex at the top of the internal barrier is a tight one whereas the collision complex is a loose one. The density of states of the latter is larger. The equation (2.47) obtained through the steady state theory still holds because $k_3 >> k_2 > k_{-2}$; that is to say the complexes crossing the internal barrier will decompose into products. Should the reaction be exothermic, and because the

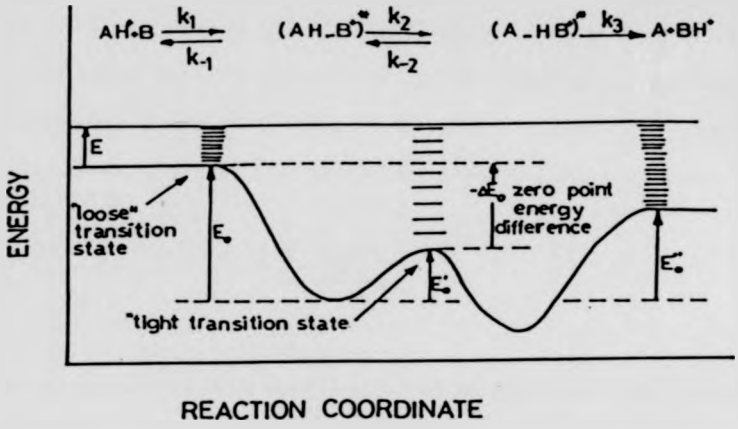

FIG. 2.8. POTENTIAL ENERGY OF REACTION COORDINATE FOR SOME PROTON TRANSFER REACTIONS

complex at E''_0 is loose, the crossing of the E''_0 barrier has to be faster than the crossing of the E'_0 barrier. In this situation where k_2 is small the efficiency ratio in equation (2.48) is necessarily lower than those for fast reactions. If $(-\Delta E_0)$ is large, it implies high efficiency since $k_2 >> k_{-1}$. In other words, the barrier E'_0 will be very small or even non existent so the conditions tend towards the initial potential energy surface shown in 2.2.2. Whether $(-\Delta E_0)$ is moderate or small the efficiency will be low. If moderate ($-\Delta E$=42−63kJ/mol)[244] the reaction will proceed at the collision rate at room temperature, but at higher temperatures, the temperature dependence will be negative. If small, $(-\Delta E_0)$, the reaction rate will reach collision rate below room temperature.

The internal barrier is considered as being caused by an electronic energy increase arising from bond modifications. Barriers were estimated by RRKM theory[245] by Brauman et al. The internal barriers were checked by experimental means. A sequence of experiments was performed for reaction (2.52).

$$AH^{+} + B \rightarrow \qquad (2.52)$$

varying B. B was chosen in such a way that the barrier will increase until it surpasses the energy level of $AH^{+}+B$. Then ΔE_0 becomes positive and the temperature dependence becomes positive also and the efficiency is lower than collision efficiency at all temperatures. These endothermic reactions whose transition states are thermally activated can be formulated by the transition state theory[2 44].

$$k = \frac{k'}{h}\frac{Q_{(AHB^{+})^{*}}}{Q_A Q_B} e^{\frac{-\Delta E_o}{RT}} \simeq A e^{\frac{-E_A}{RT}} \qquad (2.53)$$

ΔE_o - activation energy
E_A - Arrhenius activation energy

Thus one can conclude that their temperature dependence is of the Arrhenius type.

Some reactions were studied by Meot-Ner et al[2 46] for which negative temperature dependence and low efficiency is apparently due to the freezing of external rotations of the reactants and is not due to an internal barrier. This is likely to happen if steric limitations to rotation are superimposed on the reaction coordinate.

A final situation deserves comment: the occurrence of a large negative entropy change associated with low exothermicity. This leads to negative temperature dependence and inefficiency again.

This was observed by Meot-Ner and al[2 47] for a PTR where cyclisation of an aminoalcohol occurs.

In this case the reaction was said to be slightly exothermic, the internal barrier[2 44] was found to be very low and both reactants and products complexes were assumed to be loose.

A large negative entropy change means that the products complex presents a smaller density of states than the reactants complex. At high temperatures $k_2 << k_{-1}$ because of the lower density of states of the product complex and so a negative temperature dependence will arise.

2.5 Transition from Gas Phase to Condensed Phase

2.5.1 Introduction

Although one of the most important advantages of gas phase ion chemistry is the possibility of carrying out studies without solvent interference, revealing intrinsic reactivity, its versatility is enough to mimic solvated ions in solution by gradual addition of one molecule of solvent to bare ions in the gas phase.

Stepwise solvation experiments were performed for equilibria and kinetics in order eventually to produce solution behaviour and gradual change in reactivity.

This subject is reviewed briefly below.

2.5.2 The Solvent Influence

Usually the solvent acts by reducing the intrinsic effects on reactivity and consequently an attenuation effect is often observed when going from gas phase basicities and acidities to the ones in solution. Nevertheless some reversals of acidities and basicities can be found.

The following cycle[2,48] relates the effects of solvation on neutral base B and its cationic conjugated acid with the differences in $\Delta H^\circ_{prot,s}$ (standard enthalpy of protonation in solution) and PA.

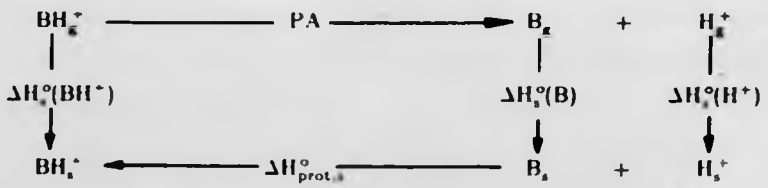

$$-\Delta H^\circ_{prot,s} = -\Delta H^\circ_s(BH^+) + PA(B) + \Delta H^\circ_s(B) + \Delta H^\circ_s(H^+) \qquad (2.54)$$

A similar cycle can be drawn to account for the solvation thermodynamics of anions.

The thermodynamics functions $\Delta H,^\circ \Delta S^\circ$ and ΔG° are supposed to result from

two factors, one internal identified with the gas phase and the other external arising from solvation. The effect of solvation[2 49] itself may be considered to be divided into two steps

1) Accommodating a neutral molecule into the solvent, leading to a hydrophobic term.

2) Interaction of the ionic charge with the solvent leading to an electrostatic term.

The latter is normally the more important one.

The substituent effects on basicity were weakened in solution as it was found[2 49] from a linear correlation of PAs vs $\Delta H^{\circ}_{prot.s}$ for alkylamines where an attenuation of 5-6 fold was seen.

This finding was rationalised in terms of compensating of electrostatic solvation contribution arising from alkylammonium solvated ions. $\Delta H^{\circ}_{prot.s}$ are proportional to PA but the relationship does not hold as well between GBs and $\Delta G^{\circ}_{prot.s}$ because $T\Delta S$ terms are able to reverse the basicity order.

A change in Proton Transfer mechanism induced by solvation was found by Kebarle et al[2 50] between two separate groups of anilines, one of them protonating on the ring and the other on the nitrogen, both in gas phase. Protonation in a given solution favoured nitrogen atoms as the site of protonation, since only gas-phase nitrogen protonated anilines give good linear correlation with aqueous protonated anilines (see figure 2.9).

The substituent effect is attenuated by a factor of 4 in solution. The formation of strong hydrogen bonds between water and nitrogen protonated anilines triggered a transfer of the proton from ring to nitrogen for m-MeS, m-OH, and mC_2H_5-anilines when monohydration took place.

Böhme[2 51] observed the effect of hydration on intrinsic reactivity of H_3O^+ and found two different types of behaviour.

$$H_3O^+.(H_2O)_n + B \rightleftharpoons BH^+(OH_2)_m + (n-m+1)H_2O \qquad (2.55)$$

In both types reduction of the specific reaction rate always took place but to a different extent.

The reduction was small up to three molecules of solvent when B was replaced by bases such as CH_3CN, $(CH_3)_2CO$, CH_3CHO, CH_3OH, C_2H_5OH, $(CH_3)_2O$ etc.

When B was replaced by H_2S, H_2SO_4 and $CHCl_3$ the reaction rates decreased dramatically, just with the addition of one molecule of solvent.

Apparently all the latter compounds may behave as H_2S. In this case[2.52] ΔG° = -15.9 kJmol^{-1} for the unsolvated reaction and ΔG°=+26.3kJmol^{-1} for the solvated reaction when n=2 at 300K. This group of reactions has low exothermicity. The hydration makes the reaction become endoergic and its direction is reversed.

The rate constant decreased accordingly from 1.9×10^{-9}cm^3 molec^{-1}s^{-1} (unhydrated reaction) to 1×10^{-12}cm^{3}molec^{-1}s^{-1} for the solvated reaction (n=1-3).

The first group remains exothermic and exoergic, its trend of a slight reduction is rationalized by the reduction in collision rate as a consequence of the increase in reduced mass of the colliding pair.

Studies by SIFT[2.53] showed that in systems such as:

$$OH^-.(H_2O)_n + CH_3OH \rightleftharpoons CH_3O^-.(H_2O)_n + H_2O \qquad (2.56)$$

$$OH^-.(CH_3OH)_n + CH_3OH \rightleftharpoons CH_3O^-.(CH_3OH)_n + H_2O \qquad (2.57)$$

K decreases sharply with the addition of one molecule of solvent (figure 2.10) and keeps decreasing slowly with solvation when n>1. The relative acidities of H_2O and methanol reverse with 2 added molecules of methanol but the same does not happen if the solvent is water.

Different studies by Bohme[2.54] concerning solvation effects on acidities (reaction 2.58),

$$B^-.S_n + AH \rightleftharpoons AS_n^- + BH \qquad (2.58)$$

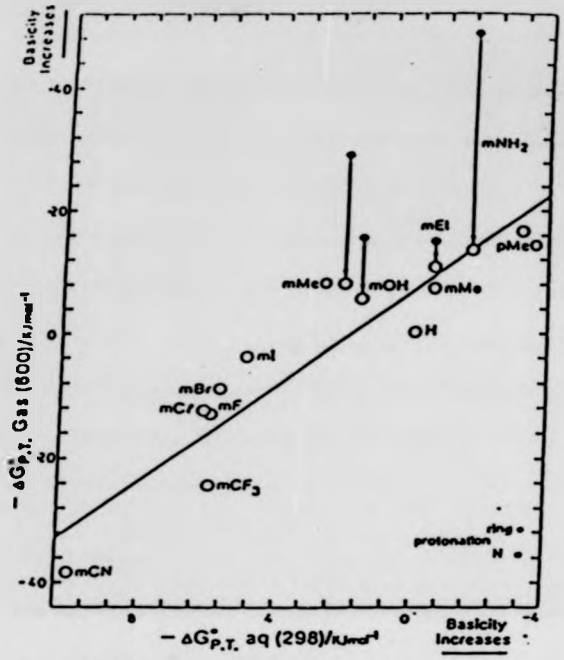

FIG. 2.9. CORRELATION BETWEEN ΔG°(gas) AND ΔG°(aq.) IN REACTION $C_6H_5NH_3^{\circ}B = C_6H_5NH_2BH^{\circ}$

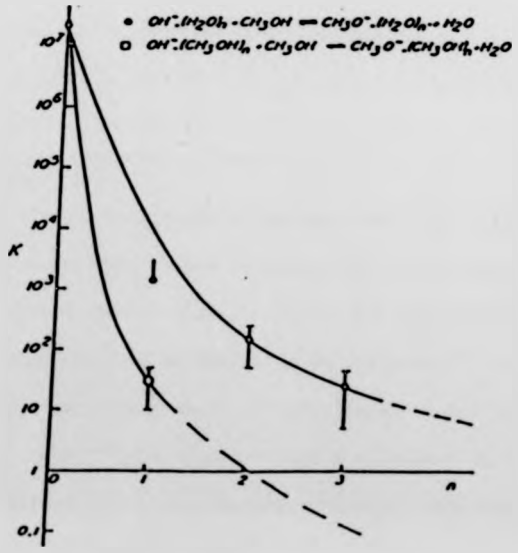

FIG 2.10. THE SHIFT IN THE EQUILIBRIUM POSITION AS FUNCTION OF SOLVATION

where for instance B⁻S = $CH_3O^-.CH_3OH$ and AH=C_2H_2, lead to the conclusion that experiments on species for which n≤3 showed agreement with some others in solution with respect to acidities and rates.

In conclusion it can be said that the most drastic attenuation of the various effects observed often took place with just one solvent molecule.

Stepwise solvation studies were performed with the addition up to 4 molecules of solvent which is an environment still far away from a real solution; nevertheless under these conditions, the separation between gas phase and condensed phase is becoming considerably reduced.

2.6 Experimental Techniques

The performance of Ion Molecule Equilibria measurements has been mainly based in three techniques whose description is given below.

2.6.1 Ion Cyclotron Resonance Spectrometry

In ICR Spectrometry[25] ion are generated by EI and they are drifted from the source region by influence of crossed electric and magnetic fields. Hence the ions inside the analyser describe a cycloidal path at a frequency ω_o

$$\omega_o = \frac{qH}{mc} \qquad (2.59)$$

q/m - charge to mass ratio of the ion
H - magnetic field

A radio frequency electric field is applied perpendicular to the magnetic field by means of a marginal oscillator. When the frequency of the marginal oscillator is equal to the cyclotron frequency of an ion ($\omega_0=\omega_1$) a signal is obtained. At this stage should the magnetic field be fixed at H all the ions of a given m/q are in resonance and they absorb energy from the radio frequency field being accelerated to a larger orbital radius. The energy absorbed is a measure of the ion intensity and it causes a decrease in the radio frequency voltage of the marginal oscillator

circuit which is amplified and detected. Two types of cells[25] have been used, drift cells and trapped cells. The first type is suitable for measurements of equilibrium constants where the proton transfer is rapid, the operating pressure is in the range (10^{-6}–10^{-3}Torr) and the drift time about 2 ms. The equilibrium constants are determined by the product of a ratio of ion intensities and a ratio of pressures of neutrals. Keeping the latter ratio constant, the total pressure is varied and equilibrium is considered reached when the ratio of intensities of ions becomes constant as function of total pressure.

The trapped cells allow residence times of at least 1 sec and the operating pressures are in the range $(1-4)\times10^{-6}$Torr.

In double resonance[255] experiments a second radio frequency is used (ω_2). If enough power is absorbed any ion resonant with this new frequency can be ejected to the sides of the cell. This allows one simultaneously to eject one particular product ion and to follow the decay of the corresponding reactant ion and vice-versa. This is advantageous in the study of very slow reactions leading to the measurement of a forward rate constant, a backward rate constant and eventually to the calculation of the associated equilibrium constant.

Pulsed experiments[213] have been set up in trapped cells, double resonance experiments[255], where a pulse of electrons causes ionisation and a detection radio frequency pulse permits the ion intensities to be followed as function of time.

Although this technique raises the doubt that the energy distribution of ions may not be Maxwell-Boltzman, it gives good agreement with data obtained by other techniques.

2.6.2 Selected Ion Flow Tube

This technique is an improved version of the flowing afterglow technique[256].

The latter technique involves a fast gas flow (velocity 10^4cms^{-1}) of a carrier gas (usually helium) in a reaction tube where typical flow tube pressure range from

0.3 to several torr. From gases introduced into the flow upstream, ions are produced and they will react with neutral molecules of reactant gases introduced downstream. At the end of the reaction tube the ions are sampled through an orifice entering a differentially pumped quadrupole mass filter. Reaction rate coefficients can be calculated from the experimental decay in the primary ion count rate with reactant neutral addition.

The basic advantage of the technique is in avoiding the possibility of neutral species becoming excited if they were in contact with the ionisation region. This aspect was improved in SIFT. Reactant ions are produced then mass analysed in a quadrupole mass spectrometer so that ions of a given m/z may be injected into the flow tube. These ions are thermalized by collison with He before meeting the neutral reactant gas downstream.

The possible selection of ions of interest reduces complications in the study of IMR avoiding for example, competing reactions from other primary ions, the presence of electrons which can compete with the reaction under study by altering the positive ion concentration. These advantages compensate largely for the possibility of mass discrimination and surface changing, both of which are likely to happen. The detection and analysis of the IMR resultant ions are analogous to those performed in FA.

Equilibrium constants are usually determined from rate constants of the forward and reverse reactions: however, equilibrium systems[2,57] are sometimes set up.

2.6.3 Pulsed High Pressure Source Mass Spectrometry

This technique was first developed by Kebarle[2,7] and it has been recognised as suitable to study ion clustering, PTR and other IMR[2,15].

Short pulses (10-50 μs) of the electron beam generate ions which react in a field free high pressure (up to 10 Torr) source[2,16]. There the ions diffuse from the reaction chamber through a very narrow ion exit slit or orifice (25 μm) into a low

pressure region where they are accelerated and mass analysed. The intensity of ions is measured as a function of time and eventually the approach to equilibrium is monitored through the progress of the ion intensity ratio as function of time until it reaches constancy.

In this technique no doubts usually arise about ions having a thermal energy.

However potential problems related to the presence of electrons, ions and neutrals in the reaction chamber are likely to be found, as well as collisonal decomposition of ions after or during acceleration since their concentrations are not measured in situ. Nevertheless the technique possesses the advantage of direct measurements and easy control of reaction time, pressure and temperature in the reactor.

A more detailed treatment of the technique will be given in the next chapter.

2.7 References

2.1 A.J. Dempster, Philos. Mag. (1916), 31, 438

2.2 T.R. Hogness and E.G. Lunn, Phys. Rev. (1925),26, 44

2.3 K.R. Jennings, Adv. Mass Spectrom (1978),7, 209

2.4 A. Harrison, "Chemical Ionisation Mass Spectrometry", (1983), C.R.C. Press Florida

2.5 D.H. Aue and M.T. Bowers, "Gas Phase Ion Chemistry", (1979), vol.2, 1-51, (ed. M.T. Bowers), Academic Press

2.6 J.L. Beauchamp, Ann. Rev. Phys. Chem. (1971), 22, 527

2.7 P. Kebarle, in "Interaction Between Ions and Molecules" Nato Advanced Study Institute, Series B, (1975), 459, (ed. P. Ausloos), Plenum Press

2.8 J.E. Bartmess and R.T. McIver, in "Gas Phase Ion Chemistry", (1979), vol.2, 87, (ed. M. Bowers), Academic Press

2.9 H.M. Rosenstock, in "Kinetics of Ion-Molecule Reactions", Nato Advanced Study Institute Series B, 1978, 246, (ed. P. Ausloos), Plenum Press

2.10 H.M. Rosenstock, K. Draxl; B.W. Steiner and J.T. Herron, J. Phys. and Chem. Ref. Data, (1977), 6, Suppl. 1

2.11 S.G. Lias, in "Kinetics of Ion-Molecule Reactions", Nato Advanced Study Institute Series B, (1978), 223, ed (P. Ausloos), Plenum Press

2.12 H.H. Rosenstock, R. Buff, M.A.A. Ferreira, S.G. Lias, A.C. Parr, R.L. Stockbauer, J.L. Holmes, J.Am. Chem. Soc., (1982), 104, 2337

2.13 R.S.Mason, "Thermochemistry and Its Applications to Chemical and Biochemical Systems", 1982, 627, ed. Ribeiro da Silva..

2.14 J.B. Cumming, P. Kebarle, Can. J. Chem., (1978), 56, 1

2.15 P. Kebarle, Ann. Rev. Phys. Chem., (1977), 28, 445

2.16 R.S. Mason, D.K. Bohme, K.R. Jennings, J. Chem. Soc., Faraday Trans I, (1982), 7, 1943

2.17 R. Yamdagni and P. Kebarle, J. Am. Chem. Soc., (1976), 98, 1320

2.18 D.K. Bohme, J.A. Stone, R.S. Mason, R.S. Stradling and K.R. Jennings, Int. J. Mass Spectrom, Ion Phys., (1981), 37, 283.

2.19 R. Yamdagni and P. Kebarle, J. Am. Chem. Soc., (1972), 95, 3504

2.20 J.P. Briggs, R. Yamdagni and P. Kebarle, J. Am. Chem. Soc., (1972), 94, 5128

2.21 K.G. Hartman and S.G. Lias, Int. J. Mass Spectrum. Ion Phys., (1978), 28, 213

2.22 W.J. Hehre and J.A. Pople, J. Am. Chem. Soc., (1972), 94, 6901

2.23 S.W. Benson, "Thermochemical Kinetics", 1976, Wiley and Son

2.24 D.R. Stull and H. Prophet, "Janaf Thermochemical Tables", Natl. Stand. Ref. Data Ser., Natl. Bur. Stand., NSRDS-NBS 37, (1971), U.S. Govt. Print.

Off., Washington, D.C.

2.25 J. Del Bene, H.D. Mettee, M.J. Frisch, B.T. Luke, J.A. Pople, J. Phys. Chem. (1983), **87**, 3279

2.26 R.L. De Kock and C.P. Jasperse, Inorg. Chem. (1983), **22**, 3839

2.27 F.S. Scott, C. Jayaraman and W.L. Jorgensen, J. Phys. Chem., (1982) **86**, 3308

2.28 Y.K. Lau and P. Kebarle, J. Am. Chem. Soc. (1976), **98**, 7452

2.29 J. Catalán and M. Yáñez, J. Chem. Soc., Perkin II (1979), 741

2.30 J.L. Devlin, J.F. Wolf, R.W. Taft, W.J. Hehre, J. Am. Chem. Soc. (1976), **98**, 1990

2.31 T. Sórdo and J. Bertrán, J. Chem. Soc., Perkin II, (1979), 1486

2.32 T.X. Carrol, S.R. Smith, T.D. Thomas, J. Am. Chem. Soc., (1975), **97**, 659

2.33 B.E. Mills, R.L. Martin, D.A. Shirley, J. Am. Chem. Soc., (1976), **98**, 2380

2.34 R.L. Martin and D.A. Shirley, J.Am. Soc. (1974), **96**, 5299

2.35 D.W. Davis and J.W. Rabalais, J. Am. Chem. Soc., (1974), **96**, 5305

2.36 J. Catalán, O. Mó, P. Pérez, M. Yáñez, J. Chem. Soc., Perkin Trans II, (1982), 1409

2.37 D.H. Aue, H.M. Webb and M.T. Bowers, J. Am. Chem. Soc., (1973), **85**, 2699

2.38 R.H. Staley, R.D. Wieting and J.L. Beauchamp, J. Am. Chem. Soc. (1977), **98**, 5964

2.39 C.R. Moylan and J.I. Brauman, Ann. Rev. Phys. Chem., (1983), **34**, 187

2.40 T. Su and M.T. Bowers, "Gas Phase Ion Chemistry", (1979), vol.1, 84, (ed. M.T. Bowers), Academic Press

2.41 D.K. Böhme, in "Interaction Between Ions and Molecules" Nato Advanced Study Institute, Series B, 1975, 489, (ed. P. Ausloos), Plenum Press

2.42 W.E. Farneth and J.I. Brauman, J. Am. Chem. Soc., (1976), **98**, 7891

2.43 J. M. Jasniski and J.I. Brauman, J. Am. Chem. Soc. (1980), **102**, 2906

2.44 T.F. Magnera and P. Kebarle, in "Ionic Processes in the Gas Phase", Nato Advanced Study Institute, Series C, 1984, 135, (ed. M.A. Almoster Ferreira), Reidel

2.45 F.K. Meyer, M.J. Pellerite and J.I. Brauman, Helv. Chim. Acta (1981), **64**, 1058

2.46 a) M. Meot-Ner and F.H. Field, J. Chem. Phys. (1976), **64**, 277

b) M. Meot-Ner, in "Gas Phase Ion Chemistry" vol. 1, (1979), 198, (ed. M. Bowers), Academic Press

2.47 M. Meot-Ner, P. Hamlet, E.P. Hunter and F.H. Field, J. Am. Chem. Soc. (1980), **102**, 6393

2.48 E.M. Arnett, Acc. Chem. Res., (1973), **6**, 404

2.49 D.H. Aue, H.M. Webb and M.T. Bowers, J. Am. Chem. Soc. (1976), **98**, 318

2.50 Y.K. Lau, K. Nishizawa, A. Tse., R.S. Brown and P. Kebarle, J. Am. Chem. Soc., (1981), **103**, 6291

2.51 D. K. Böhme, in "Ionic Processes in the Gas Phase", Nato Advanced Study Institute, Series C, 1984, 111, (ed. M.A.A. Ferreira), Reidel

2.52 D.K. Bohme, G.I. Mackay and S.D. Tanner, J.Am. Chem. Soc. (1979), **101**, 3724

2.53 B.G. Mackay and D.K. Bohme, J. Am. Chem. Soc., (1978), **100**, 327

2.54 D.K. Bohme, A.B. Rakshit and G.I. Mackay, J. Am. Chem. Soc. (1982), **104**, 1100

2.55 R.T. McIver and R. Dunbar, Int. J. Mass Spectrom. Ion Phys., (1971), **7**, 471

2.56 D. Smith and N.G. Adams, in "Gas Phase Ion Chemistry", 1979, vol.1, 2. (ed. M.T. Bowers), Academic Press

2.57 H.I. Schiff and D.K. Bõhme, Int. J. Mass Spectrom. Ion Phys. (1975), 16, 167

CHAPTER 3: INSTRUMENTATION AND EXPERIMENTAL TECHNIQUES

3.1. Instrumentation and Method

3.1.1. Description of the Source

The experiments were performed with a rebuilt MS 902 (A.E.I.) mass spectrometer to which a pulsed electron beam high pressure source was attached. This type of source was first developed by Kebarle[31] and it has provided a suitable technique for measurements of thermal equilibrium constants at high pressures, over a wide range of temperatures.

At Warwick[32] the source (figure 3.1) operates at pressures up to 6 Torr and in a temperature range of 300-770 K. In order to get such high pressures (conventional operating pressures EI≈10^{-4} to 10^{-5} Torr, CI≈0.1-1.0Torr) the reaction chamber (B) whose volume is 1 cm^3 is contained within a gold plated copper block where, the only openings are the electron entrance and the ion exit aperture (diameter≈25 μm). Copper is a suitable metal because of its high thermal conductivity. The gold plating prevents corrosion and reduces surface charging.

The apertures mentioned above were constructed from gold (Goodfellow Metals, purity 99.95%, light tight) and have several advantages over the previously used razor blades slits. They are easier to make, reduce surface charging and are readily replaceable The filament assembly (A) is attached to the source block and two plates (1 and 2) are inserted between the block and the filament.

A mesh grid (40 wires/cm, 81% transmission) is mounted equidistant (1 cm) from the source block and the beam centring plates (figure 3.1). This mesh acts both to reduce field penetration into the source and helps the pumping of gas away

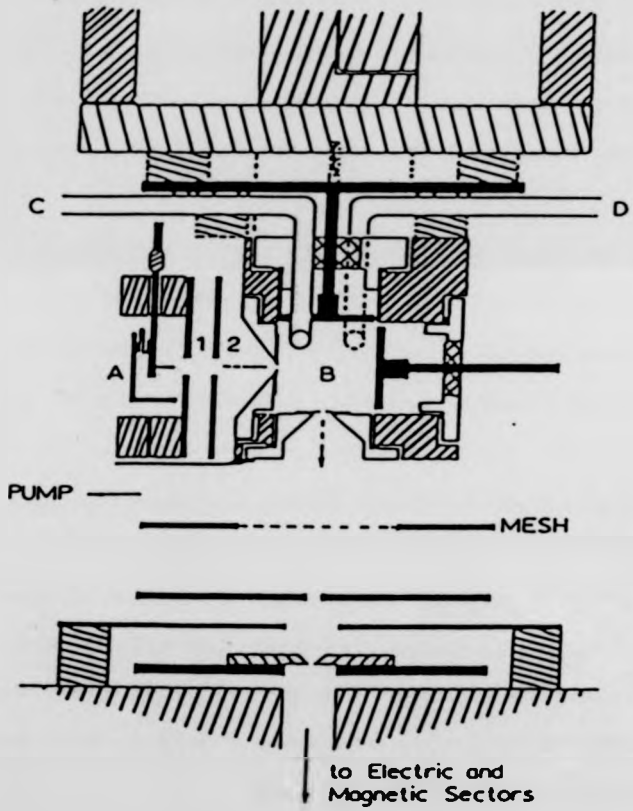

FIG. 3.1. Drawing of the pulsed high-pressure ion source.

from the ion exit aperture thus reducing collision induced decomposition (CID). This grid is maintained at <-100v with respect to the source block.

The source heating was provided by a heater, by a home built power supply and temperature control unit which associated with a platinum resistance temperature sensor controls the temperature. The heater is set into the back of the block and the platinum resistance sensor is embedded at one side of the block.

On the opposite side of the block a type K thermocouple is embedded and its leads are fed. unbroken through a hollow feedthrough in the source flange to a digital meter (Jenway 7500). This reading device gives an independent temperature measurement.

In order to perform measurements within the range 650-770 K, two additional heaters were attached to the source and connected to an extra power supply.

Cooling can be obtained within a limited range through a thick, flexible copper bellows which is in thermal contact with the source block via an electrically insulating disc.

The reactant gas mixture is introduced directly into the source through a port (C) sealed to a hollow electrical feed through in the source flange using "viton" "o" rings. In the same way the actual gas pressure in the source is measured directly, via a port (D) going to the pressure head of a capacitance manometer (MKS Baratrom type 220B). Gases entering the source come from a reservoir inlet through an automatic pressure control valve which keeps the pressure constant (Granville-Phillips series 216). Fast differential pumping is provided for the source housing by means of a 150 cm diffstack MK2 (Edwards M 160/700) via a 75cm port and 150cm diameter pumping elbow.

3.1.2. Operation of the Instrument

A schematic diagram of the instrument is shown in figure 3.2.

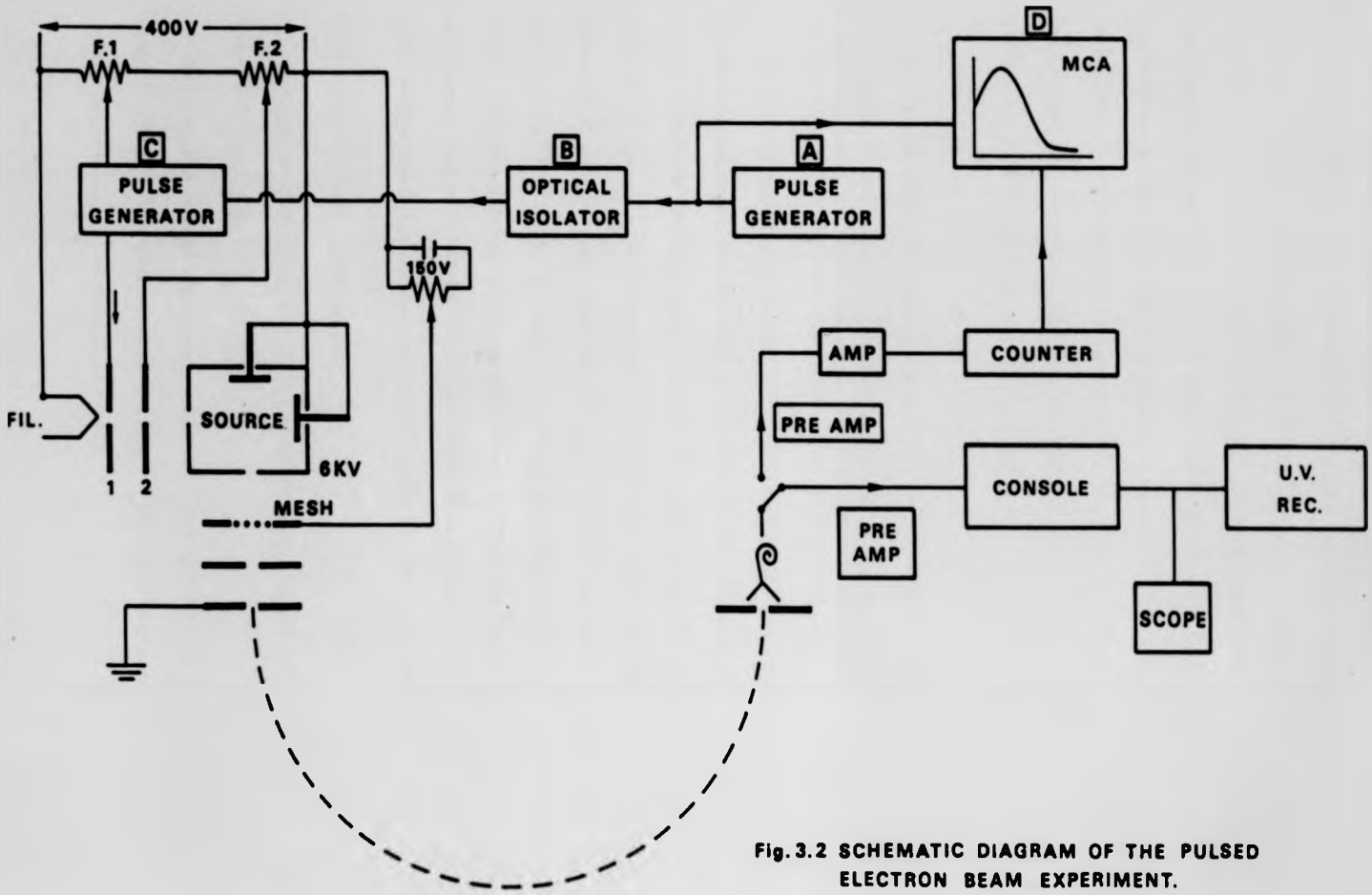

Fig. 3.2 SCHEMATIC DIAGRAM OF THE PULSED ELECTRON BEAM EXPERIMENT.

A pulse generator A (Thandar TG 105) transmits simultaneously a triggering pulse to a multi-channel-analyser D (EG & G ORTEC 7450) and via an optical isolator B (lab. made) to another pulse generator C (Farnell Pulse Generating System) which delivers a square wave pulse (+25v) to plate 1. This plate has superimposed d.c. potentials of -12.5v on pulsed mode and +12.5v on continuous mode, both with respect to filament. Continuous mode allows the standard chemical ionisation process to be performed. Plate 2 is held at +27.5v with respect to filament which is at −100v with respect to the source block.

The electron pulse duration is 10-50 μs.

Over this time ionisation takes place and as a consequence Ion Molecule Reactions (IMR) occur in the afterglow. These ions drifting out through the the ion exit slit are accelerated into the mass spectrometer for mass analysis.

Data acquisition is achieved in the pulsed mode by tunning the mass spectrometer to one particular ion whose intensity is followed as function of time for 5-10 ms after the electron pulse. The MCA, triggered by the same signal which switches on the electron beam, records and averages the time profile. Usually a minimum of 10,000 sweeps, approximately 2 minutes is necessary to obtain acceptable signals. The data are generally transferred to a microcomputer where they are treated, and the relevant information (K values) extracted. Smoothing of the data was usually accomplished by the MCA fitting a parabola to every group of five points within the displayed spectrum using a least-squares error criterion.

3.1.3. Inlet System and Samples

A diagram of the inlet system for gas handling and introduction to the source is shown in figure 3.3.

During experiments the temperature in the bulb and surroundings was maintained at 383 K . The whole system was kept at the same temperature and under vacuum when it was not in operation.

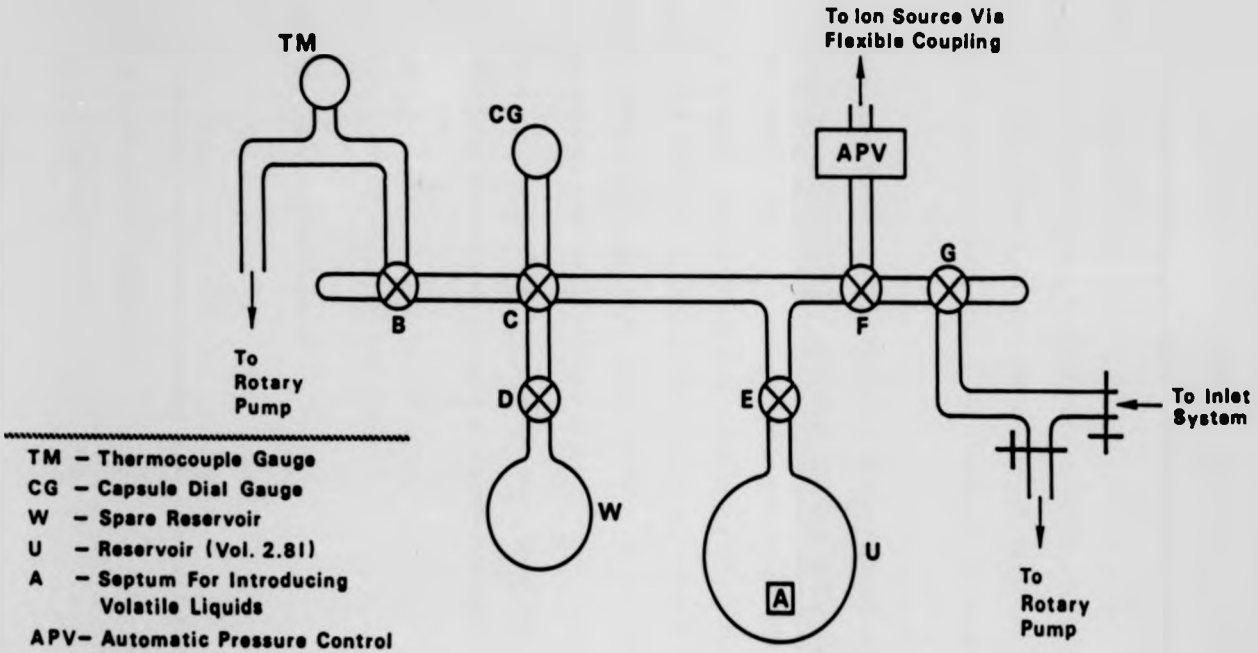

TM – Thermocouple Gauge
CG – Capsule Dial Gauge
W – Spare Reservoir
U – Reservoir (Vol. 2.8l)
A – Septum For Introducing Volatile Liquids
APV– Automatic Pressure Control Valve
B, C, D, E, F, G–Valves Or Taps

Fig. 3.3 INLET SYSTEM.

In order to feed a gas sample into the ion source the inlet system was first evacuated to below 0.05 Torr as measured by a thermocouple gauge (TM). The bulb was then filled with CH_4 (Matheson Gas Products 99.9% purity) up to 760 Torr as indicated by the capsule-dial gauge. Tap E was closed and the manifold was then evacuated to around 0.05 Torr.

The samples (2.5-50.0 µl) were injected into the bulb (2.8l) through a rubber septum and afterwards, with valve B closed, the sample and bath gas could expand inside the inlet system by opening valve E and then enter the ion source via valve F.

When the reactants were both liquids, mixtures from which the samples were extracted, were accurately prepared by weight using BDH chemicals 99%purity or Aldrich chemicals 97% purity. When the reactants were a gas and a liquid, the mixtures were directly prepared inside the bulb itself by injecting through A the adequate volumes of both chemicals to obtain the neutral concentration ratio required. SF_6 (BDH 99.9% pure) was used when necessary as an electron scavenger. The normal amounts added to the mixtures in the bulb were 7- 10 ml.

During the experiments the gas from the reservoir was maintained at a known constant pressure in the ion source by means of an automatic pressure control valve (APV).

Throughout this work valve D was always kept closed.

3.2. Conditions for Performing the Method

3.2.1. Method

In order to measure thermal equilibrium constants some experimental conditions are required which are not simply obtained.[33]

1) A temperature has to be defined.

This means that the system under study must be in thermal equilibrium with the surroundings.The product ions of Proton Transfer Reactions (PTR) are likely to have excess energy. Any excess energy can be lost by collision with a bath gas. This bath gas is present at concentrations greater than 100 times the concentration of the neutral proton transfer pair.

Considering simple collision theory at the pressures used in this work, approximately one hundred collisions are expected between reactant ion and the bath gas before the reactive collisions take place,[34] hence a Maxwell-Boltzman distribution of energy should be reached.

2) Sufficient time must be given for the system to reach equilibrium before measurement.

Since IMR are usually fast this requirement is not difficult to achieve. Equilibrium is commonly established in very short periods of time (1-3 ms). Both the above requirements are favoured by high pressures.

3) The equilibrium should not be disturbed by competing reactions.

Competing reactions and loss processes should not occur. The most commom are ion recombination, ion discharge to the walls, and proton bound dimer formation.

In order to minimise these effects one has to consider that :

a) Ion recombination is low at low charge densities.[35]

b) Ion discharge to the walls is slowed down by the bath gas.[35]

c) Proton bound dimer formation is disfavoured at high temperatures and/or low pressures because the formation occurs through third body reactions.[36]

Besides satisfying these main points the ion source has to be field free to avoid translational excitation of the reacting ions. One therefore has to pay attention to possible electric fields and space charge effects.

The pulse operating mode is particularly useful in avoiding high charge densities as would normally be obtained in continuous ionisation sources. At the same time the pulsed mode provides the facility of following the ion intensity versus time for each mass peak. To keep the source field free the ion-repeller is usually shorted to the block and magnets are not used to align the electron beam.

Having mentioned the basic requirements to perform the method it is obvious that the combination of high pressures and field free conditions in the source are essential to establish thermalisation.

All the above points must be taken into account when making measurements so it will be necessary to return to these criteria at later stages.

3.2.2. Surface Charging

A problem with surface charging was found at the beginning of this work. This has been previously discussed in the literature.[37,38] Theoretically ions travelling towards an orifice and passing through it could be considered as going through an orifice in an infinite conducting plate. It was shown[39] that the ions can be deflected to the walls before passing through the orifice because of the non uniformity of the field in the vicinity of the orifice, the mean free path of the ions and the thickness of the plate. This means a loss of charge if the walls are electrically conducting or an accumulation of charge if they are insulating. The last effect produces an attenuation in the transmitted current. Early in this work attenuation of the ion beam was observed while working in continuous mode and this was thought to be due to surface charge effects.

The problem apparently arises[3 10] from the formation of non-conducting or semi-conducting layers on the walls of the reactor. Once these layers build up on the ion exit slit they produce the insulation mentioned above and the ions are retained inside the reactor. This creats a large potential barrier which prevents thermal ions flowing through the orifice.

The application of a small positive potential to the ion-repeller pushes out the ions and restores the ion beam but under these conditions the source will not operate as field free.

Nevertheless a study was done to check the equilibrium constant dependence on the ion-repeller voltage, (figure 3.4). The test system was *para*fluorotoluene/ *ortho*chlorotoluene in methane. A voltage between 0 and 21v appears not to have any influence on the K values. This solution was not adopted because under non-charging conditions the ion-repeller voltage reduces the length of the diffusion zone (see section 3.2.3. figure 3.5).

The surface charging was finally solved by replacement of the previous razor blade slits with circular apertures (see section 3.1.1.).

As observed by other workers[3.8] plate thickness up to 25μm provided good operating conditions. Further improvement was obtained by coating the inside of the source block and plates with graphite (Aquadag, Acheson) and then baking the source at ≈523 K.

Under charging conditions the last part of the residence time profile, the free diffusion zone, becomes shorter. This shortening became an indicator of the need to clean the source and to replace the slits. The new apertures last for longer times and they lead to an improvement in mass resolution.

3.2.3. The Free Diffusion of Ions

Hiraoka and co-workers,[3.11] as well as Headley et al[3.12] recently studied the production and decay of ions in a plasma formed by EI. The study involved the use of a pulsed high pressure source mass spectrometer, the same technique used in this work.

The decay was followed after the ionising electron pulse was turned off. It was found that the decay was strongly dependent on the initial plasma density.

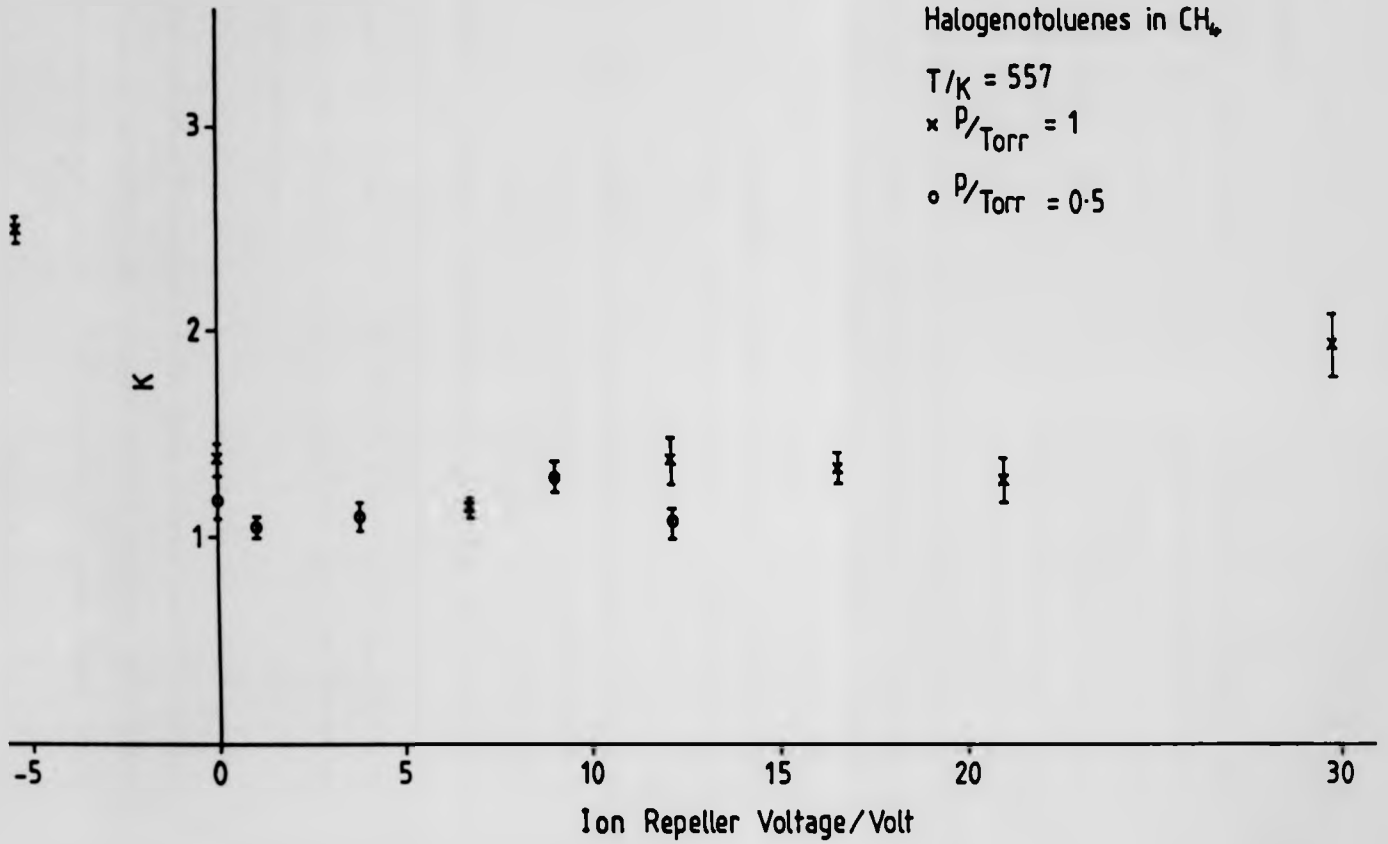

Fig.3·4 K vs. ION REPELLER VOLTAGE

The observation of IMR in the afterglow plasma is only possible if the loss of a given ion undergoing the reaction is much faster than its loss by diffusion or recombination.

Under high charge density conditions the ions do not diffuse freely towards the walls of the reactor. This is caused by fields due to the space charges.[3 9,3 13,3 14] Where charge densities are high the built up fields will retard the electron diffusion and simultaneously they will accelerate the positive ion diffusion. Over a certain period of time ions and electrons will move with a given average velocity towards the walls of the reaction chamber. This is called "ambipolar diffusion". At this stage the oppositely charged carriers, giving rise to the space charge field, show a small difference of densities compared to the density of each individual charge carrier. Under these conditions the plasma is called "quasi-neutral". Eventually a distance is reached where the electron charge density will be significantly different from the ion charge density, the quasi-neutrality is lost and the plasma under ambipolar conditions will collapse. When this distance is reached the electrons and ions will diffuse freely. During this free diffusion period charge densities are very low, the space charge will be small and its influence on the motion of the charged particles can be disregarded. When the plasma region is changed into free diffusion region, the electron-ion ambipolar diffusion is replaced either by negative-positive ion ambipolar diffusion (if negative ions are also present) or by positive free diffusion. This behaviour is visible in figure 3.5 where a typical pulsed profile is presented. Figure 3.6 shows the same peak in a logarithmic scale. The system toluene/dimethylether was chosen as an example; ion counts were plotted as a function of residence time.

The first section of the curve, A , corresponds to the formation of ions and it lasts for about 50μs. The section B is the region where the reaction is established and where the ions diffuse under ambipolar diffusion conditions. After approximately 1-2ms a change in the rate of the decay takes place when section C starts.

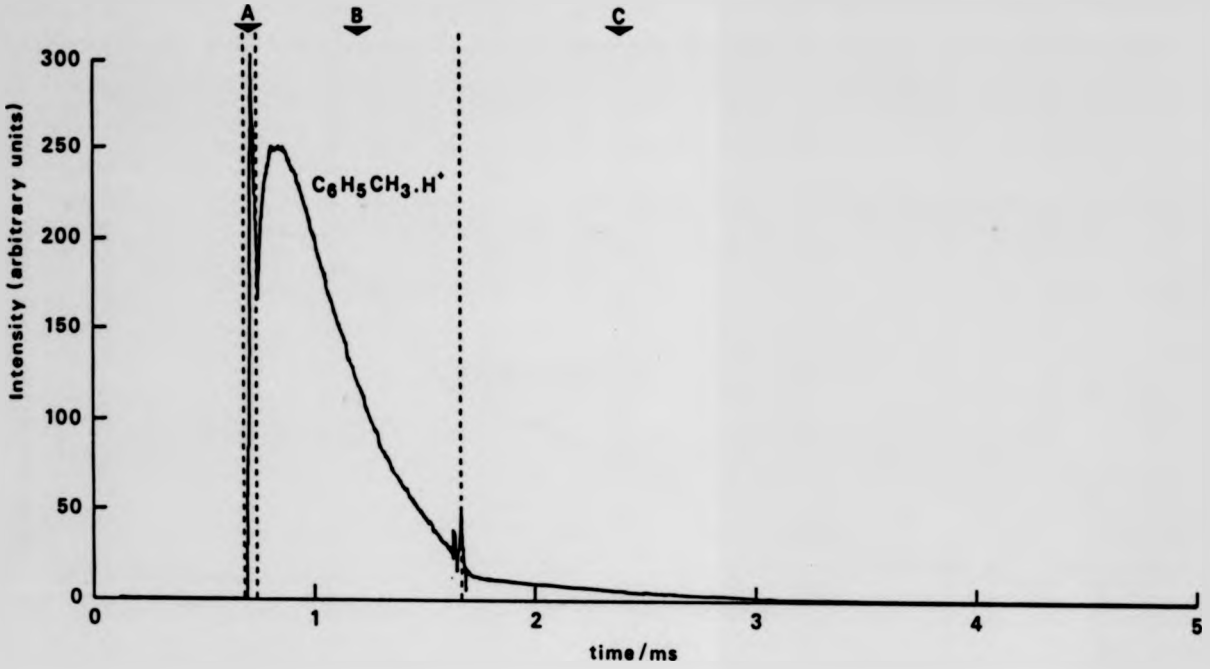

Fig. 3.5 PEAK PROFILE VERSUS RESIDENCE TIME.

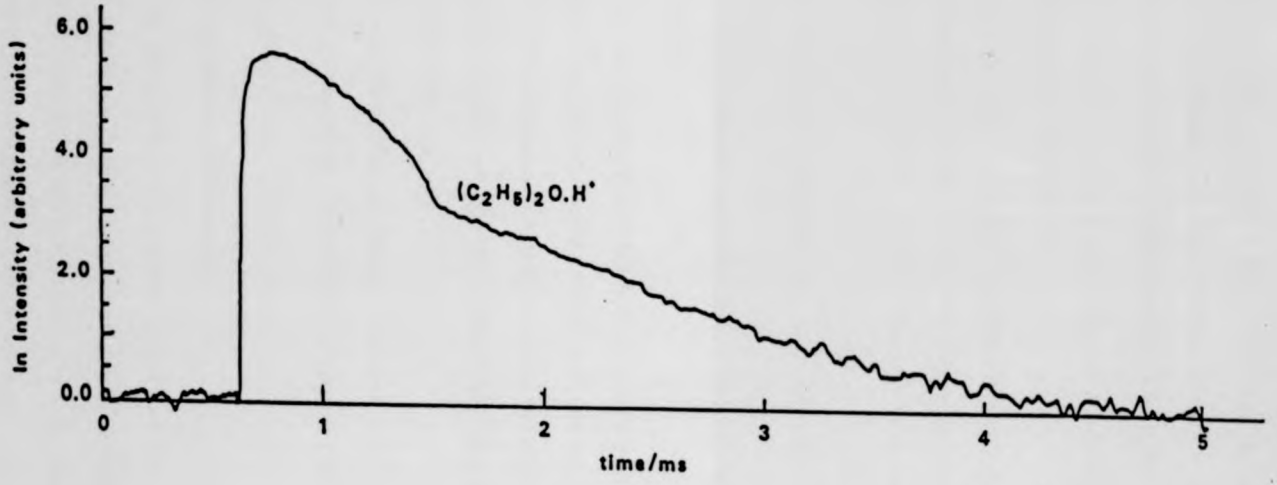

Fig.3.6 PEAK PROFILE VERSUS RESIDENCE TIME.

Then the decay of the ion intensity is slowed down over 3ms or more and it is there that equilibrium is established. The clear change observed is due to the conversion of ambipolar diffusion into free diffusion between regions B and C.

The ion current reaching the detector at the transition point between regions A and B was estimated[3 10] to be 1×10^5 ions/cm^3.

Under such conditions of charge density[3 10] the Debye length is of the same order of magnitude as the source dimensions (1 cm^3), hence at the point where zone C starts plasma conditions should not persist. Therefore it is hoped that the ion intensity decay in zone C may be due only to free positive diffusion to the walls of the reactor and to IMR. Consequently that was the region selected for taking data for measurements.

3.2.3.1 Electron Scavengers

Two well known electron scavengers[3 1] were tested to improve the shape of the decay curves. It was hoped to reduce the rate of positive ion diffusion by changing the positive ion-electron plasma to a negative-positive ion plasma. CCl_4 was found to undergo charge transfer reactions with the neutral species being studied so SF_6 was used in preference.

On changing from razor blade slits to circular apertures, the decay profiles were vastly improved and at this stage no electron scavengers were considered necessary.

3.2.4. Measurement of Equilibrium Constants

The first step was the preparation of a mixture of neutrals with a precisely known ratio of partial pressures which was diluted in a bath of methane in a proportion $<1\%$ (0.2%-0.01%). In spite of later attempts to use H_2 as reagent gas, as will be mentioned in the next paragraph, we chose methane to carry out this project.

Methane, the major gas (approx 99.95% of the mixture), is initially ionised by EI. Chemical ionisation (CI) occurs between ionised and neutral methane forming the stable CH_5^+ ion. This ion may then undergo proton transfer to neutral reagent gas. The total scheme is:[33]

$$CH_4 + e^- \rightarrow CH_4^+ + 2e^- \quad (3.1)$$

$$CH_4^+ + CH_4 \rightarrow CH_5^+ + CH_3 \quad (3.2)$$

$$CH_5^+ + \frac{A}{B} \rightarrow CH_4 + \frac{AH^+}{BH^+} \quad (3.3)$$

$$AH^+ + B \rightleftharpoons A + BH^+ \quad (3.4)$$

Step (3.2) is crucial. It is very rapid and CH_5^+ does not react further with CH_4. However CH_5^+ will transfer its proton very rapidly to any other species having a higher Proton Affinity ($-\Delta H > 30$ kJ/mol). Process (3.4) will reach equilibrium quickly if the pairs are chosen such that their PAs are close ($\Delta PA < 13$ kJ/mol).

In order to make the actual measurements the mass spectrometer was focussed on one of the two ions of interest. The averaged intensity profile of this ion was recorded as a function of time as in figure 3.7 until decay caused by diffusion to the walls of the source was complete as discussed fully in 3.2.3. The profile of the second ion was collected in the same way. Ions were followed over a period of 10ms.

Pressure and temperature were kept constant during the experiment.

A ratio of ion intensities was calculated as function of time and the equilibrium was considered reached when the ratio was constant, usually within 1 to 3 ms, (see figure 3.8).

K_T° could be determined for reaction (3.4) by the following expression

$$K = \frac{[A]}{[B]} \times \frac{[BH^+]}{[AH^+]} \quad (3.5)$$

$\frac{[A]}{[B]}$ = neutral concentration ratio

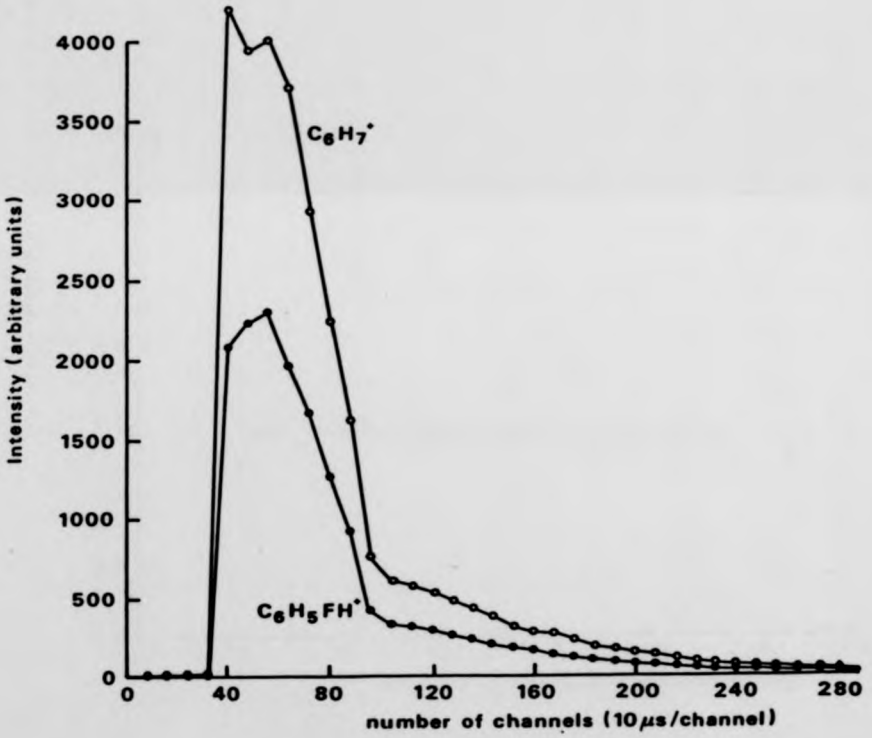

Fig. 3.7 PROFILES OF ION INTENSITIES vs NUMBER OF CHANNELS.

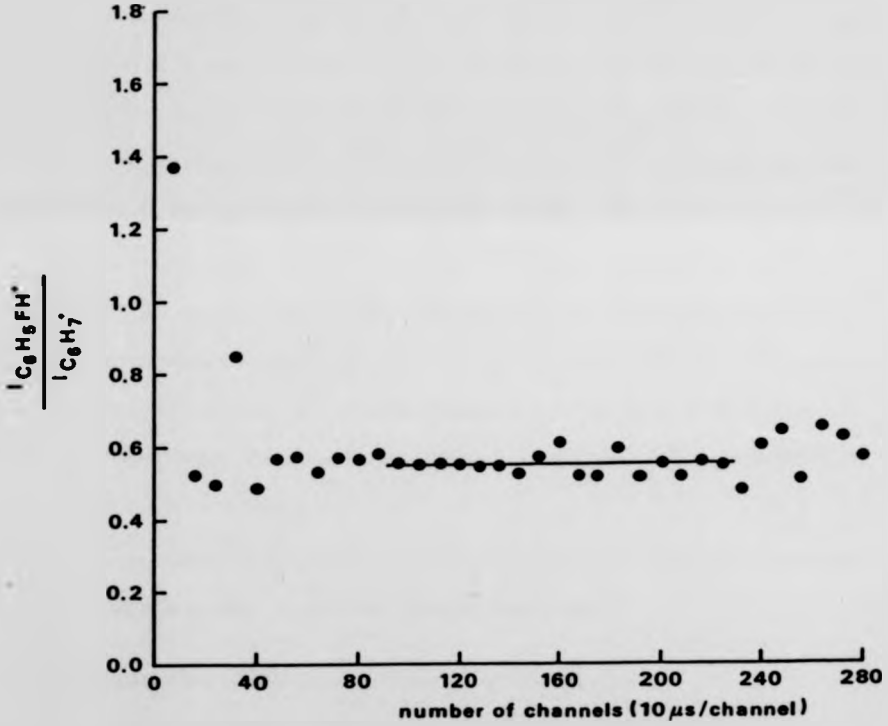

Fig. 3.8 RATIO OF INTENSITIES OF IONS IN REACTION
$C_6H_7^+ + C_6H_5F \rightleftharpoons C_6H_8 + C_6H_5FH^+$
VERSUS NUMBER OF CHANNELS.

$\frac{[BH^+]}{[AH^+]}$ = equilibrium ion intensity ratio

in which the ion intensities were observed for only one isotopic mass. Corrections were made for natural isotopic abundance and for the number of sweeps over which the signals were averaged if they were different.

The time of flight between the source and the detector are different for ions of different mass. Thus another correction had to be introduced into the measurement. Xylenes-Dimethylether systems show ion masses of interest as 107$^+$ ($CH_3C_6H_4CH_3H^+$) and 47$^+$ ($(CH_3)_2O.H^+$). By considering the geometry of the instrument the time of flight for mass 107 is 19.4μs and for mass 47 12.8μs. In order to compare the intensities at correspondent reaction time the intensity/time profile of the former ion requires a shift of 6.6μs to longer times.

The measurements described lead to the calculation of the standard free energy, $\Delta G°$, for the reaction of interest. Furthermore the measurements of K with temperature dependence lead to the construction of a van't Hoff plot. From such a plot the standard enthalpy and entropy changes can be determined from slope and intercept respectively. These plots and thermodynamic data will be presented in more detail in the next chapter.

It was necessary to check the consistency of the results and various methods were used, as will be described in the following section (3.3.).

3.3. Determination of Optimum Operating Conditions

3.3.1. Testing the Method

In order to rely on the method one has to check if one is really measuring an equilibrium constant and at the same time look for consistency of data. Various methods and parameters are available to test this.

Provided that temperature is kept constant:

1) Over a range of total pressure K should remain constant.

2) For different concentration ratios of neutrals K should stay constant.

3) Varying the partial pressure of the neutrals but keeping the same concentration ratio of neutrals. K should be unchanged.

Finally the best test for reproducibility is the internal self-consistency of the enthalpy and entropy ladders discussed in the following chapter. The ladders are built from state functions so whichever chemical route is chosen from one given initial state to one given final state the values obtained should be the same and in fact they are very close.

One particular system, *para*fluorotoluene-*ortho*chlorotoluene, was used to take measurements varying the parameters mentioned above. The reaction taking place was the following

$$1,4\text{-}FC_6H_4CH_3H^+ + 1,2\text{-}ClC_6H_4CH_3 \rightleftharpoons 1,4\text{-}FC_6H_4CH_3 + 1,2\text{-}ClC_6H_4CH_3H^+ \quad (3.6)$$

$1,4\text{-}FC_6H_4CH_3.H^+ m/z=111$

$1,2\text{-}ClC_6H_4CH_3.H^+ m/z=127$

3.3.1.1. Total Pressure

The measurements were done with mixtures of halogenotolunes whose neutral concentration ratios were accurately known.

Methane was used as a reagent gas, usually at 745 Torr, samples of halogenotolunes were in the range 5μl–25μl and 7-9 ml of SF_6 was sometimes added as an electron scavenger.

The constancy of K was checked as a function of the total pressure inside the reactor. The measurements were taken at various temperatures with parameter 3) (section 3.3.1) held constant.

The results of some experiments are shown in figures 3.9, 3.10, and 3.11. Although the reproducibility appears to be reasonable in most cases, at low temperatures the spread is always larger.

n.c.r. = 2·7

Partial Pressure
of Halogenotoluenes = 0·23 Torr

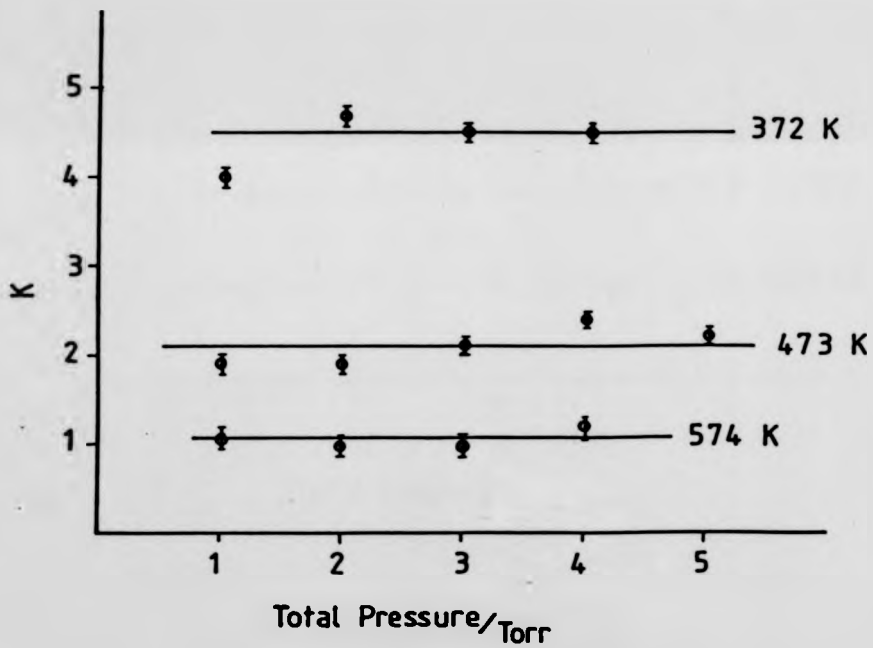

Fig. 3·9 K vs. TOTAL PRESSURE

n.c.r. = 2·7

Partial Pressure
of Halogenotoluenes = 0·9 Torr

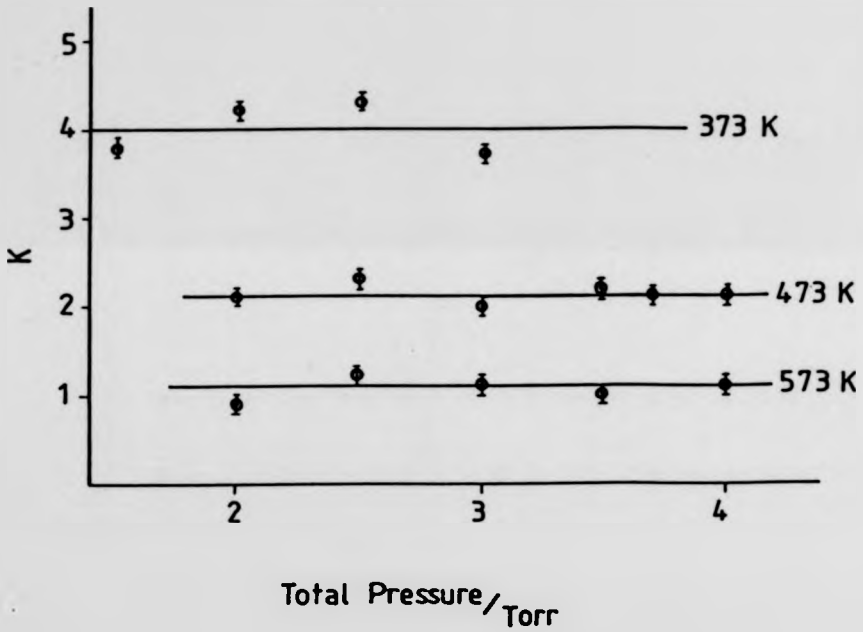

Fig. 3·10 K vs. TOTAL PRESSURE

n.c.r. = 1·0

Partial Pressure
of Halogenotoluenes = 0·45 Torr

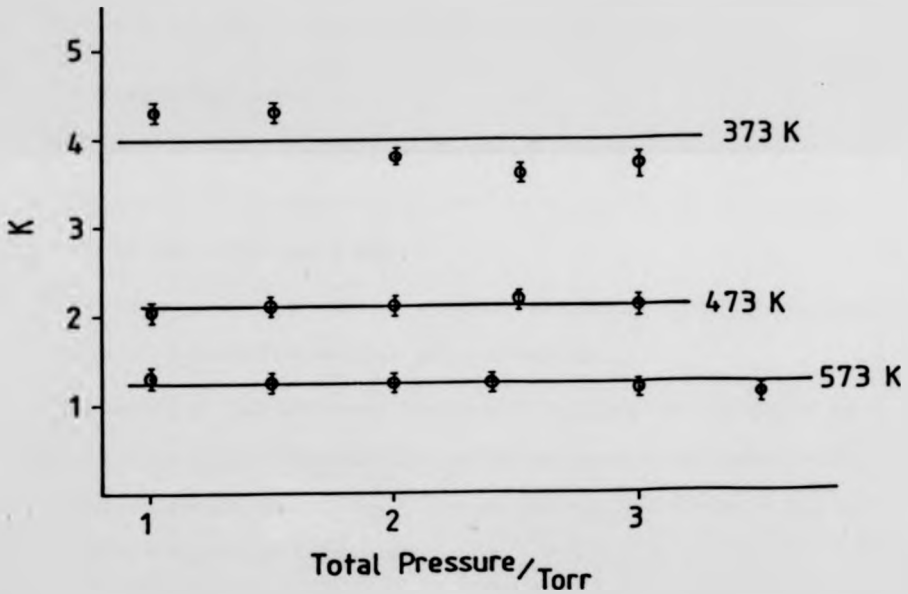

Fig. 3·11 K vs. TOTAL PRESSURE

3.3.1.2. Neutral Concentration Ratio

The second parameter being varied was the concentration ratio of the neutrals (ncr). Two different ratios were tried, 1.0 and 2.7.

Irrespective of which ratio was used, at each temperature the values of K remained constant within experimental error ($\pm 10\%$ in the least favourable cases). In figure 3.12, K as a function of pressure is shown for the two different concentration ratios taken at the same temperature. These figures confirm that K is constant over the pressure range studied. In general for each system examined such measurements were taken with various concentration ratio of neutrals.

3.3.1.3. Partial Pressures.

The third parameter examined was the partial pressure of the neutrals.

The pressures of the halogenotolunes mixtures injected in the bath gas were 0.2 Torr, 0.4 Torr. 1 Torr and 2 Torr.

For each partial pressure the ncr was kept constant and the study was done with temperature dependence and total pressure variation.

A summary of data is presented in figure 3.13. Again the variation of the parameter points to good reproducibility within the experimental error ($\pm 10\%$) and clearly the partial pressure of 0.2 Torr provides the least scatter of data so this would be used in future experiments.

3.3.1.4 The protonating Agents

The first bath/reagent gas used was methane. It was thought that competing reactions between the neutral protonating agent and reactant ions may be occurring viz:

$$FC_6H_4CH_3H^+ + CH_4 \rightarrow CH_3C_6H_4CH_3H^+ + HF \qquad (3.7)$$

CH_4 was subsequentially diluted by the neutral gas Ar.

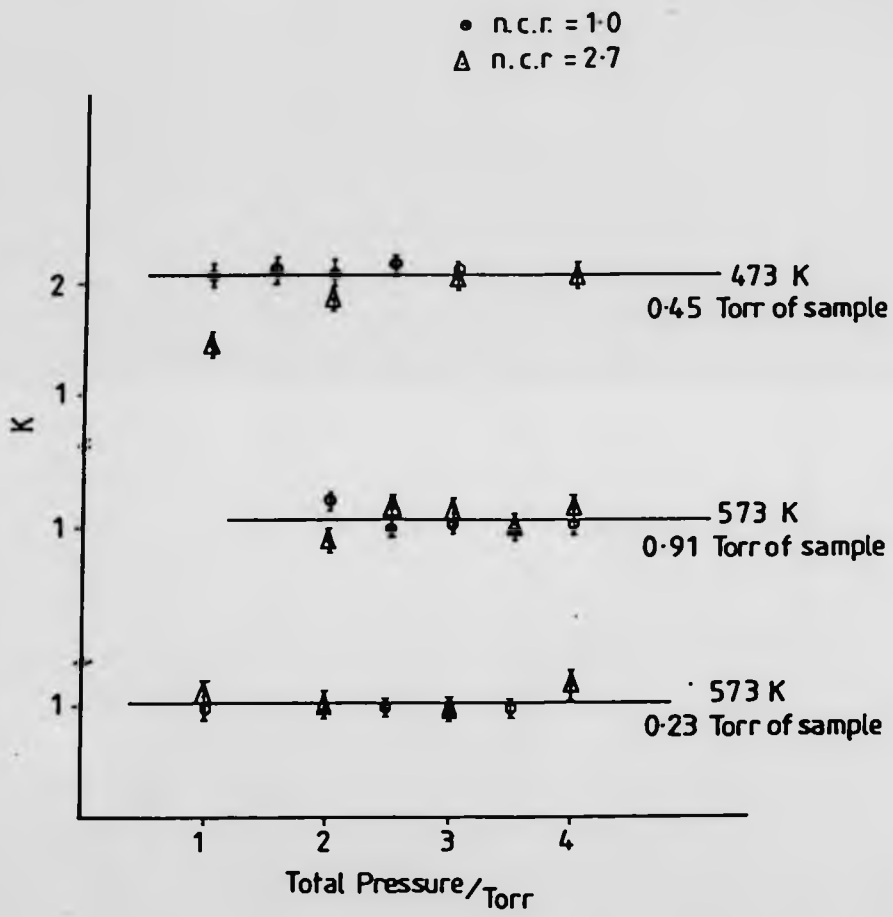

Fig. 3·12 K vs. TOTAL PRESSURE AT DIFFERENT n.c.r.

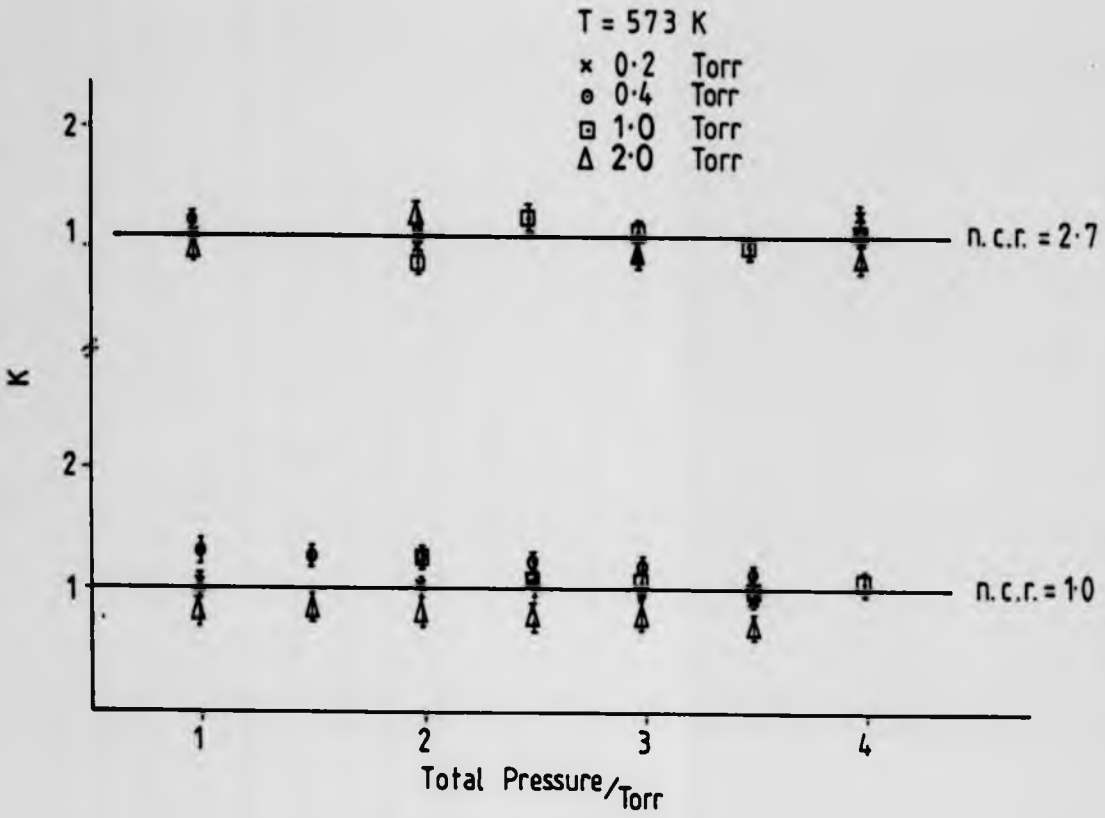

Fig.3·13 K vs. TOTAL PRESSURE FOR DIFFERENT PARTIAL PRESSURES (SAME N.C.R.)

In actual fact the mass peak $107^+(CH_3C_6H_4CH_3.H^+)$ was found (50%-70% intensity of the molecular peak) and a series of different dilutions were attempted. The best compromise of relative intensities between the mass peaks of interest was obtained with $CH_4/Ar=1/5$. Under these conditions the 107^+ peak intensity decreased to 10% of the intensity of the base peak, leaving both peaks of interest with reasonable intensities.

It was later discovered[3 15], that the actual reaction taking place was

$$XC_6H_4CH_3 + RH_2^+ \rightarrow RC_6H_4CH_3H^+ + HX \qquad (3.8)$$

X = F, Cl

$R=H \rightarrow RC_6H_4CH_3H^+.m/z=93^+$

$R=CH_3 \rightarrow RC_6H_4CH_3H^+.m/z=107^+$

which was more recently confirmed by ICR studies[3 16]. It was established that CH_5^+ ion is the precursor of the ion $m/z=107^+$. Accepting this experimental evidence for the origin of 107^+ ion, it was considered no longer necessary to dilute the bath gas with Ar, hence improving the signal of product ions.

In order to increase the reliability of the data another protonating agent was chosen, H_2. In systems with H_2, Ar was also used to dilute the reagent gas and help to achieve thermalisation because lighter collision gases were found to be less efficient as a third body.[3 4] Some of the results measured for systems with H_2 are shown in figure 3.14. At 572 K the agreement between the two concentration ratios is good and they also agree quite well with previously data measured. At 473 K the agreement between K values for the two different ncr is not so good but still within 20% experimental scatter. However the K values measured in H_2 at 473 K clearly dropped about 25% when compared with the ones measured in CH_4. This may be attributed to a higher degree of fragmentation in Cl with H_2 as a result of the greater difference in proton affinities between H_2 and the compounds under study. As a consequence more competing reactions are likely to occur under

Bath gas $\frac{H_2}{Ar} = \frac{1}{5}$

× n.c.r. = 1·0

° n.c.r. = 2·7

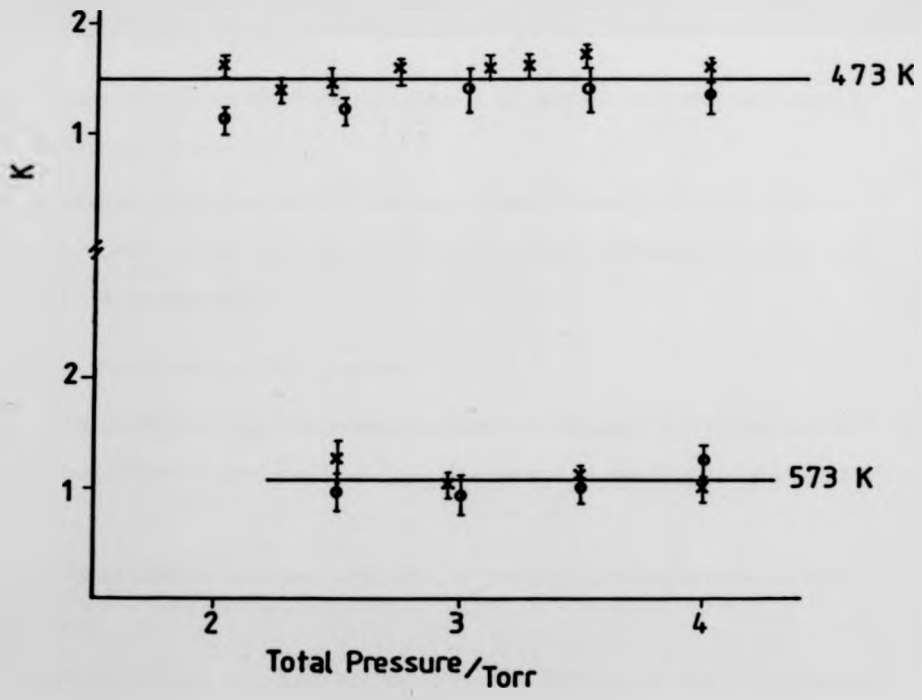

Fig. 3·14 K vs. TOTAL PRESSURE

protonation in H_2.

In chapter 4 some experimental evidence of this will be given.

3.3.1.5 Best Experimental Conditions for Performing the Method

Looking at the experimental parameters being changed one can conclude that:

1) From K versus total pressure, a higher spread in K values is visible at low temperatures (figure 3.9, 3.10, 3.11)

2) From K versus partial pressure of neutrals, again a higher spread in K values is noticeable at low temperatures and high partial pressures of neutrals (figure 3.15). In figure 3.15, K drops clearly at 2 Torr. Partial pressures above 1 Torr are not advisable.

3) From the plot of K versus ncr (figure 3.16) again is seen that low temperatures are the problem.

Thus the experimental conditions seem to be optimised by working with temperatures above 373K, with the lowest possible partial pressure of neutrals and having CH_4 as reagent gas.

3.3.1.6 Purification of Compounds

Besides varying the experimental parameters mentioned in this chapter, consideration of the effect of impurities was another way of checking the consistency of data.

Figure 4.16 shows a van't Hoff plot for the proton transfer in the following reaction:

$$1,2\text{-}ClC_6H_4CH_3H^+ + 1,3\text{-}FC_6H_4CH_3 \rightarrow 1,2\text{-}ClC_6H_4CH_3 + 1,3\text{-}FC_6H_4CH_3H \quad (3.9)$$

Three different concentration ratios were used:

$$[1,2\text{-}ClC_6H_4CH_3]/[1,3\text{-}FC_6H_4CH_3]=2$$

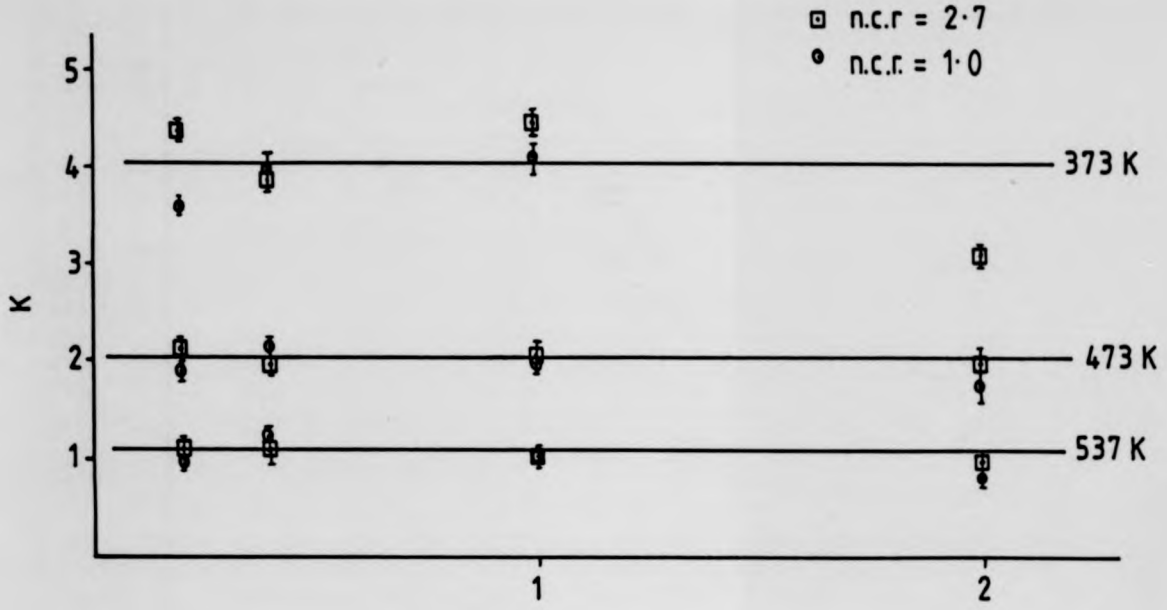

Fig. 3·15 PARTIAL PRESSURE OF NEUTRALS / TORR

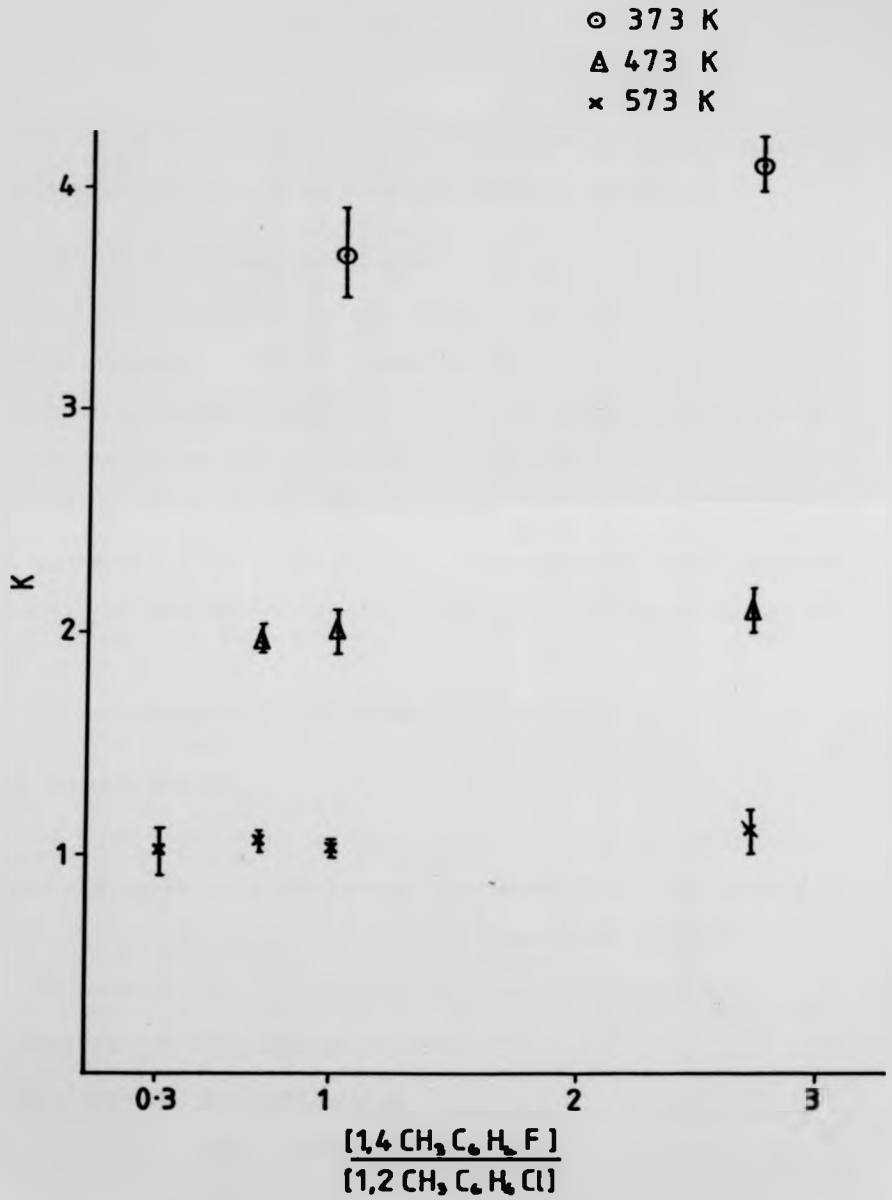

Fig. 3·16 K vs. RATIO OF CONCENTRATION OF NEUTRALS

$[1,2\text{-}ClC_6H_4CH_3]/[1.3\text{-}FC_6H_4CH_3]=50$

$[1,2\text{-}ClC_6H_4CH_3]/[1.3\text{-}FC_6H_4CH_3]=2.7$

The latter was prepared from purified compounds by gas-liquid cromatography.

On the whole all points coming from different ner show the same general trend therefore no further purification was considered necessary.

3.3.2 On Testing the Instrumentation

The consistent operation of the equipment was tested by measuring the equilibrium constant at various temperatures of the proton transfer reaction between benzene and fluorobenzene. This system had already been studied in this and other laboratories. In the former case the same technique but different equipment and in the latter case using other techniques.

Agreement had been found previously. In the particular case of this work agreement with previous data was also achieved within the limits of experimental error.

This test confirmed that the instrumentation and method are reliable.

3.3.3 Sources of Error

The signal collected and its time dependence followed through the Multi-Channel Analyser (M.C.A.) must represent how the ion concentration varies as a function of time in the reactor otherwise the measurement will not be valid.

The possible interference of some sources of error will be considered.

1) Discrimination of Ions Through the Ion Exit Slit.

2) Mass Discrimination at the Detector.

1) The Knudsen numbers defined as the ratio of the mean free path of a molecule to a specific dimension of the channel are useful to classify the type of gas flow in systems under vacuum[3 17].

When the mean free path (L) is small compared with the characteristic dimension of the channel (r) intermolecular collisions prevail over collisions of the molecules with the walls. This is called viscous flow and in these conditions the Knudsen number is given by $L/r<0.01$. The viscous flow rate is expressed by the equation:

$$F=\frac{\pi r^4}{8\eta l}P_a(P_2-P_1) \qquad (3.10)$$

r - tube radius
η - viscosity of the gas
P_a - arithmetic mean of P_1 and P_2
l - tube length
P_2 and P_1 - pressures at both sides of the ion-exit slit.

Under conditions where $L/r>1.00$ the flow is known as molecular and because L is large compared with r the molecules act as if they were independent of one another. In this situation the collisions of the ions with the walls predominate.

The molecular flow rate is given by

$$F=\frac{1}{4}v_aA(P_2-P_1) \qquad (3.11)$$

v_a - mean molecular speed

A - area of the orifice

The gas flow is said to be in the intermediate range where

$$0.01<L/r<1.00 \qquad (3.12)$$

Under the current conditions of this work the gas flow was in the intermediate range. Calculated values of L/r are for methane at 473K and pressure 4Torr $L/r=0.16$ and at 573K and 2Torr $L/r=0.36$.

The viscous flow is considered to be independent of the mass so discrimination on ion sampling is not expected under this flow. On the other hand the molecular flow depends upon the inverse of the square root of the mass. Therefore in the intermediate range some discrimination might be expected but it must be

diminutive since the compounds of interest are highly diluted with methane.

2) Mass Discrimination

Mass discrimination was not found[3 18] in plots of the average response of the detector vs. m/z in a mass range 18 to 127. The detected charge stayed constant within 10%.

Other possible errors affecting the results were also checked such as:

A) Temperature Measurement

During experiments the temperature remained constant at the preset level within ± 2 deg. Some differential heating of the source block was sought and it was found[3 18] that it was never above 2 deg.

Taking into account the pressure range under which the work was performed it is reasonable to assume that the reaction chamber and the source block are at the same temperature.

B) Pressure Measurement

The reading and controlling assembly, composed by automatic pressure control valve and "MKS" Baratrom Capacitance barometer gave pressure readings whose accuracy was ±0.02 Torr in the pressure range used throughout this work.

These two contributions seem negligible compared with the experimental scatter.

C) Multichannel Analyser

In order to test if the MCA could in any way alter the signal, the same mass peak was considered twice to calculate a ratio of intensities. The answer was always found to be in the range 1.00-1.05. No artifact had been therefore introduced by the MCA.

D) The Experimental Scatter

The maximum order of magnitude of the scatter was usually ±20%. The

scatter is likely to be caused by unsteadiness in the focusing of very low intensity ion beams through the mass spectrometer, due to charging on the slits and slight drift of the focusing potentials.

Further noise could arise from variations in the intensity of the ionising electron pulse which would induce slight changes on the time of onset of the free diffusion zone.

The onset was consequently thoroughly verified over most of the experiments. For the same pair of ions undergoing the the same experiment the onsets were always coincident. Hence the latter source of unstability is unlikely to influence the results.

E) Contributions of Error to ΔH° and ΔS°.

The errors in K measurements introduced by possible mass discrimination and ion sampling discrimination will reflect on ΔH° and ΔS° determinations.

The calculation of K is based on equation

$$\frac{[XH^+]}{[YH^+]} = \frac{I_{(XH^+)}}{I_{(YH^+)}} \times \pi_i \qquad (3.13)$$

π_i - error factor i

The mass discrimination at the detector is expected to be negligible and the discriminatory ion sampling, if any is present, must be accounted by the square root of the mass ratio of XH^+ and YH^+. The worst case (where largest mass difference was found) are the xylenes-dimethylether systems. The error factor is $\sqrt{2.28}$. How this error factor will affect ΔH° and ΔS° is shown below

$$\ln(K^\circ_{real}) = \ln(K^\circ_{obs}) + \ln(\pi_i) \qquad (3.14)$$

$$\ln(K^\circ_{real}) = \ln(K^\circ_{obs}) + \ln 1.51 \qquad (3.15)$$

$$\ln(K^\circ_{real}) = -\frac{\Delta H^\circ}{RT} + \frac{\Delta S^\circ}{R} + 0.41 \qquad (3.16)$$

A plot of $\ln K^\circ_{real}$ versus $1/T$ must not show any error effect on slope ($\Delta H^\circ_{obs} = \Delta H^\circ$) but the intercept must carry the whole error factor added.

Nevertheless even in this most unfavourable case the error factor stays within the maximum scatter of the 20% for ln K in the range 4.99-2.32.

As a general conclusion one can say that when all sources of error are considered, the main contribution comes from the scatter. The errors quoted in the tables in the next chapter are standard deviations assuming significant errors only in the K recorded.

After checking the reliability of the results varying different parameters plus the self-consistency shown in ladders (figures 4.19 and 4.20) of values of $\Delta H°$ and $\Delta S°$ measured for different systems. one can confidently state that the data are reliable.

3.4 References

3.1 P. Kebarle in "Interactions between Ions and Molecules", Nato Advanced Institute, 1955, 459. ed. P. Ausloos. Plenum Press

3.2 D.K. Bðhme, J.A. Stone, R.S. Mason. R.S. Stradling and K.R.Jennings, Inst. J. Mass Spectrom. Ion Phys., (1981), 27, 283.

3.3 R.S. Mason in "Thermochemistry and its Applications to Chemical and Biochemical Systems", Nato Advanced Study Institute. 1982, 627, ed. Ribeiro da Silva.

3.4 a) M. Meot-Ner in "Gas Phase Ion Chemistry", (1979), vol. 1, 201, ed. M. Bowers, Academic Press.

b) A.G. Harrison in "Interactions between Ions and Molecules"*, (1975), 263. ed. P. Ausloos, Plenum Press.

3.5 P Kebarle, Ann. Rev. Phys. Chem., 1977, 28. 445.

3.6 W.R. Davidson, M.T.Bowers. T.Su and D.H.Aue, Int. J. Mass Spectrom. Ion Phys., 1977, 24, 83.

3.7 W.C. Lineberger, L.J. Puckett, Phys. Rev., (1969), 187, 116.

3.8 E.E. Ferguson. F.C.Fehsenfeld and A.L.Schmeltekopt. Adv. At. Mol. Phys., (1969), 5, 1

3.9 D. Smith and I.C. Plumb, J.Phys.D: Appl. Phys., (1973). 6. 1131.

3.10 J.V. Headley. Thesis. 1981.

3.11 K. Hiraoka. K. Morise and T. Shoda. Int. J. Mass Spectrom. Ion. Proc., (1985), 67. 11.

3.12 J.V. Headley. R.S.Mason and K.R. Jennings, J. Chem. Soc. Faraday Trans. I, 1982, 78. 993.

3.13 H.J. Oskam. Philips Res. Repts. (1958). 13. 335.

3.14 D. Smith. A.G. Dean and N.G. Adams. J. Phys. D: Appl. Phys., (1974), 7, 1944.

3.15 H.W. Leungaud and A. Harrison. Can. J. Chem., 1976. 54, 3439.

3.16 R.S. Mason. D.K. Böhme and K.R. Jennings, J. Chem. Soc., Faraday Trans. I. (1982), 78, 1943.

3.17 S. Dushman and J.M. Lafferty, "Scientific Foundations of Vacuum Technique", 1962. J Wiley and sons.

3.18 R. Gallagher. Thesis. in preparation.

CHAPTER 4: THERMOCHEMISTRY OF GAS PHASE PROTON TRANSFER REACTIONS IN HALOGENO-TOLUENE MIXTURES

4.1 Introduction

The data obtained for Proton Transfer Equilibria in halogenotoluene mixtures will be presented in this chapter.

Equilibrium constants were measured for proton transfer reactions of the type (4.1) as a function of temperature.

$$CH_3C_6H_4XH^+ + CH_3C_6H_4Y \rightleftharpoons CH_3C_6H_4X + CH_3C_6H_4Y.H^+ \qquad (4.1)$$

where X,Y = Cl or F

van't Hoff plots were produced from these experimental data using the standard equation

$$\ln K = -\frac{\Delta H^\circ}{RT} + \frac{\Delta S^\circ}{R} \qquad (4.2)$$

The standard enthalpy change and entropy change of reactions (4.1) were determined from the slope and intercept of the van't Hoff plots respectively.

The results will be discussed as a whole and comparisons with other workers' results reported in the literature will be made wherever possible.

4.2 The Conventional Chemical Ionisation Spectra

The first step in this study was always the recording of normal C.I. spectra run under continuous mode conditions (see Section 3.1.2).

For seven systems of the type of reaction (4.1) these spectra were very similar, as the components of the systems were isomers. The only difference between them is the change in the position of the halogen substituent in ortho, meta or

Fig. 4·1 CI, HIGH PRESSURE SPECTRUM OF 0·025% OF 1,4 $CH_3C_6H_4F$ IN CH_4 AT 1 TORR, 551 K

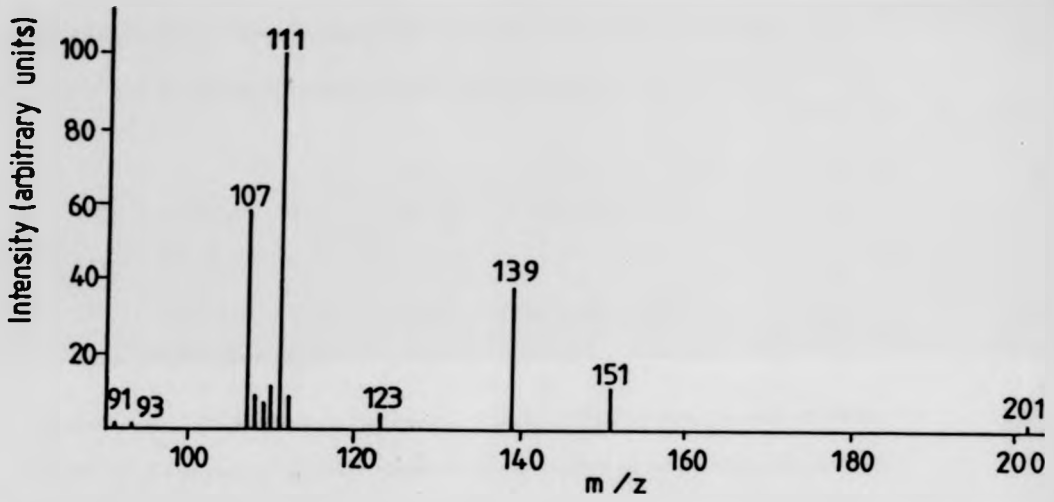

Fig. 4·2 CI, HIGH PRESSURE SPECTRUM OF 0·025% OF 1,2 $CH_3C_6H_4Cl$ IN CH_4 AT 1 TORR, 551 K

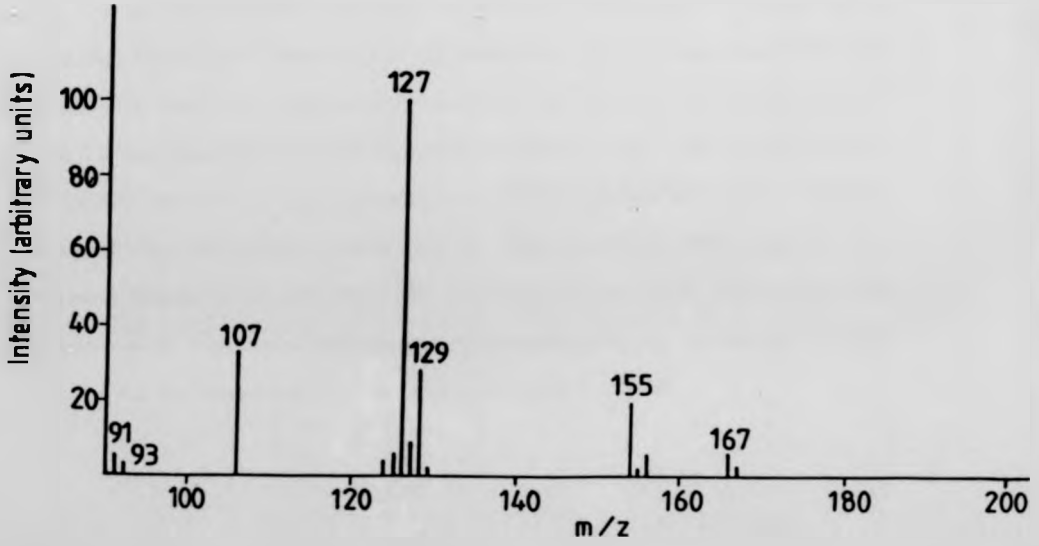

para position.

Two spectra are shown in figure 4.1 for *para*fluorotoluene and figure 4.2 for *ortho*chlorotoluene. Agreement was found between the base peaks displayed in these spectra and those reported by Harrison et al.[41] The m/z = 123 peak in figure 4.1 probably arises from the ion of m/z = 139 by loss of methane.

Main peaks in this work and Harrison[41]

m/z	Ions	m/z	Adduct Ions
107	$CH_3C_6H_4.CH_3.H^+$	139,155	$XC_6H_4CH_3C_2H_5^-$
111	$FC_6H_4.CH_3H^+$		
127	$Cl^{35}C_6H_4CH_3.H^+$	151,167	$XC_6H_4CH_3.C_3H_5^-$
129	$Cl^{37}C_6H_4CH_3.H^+$		

The only minor discrepancy is for peak 91 ($C_7H_7^-$). In this study it has an intensity of 1% of the base peak (111) intensity in the case of *para*fluorotoluene and 5% of the base peak (127) intensity in the *ortho*chlorotoluene spectrum. M/z = 93 is another tiny peak (1-3% of base peaks) probably protonated toluene. Harrison[41] found that the maximum intensity in *para*fluorotoluene spectra for 91 ($C_7H_7^+$) was 2% - 4% of the base peak. The m/z = 93 is not reported.

All the other relative intensities are similar in both studies. In all the spectra recorded, the relative intensities of the peaks were in good agreement with those reported by Harrison. Further confirmation of the pattern displayed in figure 4.1 and 4.2 was obtained from previous work by Mason et al.[42] Any slight difference in relative intensities can be ascribed to the differences in experimental conditions. Harrison and co-workers carried out the experiments at 423K and 0.5 Torr whereas Mason et al performed the measurements at 369K and 1 Torr. The present study was carried out under varying conditions, and in the case of figure 4.1 and 4.2 the pressure was 1 Torr and temperature = 551K.

In addition to the halogenotoluenes and the reagent gas CH_4, SF_6 was also present as an electron scavanger. This compound contributes to the intensity of 127^+ peak through SF_5^+.

Figures 4.3, 4.4, 4.5 show some spectra of different mixtures of halogenotoluenes run under different experimental conditions of pressure and temperature. In these spectra the intensities of the 91 and 93 mass peaks were always below 1% of the base peak.

In figure 4.3 one peak at $m/z = 117$ is attributed to a proton bound dimer of acetone $[(CH_3)_2CO]_2.H^+$. Acetone was sometimes found as an impurity peak at $m/z = 59^+$, $(CH_3)_2CO.H^+$.

Despite good agreement with the literature, further experiments were carried out to check for other possible competing reactions, using CH_4 and H_2 as reagent gases.

4.3 The Competing Reactions

Thermodynamic data can be derived from equilibrium measurements only if true equilibrium is established and interfering side-reactions are minimised. The work of Harrison et al, using CH_4 and H_2 as reagent gases was therefore repeated using reaction (4.3) as the test system.

$$1,4\text{-}FC_6H_4CH_3.H^+ + 1,2\text{-}ClC_6H_4CH_3 \rightleftharpoons 1,4\text{-}FC_6H_4CH_3 + 1,2\text{-}ClC_6H_4CH_3.H^+ \quad (4.3)$$

Fragmentation of the primary ions by loss of HX yields $C_7H_7^+$ ions, $m/z = 91$, and loss of H_2 yielded $[X{-}C_7H_6]^+$ ions at $m/z = 109$ (X=F), and $m/z = 125$ (X=Cl). Losses of H_2 and HX are competing fragmentation reactions (4.4 and 4.5) but the formation of the $C_8H_{11}^+$ ion ($m/z = 107$) is not in competition.

$$XC_6H_4CH_3.H^+ \rightarrow HX + C_6H_4CH_3^+ \quad (4.4)$$

$$XC_6H_4CH_3.H^+ \rightarrow H_2 + XC_6H_4CH_2^+ \quad (4.5)$$

The same conclusion is valid for the formation of various adducts referred in 4.2 so these will not be mentioned again.

Fig. 4·3. CI. HIGH PRESSURE MASS SPECTRUM OF 0·05% OF $\frac{[1,4\,CH_3C_6H_4F]}{[1,2\,CH_3C_6H_4Cl]}$ = 1·0 IN CH_4 AT 1 TORR 380 K

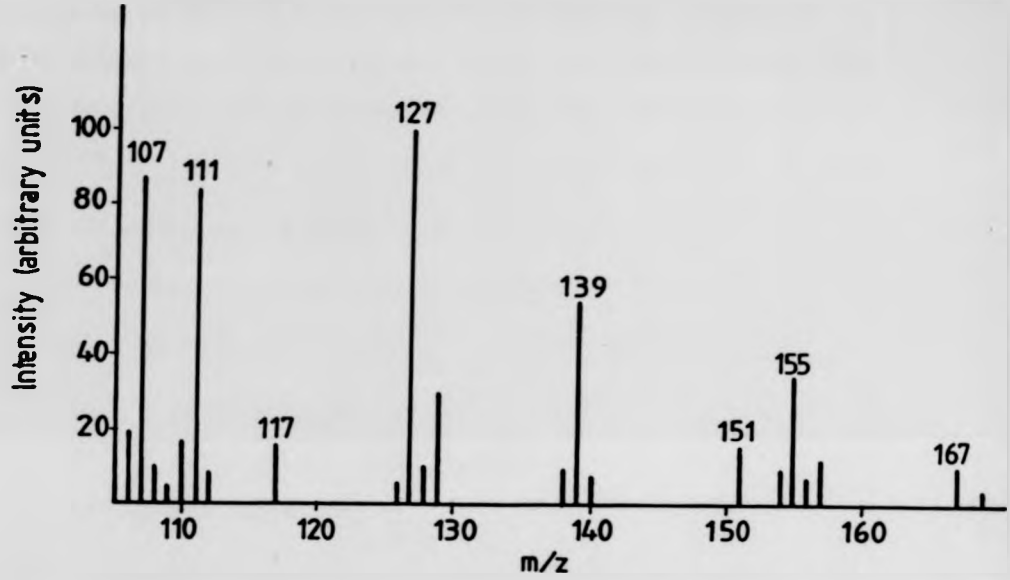

Fig. 4·4 CI. HIGH PRESSURE MASS SPECTRUM OF 0·05% OF $\frac{[1,4\,CH_3C_6H_4F]}{[1,2\,CH_3C_6H_4Cl]}$ = 2·7 IN CH_4 AT 2 TORR 437 K

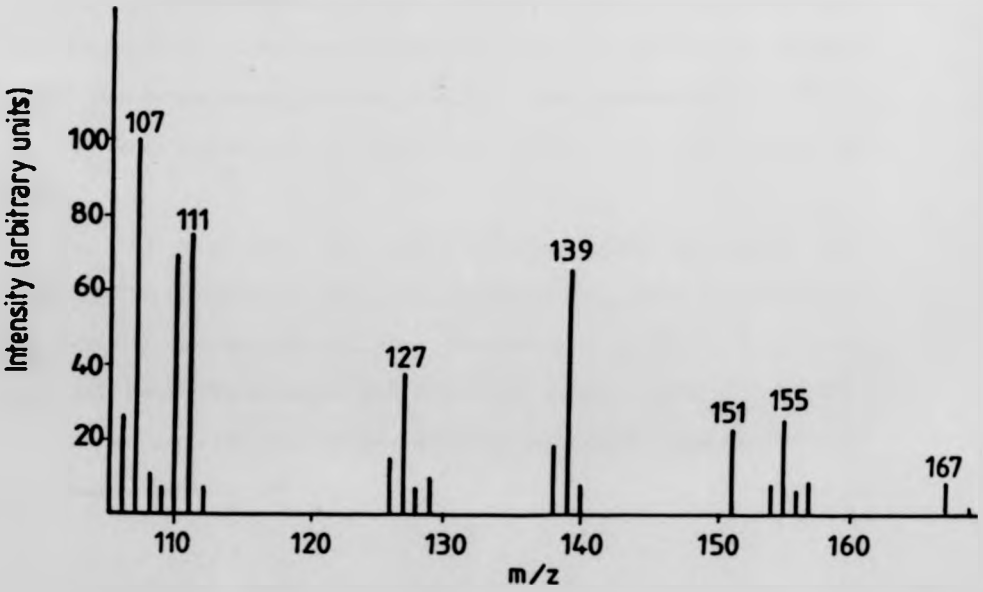

The formation of dimers and solvation with methane and SF_6 must also be considered as potentially competing reactions. The search for competing processes in both systems (CH_4 and H_2) was made for each component, *ortho*chlorotoluene and *para*fluorotoluene, individually and also with both reagents present. The observations were carried out in continuous mode with temperature and pressure variations.

4.3.1 CH_4 as protonating agent

The expected masses for proton bound dimer peaks were

m/z	Ion
221	$[(1,4\text{-}FC_6H_4CH_3)_2]H^+$
237	$[(1,4\text{-}FC_6H_4CH_3) + (1,2\text{-}ClC_6H_4CH_3)]H^+$
253	$[(1,2\text{-}ClC_6H_4CH_3)_2]H^+$

The only dimer ion observed was the 253 mass peak which had an intensity $< 1\%$ of the mass peak 127 ($1,2\text{-}ClC_6H_4CH_3.H^+$) at 2.5 Torr and 423 K. Peaks of intensity lower than 1% will not be represented in spectra. The proton bound dimer formation occurs in a three body reaction whose rate constant has a negative temperature dependence. Hence the formation of dimers is unfavoured at low pressures and/or high temperatures. This behaviour was indeed observed for the peak of mass 253 which was not present in spectra run at 551 K in a pressure range 1-3 Torr.

The solvation with CH_4 would produce peaks at masses 127 ($1,4\text{-}FC_6H_4CH_3.H^+.CH_4$) and 143 ($1,2\text{-}ClC_6H_4CH_3.H^+.CH_4$) which were not found under selected experimental conditions, temperature range 373-551K, pressure range 1-3 Torr. The solvation with SF_6 would produce peaks at m/z=257, m/z=273 but again they were not seen under the same experimental conditions as for solvation with CH_4.

Fig. 4·5 CI, HIGH PRESSURE SPECTRUM OF 0·05% OF $\frac{[1,4\,CH_3C_6H_4F]}{[1,2\,CH_3C_6H_4Cl]}$ = 0·5 IN CH_4 AT 0·7 TORR, 386 K

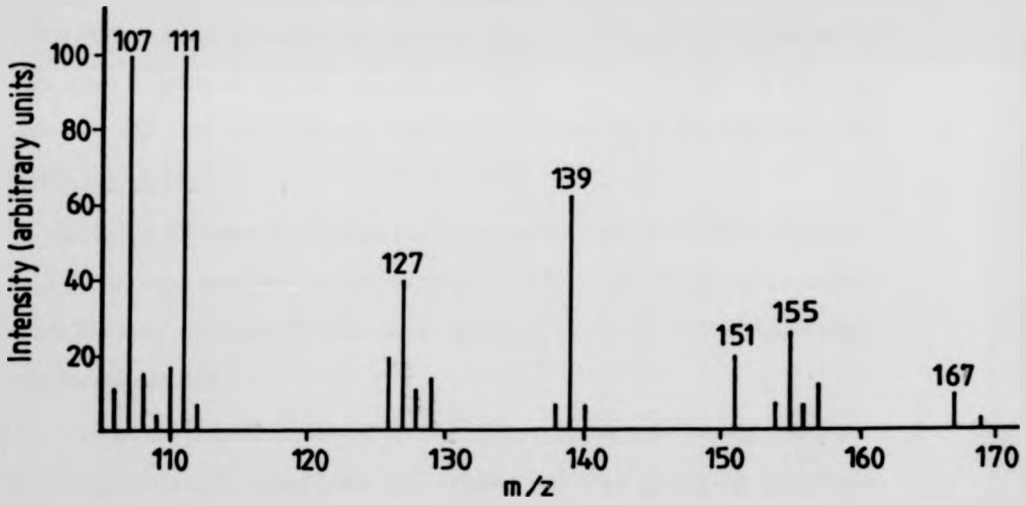

Attention will now be concentrated on reactions (4.4) and (4.5). The resultant peaks of m/z=91, 109, 125 do not look significant in figures 4.1, 4.2, 4.3, 4.4, and 4.5. In the spectrum of *para*fluorotoluene, figure 4.1, the intensities of the peaks of m/z = 91 and m/z = 109 are respectively 1% and 7% of the base peak 111 ($1,4\text{-}FC_6H_4CH_3.H^+$). In the spectrum of *ortho*chlorotoluene, figure 4.2, the intensities of ions of m/z = 91 and m/z = 125 are respectively 5% and 4% of the intensity of the base peak 127 ($1,2\text{-}ClC_6H_4CH_3.H^+$).

In figures 4.3, 4.4 and 4.5 the mass scale was not extended to the peak at mass 91 because its intensity was below 1% of base peak. The same statement is true of mass 125. These ions of mass 91 and 125 are probably not seen because in HPPS collisional stabilisation may favour the protonated molecular ion rather than their fragments. On the other hand ion of m/z = 109 had an intensity between 4% and 6% of the intensity of the ion of m/z = 111, ($1,4\text{-}FC_6H_4CH_3.H^+$).

In figures 4.1 and 4.2 two weak peaks, whose intensities were about 1% of the base peaks, were observed at m/z = 201 and m/z = 217. They are considered negligible here but one will come to them again, in the H_2 system where they become more intense.

Not all the records are shown for the whole range of experimental conditions that were attempted. Nevertheless the product ions from potentially competing reaction channels never became more intense than in the spectra shown.

In conclusion the most important interference seems to be the decomposition of $1,4\text{-}FC_6H_4CH_3.H^+$ (m/z = 111) by loss of H_2 through reaction (4.5). The subsequent formation of an ion with m/z = 109 should affect the values of the equilibrium constant by increasing them. However this effect was never clearly found when studies were done to check the constancy of K (section 3.3.1.2) with n.c.r. variation.

4.3.2 H_2 as protonating agent

Following a similar sequence to that described in section 4.3.1. the proton bound dimer ions will be considered first. In figures 4.6, 4.7, and 4.10 a peak of m/z = 253 is present. At 428K and 1 Torr the intensity is 6% of base peak 127 (figure 4.7). A comparison between 4.6 and 4.7, spectra of (1,2-$ClC_6H_4CH_3$) on its own, shows that the behaviour of ion of m/z = 253 is typical of a proton bound dimer as far as the pressure is concerned. When the pressure varied from 1 Torr to 3.5 Torr, at 428K, the intensity of the 253 mass peak was increased by a factor of five. In figures 4.8 and 4.9 where 1,4-$FC_6H_4CH_3$ was run on its own no dimer at m/z = 221 was found. In figures 4.10 and 4.11 where both halogenotoluenes are simultaneously present, peaks resulting from formation of dimers at m/z = 221, again were not found. Nevertheless a dimer ion at m/z = 237 is visible and another one at m/z = 253 whose intensities are respectively 1% and <1% of 1,4-$FC_6H_4CH_3.H^+$ (m/z = 111) and the latter 2.5% of 1,2-$ClC_6H_4.H^+$. Ions resulting from m/z = 237 and m/z = 253 by loss of H_2 are also visible at m/z = 235 and m/z = 251. Their intensities are twice the intensity of the potential precursors. Again the comparison of figures 4.10 and 4.11 as far as proton bound dimers are concerned, is in accordance with expectations. Both spectra were run at the same pressure and as temperature increased from 127K to 571K the proton bound dimer peaks vanished.

In figures 4.10 and 4.11 solvation with SF_6 is not observable either, as the peaks at m/z = 257 and 273 are not present.

Other types of possible competing reactions are (4.4) and (4.5). In figure 4.6 spectra of 1,2-$ClC_6H_4CH_3$, ions of m/z = 91 and 125 have respectively intensities of 37% and 8% of the intensity of the base peak m/z = 127 (1,2-$ClC_6H_4CH_3.H^+$). This pattern is similar in figure 4.7.

In CI spectra of 1,4-$FC_6H_4CH_3$, figures 4.8, 4.9, the ions of m/z = 91 and

CI, HIGH PRESSURE SPECTRA OF 0·05% OF 1,2 $CH_3C_6H_4Cl$ IN H_2 AT 428 K, 3·5 TORR (Fig. 4·6), 1 TORR (Fig. 4·7)

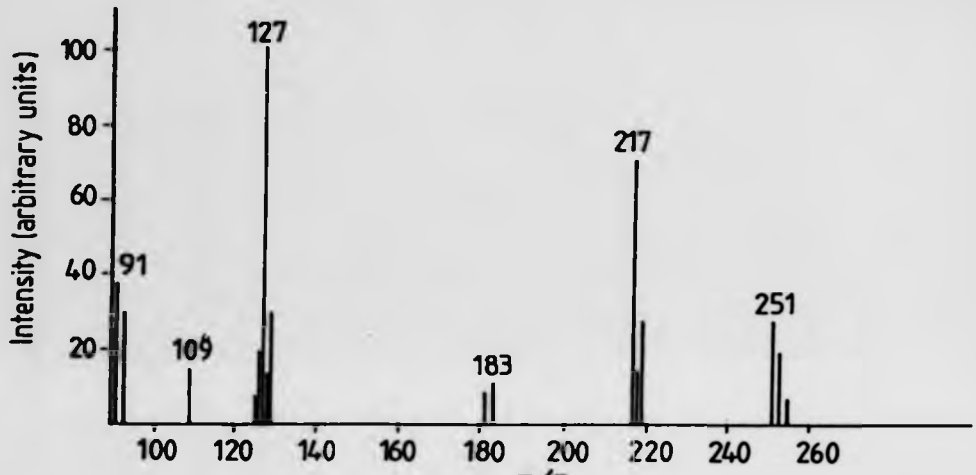

Fig. 4·6

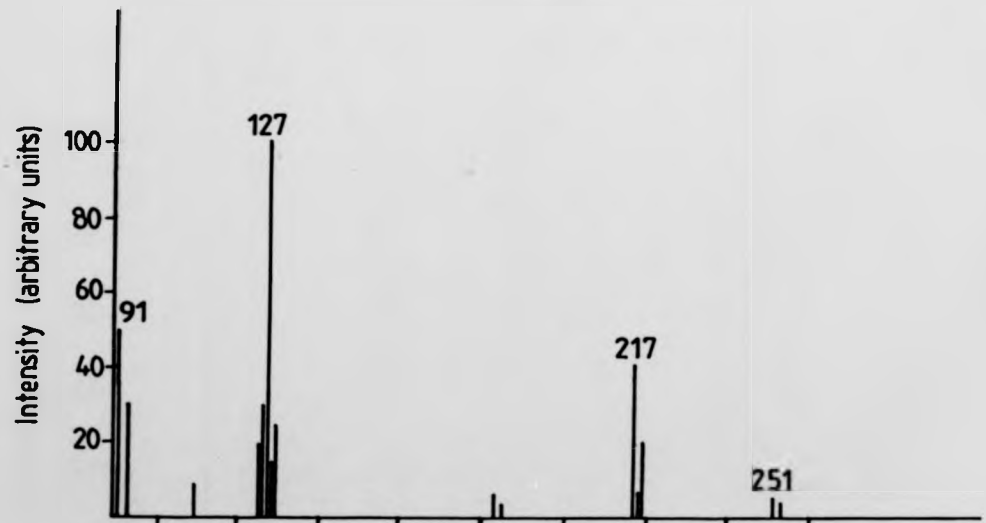

Fig. 4·7

CI, HIGH PRESSURE SPECTRA OF 0·05% OF 1,4 $CH_3C_4H_4F$ IN $\frac{H_2}{Ar} = \frac{1}{5}$ AT 2 TORR. 420 K (Fig. 4·8), 532 K (Fig. 4·9)

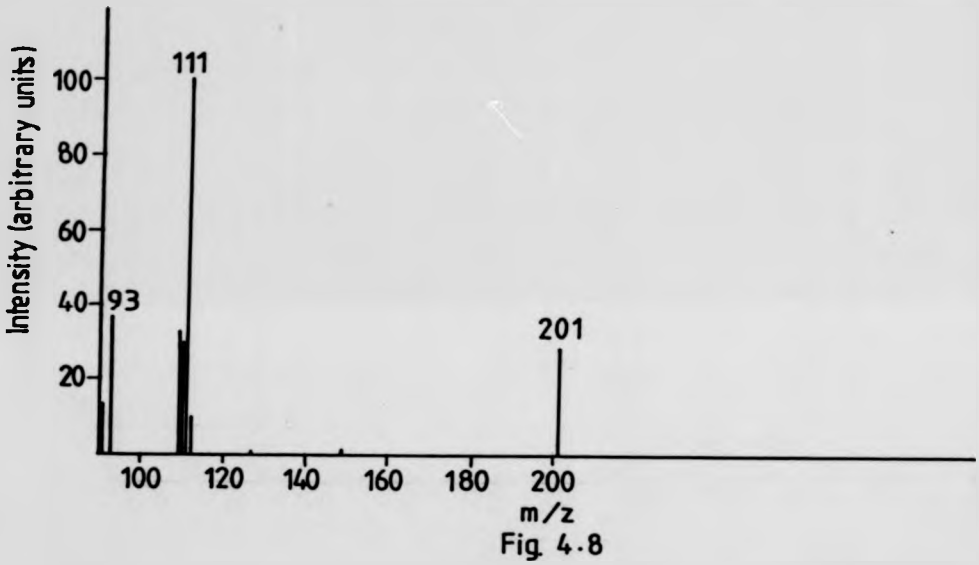

Fig. 4·8

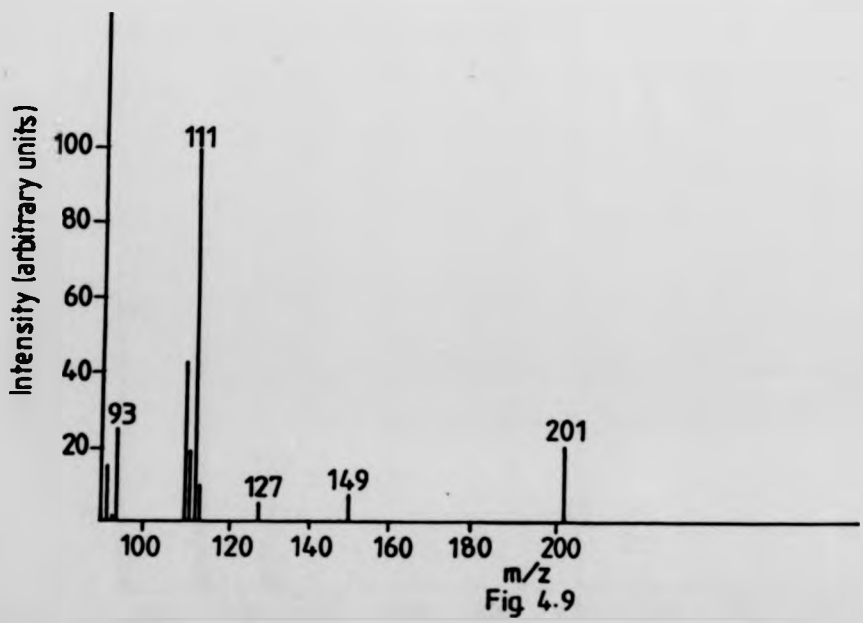

Fig. 4·9

CI, HIGH PRESSURE SPECTRA OF 0·05% OF $\frac{[1,4\ CH_3C_6H_4F]}{[1,2\ CH_3C_6H_4Cl]} = 2{\cdot}7$

IN $\frac{H_2}{Ar} = \frac{1}{5}$ AT 1 TORR, 427 K (Fig. 4.10), 571 K (Fig. 4.11)

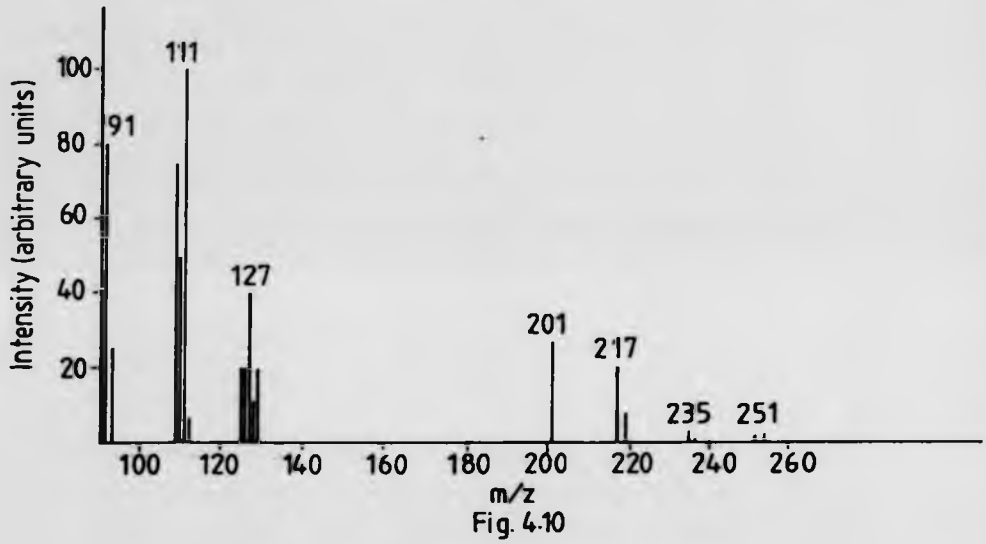

Fig. 4.10

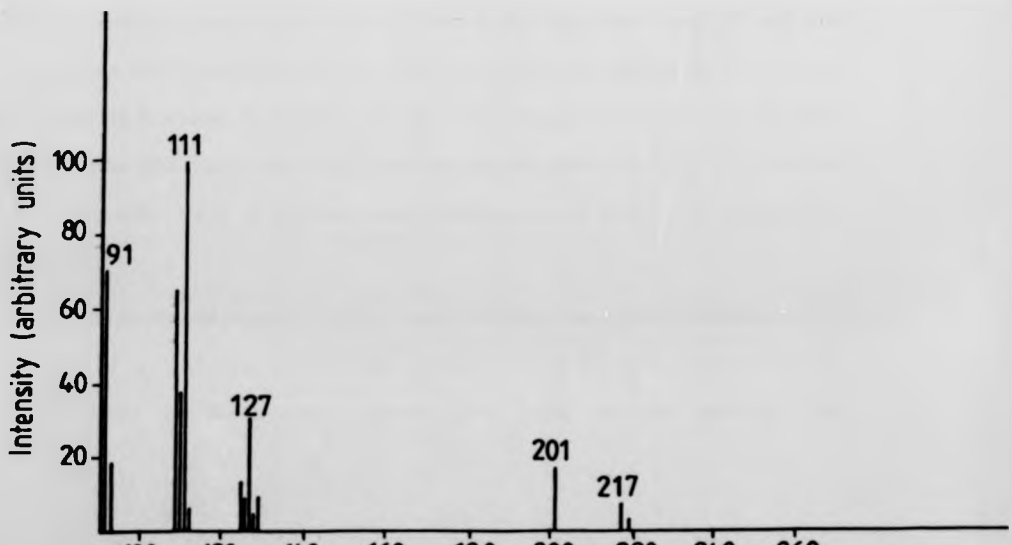

Fig. 4.11

109 are present. In figure 4.8 the intensity of m/z = 91 is 14% of the base peak intensity (m/z = 111). The pattern again receives support from Harrison et al[4.1] who noticed a lower intensity of MH^+ ions for chlorotoluenes (see figures 4.10 and 4.11) and a lower intensity of $C_7H_7^+$ (m/z = 91) for fluorotoluenes. The intensity of peak of m/z = 109 is approximately 30 - 40% of the intensity of $1,4\text{-}FC_6H_4CH_3.H^+$ (m/z = 111) in both figures 4.8 and 4.9. Still regarding the same competing reactions, (4.4) and (4.5), in figure 4.10 the peaks of m/z = 91 and 109 increase. Their intensities are respectively 80% and 75% of the peak of m/z = 111. The m/z = 125 peak has an intensity of 50% of the intensity of $1,2\text{-}ClC_6H_4CH_3.H^+$ (m/z = 127). The ion $C_7H_9^+$ (m/z = 93) need not be taken into account in the study of competing reactions because its formation does not alter the concentration of ionic species $XC_6H_4CH_3$.

$$H_3^+ + XC_6H_4CH_3 \rightarrow HX + C_6H_4CH_3H^+ \qquad (4.6)$$

where X = F, Cl

Two unexpected peaks were observed in figures 4.6 to 4.11 with m/z = 201 and 217. It was thought that they could arise from one of two sources. Either from a proton bound dimer of the type $M_1M_1H^+$, $M_2M_2H^+$ losing XH (X = F,Cl) or from the combination of ion $C_7H_7^+$ (m/z = 91) with a neutral, $XC_6H_4CH_3$. The second hypothesis seemed more likely. First of all comparing figures 4.6 and 4.7, the intensity of 217 increases with pressure (secondary process) as the intensity of mass peak 91 decreases. Secondly in section 4.3.1 the peaks of m/z = 217 and 201 also had intensities lower than 1% of the base peaks whilst ion $C_7H_7^+$ (m/z = 91) had an intensity $\leq 1\%$ of the base peak. Furthermore in that study dimers were not found.

A comparison of figure 4.8 with figure 4.9 offers no further explanation for the origin of peak of m/z = 201. The intensity of 201 seems to decrease slightly with increase in temperature. Spectra run with pressure variation for

1,4-$FC_6H_4CH_3$ were inconclusive. The intensity remained as 10% of m/z = 111 in a range of 0.9 - 2 Torr.

In figures 4.10 and 4.11 those peaks remain present. The possibility of their arising from dimer formation seems to be out of the question as dimers are absent in figure 4.11. Nevertheless a possible formation based on 91+M is not completely ruled out.

In summary, although dimers are not very intense in H_2 they are present under certain conditions unlike in CH_4. The most intense ion from a competing process is $C_7H_7^+$ (m/z = 91) which is not relevant in CH_4. The almost non-existent ions $[(CH_3C_6H_4)_2X]^+$ (X = F, Cl), in the methane systems are fairly intense in the H_2 system probably formed by $[C_7H_7^+ + CH_3C_6H_4X]$

As expected (section 3.3.1.4) the use of H_2 as protonating agent leads to a greater fragmentation than CH_4 and consequently various competing reactions occur. This explains the smaller equilibrium constants measured in H_2 systems than in CH_4 systems under the same experimental conditions at 473K (see figure 3.14).

The competing reactions taking place in H_2 systems are more severe in 1,2-$ClC_6H_4CH_3$ than in 1,4-$FC_6H_4CH_3$. This may lead to a higher attenuation of the intensity of the ion 1,2-$ClC_6H_4CH_3.H^+$ (m/z = 127) compared to the intensity of ion 1,4-$FC_6H_4CH_3H^+$. A drop in K values would be expected, as was demonstrated in section 3.3.1.4, figure 3.14. Hydrogen was considered unsuitable as a reagent/bath gas and abandoned in favour of methane.

4.4 The Measurements of the equilibrium constants

Using the best experimental conditions established in Section 3.3.1.5 and having chosen methane as the better reagent gas the next step was to measure equilibrium constants of PTR in halogenotoluene mixtures.

The van't Hoff plots of the seven systems of the type (4.1) studied are shown in figures 4.12 to 4.18. Values of ΔH° and ΔS° were derived from these van't Hoff plots by linear regression. They are summarised in table 4.1 where the number of measurements and the n.c.r. used for each system are also tabulated. The errors stated in the table are the standard deviations evaluated by considering that the errors are significant only in the values of K measured. The plots in fugures 4.14 and 4.16 were deliberately drawn in such a way that the extrapolation could be seen. Two graphs, 4.12 and 4.16, are the most scattered. In spite of this the presentation of the data in the form of two ladders, figures 4.19 and 4.20, displays a very good internal self-consistency. Figure 4.19 lists the relative proton affinities in the form of a ladder and figure 4.20 uses the same form for relative entropy changes.

The most surprising aspect of these data is the large entropy changes measured for some of the systems. A case in point is reaction (3), in table 4.1, where the proton transfer occurs between 1,4--chloro and 1,2-fluorotoluenes. The possibility of an artifact or interfering side-reactions being responsible for this seems unlikely. The thorough investigation of potential effects arising from varying a range of experimental parameters (section 3.3), impurities (section 3.3.1.6) and competing processes (4.3), led to the choice of ultimate experimental conditions. Under these conditions the results obtained were always consistent with the values in table 4.1. This together with the good internal self-consistency observed in the ladders of ΔH° and ΔS° for the seven systems points to the conclusion that there is a real effect.

Moreover a correlation between ΔH° and ΔS° was found as shown in figure 4.21. This plot illustrates the compensation effect, often observed. A linear correlation between ΔH and ΔS is well known[4.3] in solution and it is usually designated by an isokinetic or isoequilibrium relationship. The occurrence of this correlation not only confirms the reliability of the data but it points to a common pattern.

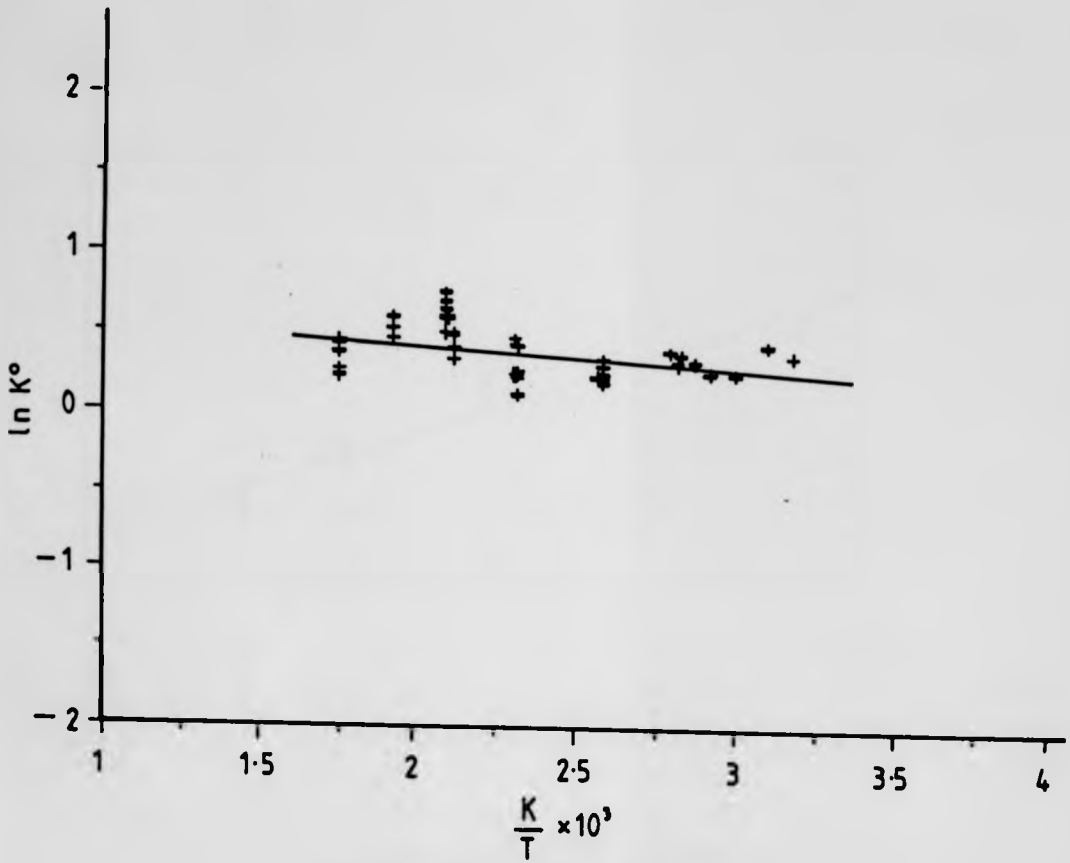

Fig. 4·12 van't Hoff Plot for Reaction

$$1,4\ CH_3C_6H_4F.H^+ + 1,4\ CH_3C_6H_4Cl \rightleftharpoons 1,4\ CH_3C_6H_4F + 1,4\ CH_3C_6H_4Cl.H^+$$

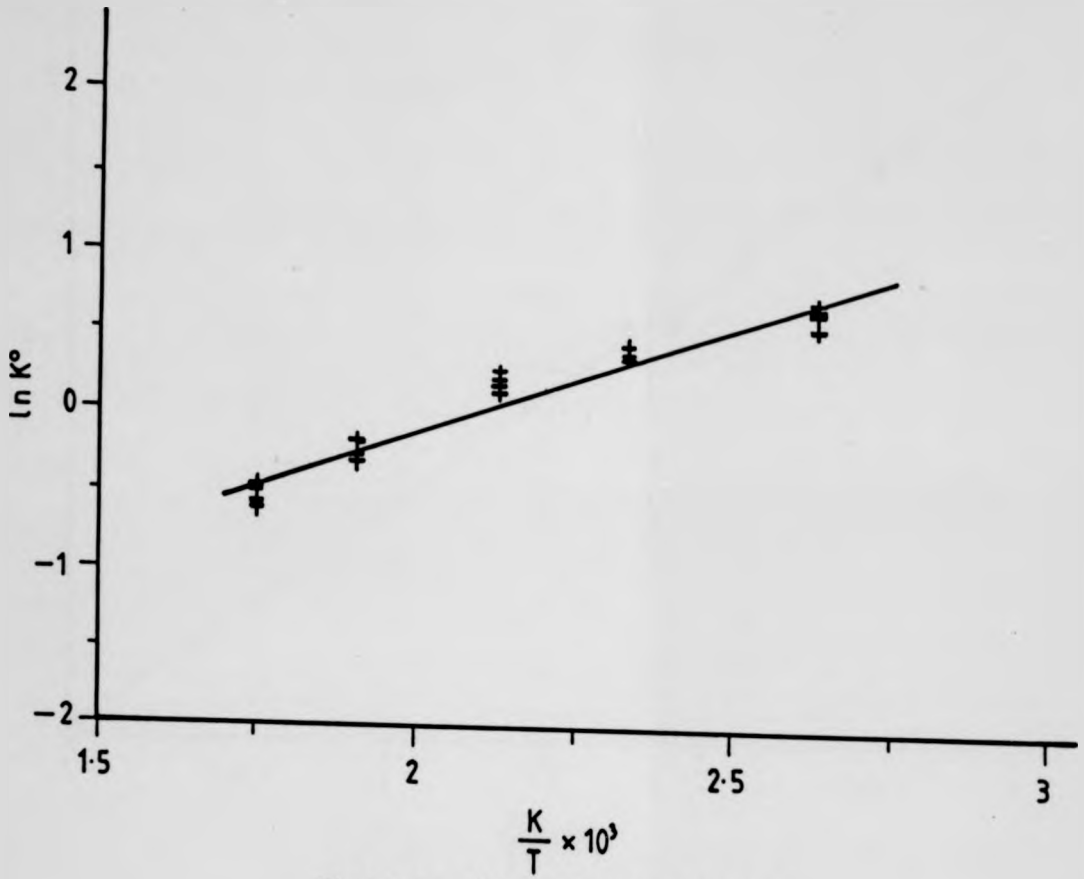

Fig. 4·13 van't Hoff Plot for Reaction

$1,2\ CH_3C_6H_4Cl.H^+ + 1,2\ CH_3C_6H_4F \rightleftharpoons 1,2\ CH_3C_6H_4Cl + 1,2\ CH_3C_6H_4F.H^+$

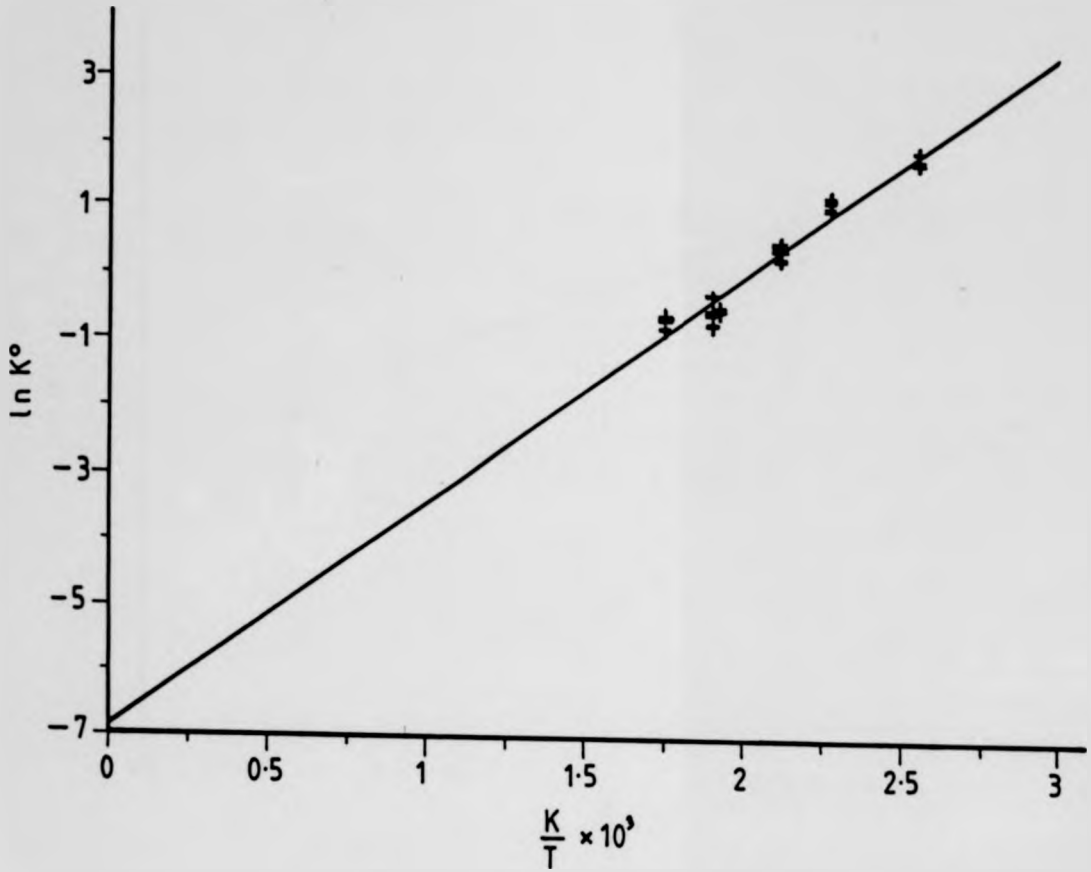

Fig. 4·14 van't Hoff Plot for Reaction

$$1,4\ CH_3C_6H_4Cl.H^+ + 1,2\ CH_3C_6H_4F \rightleftharpoons 1,4\ CH_3C_6H_4Cl + 1,2\ CH_3C_6H_4F.H^+$$

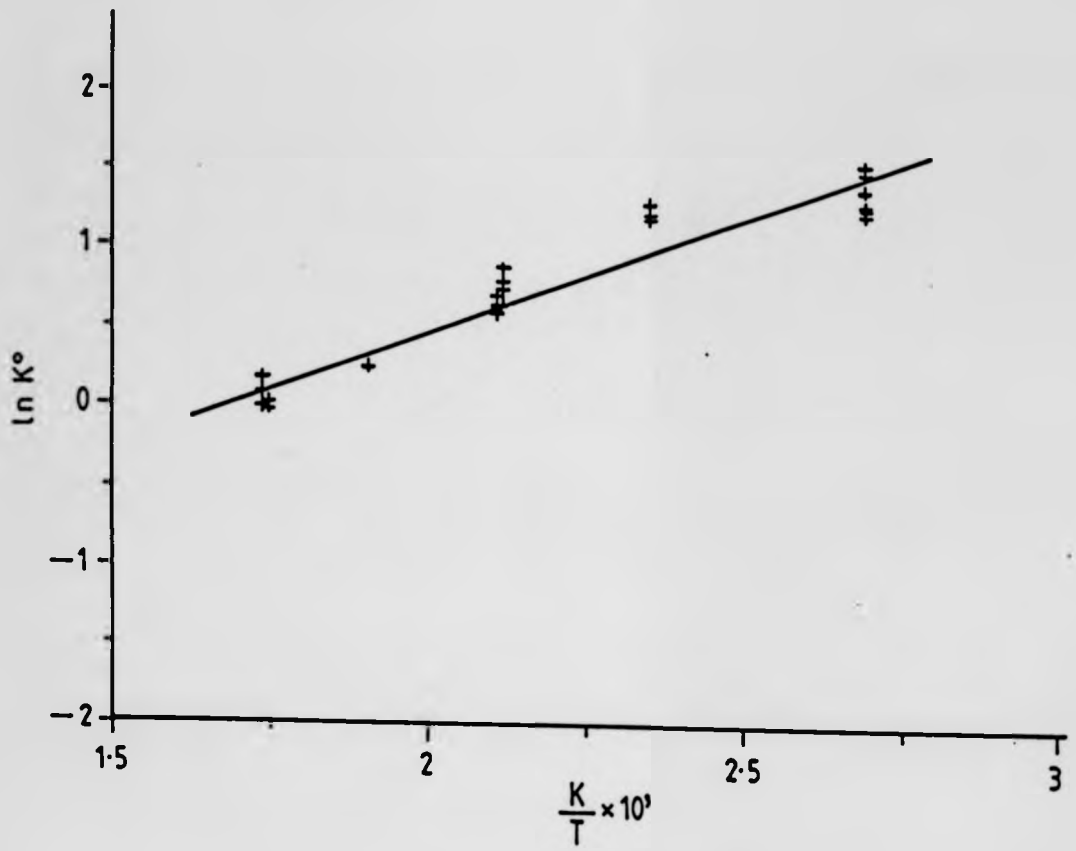

Fig.4·15 van't Hoff Plot for Reaction

$$1,4\ CH_3C_6H_4F.H^+ + 1,2\ CH_3C_6H_4Cl \rightleftharpoons 1,4\ CH_3C_6H_4F + 1,2\ CH_3C_6H_4Cl.H^+$$

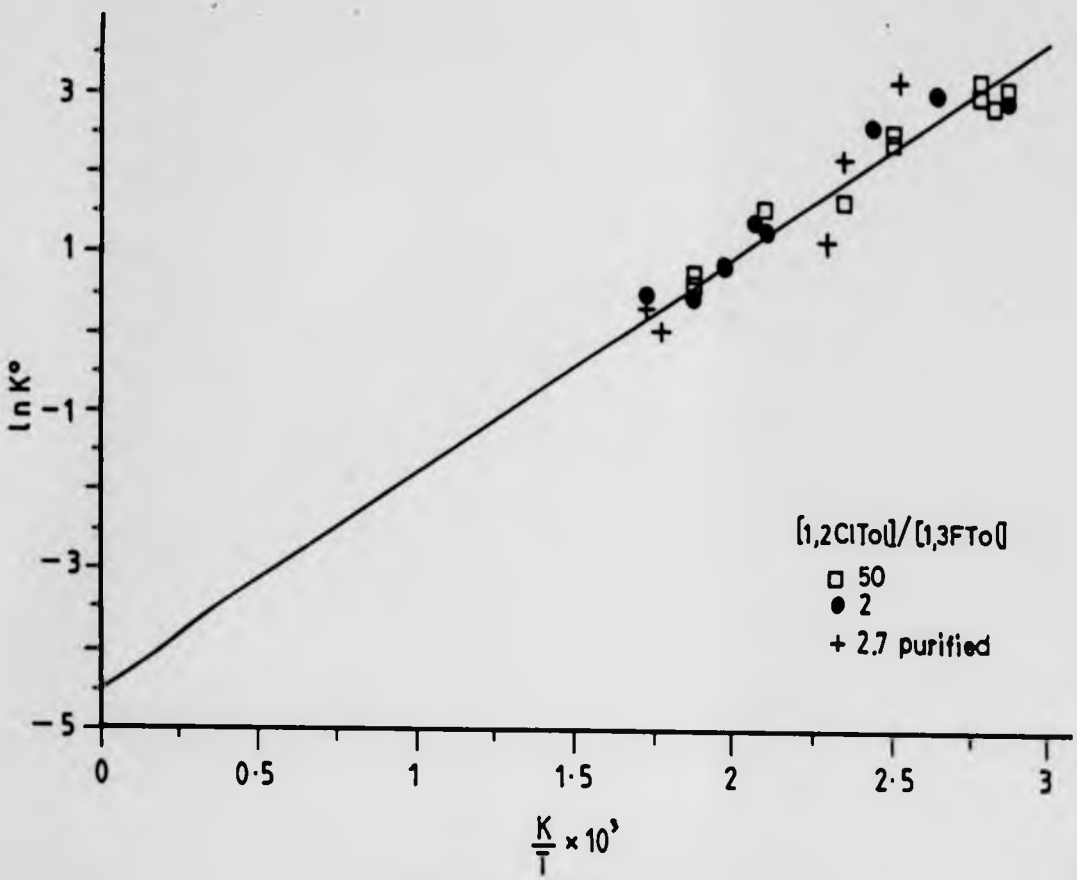

Fig. 4·16 van't Hoff Plot for Reaction

$$1,2\ Cl\ C_6H_4CH_3.H^+ + 1,3\ F\ C_6H_4CH_3 \rightleftharpoons 1,2\ Cl\ C_6H_4CH_3 + 1,3\ F\ C_6H_4CH_3.H^+$$

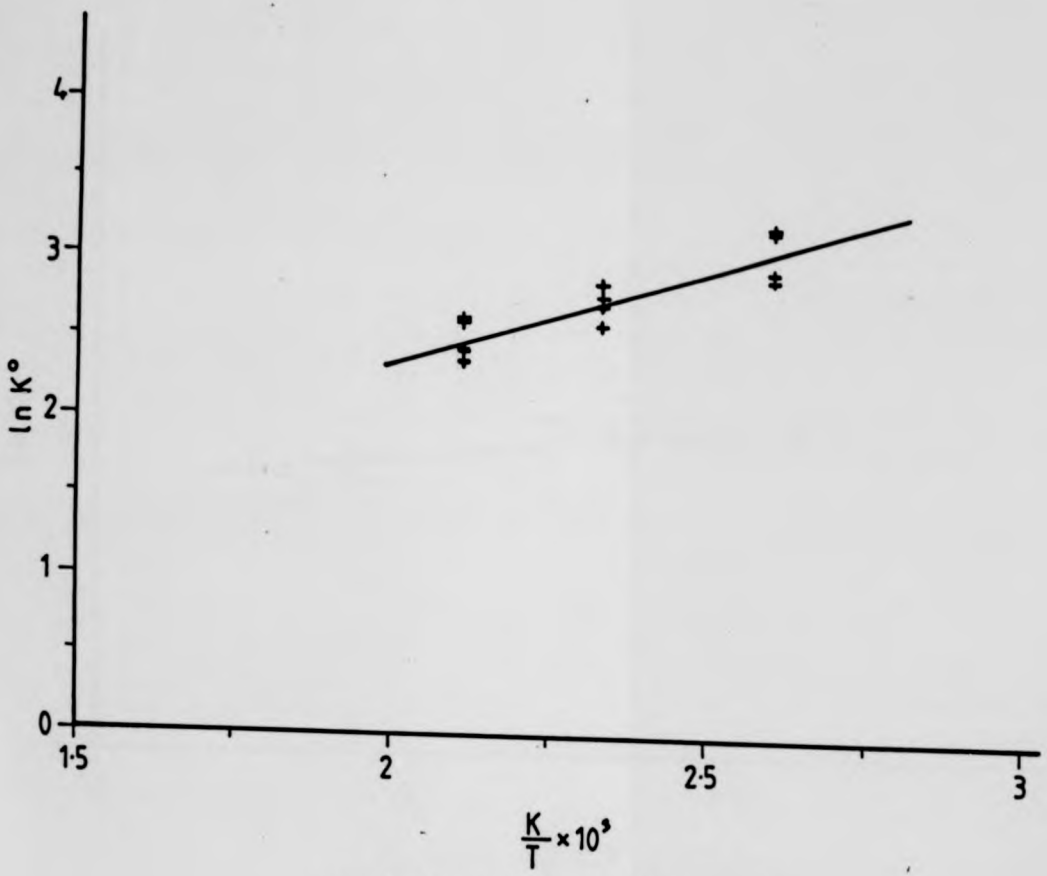

Fig. 4·17 van't Hoff Plot for Reaction

$$1,2\,CH_3C_6H_4F.H^+ + 1,3\,CH_3C_6H_4Cl \rightleftharpoons 1,2\,CH_3C_6H_4F + 1,3\,CH_3C_6H_4Cl.H^+$$

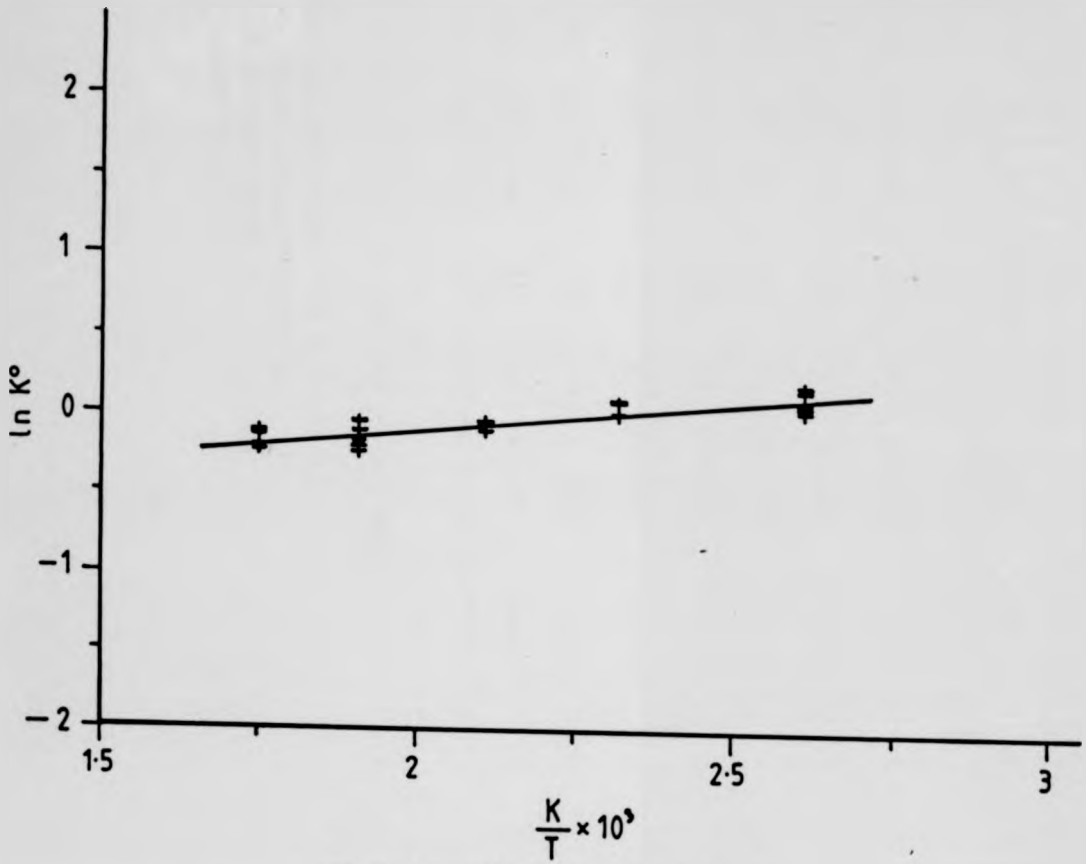

Fig. 4·18 van't Hoff Plot for Reaction

$$1,3\,CH_3C_6H_4Cl.H^+ + 1,3\,CH_3C_6H_4F \rightleftharpoons 1,3\,CH_3C_6H_4Cl + 1,3\,CH_3C_6H_4F.H^+$$

Table 4.1

Summary of Results

	A	B	[A]/[B]	(n)	$-\Delta H^\circ$ $kJmol^{-1}$	$-\Delta S^\circ$ $JK^{-1}mol^{-1}$	ΔS_{rot} $JK^{-1}mol^{-1}$
(1)	pCl	pF	1.7 0.9	51	1.2±0.4	5.8±1	0
(2)	pF	oCl	1.0 2.7	32	14.±0.5	23.3±1	0
(3)	pCl	oF	5.8	31	28.±1.0	56.5±2	0
(4)	oCl	oF	0.5 0.9	24	11.3±0.5	24.0±1	0
(5)	oCl	mF	51.7 2.5	25	22.8±0.5	37.4±1	0
(6)	oF	mCl	18.3	13	9.3±0.3	0.7±0.5	0
(7)	mCl	mF	1.1 0.6	24	3.0±0.3	7.0±0.6	0

$$AH^+ + B \rightleftharpoons A + BH^+$$

p = para (1,4), o = ortho (1,2), m = meta (1,3)

* assumes protonation on the ring

A and B are halotoluenes

n = number of experiments

PROTON AFFINITY LADDER

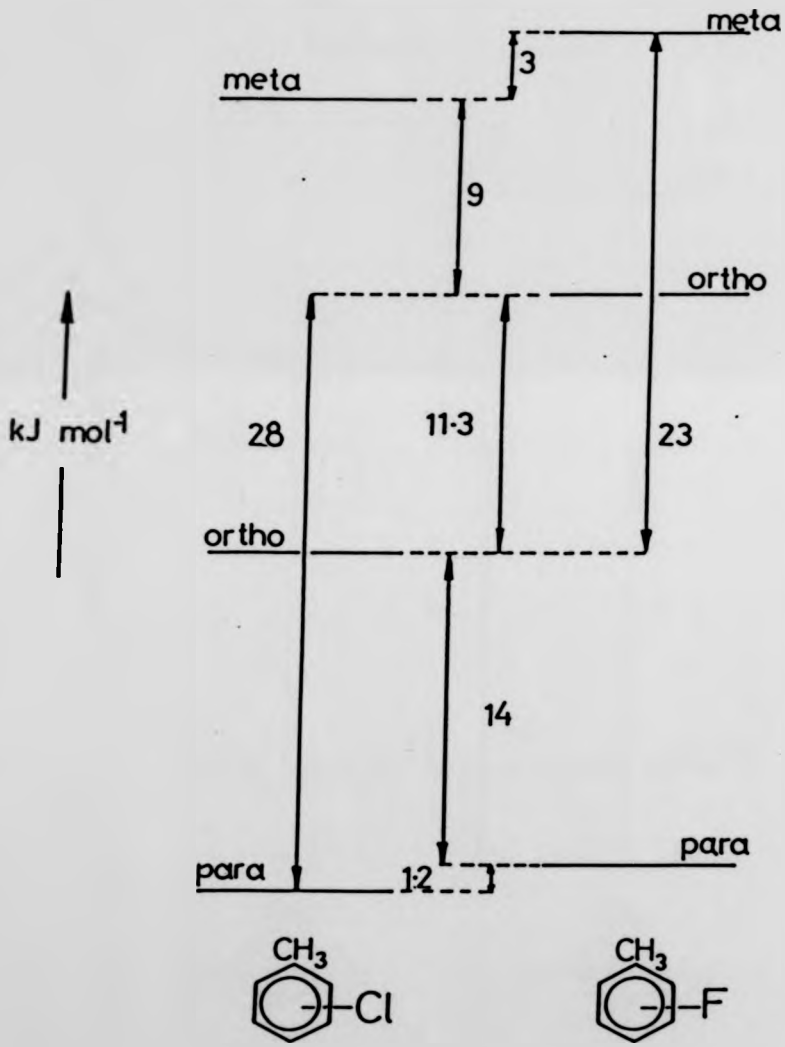

FIG. 4.19

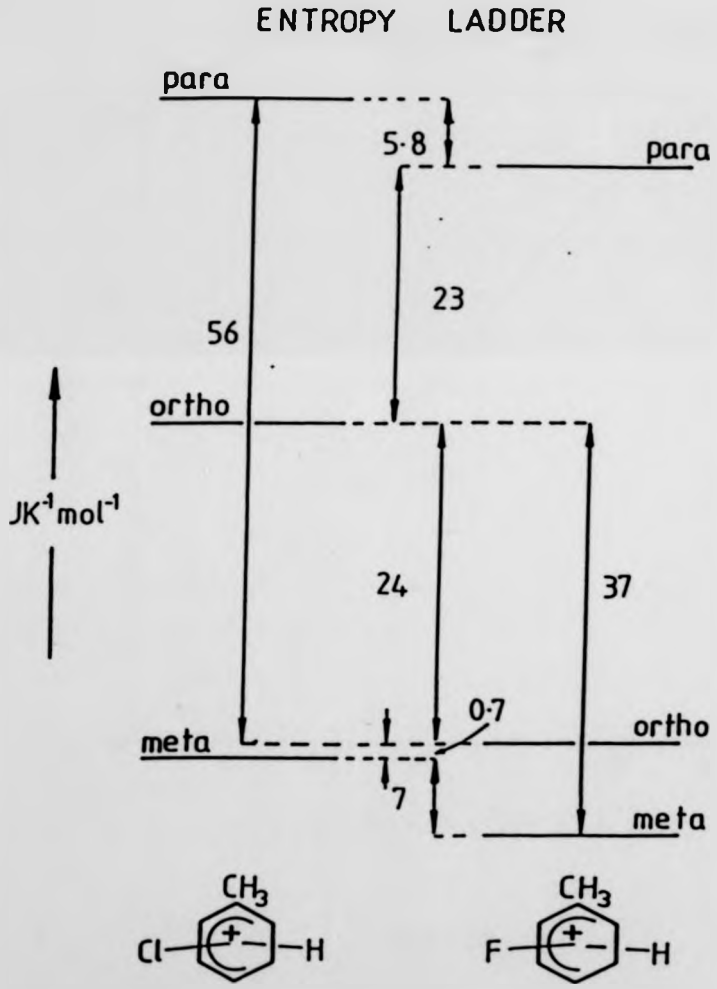
ENTROPY LADDER
para
5·8
para
23
56
ortho
JK⁻¹mol⁻¹
24
37
0·7
ortho
meta
7
meta
CH3
Cl
H
CH3
F
H

FIG.4.20

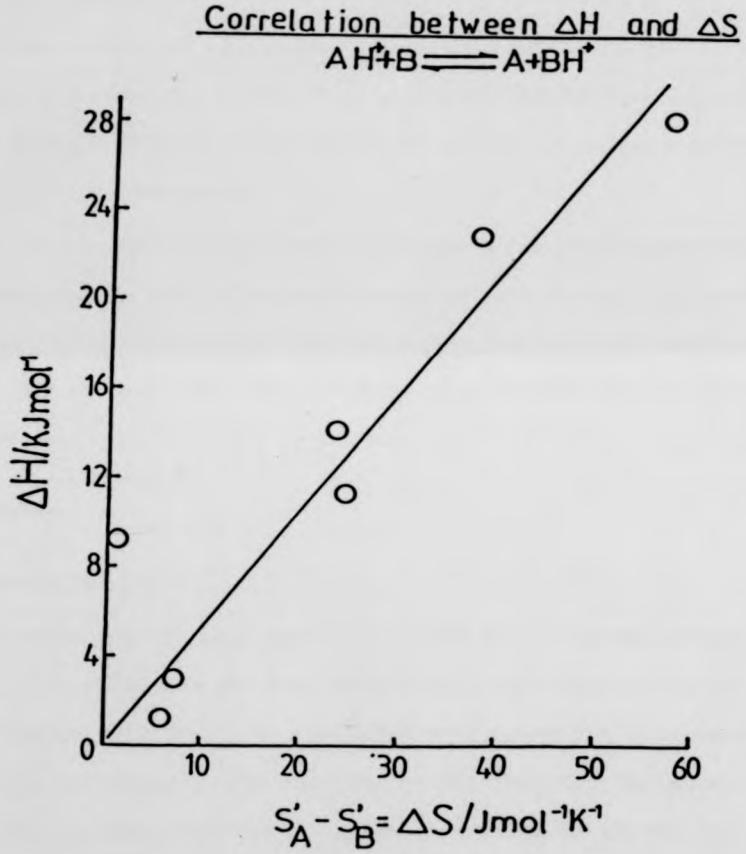
Correlation between ΔH and ΔS
AH⁺+B ⇌ A+BH⁺
ΔH/KJmol⁻¹
0
4
8
12
16
20
24
28
10
20
30
40
50
60
S'A - S'B = ΔS/Jmol⁻¹K⁻¹

FIG. 4.21

Only one point is shifted from the straight line for reaction (6) in table 4.1. This system has the smallest number of measurements but its van't Hoff plot is not the most scattered.

4.5 Previous Measurements in the Literature: A Comparison.

Earlier measurements of ΔG° for halogenotoluene systems had been carried out at 369K[42] and for fluorotoluenes at 478K[44]. The data in Table 4.1 were converted to basicity values at 369K and 478K, relative to $1.3FC_6H_4CH_3$ and compared in Table 4.2 with the previous results.

The qualitative agreement is fairly good between the results from this work and previous data. The order of basicities remains the same although the former values are smaller by 2 to 7 kJ mol^{-1}; they are more trustwothy as they are more extensive. Large differences were found in the gas phase basicities of the isomeric halogenotoluenes.

4.6 Discussion

4.6.1 Introduction

The previous study of halogenotoluenes[42], made at Warwick, at a single temperature 369K, led to the relative gas phase basicities of isomers whose values were different. This was rationalised in terms of differently favoured sites for protonation due to the combination of ortho and para directing effects from the two substituents, the methyl group and halogen. Apparently more than one site was available (figure 4.23).

Theoretical calculations[42] showed that the protonation of *para*fluorotoluene could occur preferentially at the carbon atom bearing the methyl group.

These results led to interest in the determination of proton affinities of the various isomeric halogenotoluenes and in clarifying whether the differences in their gas phase basicities were due to ΔH° or ΔS° variations.

TABLE 4.2

BASICITIES (ΔG/kJ mol^{-1}) RELATIVE TO 1,3-FLUOROTOLUENE
COMPARISON WITH PREVIOUS DATA

Substance	ΔG_{369}(a)	ΔG_{369}(b)	ΔG_{478}(b)	ΔG_{478}(c)
Toluene	-1.2			-0.84
1,3-F	0	0	0	0
1,3-Cl	2.0	0.4	-0.4	
1,2-F	11.8	6.4	5.3	12.3
1,2-Cl	12.9	8.8	5.1	
1,4-Cl	17.4	13.5	6.5	
1,4-F	18.7	14.5	8.2	14.8

(a) Ref. 4.2

(b) Estimated using ΔH and ΔS values from Table 1

(C) Ref. 4.4

In the previous study the entropy changes were considered to be small due to the low symmetry numbers of all components of the systems. In the present study it was hoped that the experimental determinations of entropy changes. in proton transfer between fluoro-chlorotoluenes, would eventually give information about the structure of the protonated species.

4.6.2 Protonation on the ring

In this work it was considered that the protonation of halogenotoluenes takes place on the ring. Evidence in support of this is given below.

As an electrophilic attack protonation is likely to occur at high electronic density sites in molecules. In non-aromatic molecules the existence of heteroatoms make them preferential targets for protonation as they have non bonding pairs of electrons[4.5]. For instance compounds whose composition contains O and N atoms have proton affinities on the top half of the scale (see table 2.1) within the interval 750-900 kJ mol^{-1}. The aromatic ring itself is a good candidate for protonation. However, when benzene is mono or disubstituted and the substituent itself contains heteroatoms, a doubt can arise about the competition for the proton between ring and heteroatoms. An attempt is made here to clarify the situation in the case of the halogenotoluenes. It is shown in figure 4.22 that for two groups of aliphatic molecules, hydrogen halides and alkyl halides, it is the polarizability[4.6,4.7] of the substituent that controls the proton affinities. On the other hand the behaviour of proton affinities of halobenzenes and halogenotoluenes, against polarizability is quite different from hydrogen and the alkyl halides. The proton affinities of halobenzenes and halogenotoluenes are very similar to the proton affinities of benzene and toluene respectively (see figure 4.22). No apparent influence of the polarizability of the halogen on proton affinities is found for monohalobenzenes and halogenotoluenes. This led to the conclusion that for both latter species the preferential site for protonation is the aromatic ring. An addi-

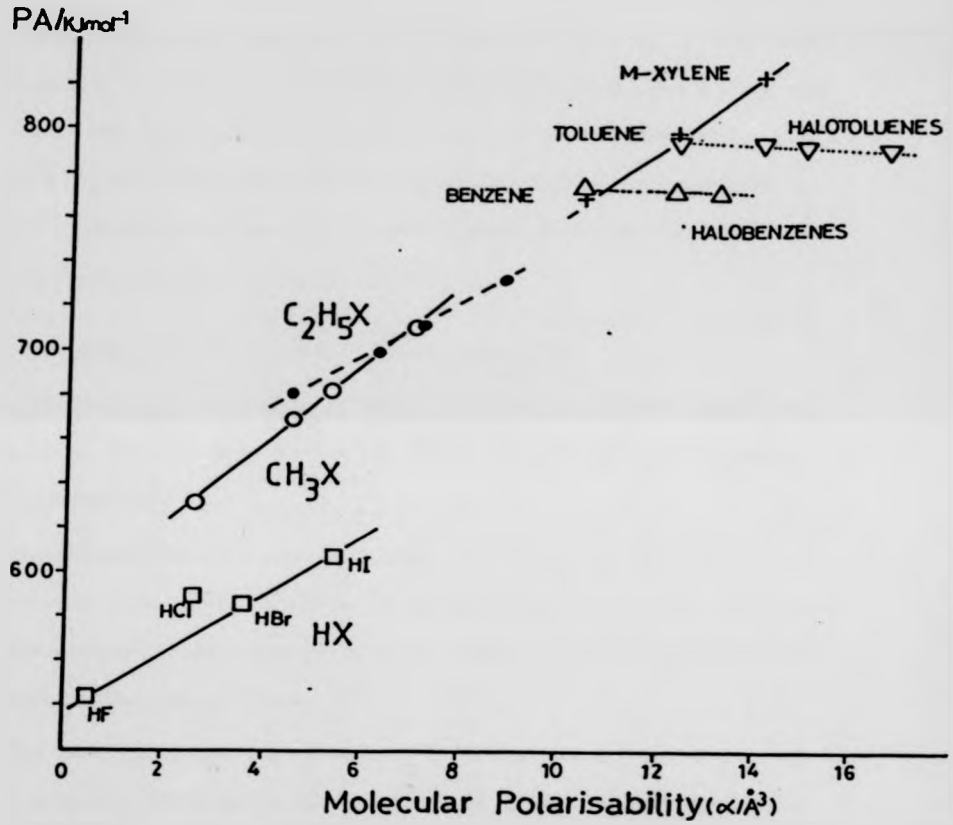

FIG.4.22. PROTON AFFINITY vs. POLARISABILITY

tional example is given by monoalkylbenzenes whose proton affinities are all close to $803 \pm 5 kJ\ mol^{-1}$ although the proton affinities of aliphatic compounds depend on the polarizability of alkyl substituent.

Further evidence for protonation on the ring was drawn from *ab initio* calculations (section 7.4). Once the protonation on the ring is established it is obvious that within the ring the preferred carbon atoms for protonation will be those where the negative charge density is the highest. For halogenotoluenes as well as for other disubstituted benzenes, these sites and their electron density will depend upon the substituents and their relative positions.

4.6.3 The Effect of Substituent on Protonation Sites

The interaction of a given substituent with an aromatic ring decides its reactivity and stability. This has been discussed in terms of the inductive effect, polarisation, and resonance[4 8]

The charge distribution around the ring, the action of electron withdrawing or electron donating groups, determine the proton affinity of a molecule. Furthermore these effects also determine the relative availability of more than one site for protonation in the same molelcule.

The methyl group has been considered[4 9,4 10] as a weak π donor, justified by hyperconjugation. This seems to determine why toluene has a higher proton affinity than benzene[4 11]. The halogens, although σ electron acceptors, are also π electron donors. The introduction of a fluorine atom in the benzene ring will slightly increase its proton affinity relative to benzene[4 12] but this effect decreases in the following order, F>Cl>Br. Two fluorine substitution decreases the PA relative to benzene[4 13]. This decrease can be understood on the basis of the duality of halogens with respect to stabilisation of the ring. Their π donation favours the stabilisation, but, on the other hand, the σ withdrawal provokes destabilisation of the protonated species.

These two π electron donating groups will stabilise the protonated ring ion. Both substituents, methyl group and halogen, are separately para and orthodirecting in terms of electrophilic attack. Hence, in toluenes and halobenzenes, the maximum stabilisation of the protonated species occurs when protonation happens at para and ortho positions. This is shown in the first row of figure 4.23. The second row of the same figure shows the combination of these "driving" effects if both substituents are simultaneously present on the ring. In *meta*halogenotoluenes it is possible to find suitable protonation positions being at the same time para to one of the substituents and ortho to the other. These compounds would be expected, therefore, to have the highest proton affinity since they present the most stable combination. The same kind of arguments can be used to predict that *para*halogenotoluenes have the most unstable conditions for protonation. Any unsubstituted carbon atom will always be ortho to one of the substituents and meta to the other; this is a combination of the two most unfavourable conditions for protonation. Consequently the *para*halogenotoluenes have the lowest proton affinity amongst halogenotoluenes. The *ortho*halogenotoluenes lie in between. The expected order for gas phase basicities is then

meta > ortho > para

This was the order actually found for gas phase basicities in the work of reference 4.2 which was confirmed by the proton affinity measurements made in this work. Some of the proton affinity values are larger than previously expected but this is due to some surprisingly large values measured for ΔS° which will be considered in more detail in the next section.

Having compared the relative order of proton affinities for meta, ortho and para halogenotoluenes, one can now compare the proton affinities for fluorotoluenes and chlorotoluenes. *Meta*fluorotoluene has higher proton affinity than *meta*chlorotoluene and the same is true for ortho and para compounds. This is consistent with the scale mentioned above F > Cl > Br based on the association

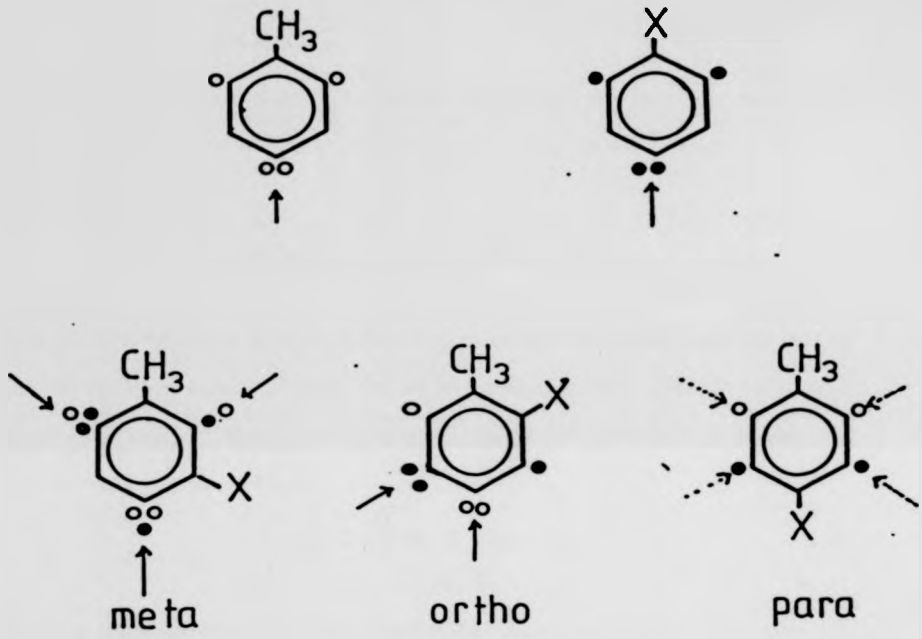

FIG. 4.23. EXPECTED SITES OF PROTONATION

of π-donation and σ withdrawal of electrons. The extent of π-donation seems to decrease with the increase of size of the halogen.

4.6.4 The Entropy Changes

As it was pointed out in section 2.2.4 the entropy change in a proton transfer reactions can be calculated by statistical thermodynamics as being made up of four contributions.

$$\Delta S^{\circ} = \Delta S^{\circ}_{trans} + \Delta S^{\circ}_{rot} + \Delta S^{\circ}_{vib} + \Delta S^{\circ}_{elect} \qquad (4.7)$$

It was then shown that the main contribution usually results from ΔS_{rot} . However a fifth contribution must be taken into account when more than one site is available for protonation. all with the same energy content. This is called the entropy of mixing[4 17]. Recalling the general reaction (4.8) entropy of mixing can be expressed by equation (4.9).

$$AH^{+} + B \rightleftharpoons A + BH^{+} \qquad (4.8)$$

$$\Delta S_{mix} = R\ln\frac{m}{n} \qquad (4.9)$$

where m is the number of isomers for species BH^{+} and n the number of isomers for species AH^{+}.

Equation (2.23) proves that ΔS_{rot} must depend on rotational symmetry variations[4 2,4 12]. The external symmetry numbers are given by the number of indistinguishable configurations arrived at by rigid rotation of the species around symmetry axes[4 7]. If the species possesses any hindered rotation then the symmetry contribution arising from this internal rotation must be added to the external term.

For the systems in table 4.1 the symmetry numbers arising from external rotation will always be 1 in every case for all species. If there is any internal hindered rotational contribution it must be given by $R\ln 3 = 9.1 Jmol^{-1}K^{-1}$. These contributions must be equivalent on both sides of the proton transfer reaction and so they are likely to cancel.

For at least four systems the experimental values of ΔS were found to be strikingly large compared with the rotational contributions just described or the entropy of mixing defined above.

In order to establish upper and lower limits for ΔS_{mix} one can use figure 4.23 and its predictions. For meta derivatives two sites are predicted to have equivalent proton affinities and a third position is expected to protonate to a lesser extent. For *ortho* derivatives two sites are predicted to have equivalent proton affinities and the other two sites must have equivalent lower proton affinities than the latter. In the case of paraderivatives all four carbon atoms non substituted must have the same proton affinity.

For *ortho* and *para*halogenotoluenes semiempirical calculations[4,2] suggested the possibility of protonation on the carbon atom bearing the methyl group. The ipsoprotonation would lead to a maximum number of three isomers for *para*halogenotoluenes and three or five for *ortho*halogenotoluenes. In fact the five sites would not be enough to give an entropy of mixing accounting for the largest ΔS^o measured. The maximum contribution of entropy of mixing would arise from a situation where one component had five isomers and the other none. $\Delta S_{mix}=R\ln 5=13.4 Jmol^{-1}K^{-1}$. This situation is unlikely to occur since the existence of at least two isomers for any compound looks highly favourable. One can possibly expect $\Delta S_{mix}=R\ln(m/n)$ within a range 1.9 to 7.6 $Jmol^{-1}K^{-1}$ if $n = m = 2,3,4,5$. In summary if ΔS_{rot} cannot explain the high values of entropy changes measured neither can ΔS_{mix} account for them. Evidence will be given in chapter 7 that the maximum value of 7.6 $JK^{-1}mol^{-1}$ can be reduced by taking into account the number of allowed positions for proton attachment with similar PA, as found from theoretical calculations.

In section 2.2.4 evidence was given that ΔS°_{trans} and ΔS°_{elect} are close to zero for PTR. Thus one is left with the possibility of a considerable entropy change

arising from ΔS°_{vib} for reaction (4.1). This is also unlikely. A look at table 4.4 shows that additional vibration frequencies arising from the new bond formation lead to $\Delta S_{vib} < 3 Jmol^{-1}K^{-1}$.

On the other hand if the entropy change in reaction (4.8) is expressed in terms of the entropies of the species involved, it will lead to the following equation.

$$\Delta S = (S_{BH^+} - S_B) - (S_{AH^+} - S_A) = S'_B - S'_A \qquad (4.10)$$

S'_A is the excess entropy arising from protonation of molecule A. This will be designated from now on as the " entropy of protonation".

4.6.5 Isoequilibrium Relationship

In section 4.6.3 the influence of substituents on protonation of the aromatic ring was analysed. This effect is included in the semi-quantitative expression of the binary structure/reactivity given by the linear free energy relationships (LFER). The Hammett equation is an example of these relationships and can be given[4.15] by

$$\log k_x = \rho \log K_x + c \qquad (4.11)$$

or converted to

$$\log \frac{k_x}{k_H} = \rho \sigma_x \qquad (4.12)$$

K_x- Equilibrium constant of a given reaction for a given species where x is a particular substituent in the benzene ring.

k_x - rate constant of a given reaction (different from reaction whose K is being determined above) same species as above

k_H - rate constant for the unsubstituted species

ρ - reaction constant

σ_x - substituent constant.

hold[43] and a common reaction mechanism to take place. The constant β has dimension of temperature and is given by the slope of the correlation. Its physical meaning is that of a temperature for which reactivity is reversed.

This compensation effect is well understood in terms of C_p° and ΔC_p° variation with temperature. Over a given temperature range C_p° is usually expressed as a polynomial expression in the range ΔT, quadratic or cubic, in T or ΔT. ΔC_p° has a lower variation thus it can be expressed by a linear or quadratic function of T, even if ΔT is wide.

$$\Delta C_p^\circ(T) = a + bT + cT^2 \qquad (4.15)$$

Hence ΔH_T° and ΔS_T° are given by

$$\Delta H_T^\circ = \Delta H_{T_-}^\circ + \int_{T_-}^{T} (\Delta C_p^\circ) dT \qquad (4.16)$$

$$\Delta S_T^\circ = \Delta S_{T_-}^\circ + \int_{T_-}^{T} \left(\frac{\Delta C_p^\circ}{T} \right) dT \qquad (4.17)$$

If $\Delta C_p^\circ(T)$ is not small ΔH° and ΔS° must change considerably with temperature but even so they will change in the same way and will cancel in the expression for ΔG°. Thus the calculation of ΔG°_T based on $\Delta H_{T_-}^\circ$ and $\Delta S_{T_-}^\circ$ may only be affected by very small errors.

An isokinetic relationship was observed for proton transfer reactions between the halogenotoluenes. The correlation was shown in section 4.4 figure 4.21. Among the compounds in this series the 1,4-chlorotoluene has the lowest proton affinity and the 1,3-fluorotoluene has the lowest value of entropy of protonation S'_A. These two values were used as comparative co-ordinates for relative scales of proton affinities and entropies of protonation of all halogenotoluenes studied. All the relative values are gathered in table 4.3 and they are plotted in figure 4.24. The error bars are the maximum variation in both parameters arising from the use of different thermochemical cycles when determining these values. The slope of the plot leads to a value of 589±50K for β, the isokinetic temperature. This value

TABLE.43

PROTON AFFINITIES, PA , OF FLUORO- AND CHLOROTOLUENES RELATIVE TO PARA-CHLOROTOLUENE, AND ENTROPIES OF PROTON S°_{A} , RELATIVE TO META-FLUOROTOLUENE

Substance	PA /kJ mol^{-1}	S°_{A} /J K^{-1} mol^{-1}
P-Cl-Toluene	0	61-66
P-F	1.2	55-60
O-Cl	15.2-16.7	32-37
O-F	26.5-29.2	7.7-13
M-Cl	35.5-38.2	7
M-F	36.5-41.2	0

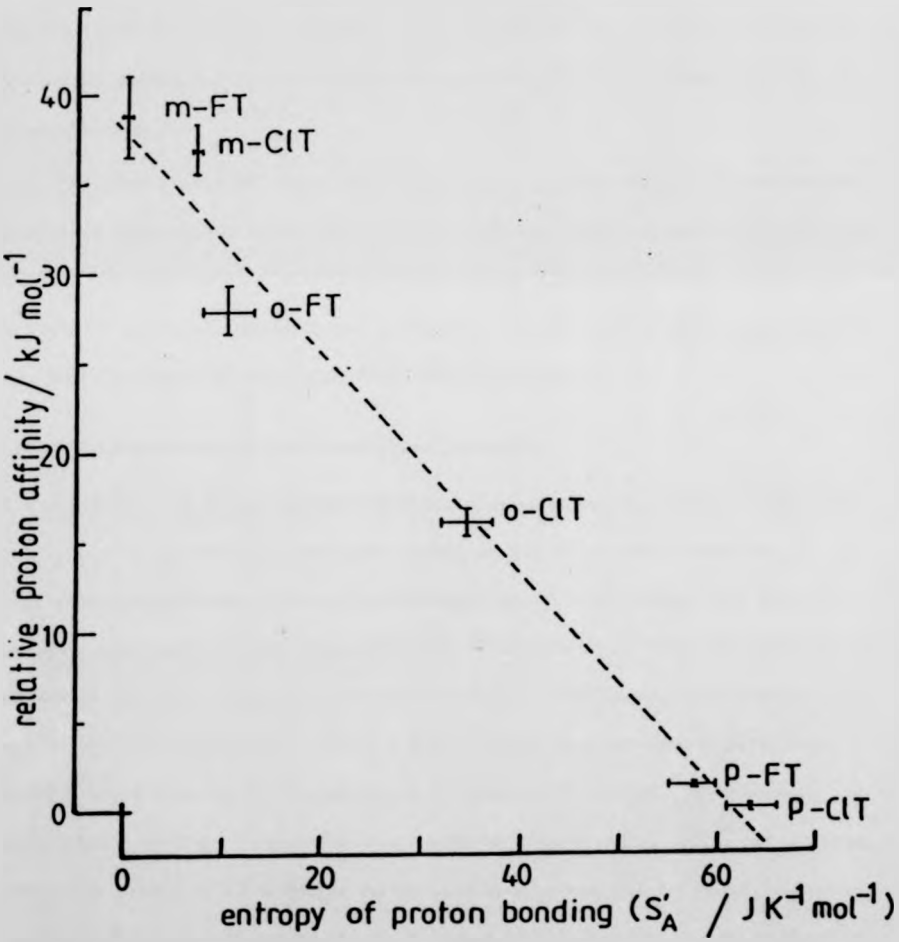

FIG.4.24 THE ISOKINETIC EFFECT

of β is 100° above the mean temperature, 450K, of the experiments. In previous works in solution β was sometimes found to be close to this mean temperature. This was often attributed to an artifact. Furthermore in this study a wide range of experimental values is considered, so statistically[43] the effect observed must be real.

The isokinetic or isoequilibrium relationship serves here as a confirmation of the reliability of the large entropy changes measured. On the other hand it indicates some connection between those entropy changes and the structure of the protonated species.

The observation of these correlations raises another subject for discussion. They have been mainly attributed to solvent effects. Some of the previous studies involved aromatic systems also containing ionic species. Since such correlation can be observed in the gas-phase, in the absence of solvent, it seems likely that the reasons for this cannot be entirely ascribed to solvent effects.

4.6.6 The Structure of the Protonated Species

It was pointed out in section 2.2.4 that some insight into structure of protonated species can be gained from entropy changes in proton transfer reactions. In the case of halogenotoluenes proton transfer reactions it was verified that more than one site was available for protonation in the molecules. This conclusion was arrived at through classical mechanistic considerations discussed in section 4.6.3 and theoretical calculations.[42] Thus it was expected that the experimental entropy changes could contain the contribution of entropy of mixing. Nevertheless, the experimental entropy changes in some systems exceed $\Delta S_{rot}+\Delta S_{mix}$ by a large amount as shown in 4.6.4. So far no obvious conclusions can be arrived at about structure of protonated species since ΔS experimental does not match adequately any of the calculated contributions or their sum.

TABLE 4.4

ENTROPY CONTRIBUTIONS AND CHANGES FOR VARIOUS PROCESSES

System	S or ΔS JK^{-1} mol^{-1}	Reference
PROTON TRANSFER		
$BH^+ + CH_3(CH_2)_3NH_2 \longrightarrow B + CH_3(CH_2)_3NH_3^+$	0	4.18
$BH^+ + NH_2(CH_2)_3NH_2 \longrightarrow B + NH_2(CH_2)_3NH_3^+$	− 86.	4.18
$AH^+ + B \rightleftharpoons A + BH^+$		
ΔS Rotation, e.g. σ = 1 1 1 1	0	See text
ΔS Mixing, e.g. m = 1 n = 5	< 13	See text
p-chlorotolueneH$^+$ + o-fluorotoluene		
p-chlorotoluene + o-fluorotolueneH$^+$	− 56.	Table 4.1
FREE INTERNAL ROTATION		
Methyl group of toluene at 450 K	26.5	4.7
VIBRATIONAL CONTRIBUTIONS		
(S = R + Rln (1.44 ν/T)) at T = 450 K		4.7
ν cm^{-1}		
3100 (e.g. C-H stretch)	0	
700 (e.g. C-C-H bend)	2.9	
50	23.6	

Perhaps some informative clue is contained in these experimental entropy changes. Having checked the impossibility of $\Delta S_{rot}+\Delta S_{mix}$ accounting for the large values of ΔS_{exp} it was decided to investigate thoroughly any other possible contributions. Table 4.4 includes some typical cases. The first two rows illustrate the well known (see section 2.3) cyclisation process leading to large values of ΔS. This has been explained on the basis of formation and breaking of hydrogen bonds. In the halogenotoluene systems such a process, which would certainly lead to a higher value of ΔS experimental than measured, seems unlikely. The next rows give a summary of some of the contributions mentioned above, both calculated and measured.

The entropy associated with the free internal rotation of the methyl group in toluene is 26.5 J $mol^{-1}K^{-1}$. If the value for the same process was similar in halogenotoluenes, this contribution would not account for the high experimental values. It appears unlikely that the introduction of a second substituent could double the contribution in this case. On the other hand the para and ortho directing effect of $-CH_3$ group has been rationalised in terms of hyperconjugation and this must prevent the free internal rotation in the four species present in proton transfer reactions. Furthermore if instead of the free rotation a hindered rotation occurred, contributing through an internal rotation entropy term (Rln3) the net entropy of the four species involved would be zero.

As was expected above, (4.6.4) the increase in entropy arising from protonation can sometimes be ascribed to contributions from additional vibrations or to changes in vibrational frequencies or internal rotations within the molecule. This was also ruled out in the present case by examination of Table 4.4. There, are given the vibrational contributions for ΔS from stretching and bending associated with a C-H in neutral species. It is hoped that in the protonated species similar vibrations may produce similar ΔS contributions. These values in Table 4.4 are very small, indeed they were considered negligible. In fact in the protonated

species they may be even smaller as proton affinity are in the range 750-800 kJ mol^{-1} which are larger than C-H bond energies,[4.19] which are typically $<500 kJmol^{-1}$.

All these possibilities do not suggest an acceptable explanation in the experimental data. Nevertheless a suggestion was found in the literature from studies in solution and in gas phase.

Olah[4.20] reports the protonation of benzene with formation of $C_6H_7^+$ ion in solution. Studies by NMR in superacid media showed hydrogen intramolecular rearrangement arising from very rapid 1,2 shifts. The activation energy for intramolecular proton exchange was estimated to be 40 $kJmol^{-1}$.

In gas phase Bruins and Nibbering[4.21] ionised $C_6D_5CD_2NH_2$ by E.I. The $C_6D_5H_2^+$ ion was generated from the resultant ion $[M-D]^+$ by elimination of DCN.

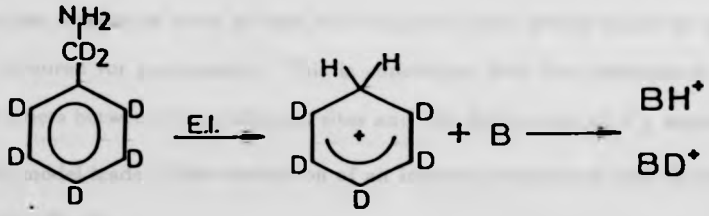

That $C_6D_5H_2^+$ ion swaps its proton with base B and because the ratio $\frac{BH^+}{BD^+}$ equals $\frac{2}{5}$ it is concluded that intra- molecular H/D exchange around the ring takes place for protonated benzene.

This evidence for mobility of the proton in protonated benzene suggested that in the protonated species being studied here something similar is taking place.

What is proposed is a model matching mobility with high proton affinities and high values of S'_A. This may be visualized as a proton firmly bound to the aromatic ring but able to circulate within the ring, being shared by two or more of

the ring carbon atoms.

It is easily concluded from figure 4.24 that the more tightly bound the proton is the less the entropy of protonation (metacompound). In fact for metacompounds $S'_A \approx 0$ and it may be seen from figure 4.23 that all favoured sites for protonation are predicted on alternate carbon atoms. If one assumes that high energy barriers are present at the alternative carbon atoms where protonation is not favoured the motion of the proton around the aromatic ring will be minimal leading to $S'_A \approx 0$. This agrees with the fact that *meta*halogenotoluenes have the highest proton affinity of the compounds studied. Hence, the benzenium† ion must be an acceptable picture for these ions. This benzenium ion[4,19] structure has been proposed as an adequate structure for protonated benzene. In such an ion the proton is attached to a specific carbon atom which exhibits a tetrahedral sp^3 configuration. On the other hand, *para* and *ortho* halogenotoluenes whose proton affinities are smaller do have at least four adjacent sites which might be roughly equally favoured for protonation. This is consistent with the assumption of low energy barriers between those adjacent sites and the high values of S'_A measured.

This model leads to the conception of an internal translation contribution, to the entropy change.

In the previous studies, supporting this idea, the observations were rationalised in terms of rapid isomerisation. This work gives negative evidence of such phenomenon, for ΔS measured are much larger than ΔS_{mix}. The present work suggests that above 300K, in gas phase, for *ortho* and *para*halogenotoluenes the proton has enough mobility to proceed rapidly, generating a dynamic structure rather than isomerization.

Having regarded the process in this way, one was led to the necessity of carrying out *ab initio* calculations on the potential energy surface. It was decided to

† Nomenclature according to Pople et al[1,22] and references t-erein.

look simultaneously for other systems where a similar effect could take place in order to confirm it.

Furthermore if the basic idea was correct ΔS of internal translation would not occur on compounds protonating on the substituent. Therefore experiments in these conditions would produce ΔS°_{exp} close to the usual contributions ΔS_{rot} and ΔS_{mix}.

The following chapters will give an account along these different lines of search.

4.7 References

4.1 a) A. G. Harrison and P-H Lin. Can J. Chem. (1975), 53. 1314

b) H. W. Leung and A. G. Harrison. Can. J. Chem., (1976), 54, 3439

4.2 R. S. Mason, D.K. Böhme and K.R. Jennings. J. Chem. Soc. Faraday Trans. I. (1982), 78. 1943.

4.3 O. Exener, Prog. Phys. Org. Chem. (1973), 10, 411

4.4 J.A. Stone, D.E. Splinter and S.J. Kong, Can. J. Chem. (1982), 60, 910

4.5 R.W. Taft, in "Kinetics of Ion Molecule Reactions", ed. P. Ausloos, Nato Advanced Study Institute Series B, (1979) vol. 40, 271 Plenum Press

4.6 C.J.F. Böttcher and P. Borderwijk, "Theory of Electric Polarization", (1978), vol.2, table 4.3, Elsevier

4.7 S.W. Benson "Themochemical Kinetics", Wiley and Sons, New York, 1976

4.8 J. Hine, "Structural Effects on Equilibrium in Organic Chemistry", (1975), Wiley and Sons.

4.9 A. Pross, L. Radom and R.W. Taft, J. Org. Chem. (1980), 45, 818

4.10 G. Kemister, A. Pross, L. Radom and R.W. Taft, J. Org. Chem. (1980), 45,1056

4.11 J.L. Devlin, J.F. Wolt, R.W. Taft and W.J. Hehre, J. Am. Chem. Soc. (1976), 98, 1990

4.12 D.K. Bŏhme, J.A. Stone, R.S. Mason, R.S. Stradling and K.R. Jennings, Int. J. Mass Spectrom. Ion Phys., (1981), 37, 1283

4.13 R. Yamdagni and P. Kebarle, J. Am. Chem. Soc. (1976), 98, 1320

4.14 S.G. Lias, J.F. Liebman, R.D. Levin, J. Phys. Chem. Ref. Data, (1984), 13, 695

4.15 L.P. Hammett, "Physical Organic Chemistry", McGraw-Hill New York, 1970

4.16 Y. K. Lau and P. Kebarle, J.Am. Chem. Soc. (1976), 98, 7452

4.17 J.E. Leffler, J. Org. Chem., (1955), 20, 1202

4.18 R. Yamdagni and P. Kebarle, J. Am. Chem. Soc., (1973), 95, 3504

4.19 J.A. Kerr and Trotman - Dickenson, CRC Handbook of Chemistry and Physics, 58th edition ed. R.C. Weast, CRC Press, Inc. 1977-78, F 231

4.20 G. Olah, R.H. Schlosberg, R.D. Porter, , D.P. Kelly and G.D. Mateescu, J. Am. Chem. Soc., (1972), 94, 2034

4.21 A.P. Bruins and N.M.M. Nibbering, Org. Mass Spectrom (1976), 11, 950

4.22 W.J. Hehre and J.A. Pople, J. Am. Chem. Soc. (1972), 94, 6901

CHAPTER 5: THERMOCHEMISTRY OF GAS PHASE PROTON TRANSFER REACTIONS BETWEEN XYLENES AND DIMETHYLETHER

5.1 Introduction

The study of Proton Transfer Reaction (PTR) between xylenes and dimethylether will be dealt with in this chapter. The results obtained for equilibrium constants at different temperatures will be presented in the form of van't Hoff plots. The subsequent values of standard enthalpy and entropy changes will be given for the following reaction:

$$C_6H_4(CH_3)_2 + (CH_3)_2O.H^+ = C_6H_4(CH_3)_2H^+ + (CH_3)_2O \qquad (5.1)$$

This reaction applies to the different isomers ortho, meta and para. These data will be discussed and compared with literature values. The behaviour of the xylenes will be compared with the halogenotoluenes with respect to the PTR.

5.2 The Conventional CI Spectra

CI spectra were run in continuous mode (see section 3.1.2) in order to check the underlying chemistry. The reagent/bath gas used was CH_4 as had been chosen in section 4.3.

The spectra found for dimethylether (figure 5.1), *para*xylene (figure 5.2) and a mixture of both compounds, (figures 5.3 - 5.5) do not show any unexpected peaks.

In figure 5.1 the main peaks are seen at m/z= 47, 93 which correspond to ions $(CH_3)_2O.H^+$ and $[(CH_3)_2O]_2H^+$. The peaks at m/z = 41, 43, 57 must arise directly from methane[5.1] which creates respectively the ions $C_3H_5^+$,$C_3H_7^+$,$C_4H_9^+$. The peak at m/z = 45 could either be an ion cluster $C_2H_5^+.CH_4$ that at T>250K dissociates into $C_3H_7^+$ and H_2, or an ion arising from the protonated molecular ion

Fig. 5·1. CI. HIGH PRESSURE SPECTRUM OF 0·026% OF $(CH_3)_2O$ IN CH_4 AT 2 TORR, 473 K

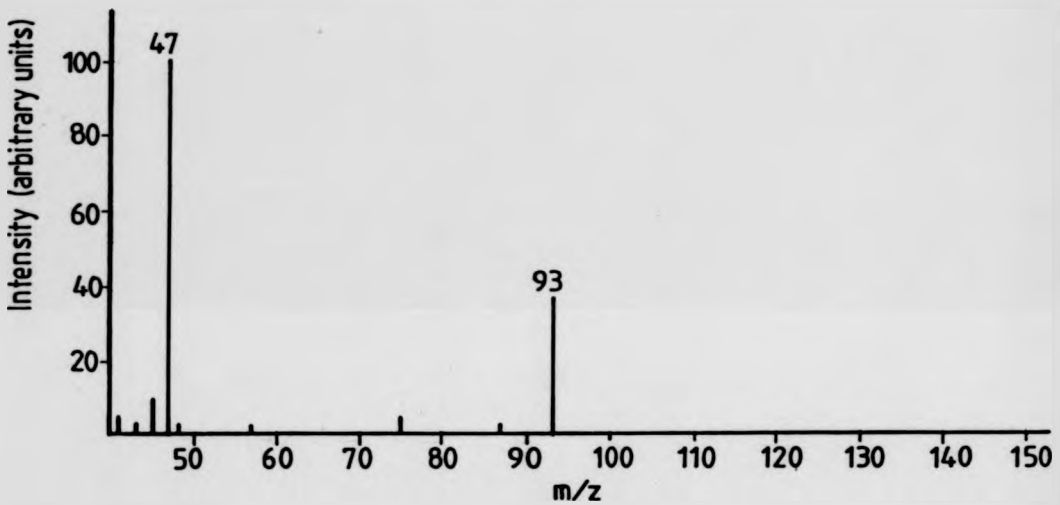

Fig. 5·2. CI. HIGH PRESSURE SPECTRUM OF 0·026% OF 1.4 $CH_3C_6H_4CH_3$ IN CH_4 AT 1 TORR. 473 K

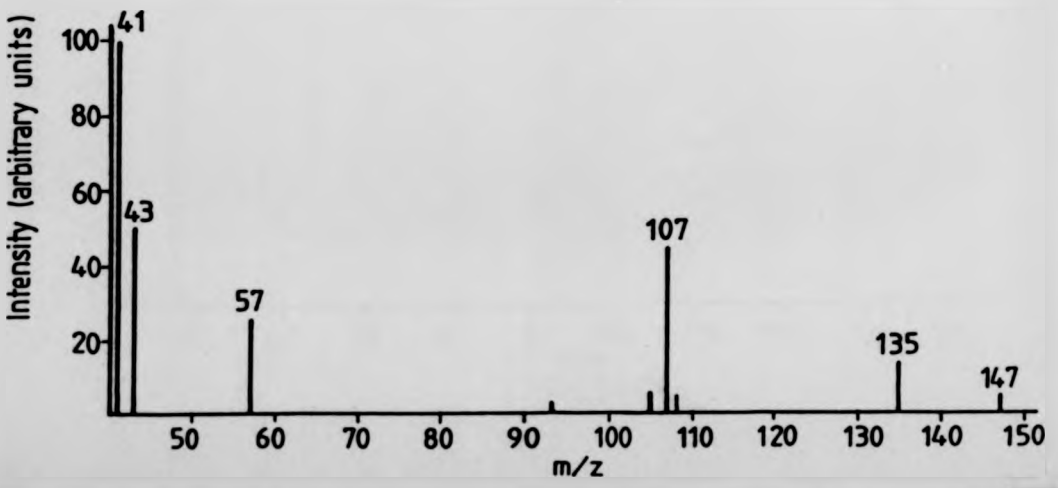

CI, HIGH PRESSURE MASS SPECTRA OF 0·025% OF

$\frac{1,4\,[CH_3C_6H_4CH_3]}{[(CH_3)_2O]}$ = 15·3 AT 473 K, 2 TORR (Fig. 5·3)

0·5 TORR (Fig 5·4)

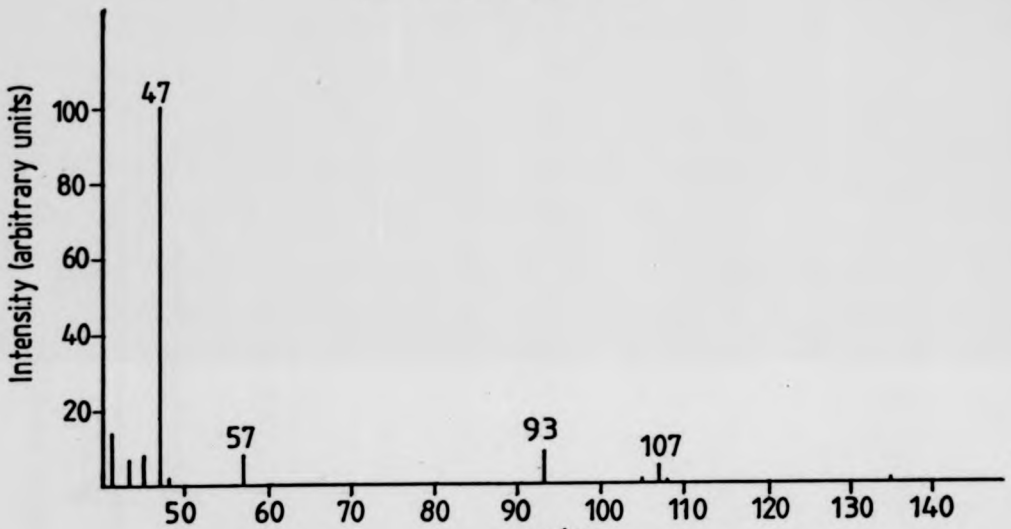

Fig. 5·3

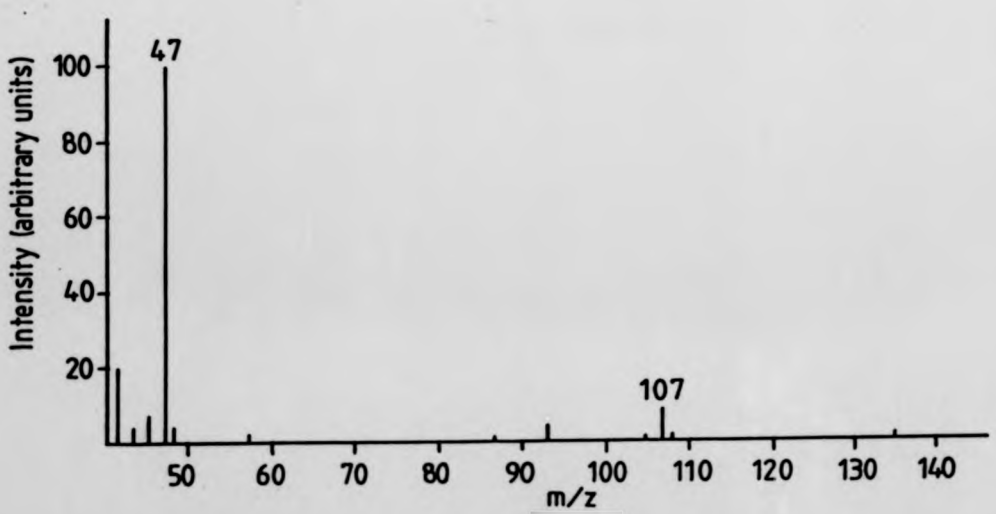

Fig. 5·4

CI. HIGH PRESSURE SPECTRUM OF 0·025% OF

$\frac{[1,4\ CH_3C_6H_4CH_3]}{[(CH_3)_2O]}$ = 15·3 IN CH_4 AT 2 TORR. 608 K

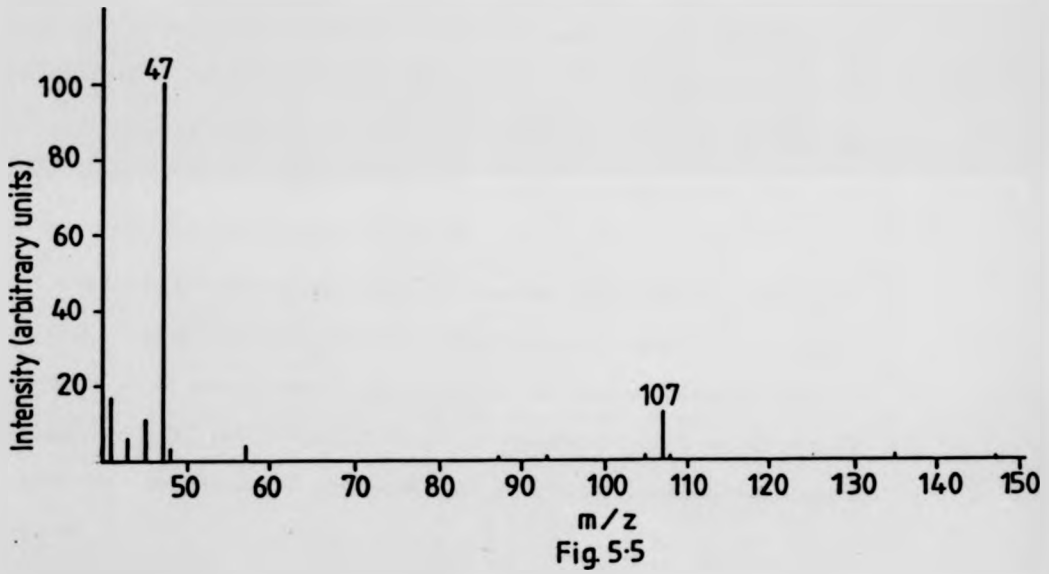

Fig. 5·5

of dimethylether by loss of H_2. The peaks at m/z = 75 and 87 are the adduct ions arising from dimethylether (m/z = 46) plus $C_2H_5^+$ (m/z = 29) and $C_3H_5^+$ (m/z = 41) respectively. These adducts are usually seen in CI with CH_4. These adduct ions are not competing with PTR under study but rather they are formed from the neutrals. The neutrals are present in very large amounts compared with the ions of interest and so their concentration is assumed to be kept constant during experiments.[5.2] The formation of ion at m/z = 45 can compete with PTR if it arises from decomposition of the ion of m/z = 47. Nevertheless its intensity is never above 10% of m/z = 47, consequently the interference would be within the experimental error.

The cause of concern is the proton bound dimer at m/z = 93. This certainly, consumes, in its formation, one of the basic ions of the PTR under study, the protonated molecular ion of dimethylether (m/z = 47).

The figure 5.2 shows a spectrum of *para*xylene. Again the ions $C_3H_5^+$, $C_3H_7^+$ and $C_4H_9^+$ arising from the methane CI spectrum are present. The protonated molecular ion of *para*xylene is seen at m/z = 107 and its adducts formed by $(CH_3)_2C_6H_4+C_2H_5^+$ and $(CH_3)_2C_6H_4+C_3H_5^+$ are displayed at m/z = 135 and 147 respectively. In the case of the *para*xylene no sign of competing reactions is observed.

In figures 5.3, 5.4, and 5.5, both reagents are present. The basic peaks are still the same. The peak of mass 93 has a typical behaviour as a dimer. At 473K as the pressure decreases from 2 Torr to 0.5 Torr the intensity of peak 93^+ decreases from 9% to 4% of the intensity of peak 47^+, (figures 5.3 and 5.4). On the other hand at a constant total pressure of 2 Torr, the intensity of peak 93^+ changes from 9% of 47^+ intensity to 1.2% intensity, as the temperature is raised from 473K to 608K (see figures 5.3 and 5.5).

An analogous pattern is shown in figures 5.9 and 5.10 where *ortho*-

xylene/dimethylether and *meta*-xylene/dimethylether spectra are recorded.

5.3 The Competing Reactions

The observation of an ion with m/z=93 in the dimethylether spectrum indicated existence of a proton bound dimer ion $[(CH_3)_2O]_2.H^+$. The intensity of the dimer peak seemed considerably reduced at 608K; it is shown in figure 5.5 to be only 1.2% of the intensity of peak 47.

Measurements of K with temperature dependence could not be performed as temperature above 608K were not attainable due to equipment limitations. It was critical to find out how the competing process, leading to the dimer ion, was affecting the actual PTR of interest. Firstly, measurements of K were made using different concentration ratios of neutrals by varying the partial pressure of dimethylether and keeping the total pressure constant. Secondly a comparison between the behaviour of K versus total pressure and the behaviour of the ratio of intensities of the ions of m/z = 93 and 47 versus total pressure, was also made.

The results of the former study are displayed in figure 5.6. At 571°K and at a total pressure of 2.5 Torr in the reactor, the amount of *para*xylene was kept at 0.1μl ($7x10^{-3}$) Torr for 760 Torr of CH_4 in the inlet system and the amount of dimethylether (DME) from 0.05 Torr to 0.2 Torr was varied. It is apparent from figure 5.6 that for a partial pressure of DME $<$ 0.1 Torr the equilibrium constant remain reasonably constant, thus any neutral concentration ratio used must fulfil this requirement. The behaviour of ratio $I_{93}+/I_{47}+$ was also observed under the same conditions. The values of the ratios keep constant at very low values (0.1) so their influence seems to be negligible. This confirms the very low intensities of ions 93 observed at values above 575K, for example at 608K. Experiments made under the same conditions but with 0.2μl of *para*xylene and keeping amounts of DME above 0.2 Torr give results consistent with previous experiments. This confirms that the dependence of K on partial pressure is associated with DME.

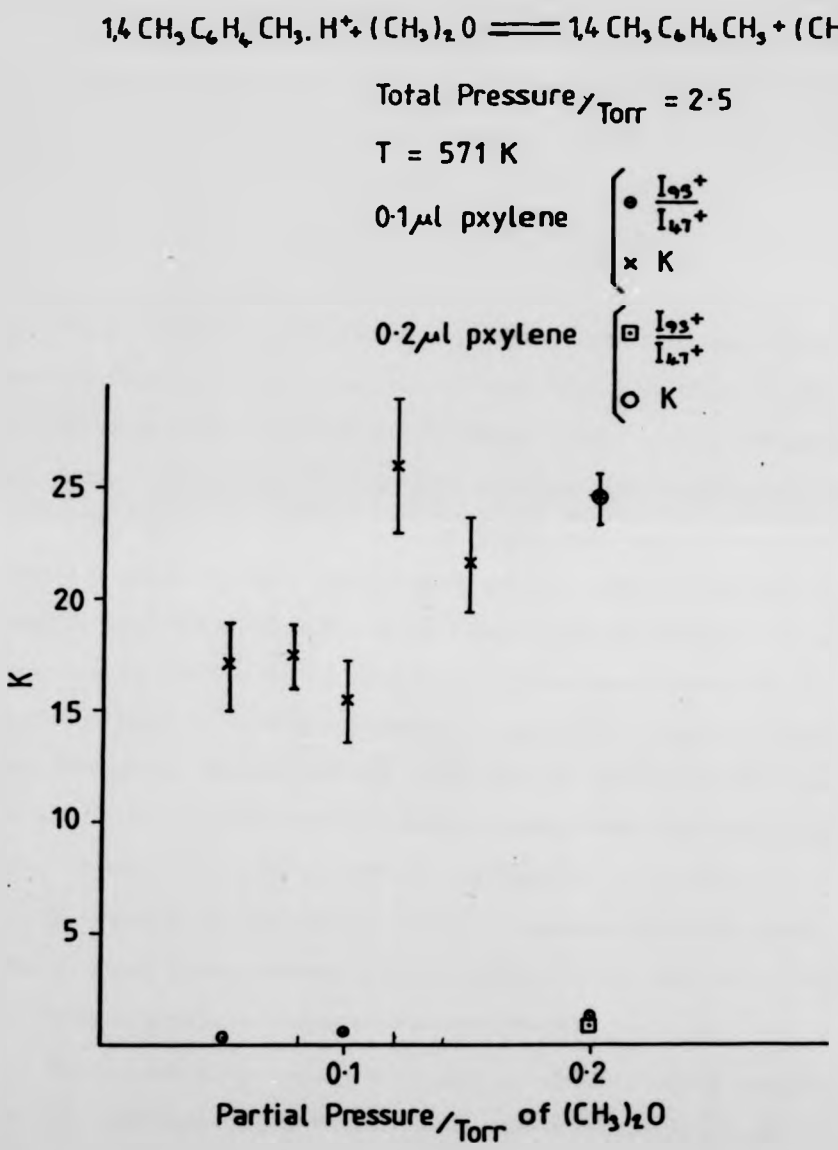

Fig. 5·6 K and $\frac{I_{93}^+}{I_{47}^+}$ vs. PARTIAL PRESSURE OF $(CH_3)_2O$

The results of the second study can be seen in figure 5.7. The very first measurements of K at 475K and 571K up to 3 Torr led to doubts of an equilibrium being reached since K seemed to be varying with total pressure. The extension of the pressure range up to 4 Torr proved that at 475K either equilibrium was being reached or a steady state was occurring. At 571K as the ratio of I_{93^+}/I_{47^+} was negligible an equilibrium state was being reached. This last finding agrees again with the low intensities of peak 93^+ around 608K.

These studies were not very conclusive. The positive conclusions to be drawn were that amounts of DME should be kept below 0.1 Torr, and that equilibrium was reached at 571K as expected. At 475K the variation of I_{93^+}/I_{47^+} with pressure was similar to the variation of K with pressure. Although K is constant above 2.5 Torr doubts still remain as to whether a true equilibrium or a steady state is being reached as mentioned above. The attempt to avoid the dimer by choosing a small range of temperature, 473—608K, to make the experiments and using low pressures, was not suitable for the calculation of thermodynamic properties, which have to be based on the widest temperature range possible. It had been thought that although the competing reaction might affect the equilibrium under study, the effect could fall within the 20% of maximum scatter, quite often found in these measurements, as the intensity of peak 93^+ was 9% of peak 47^+ at 473K.

At this stage two alternatives seemed to be available to solve the problem; either to choose another reference compound to substitute for DME or to modify the heating in order to perform experiments above 608K.

The first alternative was abandoned after an attempt involving nbutylbenzene (PA = 804kJmol^{-1} vs 803kJmol^{-1} for *para*xylene[5.3]) whose spectra showed a peak at m/z = 107. The protonated molecular peak of *para*xylene has the same m/z and in this case they were not separable by high resolution.

Although difficult, the second alternative was the only one left and it was

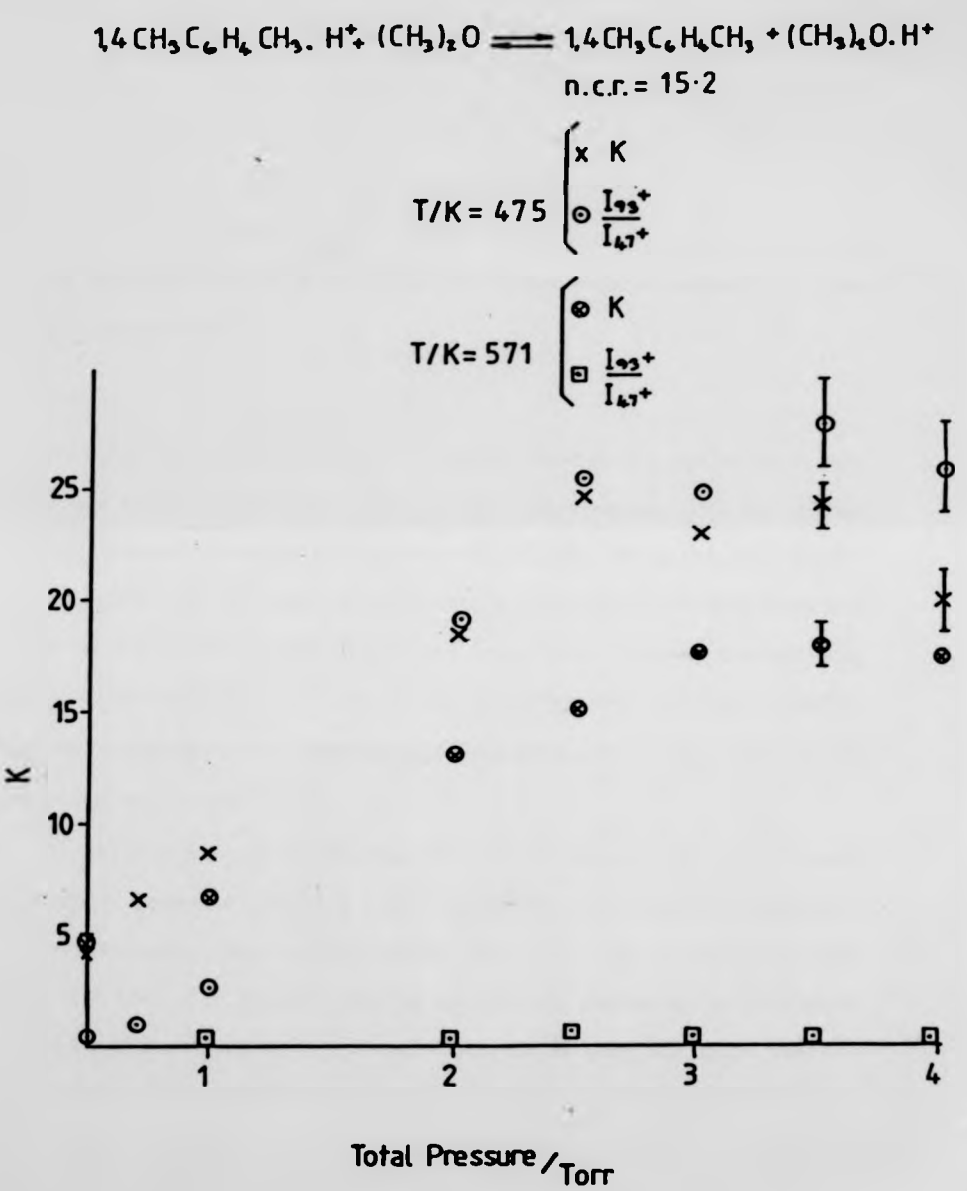

Fig. 5·7 K and $\frac{I_{93}^+}{I_{47}^+}$ vs. TOTAL PRESSURE

decided to try it. Two new heaters were attached to the source block and a spare power supply was used. After that, temperatures of up to 758K. (section 3.1.1) were attainable.

Spectra taken under the new conditions are recorded in figures 5.8, 5.9 and 5.10. At 758K (Fig. 5.8) the dimer peak is not seen at all. Spectra run for *ortho*xylene and *meta*xylene are presented in figures 5.9 and 5.10 respectively. The pattern displayed there, is in agreement with the description outlined along this section for *para*xylene.

5.4 Results

Initially, given the conclusions in section 5.3, the temperature range for the experiments was chosen to be 571K−750K. As the measurements of K. for proton transfer between *para*xylene-dimethylether showed that the temperature dependence appeared to be very small or zero, measurements below 571K were made and the results were consistent with the previous data. Hence one could conclude that the formation of $[(CH_3)_2O]_2.H^+$ ion was not competing with the proton transfer. Since then the experiments for these systems have been performed at a wider range of temperatures from 370−750K.

As in Chapter 4 the experimental data were gathered in the form of van't Hoff plots in figures 5.11, 5.12 and 5.13 for *meta*xylene-dimethyleter, *ortho*xylene-dimethylether and *para*xylene-dimethylether respectively. The pressure range was always 1-6 Torr. The standard enthalpy and entropy changes for reaction (5.1) derived from those van't Hoff plots were summarised in table 5.1. Again, exactly as in Chapter 4, the errors referred to in this table are standard deviations.

CI, HIGH PRESSURE SPECTRUM OF 0·025 % OF

$\frac{[1,4\,CH_3C_6H_4CH_3]}{[(CH_3)_2O]}$ = 15·3 IN CH_4 AT 2 TORR, 758 K

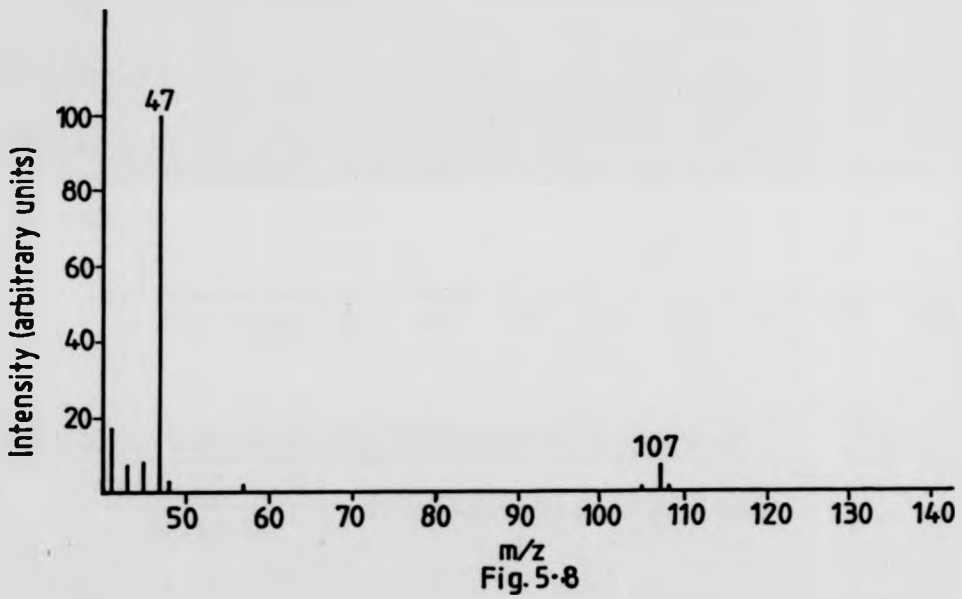

Fig. 5·8

Fig. 5·9 CI. HIGH PRESSURE SPECTRUM OF 0·025% OF $\frac{[1,2\,CH_3C_6H_4CH_3]}{[(CH_3)_2O]}$ = 25·5 IN CH_4 AT 2·5 TORR, 623 K

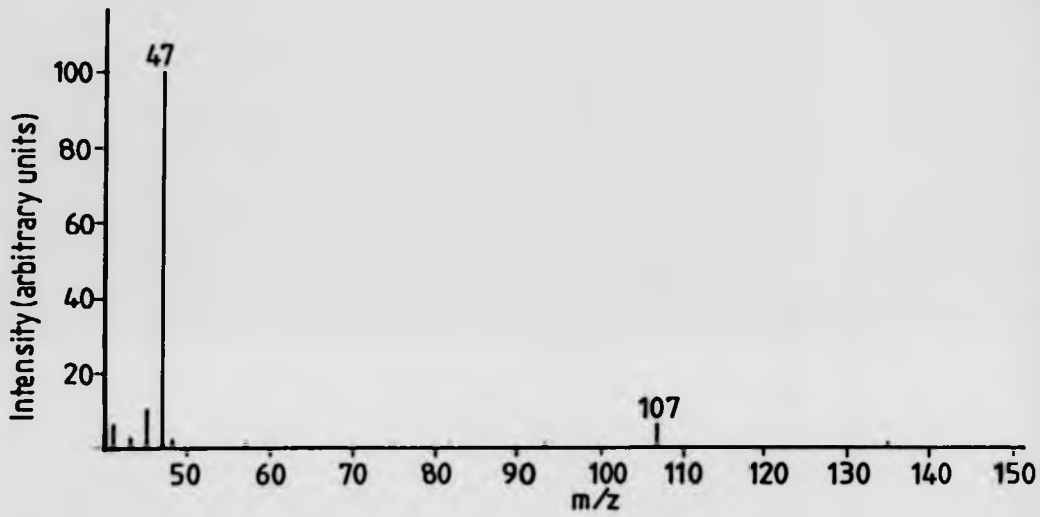

Fig. 5·10 CI, HIGH PRESSURE SPECTRUM OF 0·025% OF $\frac{[1,3\,CH_3C_6H_4CH_3]}{[(CH_3)_2O]}$ = 51·3 IN CH_4 AT 5 TORR, 623 K

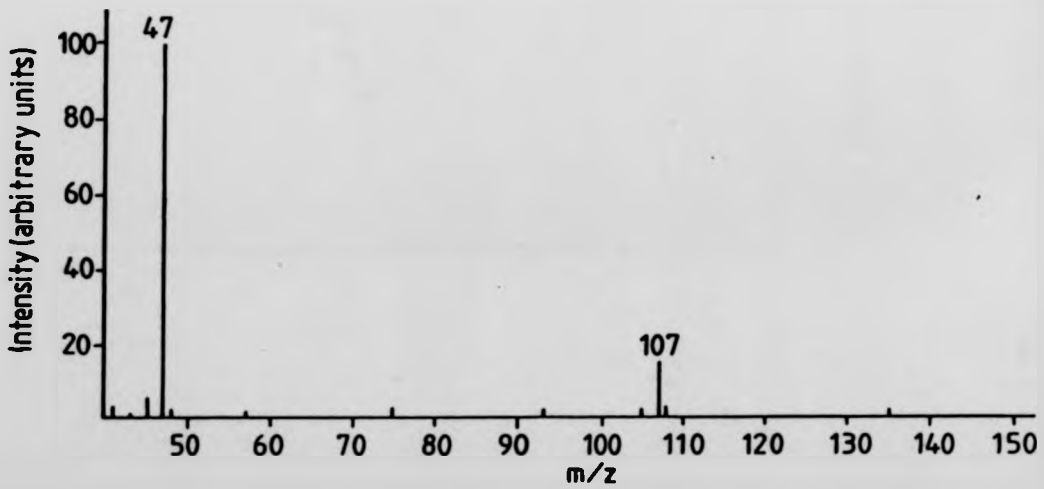

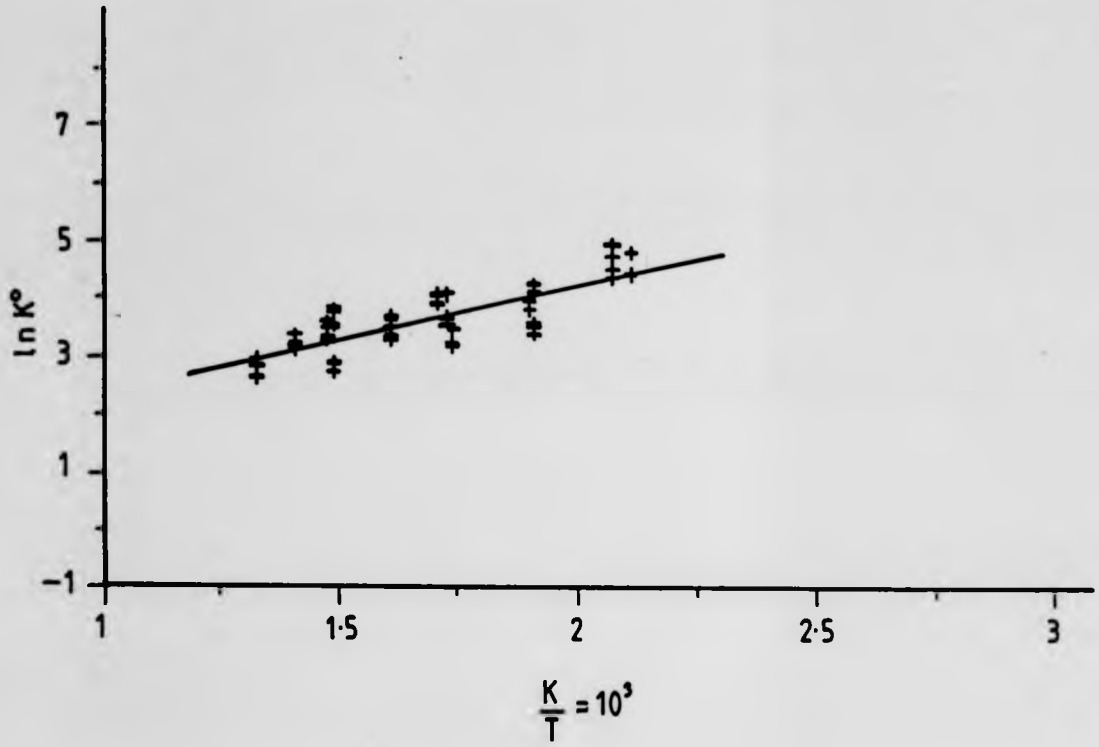

Fig. 5·11 van't Hoff Plot for Reaction

$$(CH_3)_2O{\cdot}H^+ + 1{,}3\,(CH_3)_2C_6H_4 \rightleftharpoons (CH_3)_2O + 1{,}3\,(CH_3)_2C_6H_4H^+$$

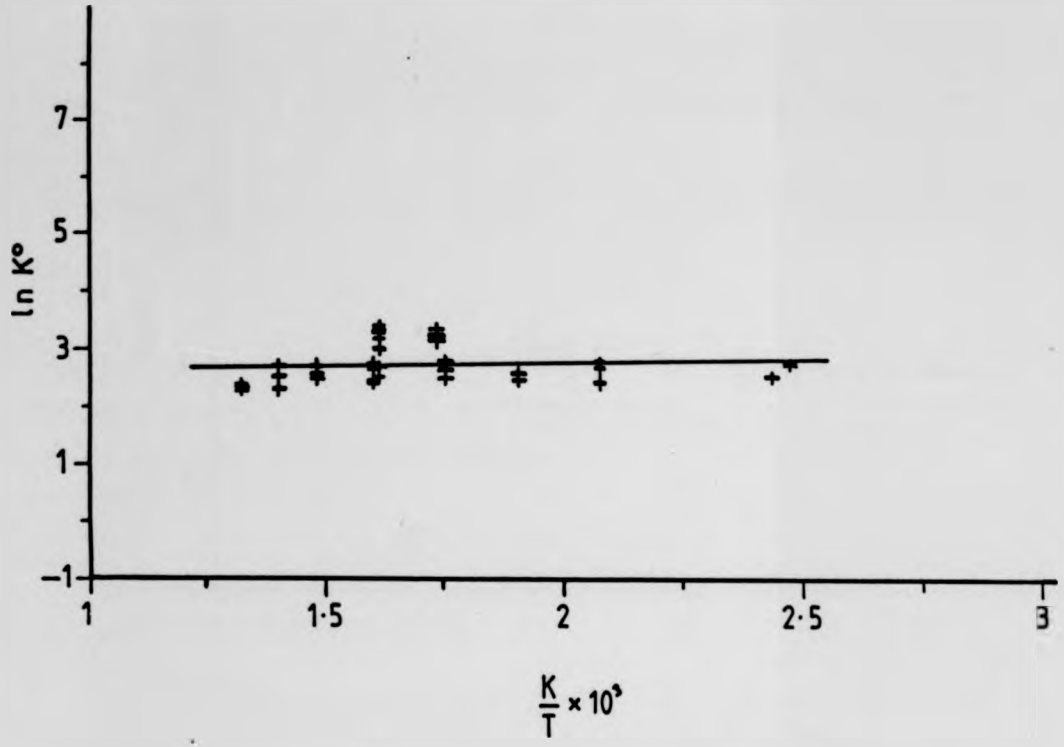

Fig. 5·12 van't Hoff Plot for Reaction

$(CH_3)_2O.H^+ + 1,2\,(CH_3)_2C_6H_4 \rightleftharpoons (CH_3)O + 1,2\,(CH_3)_2C_6H_4H^+$

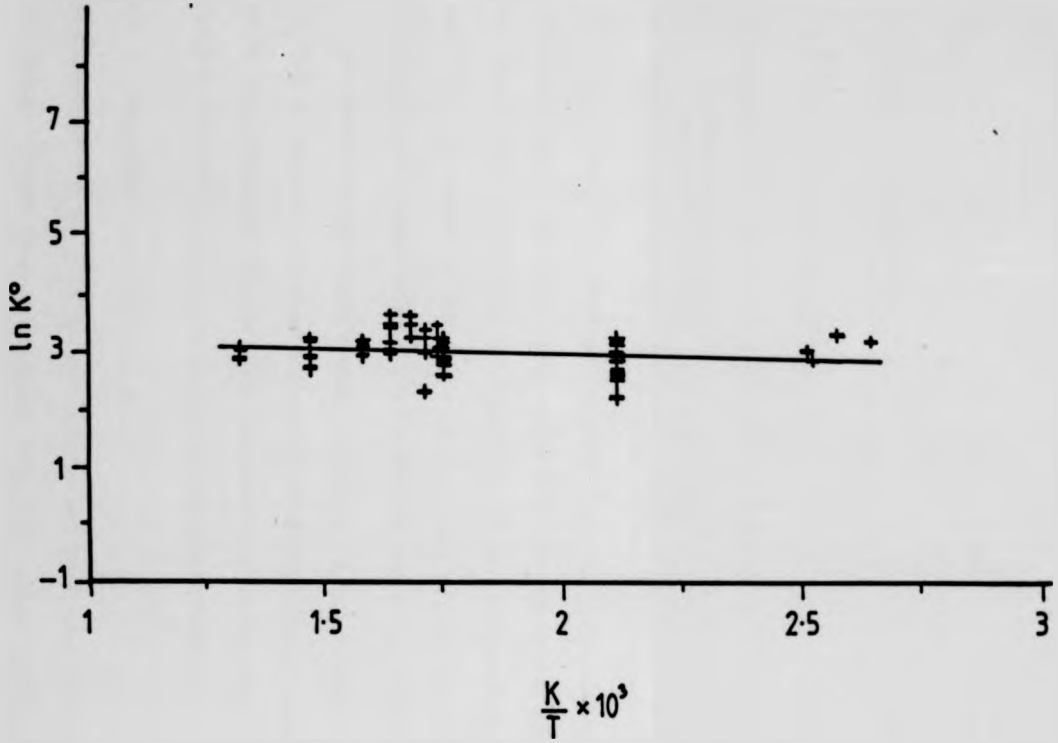

Fig. 5·13 van't Hoff Plot for Reaction

$$(CH_3)_2O{\cdot}H^+ + 1,4\,(CH_3)_2C_6H_4 \rightleftharpoons (CH_3)_2O + 1,4\,(CH_3)_2C_6H_4{\cdot}H^+$$

Table 5.1

Summary of Data

$AH^+ + B \rightleftharpoons A + BH^+$

A	B	n	[A]/[B]	ΔH° $kJmol^{-1}$	ΔS° $Jmol^{-1}K^{-1}$	ΔS^a_{rot} $Jmol^{-1}K^{-1}$
$(CH_3)_2O$	1,3-$C_6H_4(CH_3)_2$	62	15.3 30.6	-17.1±1.2	2.7±2.0	0 or 5.8
$(CH_3)_2O$	1,2-$C_6H_4(CH_3)_2$	43	25.6 15.3	-1.5±1.7	20.4±2.9	5.8
$(CH_3)_2O$	1,4-$C_6H_4(CH_3)_2$	60	15.3 7.7 31.1 23.3 19.4	1.5±1.1	27.7±2.0	5.8

n - Number of experiments
a - protonation assumed to be on the ring

Table 5.1 also contains the calculated rotational entropies for each system. The ΔS_{mix} is likely to lie between 0 - 7.6$JK^{-1}mol^{-1}$. This is concluded from the assumption that for xylenes a similar picture for favoured sites of protonation can be drawn from mechanistic considerations as for halogenotoluenes (section 4.6.3).Thus the number of distinguishable forms may take the values 2, 3, 4 and 5. The ΔS_{mix} became more precise after *ab initio* calculations reported in chapter 7.

In figure 5.14 the relative proton affinities and entropy changes are given in the form of diagrams. Although the entropy changes are not so large as the largest for the halogenotoluenes they show the same order, as expected. Also the relative proton affinities show the same order as in halogenotoluenes.

5.5 A comparison with previous data

Measurements of K for PTR between xylenes and DME were made by Franklin and Chong[5.4]. From these experiments ΔG°_{340} and proton affinities of xylenes relative to DME were obtained. In table 5.2 ΔG° at 340K for the systems studied in this work are compared with the values from Franklin. Also ΔG° at 300K for the same reactions studied here are compared with ΔG° at 300K calculated from

RELATIVE PROTON AFFINITIES

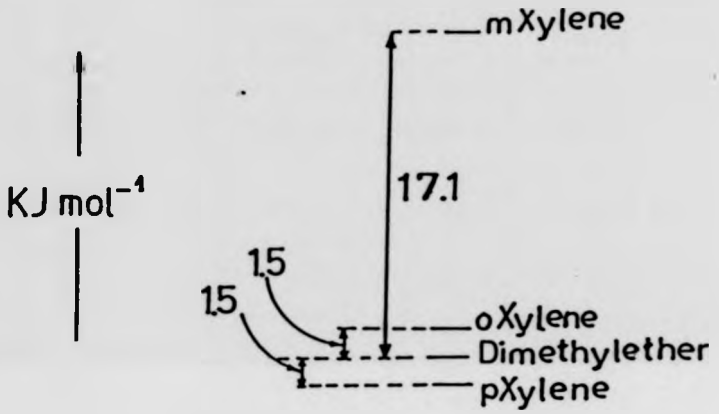

ENTROPY CHANGES

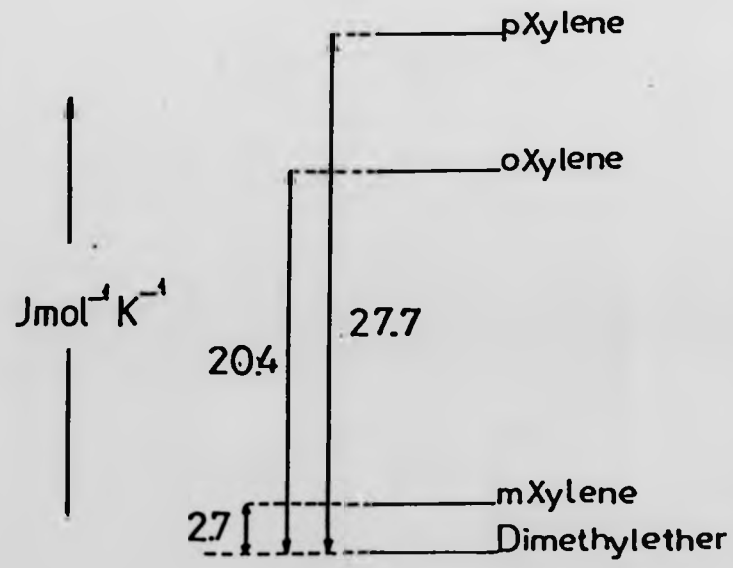

FIG. 5.14

values of gas phase basicities for xylenes and DME recommended by Lias et al.[5.3]

Table 5.2

$$AH^+ + B \rightleftharpoons A + BH^+$$

A	B	$-\Delta G^\circ_{340K}$ [a] ($kJmol^{-1}$)	$-\Delta G^\circ_{340K}$ [b] ($kJmol^{-1}$)	$-\Delta G^\circ_{300K}$ [b] ($kJmol^{-1}$)	$-\Delta G^\circ_{300K}$ [c] ($kJmol^{-1}$)
$(CH_3)_2O$	1,3-$(CH_3)_2C_6H_4$	1.33±0.3	18.0±1.9	17.9±1.8	16.0
$(CH_3)_2O$	1,2-$(CH_3)_2C_6H_4$	1.29±0.2	8.4±2.7	7.6±2.2	8.0
$(CH_3)_2O$	1,4-$(CH_3)_2C_6H_4$	0.97±0.4	7.9±1.8	6.8±1.4	1.0

a - Reference 5.1
b - This work
c - Reference 5.2

In table 5.3 the proton affinities of meta, ortho, and para, xylenes obtained in this work are compared with proton affinities for xylenes determined by Franklin et al[5.4] and with the values recommended by Lias et al[5.3] and coworkers in a compilation based on various measurements.

Table 5.3

	PA[a] $kJmol^{-1}$	PA[b] $kJmol^{-1}$	PA[c] $kJmol^{-1}$
1,3-$(CH_3)_2C_6H_4$	785.0±4.5	820	821.1±1.2
1,2-$(CH_3)_2C_6H_4$	784.9±4.4	809	805.5±1.7
1,4-$(CH_3)_2C_6H_4$	784.6±4.6	803	802.5±1.1

a - Reference 5.1
b - Reference 5.2
c - This study. The PAs are relative to DME whose PA was considered to be 804$kJmol^{-1}$ from Reference 5.2.

In both tables the agreement between data from this work and work from Franklin, is fairly good from the qualitative point of view. Franklin et al[5 4] found the order of proton affinities for xylenes agreed with the order found in solution which is the same as in this study. The fact that the quantitative agreement is not so good is not so surprising. Those early experiments[5 4] were performed at one temperature and the experimental conditions were not very reliable. The pressures used were usually below 0.4 Torr so thermalisation was probably not occurring. The ionisation was continuous rather than pulsed. Moreover, the formation of a proton bound dimer ion, $[(CH_3)_2O]_2H^+$, although reported by Franklin as an interference in measurements of K for the system toluene-dimethylether, was not considered as such in xylenes experiments with dimethylether. Thus the data from this work are more extensive and reliable in terms of the thermalisation achieved before measurement, and interference free since much smaller samples of DME were used.

The agreement with Lias et al is much better. In table 5.3 the proton affinities values are fairly consistent, confirming the reliability of the data from this study.

The deviation of Franklin values is justified by the reasons mentioned above and the assumption made that the entropy change for reactions under study was zero.

In table 5.2 qualitative and quantitative agreement with Lias is also good. Only in the case of *para*xylene is the quantitative agreement not so satisfactory.

5.6 Discussion

In Chapter 4 it was stated that the large entropies of protonation found for para and ortho isomers of halogenotoluenes resulted from a genuine effect. Confirmation for this could be sought from studies of proton transfer reactions in systems where the same behaviour ought to be expected.

The explanation outlined in section 4.6.6 was partially based on the relative position of the sites for protonation, and this was determined by the substituents on the aromatic nucleus. In fact, if one recalls section 4.6.3, the replacement of the halogen substituent by a methyl group should not alter the trend qualitatively.

The methyl group and halogen are both electron π donors and para and ortho directing groups for electrophilic attacks as outlined in Section 4.4.3. For xylenes the same combination as in figure 4.23, second row, must be observed, for the substitution of X by CH_3 would induce protonation on the same positions. Consequently the aromatic nucleus is still the expected site for the proton attachment.

Therefore the xylenes appear to be a good choice for providing further evidence for the observed effect in halogenotoluenes. Moreover for the claimed mobility of the proton around the ring, the role of aromaticity was important. Then it was thought that the use of a non aromatic reference compound for xylenes could reinforce the referred effect. These were the reasons for electing the systems studied in this chapter.

Proton Transfer Equilibria involving xylenes had been studied[5 4.5 3.5 5], at one temperature. The entropy changes had been either considered to be zero or estimated from rotational symmetry variation. It is obvious that such experiments could not show any peculiarities in the entropy changes. Only a temperature dependence study could give conclusive evidence about such changes.

For systems with ortho and para compounds the ΔS° measured are larger than the usual ΔS_{rot} and ΔS_{mix}. The data for xylenes show up the same trend already seen for halogenotoluenes. The proton affinities of the different isomers of xylenes are in the same order as those for halogenotoluenes:

$$PA_{meta} > PA_{ortho} > PA_{para}$$

The entropies of protonation (see Section 8.1, Figure 8.2), although not as large as

for some halogenotoluenes, they fall in the same order.

$$S'_{para} > S'_{ortho} > S'_{meta}$$

The fact that the entropies of protonation are lower than for halogenotoluenes is probably due to a smaller donation of π charge to the ring, by the methyl group than by fluorine[5.6]. These studies of Hehre et al[5.6] were performed for toluene and fluorobenzene but the conclusion probably still holds in the compounds under study. The entropy changes for reaction 5.1 are definitely higher ($28 JK^{-1}mol^{-1}$ for paraxylene) than they had been assumed in previous studies. These results confirmed the predictions made earlier.

Agreement is obtained from *ab initio* calculations[5.7] STO-3G with the order shown above. From the same reference the most stable protonated species for each isomer are:

Metaxylene Orthoxylene Paraxylene

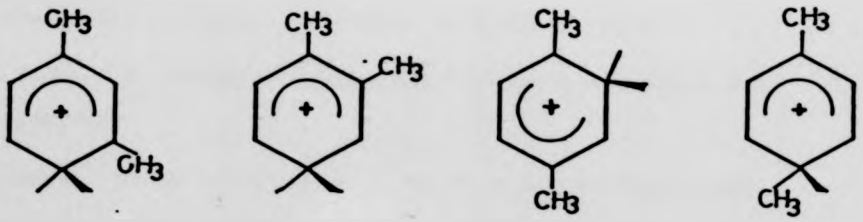

The three first structures had been predicted in section 4.6.3 (see figure 4.23). The fourth has also received support from CNDO/2 calculations[5.8] for halogenotoluenes.

Another point that deserves to be stressed is the relation between $\Delta H°$ and $\Delta S°$ values which is here opposite to that found for halogenotoluenes where large

ΔH° values were associated with large ΔS° values. In the xylenes the proton affinities of dimethylether is close to that for *para* and *ortho*xylene. This gave rise to a shallow slope of the van't Hoff plot (small ΔH°) and a high intercept (large ΔS°). No doubts can arise, now, about consistent errors in the large slopes of halogenotoluenes being magnified at the intercept from which anomalously large entropy changes would arise. This was extensively discussed in ref 4.3 in terms of the isokinetic relationship.

5.7 References

5.1 P. Kebarle, R. Yamdagni, K. Hiraoka and T.B. McMahon, Int. J. Mass Spectrom. Ion Phys. 1976, 19, 71

5.2 K.G. Hartman and S.G. Lias, Int. J. Mass Spectrom. Ion Phys., (1978), 28, 213

5.3 S.G. Lias, J.F. Liebman and R.D. Levin, J. Phys. Chem. Ref. Data (1984), 13

5.4 S.L. Chong and J.L. Franklin, J. Am. Chem. Soc. (1972), 94, 6630

5.5 W.J. Hehre, R.T. McIver, J.A. Pople, P.R. Schleyer, J. Am. Chem. Soc. (1974), 96, 7162

5.6 W.J. Hehre, L. Radom and J.A. Pople, J. Am. Chem. Soc., (1972), 94, 1496

5.7 J.L. Devlin, J.F. Wolf, R.W. Taft, W.J. Hehre, J. Am. Chem. Soc., (1976), 98, 1990

5.8 J . Burdon, personal communication (Chemistry Department, University of Birmingham)

CHAPTER 6: THERMOCHEMISTRY OF GAS PHASE PROTON TRANSFER REACTIONS IN MIXTURES CONTAINING BENZENE OR OTHER SUBSTITUTED BENZENES

6.1 INTRODUCTION

In this chapter data will be presented for proton transfer reactions in systems involving benzene and mono- and di-substituted benzenes. In an attempt to relate the various systems studied so far, measurements on the following group of systems were carried out:

benzene–*para*fluorotoluene
toluene–*meta*fluorotoluene
toluene–dimethylether

A final system, benzaldehyde–diethylether, was chosen, where protonation was expected to take place on the substituent, unlike the other systems studied.

6.2.1 The benzene–*para*fluorotoluene system

When the real proton affinities of halogenotoluenes were first measured, it was predicted that the proton affinity of benzene would probably be much closer to proton affinity of *para*fluorotoluene than had been established in previously published data[6.1]. This was expected to occur in the temperature range 330-575K over which the experiments on halogenotoluenes were carried out.

On the other hand, for the large entropy excess measured due to the protonation of para and ortho halogenotoluenes and xylenes, the rationalisation proposed, in section 4.6, indicated that benzene could also have a large entropy due to protonation.

The experiments with benzene were first carried out with *para*fluorotoluene

as reference compound. Attempts to perform experiments with an aliphatic reference compound were abandoned because of competing reactions.

6.2.1.2. Results

From the chemical ionisation (CI) spectra shown in figure 6.1 to 6.4 and figure 4.1 it can be shown that the chemistry of the systems is apparently very simple.

The main peaks in figure 6.1 occur at m/z=79, 107 and 119 which correspond to the protonated molecular ion and adduct ions $(M+C_2H_5)^+$ and $(M+C_3H_5)^+$ respectively. As has been pointed out in previous chapters, the formation of this type of adduct ions, in methane, does not occur through interfering side reactions of proton transfer. The same arguments can be used to predict the absence of competing reactions in *para*fluorotoluene. In the spectrum in figure 4.1, besides the protonated molecular peak and equivalent adduct peaks, a peak at m/z=107 can be seen; that peak does not arise from any competing reaction was justified in section 4.3.

Both compounds of the system are simultaneously present in spectra displayed in figure 6.2 to figure 6.4. No newly formed ionic species can be observed.

The measurements of equilibrium constants for

$$C_6H_7^+ + CH_3C_6H_4F \rightleftharpoons C_6H_6 + CH_3C_6H_4F.H^+ \qquad (6.1)$$

were performed in the temperature range 330 - 570K.

The van't Hoff plot of the experimental data has a curved shape. The curvature starts at 480K and is directed upwards, as can be seen in figure 6.5, producing extremely large K values at the upper temperature limit.

The pattern of spectra at temperatures above 480K was always similar to figure 6.4. As was mentioned above, a thorough check for any reactions producing new species which might account for the observations, was negative. No obvious interpretation for the diverging van't Hoff plot was found at the time, although a

Fig. 6·1 CI. HIGH PRESSURE SPECTRUM OF 0·05% C_6H_6 IN CH_4 AT 2 TORR, 443 K

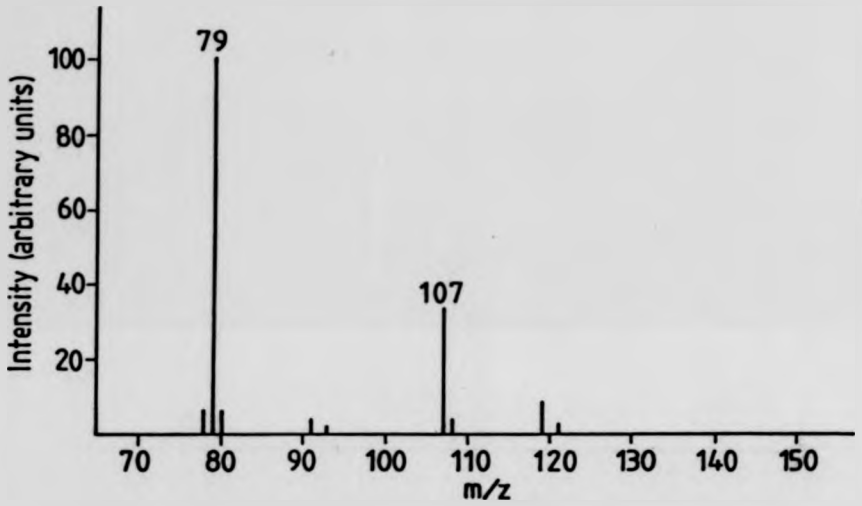

Fig. 6·2 CI, HIGH PRESSURE SPECTRUM OF 0·05% OF $\frac{[C_6H_6]}{[1,4\,CH_3C_6H_4F]}$ = 2·9 IN CH_4 AT 2 TORR, 343 K

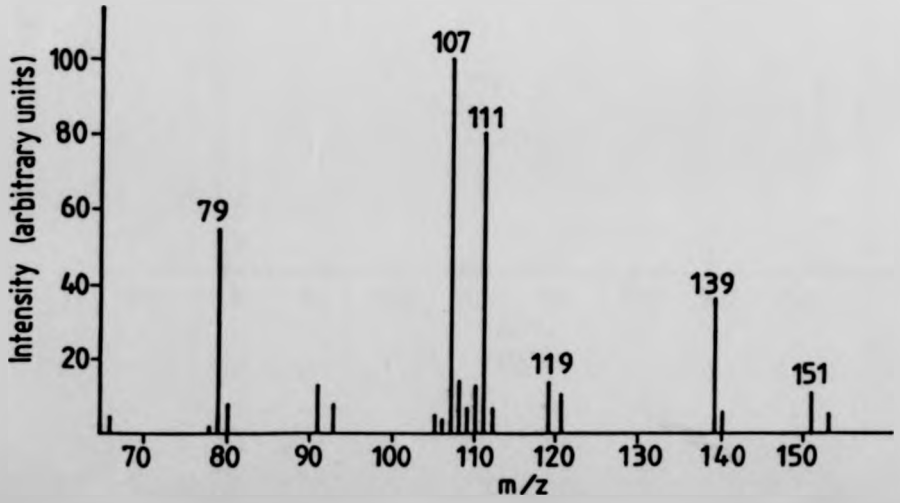

CI, HIGH PRESSURE SPECTRA OF 0·05% OF

$\frac{[C_6H_6]}{[1,4\,CH_3C_6H_4F]}$ = 15·1 IN CH_4 AT 1·5 TORR, 514 K (Fig. 6·4)

2 TORR, 443 K (Fig. 6·3)

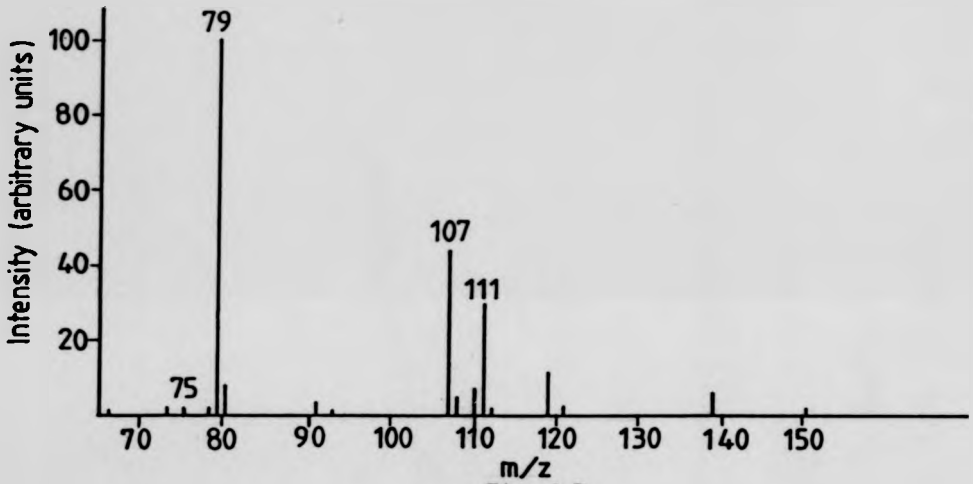

Fig. 6·3

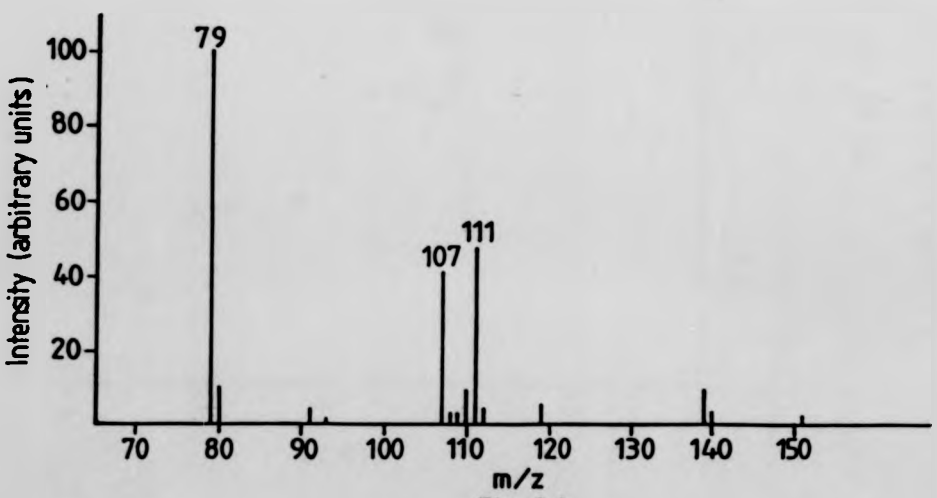

Fig. 6·4

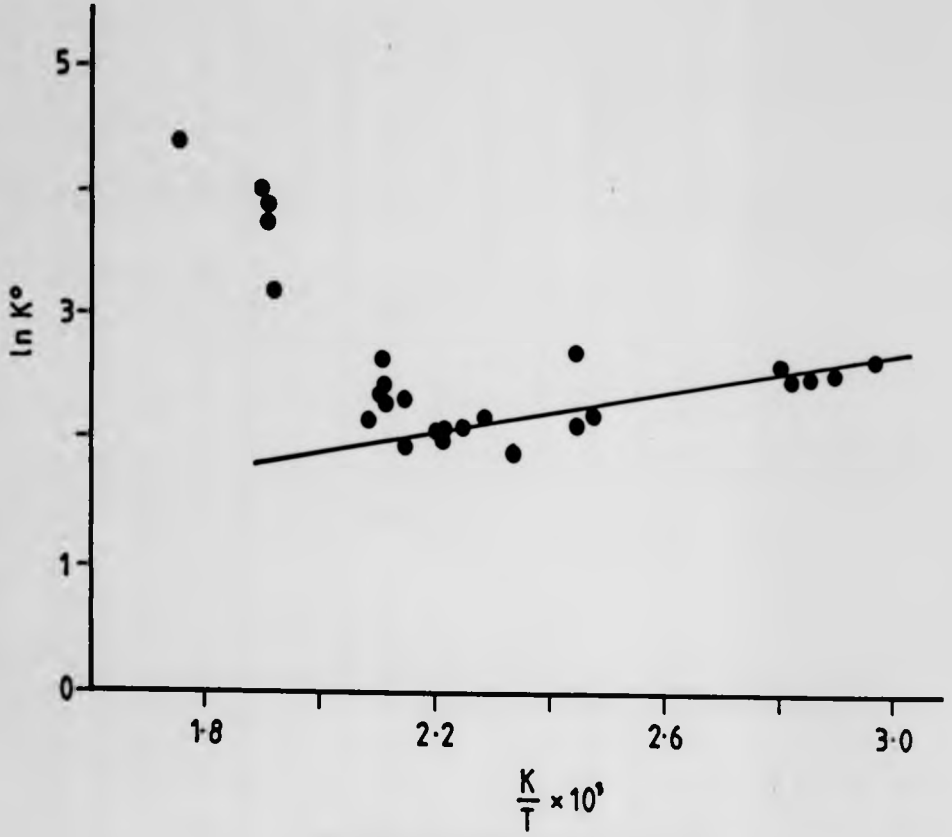

Fig. 6.5 van't Hoff Plot for Reaction

$C_6H_7^+ + CH_3C_6H_4F \rightleftharpoons C_6H_6 + CH_3C_6H_4F.H^+$

suggestion by Mason et al.[62] will appear in the literature in the near future. In order to avoid the divergent region the thermodynamic properties were determined from measurements taken at temperatures below 480K.

A summary of thermodynamic data from various sources is gathered in table 6.1.

Table 6.1

$-\Delta H^{o(a)}$	$-\Delta H^{o(b)}$	$-\Delta G^{\circ}_{400}{}^{(c)}$	$-\Delta G^{\circ}_{400}{}^{(b)}$	$\Delta S^{o(a)}$	$\Delta S_{rot}{}^{(d)}$	$\Delta S_{mix}{}^{(e)}$
3.9±1	18.3	7.9	13.6	9.9±3	-14.9	+9.1

Units
$\Delta H°/kJmol^{-1}$
$\Delta G°/kJmol^{-1}$
$\Delta S°/JK^{-1}mol^{-1}$

References
(a) this work
(b) from ref 6.1
(c) this work, calculated at 400K
(d) calculated, $\Delta S_{rot}=R\ln\frac{3x1}{12\pi1}$
(e) calculated, $\Delta S_{mix}=R\ln3$ (see figure 7.1)

6.2.1.3 Discussion and conclusions

The study of reactions (6.1) with temperature variation confirmed the prediction about the proton affinity of C_6H_6. In table 6.1 the difference in proton affinities between benzene and *para*fluorotoluene is established to be 3.9 in the range of temperature of the experiments rather than the 18.3 $kJmol^{-1}$ found[61] previously.

The entropy change must be carefully analysed. The proposed model discussed in section 4.6 which rationalised the large entropy changes measured in terms of the occurrence of an internal translational contribution to entropy, must be applicable to benzene. The model was based on the possibility of intramolecular exchange of the proton when equally favoured adjacent sites for protonation are available. Furthermore if the adjacent positions have a similar energy content the barrier for the proton transfer between them must be low, allowing internal translation. This makes benzene an amenable compound for such observations as it possesses six equivalent positions for protonation. The intramolecular exchange of the proton was previously observed for protonated benzene in liquid and gas phase[63,64]. Values for these barriers will be discussed in chapters 7 and 8.

The entropy change measured for reaction (6.1) is not very large when compared to the largest changes measured for the halogenotoluene mixtures or xylene systems. Nevertheless this is not in disagreement with the expectation for benzene because both compounds involved, C_6H_6 and 1,4-$FC_6H_4CH_3$ (5 positions nearly equally favoured for protonation, see section 4.6.4 and chapter 7), are supposed to contain large internal translational entropy contributions which are likely to cancel to a large extent. Furthermore the expections of a large entropy of protonation for benzene are confirmed. For the sake of comparison if one expresses the entropy of protonation of C_6H_6 relative to 1,3-$FC_6H_4CH_3$, (see figure 8.2) the actual value is 50 $JK^{-1}mol^{-1}$ which is rather large. It cannot be compared with the rotational and mixing contributions.

What is surprising at first sight is that the entropy change is positive as C_6H_6 would be expected to have a larger $S'_{C_6H_6}$ (entropy of protonation) than 1,4-$FC_6H_4CH_3$. Although the values for barrier heights, calculated by *ab initio* and semi-empirical methods (see chapters 7 and 8), for internal proton migration in benzene do not appear to be definite it seems reasonable to assume that they might be higher in C_6H_6 than in 1,4-$FC_6H_4CH_3$. This assumption would account for the entropy of protonation of 1,4-$FC_6H_3CH_3$ being larger than entropy of protonation of C_6H_6.

6.2.1.4 Another reference compound for benzene

Two reasons were decisive in the choice of another reference compound for benzene. Firstly it was felt that the use of an aliphatic reference compound would enhance the entropy of protonation of benzene. Secondly a new system would probably overcome the problem of the curved van't Hoff plot allowing a wider temperature range.

The choice is always restricted by the exothermicity of the reaction. The difference in proton affinities recommended is circa 20 kJ $mole^{-1}$.

Methanol was readily available and the proton affinity difference was about 2 $kJmole^{-1}$ for both reactants involved in reaction 6.2.

$$C_6H_6 + CH_3OH.H^+ \rightleftharpoons C_6H_7^+ + CH_3OH \qquad (6.2)$$

Unfortunately it was impossible to overcome the formation of proton bound dimers.

For a neutral concentration ratio of 6. reaction (6.2) shows the pattern in figure 6.6 under the experimental conditions of the measurements taken to produce the graph. The usual peaks arising from the protonated molecular ions occur at $m/z = 33$ and 79 for methanol and benzene respectively. The peaks resulting from adduct ions formed in methane. with general formula $(M + C_2H_5)^+$ and $(M + C_3H_5)^+$, are at $m/z = 107$ and 119 for C_6H_6.

Furthermore methanol shows an intense dimer ion $(CH_3OH)_2.H^+$, whose peak is situated at $m/z = 65$ and another peak at $m/z = 47$ which probably results from the dimer ion by loss of water. A similar reaction must produce a peak of mass 79 from a proton bound trimer ion since 79 mass peak was found to be composite.

Given that the intensity of the dimer peak is as large as the intensity of the molecular peak, a smaller neutral concentration ratio was tried by reducing the concentration of methanol. Thus in figure 6.7 the dimer peak of methanol has its intensity reduced to 21% of the molecular peak. Under these experimental conditions the observation of peaks of mass 33, 65 and 79 in pulsed mode showed a very poor pulsed profile for the two first peaks. The decay was very sharp for both, not having a proper free diffusion zone. Within 25.000 sweeps the number of counts was just 45 for the peak of mass 33 and 50 counts for the peak of mass 65 which is a very low number of counts, close to noise signals. The peak of mass 79 had a better pulsed profile, an acceptable number of counts, 200, at the beginning of the free diffusion zone, but was still not very high compared with the usual range, 150

C.I. HIGH PRESSURE SPECTRA IN CH_4 OF 0·026% OF $\frac{[C_6H_6]}{[CH_3OH]}$ AT 4 TORR, 570 K IN (Fig 6·6) n.c.r. = 6 IN (Fig 6·7) n.c.r. = 0·6

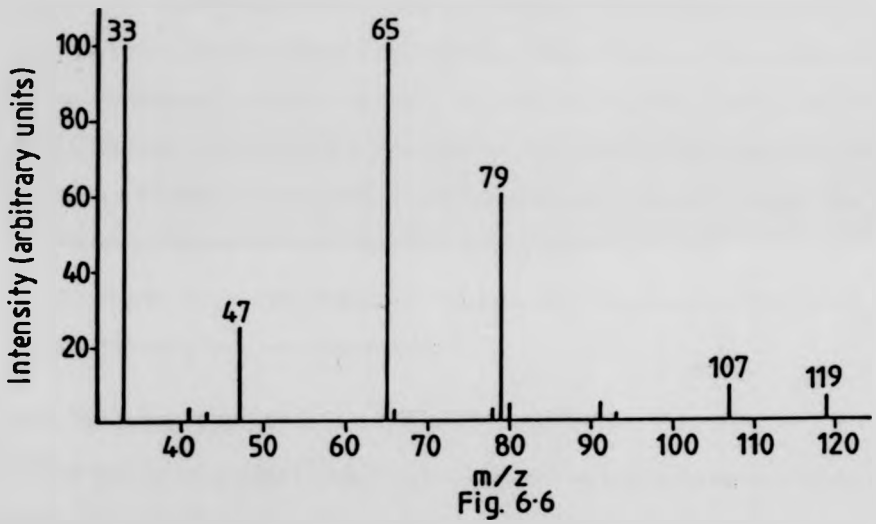

Fig. 6·6

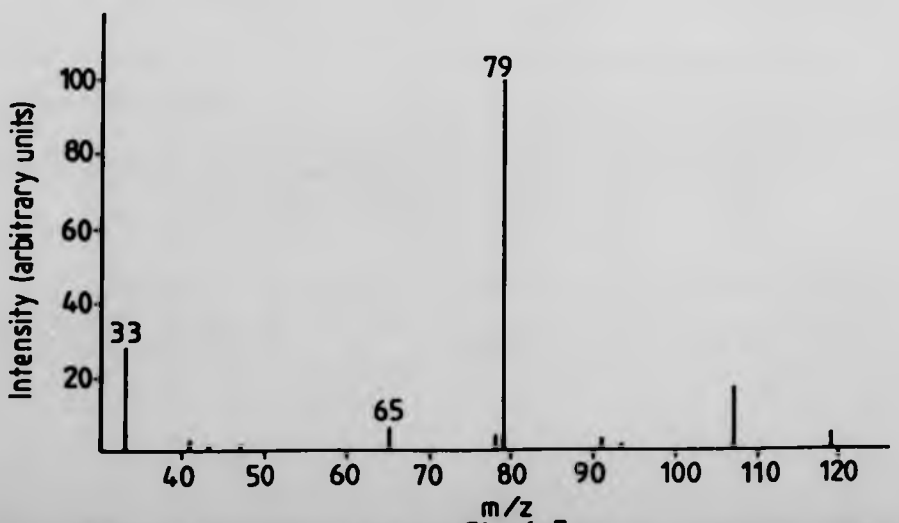

Fig. 6·7

to 1000 counts, at the beginning of the free diffusion zone.

One last attempt with a neutral concentration ratio equal to 1.68 did not significantly improve this picture.

This system presented various difficulties: first of all a double peak of mass 79. secondly the occurrence of strong dimers. In order to overcome the formation of dimers a temperature much higher than 573K would be necessary as a starting temperature. With a n.c.r. of 0.6 at 573K the intensity of the dimer was still 21% of the molecular peak of methanol. Nevertheless it would be necessary to raise the amount of methanol in order to improve the pulsed profile of the peak at m/z = 33. If 573K could not be used as a lower limit for n.c.r. = 0.6. an increase of n.c.r. would raise further the lower limit of the experimental temperature range. This would narrow, dramatically, the temperature range of the experiments.

Eventually it was concluded that a satisfactory compromise could not be achieved and the system was abandonned.

6.2.2 The toluene systems

Toluene has a proton affinity such that it can be used as a link among the various systems whose study has been discussed.

The very first system, involving toluene, whose equilibrium was studied with temperature dependence, was toluene – *meta*fluorotoluene. This system is used to relate the proton affinity of toluene with the halogenotoluenes. The relationship between toluene and the xylenes was established by examining the toluene – dimethylether system.

6.2.2.1 Toluene – *meta*fluorotoluene

Some chemical ionisation (CI) spectra for the following system

$$C_6H_5CH_3 + 1,3FC_6H_4CH_3H^+ = C_6H_5CH_3H^+ + 1,3FC_6H_4CH_3 \qquad (6.3)$$

are available in figure 6.8, 6.9 and 4.1. The latter is not a spectrum of

*meta*fluorotoluene, but the pattern is similar. From these spectra, where each compound is on its own, interferences are not obvious. Both figure 6.8 and 6.9 show as main peaks m/z = 93, 121 and 133 which correspond to the $C_6H_5.CH_3.H^+$ ion and adduct ions $(C_6H_5CH_3.C_2H_5)^+$ and $(C_6H_5CH_3.C_3H_5)^+$ resepctively. The proton bound dimer ion of toluene $(C_6H_5CH_3)_2H^+$ would produce a peak of m/z = 185. figure. 6.8 is the only spectrum where it was recorded but its intensity is negligible.

One possible interference could be the 93 mass peak occurring in the *meta*fluorotoluene spectrum but its intensity was never above 1% of the intensity of the base peak if it was present. Other interfering reactions caused by *meta*fluorotoluene were not found in section 4.3.1; spectra of the two compounds mixed together did not display any new ionic species.

The temperature range within which the measurements of the equilibrium constant for reaction (6.3) were made was 373-573K.

6.2.2.2 Toluene – dimethylether

In this system the reaction under study was

$$C_6H_5CH_3.H^+ + (CH_3)_2O \rightleftharpoons C_6H_5CH_3 + (CH_3)_2OH^+ \qquad (6.4)$$

whose equilibrium constants were measured without temperature dependence, only at 575K. Once more the examination of the chemical ionisation spectra led to some conclusions about the chemistry of the system.

The chemical ionisation spectra of toluene in methane, shown in figure 6.8 and 6.9, were described in section 6.2.2.1. The spectrum of dimethylether in methane is shown in chapter 5 in figure 5.1. The main peaks are at m/z = 47 and 93 which are the masses for the protonated molecular ion $(CH_3)_2O.H^+$ and the proton bound dimer ion $[(CH_3)_2O]_2.H^+$ respectively.

Spectra of both compounds in methane, recorded in continuous mode, are displayed in figure 6.10 and 6.11. The adduct ions producing peaks at masses 121 and 133 are not interferences. Under the experimental conditions in figure 6.9 the

CI, HIGH PRESSURE SPECTRA OF 0·05% OF $C_6H_5CH_3$ IN CH_4 AT 2 TORR, 473 K IN (Fig. 6·8), AT 5 TORR, 573 K IN (Fig. 6·9)

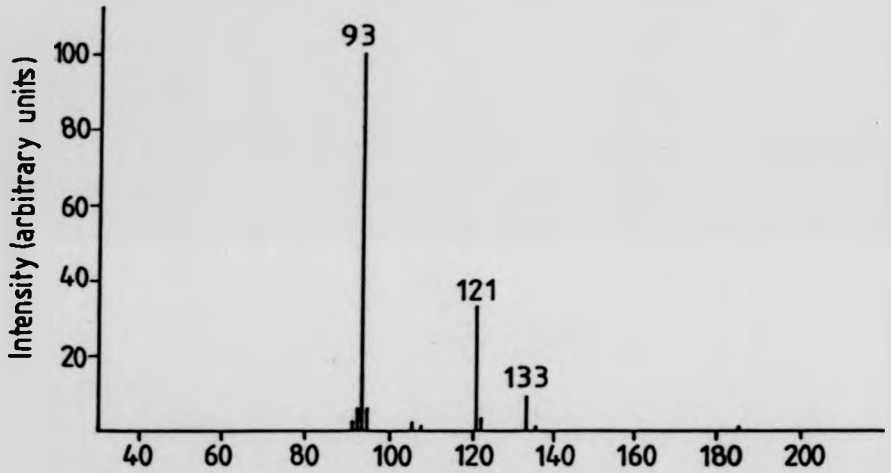

Fig. 6·8

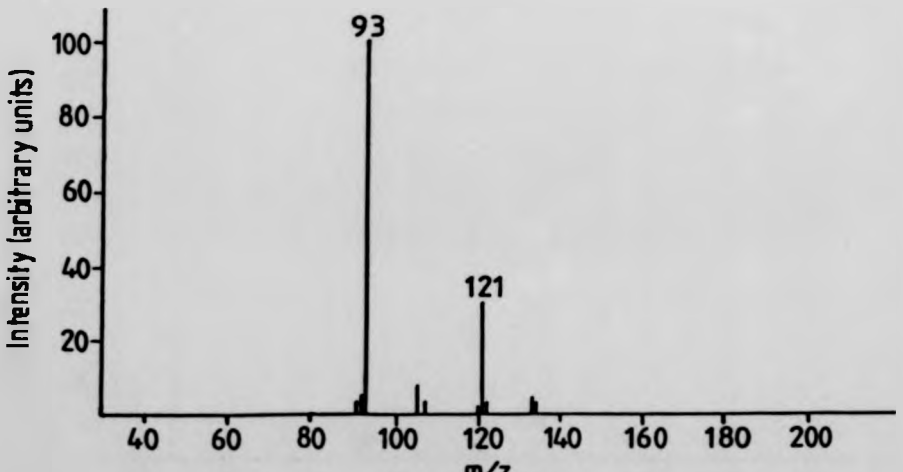

Fig. 6·9

CI, HIGH PRESSURE SPECTRA OF 0·025% OF $\frac{[C_6H_5CH_3]}{[(CH_3)_2O]} = 16$ IN CH_4 AT 1·5 TORR, 342 K (Fig. 6·10), AT 6 TORR, 573 K IN (Fig. 6·11)

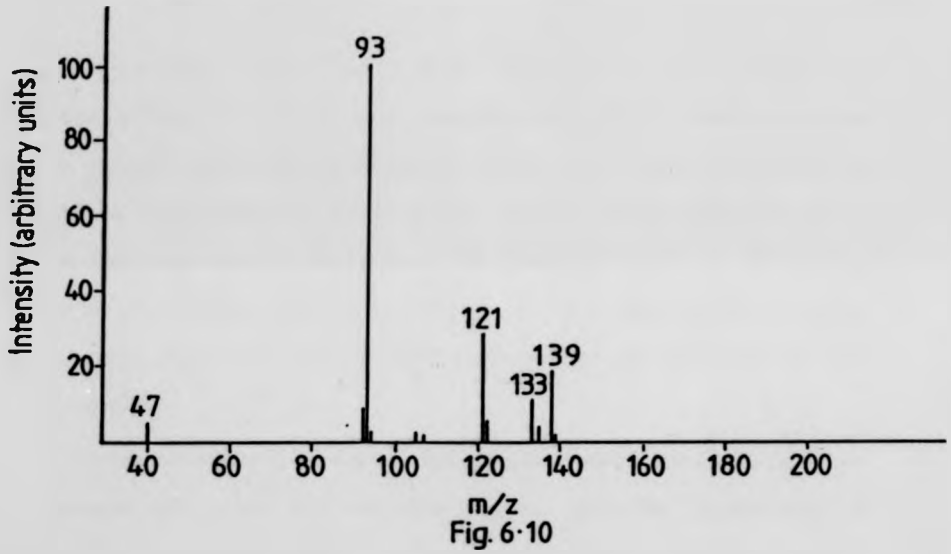

Fig. 6·10

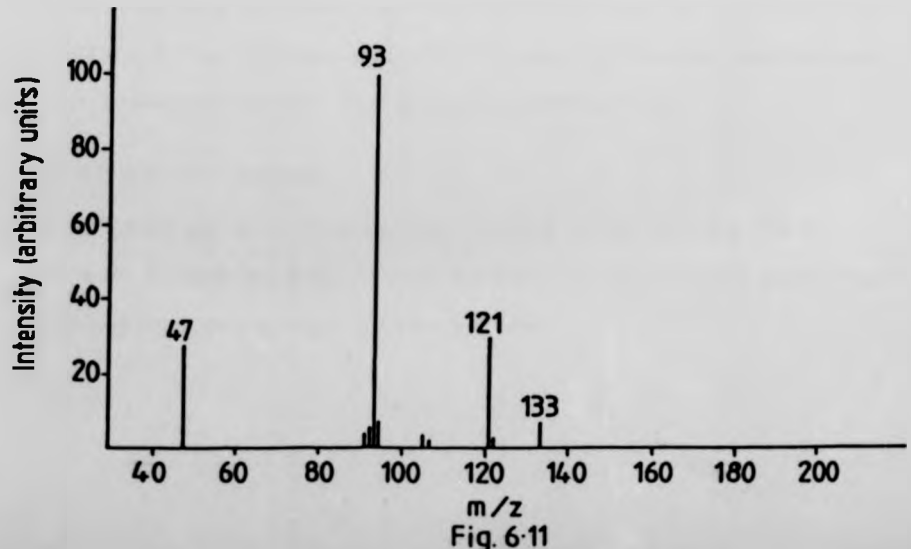

Fig. 6·11

intensities of peaks of mass 105 and 107, probably arising from ions $C_8H_9^+$ and $C_8H_{11}^+$, increased. Their intensities are negligible in figure 6.10 and 6.11. In figure 6.10 the proton bound dimer ion $[(CH_3)_2O.C_6H_5CH_3].H^+$ produced a peak at m/z = 139. The intensity of peak of mass 47 is very low, owing to the formation of more than one proton bound dimer which is favoured at the low temperature of the run. The conditions chosen to perform the experiments are shown in figure 6.11.

The following conditions had to be met in order to obtain reasonable measurements. Firstly the work had to be carried out above 573K to reduce the intensity of the peak relative to the dimer ion $[(CH_3)_2O]_2.H^+$ (m/z = 93) to be less than 5% of the intensity of peak of mass 47. Secondly, the use of neutral concentration ratios (ncr) with a reduced amount of dimethylether (50 μl). Ncr equal to 16 and 32 were found to keep an acceptable intensity of peak 47 without raising the intensity of the dimer peak, mass 93, above 5% of the intensity of the base peak, mass 47.

Once this was established high resolution measurements had to be carried out to separate both peaks with the same nominal mass 93, corresponding to $[(CH_3)_2O]_2.H^+$ and $C_6H_5CH_3.H^+$ ions. This reduction of intensity of the beam introduced instability and decreased the signal to noise ratio.

The difficulties mentioned above pointed to the necessity of toluene being used with a different reference compound. Because of instrumental problems only one set of measurements was collected with this system at 575K.

6.2.2.3 Data and discussion

The van't Hoff plot of the former system discussed in this section is displayed in figure 6.12. In table 6.2 data from the literature and the thermodynamic data determined from the van't Hoff plot are presented.

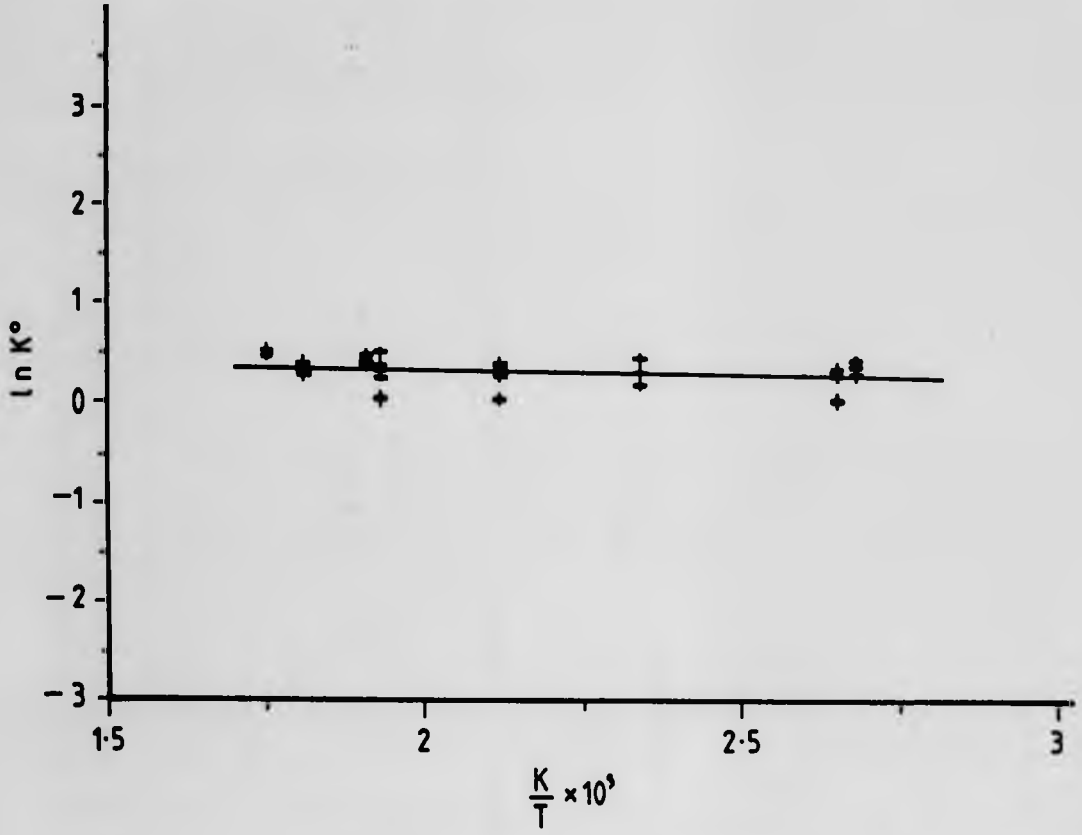

Fig. 6·12 van't Hoff Plot for Reaction

$1,3\,CH_3C_6H_4F.H^+ + C_6H_5CH_3 \rightleftharpoons 1,3\,CH_3C_6H_4F + C_6H_5CH_3.H^+$

The measured entropy changes cannot be compared with previous measurements because values are not available in the literature. For the systems here reported the ratio $\frac{\sigma_X}{\sigma_{XH^+}}$ from equation (2.2.4.) is always 1 so the rotational entropy contribution was expected to be zero. Any contribution from hindered internal rotation arising from the methyl group cancels as it is present on both sides of reaction (6.3).

Table 6.2

$$XH^+ + Y \rightleftharpoons X + YH^+$$

X	Y	[X]/[Y]	ΔG°_{575}/kJmol^{-1}	ΔS°/Jmol^{-1}K^{-1}
1,3FC$_6$H$_4$CH$_3$	C$_6$H$_5$CH$_3$	2.1 6.9	–	3.9±1.4
C$_6$H$_5$CH$_3$	(CH$_3$)$_2$O	15.2	-10.8±1	1.4[c]

X	Y	[X]/[Y]	ΔH°/kJmol^{-1}[a]	ΔH°/kJmol^{-1}[b]
1,3F$_6$H$_4$CH$_3$	C$_6$H$_5$CH$_3$	2.1 6.9	0.7±0.7	2.0
C$_6$H$_5$CH$_3$	(CH$_3$)$_2$O	15.2	–	10.0

(a) this work
(b) reference 6.1
(c) measurements of K at one temperature. ΔS calculated, based on ΔH from ref. 6.1 and ΔG from this work.

The novel internal translational entropy contribution is expected, in the system under study in this section, to be close to zero. In chapter 4 it was observed that the predicted sites for protonation in mechanistic terms, were not adjacent for *meta*fluorotoluene. This will be confirmed by *ab initio* calculations which will be produced in the next chapter. Devlin et al[6.5,6.6] from *ab initio* calculations suggest that the para position in toluene is energetically favoured for protonation. According to them the theoretical PA in the para position is higher than the PA in the ortho by 8.4 kJ mol^{-1} and the PA in the ortho position exceeds the PA in the meta by 18.8 kJ mol^{-1}. Catalán and Yá nez,[6.7] from *ab initio* calculations, arrive at very close PAs for the ortho and para positions in toluene. In contradiction to Devlin et al[6.6] they found the PA in the ortho position higher than the PA in the

para by 3.8 kJ mol^{-1} and the PA in ortho exceeding that in the meta by 19.2 kJ mol^{-1}. Whether the protonation occurs only in para position or in ortho and para simultaneously it will lead to the situation where the proton is attached to one site or more than one but never on adjacent sites. In this case the proton would hardly be labile and internal translation is not expected.

On the other hand ΔS_{mix} will be given by Rln(1/2) for two isomers of *meta*fluorotoluene and one isomer of toluene or by Rln(2/2) if two isomers of toluene are considered. If para and two ortho positions are equally favoured for proton attachment they only give rise to two distinguishable forms. That is to say that ΔS_{mix} must lie in a range 0 to $-5.8\ JK^{-1}mol^{-1}$. The experimental $\Delta S°$ seems preferentially to confirm the predictions of Catalán et al[67].

The $S'_{C_7H_8}$ relative to $1,3-FC_6H_4CH_3$ does agree with expectations as it is much lower than the entropies of protonation measured for ortho and para substituted toluenes (see chapter 4 and 5).

The latter system, whose components are in a similar situation as far as non-adjacent sites for proton attachment are concerned, must not have any internal translational entropy, nor rotational entropy contributions. The entropy of mixing is probably small contained in the range 0 to -5.8 $JK^{-1}mol^{-1}$ assuming no isomer for dimethylether and 1 or 2 for toluene. For the toluene/dimethylether system gas phase basicities were measured only at 575K. Using the published[61] PAs for both compounds to determine the $\Delta H°$ of the reaction it was possible to determine indirectly a temporary $\Delta S°$. This permitted the desired connection to be made between xylenes and the other systems measured so far, as displayed in figure 8.2.

In order to establish a better link between toluene and xylenes more measurements would be needed for toluene — dimethylether. The use of a different reference compound is strongly recommended considering the experimental problems

found with this latter system and the discrepencies in the literature about protonation sites.

6.3 The benzaldehyde – diethylether system

In all systems that have been reported in this work, it has been assumed that the protonation of the aromatics involved takes place on the ring. This is a necessary condition for the interpretation of the thermodynamic data proposed in section 4.6.6. to hold. In contrast an experiment involving an aromatic protonating on a substituent group should not produce any internal translational entropy contribution. Hence any entropy change measured would be, in the latter case, due to the classical contributions from external rotation and/or mixing. It has been suggested in section 4.6.6 that an experiment of this type would supply further evidence for the proposed model.

Protonation occurring on the substituent, i.e. benzaldehyde, nitrobenzene and cyanobenzene is supported by evidence found in the literature.[68,69] The two former compounds were tried. In order to avoid any possible internal translational contributions from reference compounds, aliphatic reference compounds were chosen.

The benzaldehyde – diethylether system gave better experimental conditions than that of nitrobenzene – dimethylether.

6.3.1 The results

The first reaction studied was

$$(CH_3)_2O.H^+ + C_6H_5NO_2 \rightleftharpoons C_6H_5NO_2.H^+ + (CH_3)_2O \qquad (6.5)$$

for which some aspects of the chemistry are shown in figure 6.13 and 6.14. The main peaks of the CI spectrum of nitrobenzene are displayed in figure 6.13. The protonated molecular peak, $(M+1)^+$, is at m/z = 124 and the peaks at m/z = 152 and 164 are the usual adduct ions formed in methane, $(M+29)^+$ and $(M+41)^+$.

Fig. 6·13 CI, HIGH PRESSURE SPECTRUM OF 0·025% OF $C_6H_5NO_2$ IN CH_4 AT 3 TORR, 573 K

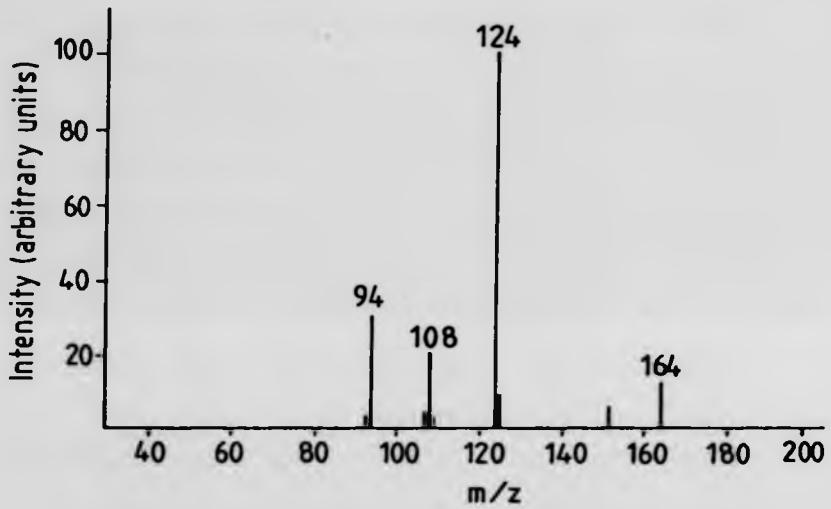

Fig. 6·14 CI, HIGH PRESSURE SPECTRUM OF 0·025% OF $\frac{[C_6H_5NO_2]}{[(CH_3)_2O]}$ = 0·42 IN CH_4 AT 3 TORR, 573 K

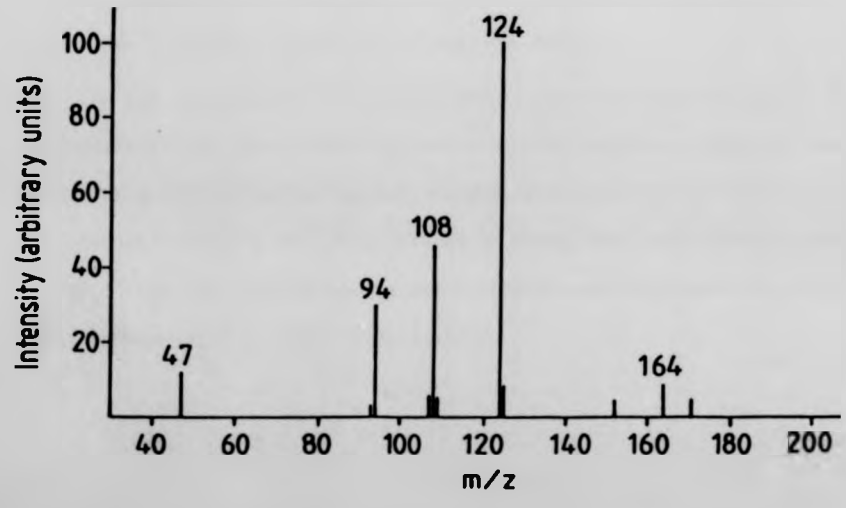

Two other peaks at m/z = 94 and 108 are apparently due to loss of NO and O respectively. The latter two peaks may interfere with the proton transfer reaction. A CI spectrum of dimethylether is shown in chapter 5.

A CI spectrum of nitrobenzene and dimethylether is recorded in figure 6.14. In this spectrum a neutral concentration ratio, n.c.r. = 0.42, was tried in order to use a smaller amount of dimethylether than nitrobenzene in an attempt to reduce its dimer peak at m/z = 93. This was not satisfactory because the dimer ions $[(CH_3)_2O]_2.H^+$ and $[NO_2C_6H_5.(CH_3)_2O].H^+$ at masses 93 and 170 respectively, whose intensities are 27% and 45% of peak of mass 47, are still not sufficiently reduced. Furthermore this ncr significantly reduced the intensity of the protonated molecular peak of dimethylether producing a very weak peak whose pulsed profile was very poor. All these problems did not recommend the study of this system.

The next attempt was the proton transfer in the following system.

$$(C_2H_5)_2O.H^+ + C_6H_5CHO \rightleftharpoons (C_2H_5)_2O + C_6H_5CHO.H^+ \qquad (6.6)$$

According to Lias et al[6 1] the proton affinities were expected to be equal.

A series of spectra of the system is shown in figure 6.15 to figure 6.18. It can be easily concluded from figure 6.15 that the CI spectrum of C_6H_5CHO at T/K = 385 is mainly composed of the protonated molecular peak $(M+1)^+$ = 107, the adduct peaks, $(M+29)^+$ = 135 and $(M+41)^+$ = 147, the dimer peak, $(2M+1)^+$ = 213 and a peak of mass 79 formed by loss of CO. The latter is negligible having an intensity of only 3% of the intensity of the base peak.

The spectra in figure 6.16 and 6.17 are much cleaner than in figure 6.15. In spectrum 6.16 the dimer peak disappeared by the temperature increase but the peak of mass 79 increased its intensity to 11% of the intensity of the base peak. In the joint spectrum 6.17 at T/K = 573, peaks arising from the possible competing reactions have their intensities very much reduced even at pressures as high as 4 Torr. A summary of the peaks is given below:

CI. HIGH PRESSURE SPECTRA OF 0·025% OF C_4H_5CHO IN CH_4 AT 0·5 TORR, 385 K (Fig. 6·15), 573 K (Fig. 6·16)

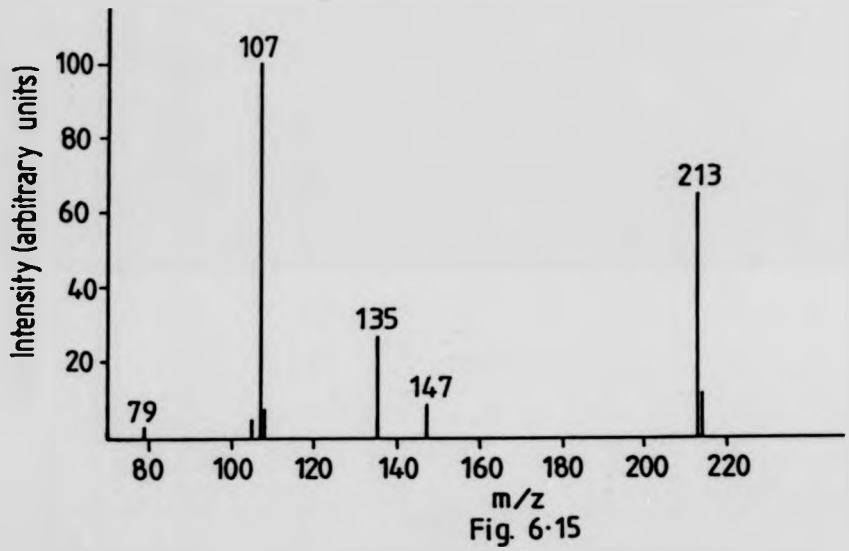

Fig. 6·15

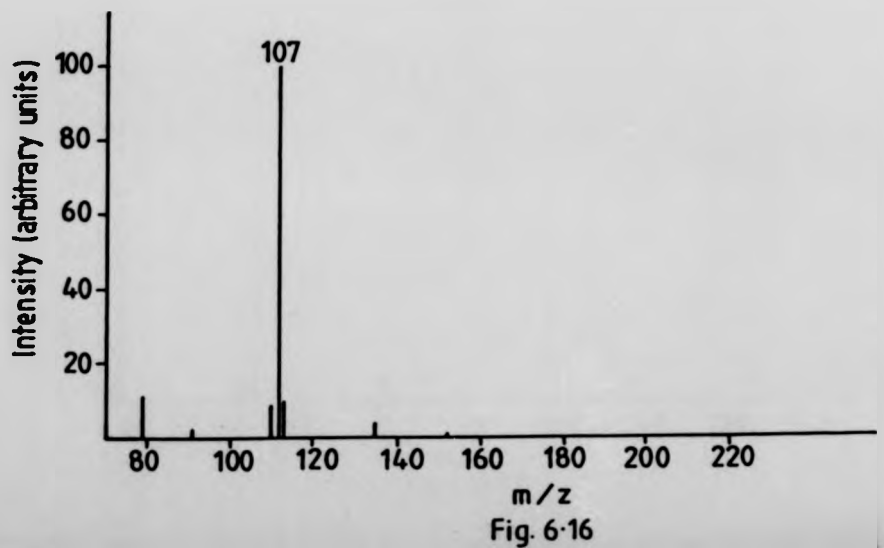

Fig. 6·16

C.I. HIGH PRESSURE SPECTRA OF 0·026 % OF $\frac{[C_6H_5CHO]}{[(C_2H_5)_2O]} = 1{\cdot}0$ IN CH_4 AT 4 TORR, 578 K (Fig. 6·17), 633 K (Fig. 6·18)

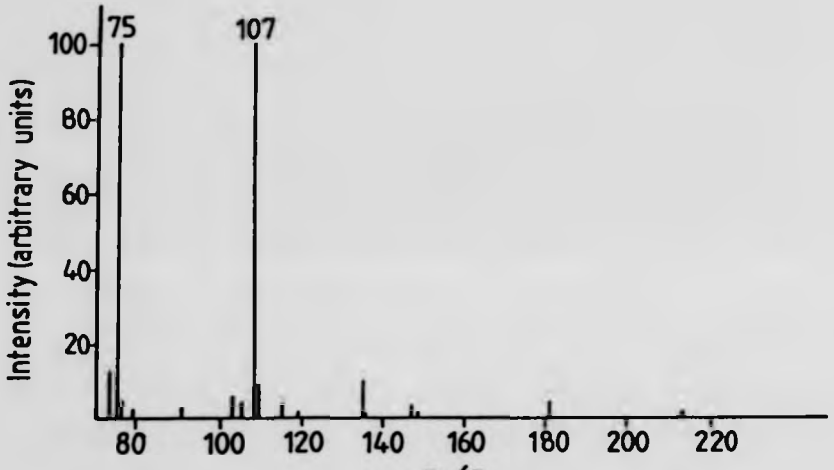

Fig. 6·17

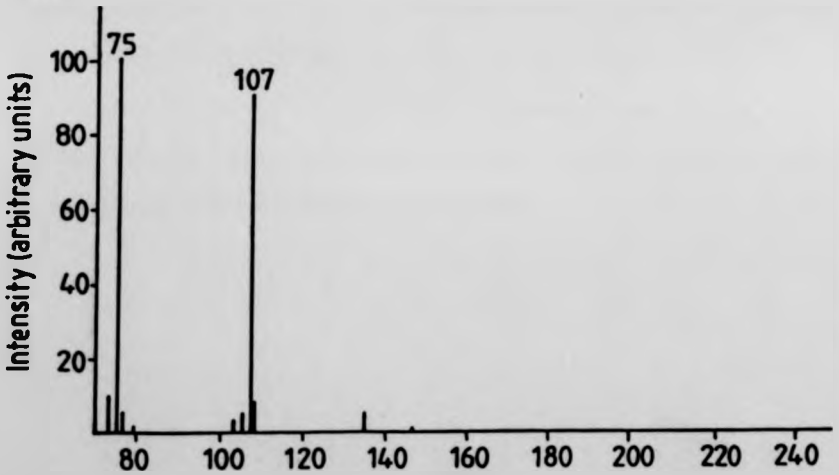

Fig. 6·18

m/z	ions
75	$(C_2H_5)_2O.H^+$
103	$(C_2H_5)_2O.C_2H_5^+$
107	$C_6H_5CHO.H^+$
115	$(C_2H_5)_2O.C_3H_5^+$
135	$C_6H_5CHO.C_2H_5^+$
147	$C_6H_5CHO.C_3H_5^+$
149	$[(C_2H_5)_2O]_2.H^+$
180	$[C_6H_5CHO.(C_2H_5)_2O].H^+$
213	$(C_6H_5CHO)_2.H^+$

The dimers are the most likely interferences but under the experimental conditions of spectrum 6.18 their intensities are negligible, smaller than 4% of the intensities of the base peaks. The peak at mass 79 now has its intensity reduced to 3% of the base peak. Furthermore both peaks of interest, m/z = 75 and 107 are intense providing good pulsed profiles well above the number of counts due to noise. (Minimum number of counts used was 250 and the maximum number of counts was 1218.)

Thus T/K = 578 is suitable as the lowest temperature limit for experiments. In figure 6.18 the trend is improved. The temperature interval for measurements was established to be 573 - 725K.

Figure 6.19 contains the van't Hoff plot determined for reaction (6.6). The standard enthalpy change and standard entropy change are given in Table 6.3 where comparison with literature data is available.

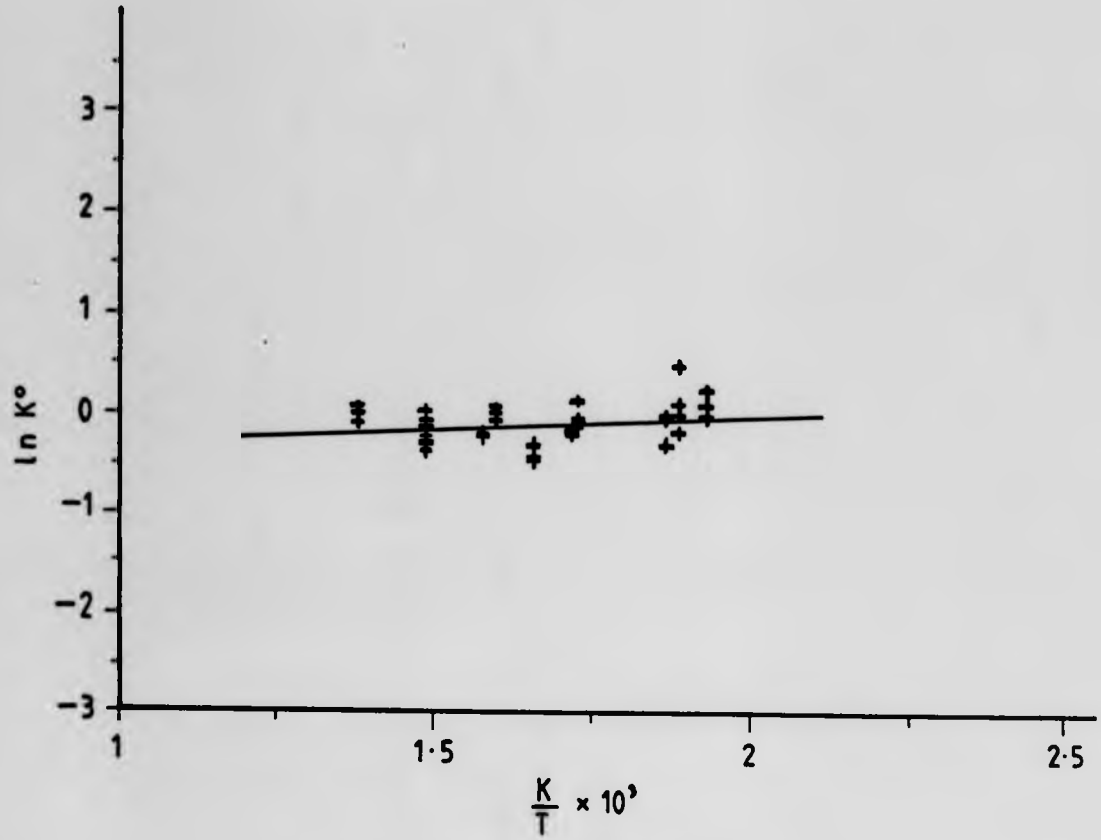

Fig. 6·19 van't Hoff Plot for Reaction

$(C_2H_5)_2O.H^+ + C_6H_5CHO \rightleftharpoons (C_2H_5)O + C_6H_5CHO.H^+$

Table 6.3

$-\Delta H°/kJmol^{-1}$[a]	$-\Delta S°/JK^{-1}mol^{-1}$[a]	$\Delta H°/kJmol^{-1}$[b]	$\Delta S°_{rot}/JK^{-1}mol^{-1}$[c]
3.3±1.3	6±2	0	0

(a) this work
(b) Reference 6.1
(c) Calculated from statistical thermodynamics

6.3.2 Discussion and conclusions

The values of the thermodynamic properties measured and collected in Table 6.3 are consistent with expectations. The difference in proton affinities between both compounds was expected to be, according to Lias et al.[6.1] close to zero. The standard enthalpy measured, which is equal to the difference in proton affinities is quite small, -3kJmol^{-1}, benzaldehyde having a slightly higher PA than diethylether.

The entropy change was at first expected to be zero on the grounds of the rotational entropy term to be the main contribution. The rotational symmetry numbers are the same for neutrals and the corresponding ions, leading to a ratio of symmetry numbers equal to one which would produce $\Delta S_{rot}=0$. The experimental value of $\Delta S°=-6JK^{-1}mol^{-1}$, although small when compared to values measured previously for some proton transfer reactions involving para and ortho substituted toluenes, is still different from zero.

In looking for some possible contributions for entropy certain vibrational terms were checked (table 6.4).

In benzaldehyde at 600K a vibrational contribution of 1.25 $JK^{-1}mol^{-1}$ may arise by replacement of the first bond stretch of table 6.4 by the last stretch and bending.

Table 6.4

Bond stretch	$\nu/(cm^{-1})$	$S°/JK^{-1}mol^{-1}$[a]
C=O	1700	0.84
O–H	3100	0.0
Bond bending		
C – O – H	1200	2.09

(a) Reference 6.10

The ether does not seem to give any contribution at 600K. The bending and stretching of

$$C - O - C \quad \nu/cm^{-1} = 100$$
$$C - O \quad \nu/cm^{-1} = 1100$$

are kept at both sides of reaction (6.7). The new bond O – H does not contribute either in vibrational terms for its stretch frequency is 3100 cm^{-1} which at 600K gives an entropy of zero.

The planar geometry for benzaldehyde is the more favoured[6.11,6.12] due to resonance.

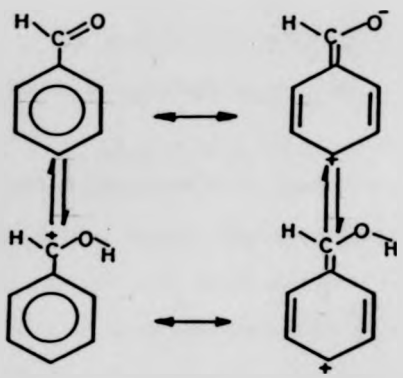

(6.7)

This resonance in equilibrium (6.7), leads to restriction of the free rotation of the aldehyde group. This effect is not accounted for by the entropy change of the reaction (6.6) because it must be cancelled at both sides of the reaction. The entropy contribution due to free rotation of the ethyl group of the diethylether must cancel also since it occurs on both the neutral and the ion.

Defining the entropy change in terms of the individual species of reaction

(6.6).

$$\Delta S^{\circ} = S^{\circ}_{C_6H_5CHO\ H^+} - S^{\circ}_{(C_2H_5)_2OH^+} \qquad (6.6)$$

The sign of the entropy change measured seems to indicate that diethylether must suffer a larger entropy change in the reaction than benzaldehyde. On the other hand the value of 6 $Jmol^{-1}K^{-1}$ is reminiscent of the very ordinary value of 5.8 $Jmol^{-1}K^{-1}=R\ln 2$.

Having ruled out the vibrational and rotational contributions as accounting for the experimental value, what is left is the entropy of mixing. In fact two rotational conformers were found for diethylether by Raman spectroscopy[6 13,6 14] in the gas phase, pure liquid and solutions. The two isomers are the two forms: trans-gauche (TG) and trans-trans (TT). The former has a symmetry C_1 and the latter, which predominates, has a symmetry C_{2v}. The TT form was found to be more stable than TG by 4.18 $kJmol^{-1}$ up to 300K. At the higher temperatures of the experiments in this work it may be that both conformers will be equally favoured leading to an entropy of mixing given by

$$\Delta S_{mix} = R\ln 2 = 5.8 Jmol^{-1}K^{-1}$$

However the important conclusion to be drawn from the study of this system is that the standard entropy change experimentally obtained is small, comparable with values previously measured, which accounted for the classical contributions of entropy of mixing or small rotational entropy terms. As expected, a much smaller entropy change was measured than for systems where internal translation is predicted.

6.4 References

6.1 S.G. Lias, J.F. Liebman and R.D. Levin, J. Phys. Chem. Ref. Data, (1984), 13, 694

6.2 R.S. Mason, M.T. Fernandez and K.R. Jennings, J. Chem. Soc., Faraday Trans., in press

6.3 G.A. Olah, R.H. Schlosberg, R.D. Porter, Y.K. Mo, D.P. Kelly and G.D. Mateescu. J. Am. Chem. Soc., (1972), 94, 2034

6.4 A. P. Bruins and N.M.m. Nibbering, Org. Mass. Spectrom., (1976), 11, 950

6.5 J.L. Devlin, J.F. Wolf, R.W. Taft and W.J. Hehre. J. Amer. Chem. Soc. (1976), 98, 1990

6.6 J.F. Wolf, J.L. Devlin, D.J. DeFrees, R.W. Taft and W.J. Hehre. J. Amer. Chem. Soc., (1976), 98, 5097

6.7 J. Calalán and M. Yáñez. Chem. Phys. Letters. (1979), 60. 199

6.8 F.M. Benoit and A.G. Harrison. J. Amer. Chem. Soc. (1977), 99. 3980

6.9 J.K. Lau and P. Kebarle, J. Am. Chem. Soc. (1976), 98. 7452

6.10 S.W. Benson, "Thermochemical Kinetics", Wiley and Sons, New York, (1976).

6.11 F.A. L. Anet, M. Ahmad. J. Amer. Chem. Soc. (1964), 86, 119

6.12 W.J. Hehre, L. Radom and J.A. Pople, J. Amer. Chem. Soc. (1972), 94, 1496

6.13 H. Wieser, W.G. Laidlaw, P.J. Krueger and H. Fuhrer, Spectroc. Acta (1968), 24, 1055

6.14 J.P. Perchard, J.C. Morrier and P. Dizabo, Spectroc. Acta (1971), 27A, 447.

CHAPTER 7: MOLECULAR ORBITAL CALCULATIONS

7.1 Introduction

Ab initio calculations were carried out in order to obtain some more support for the model sketched in section 4.6.6. It was thought that the presence of substituents in the aromatic ring could decrease the energy required for the migration of a proton from one carbon to another. An attempt to estimate this was made through an energy determination of a bridged intermediate structure of *para*fluorotoluene.

Theoretical proton affinities were also calculated, using 4-31G basis set level, for all the carbon atoms in the aromatic ring of all three fluorotoluenes, ortho, meta and para. Allowances were made by the above calculations for drawing sections of the potential energy surfaces for the three fluorotoluene isomers.

7.2 Basic Concepts

7.2.1 The Hartree-Fock Self-Consistent Field Method

In this section basic principles which are the foundation for molecular orbital calculations for many electron systems will be explained. The calculation of wave functions for these systems by the Hartree-Fock Self-Consistent Field (H-F SCF) method will be outlined. Only closed shell systems procedure will be dealt with.

Fundamentally, the problem is to solve the time independent Schrödinger equation[7.1].

$$H\Psi = E\Psi \qquad (7.1)$$

where Ψ is the electronic wave function for a N electron system, H the N electron hamiltonian operator and E the energy. Only the electronic part of the wave

function is considered as the clamped nucleus approximation is applied.

Equation (7.1) has no exact solution for many electron systems. An approximate solution of the equation must minimise the energy of the system

$$E = \frac{\int \Psi^{*} H \Psi d\tau}{\int \Psi^{*} \Psi d\tau} \geq E_{o} \qquad (7.2)$$

The minimisation of the energy uses the Variation Principle[7.2] which states the inequality present in equation (7.2). This is the first approximation being introduced to solve our problem, in this case Ψ in (7.2) is called a trial variation function and E_0 is the ground state energy of the system. In fact the Variation Principle is only applicable to the lowest energy state of a given symmetry.

Moreover in the Hartree-Fock approximation the wave function for closed-shell systems is given by a product of one electron orbitals[7.3].

$$\Psi = A(n)\Phi_1(1)\Phi_2(2)...\Phi_n(n) \qquad (7.3)$$

where A(n) is an antisymmetriser for N electrons since Ψ must be antisymmetric with respect to electron interchange. The wave function is better represented by a Slater determinant of the form

$$\Psi = \frac{1}{\sqrt{n!}} \begin{vmatrix} \Phi_1(1) & \Phi_1(2) & \cdots & \Phi_1(n) \\ \Phi_2(1) & \Phi_2(2) & \cdots & \Phi_2(n) \\ \vdots & \vdots & \cdots & \vdots \\ \Phi_n(1) & \Phi_n(2) & \cdots & \Phi_n(n) \end{vmatrix} \qquad (7.4)$$

The Φ molecular orbitals are called spinorbitals composed of the product of a space function (λ_i) and a spin function (γ).

$$\Phi_i = \gamma\lambda_i \qquad (7.5)$$

where γ can be α or β allowing for two electrons with opposite spin in the same orbital.

A linear combination of Slater determinants is also a solution of the Schrödinger equation. This will be referred to in section 7.2.3

On the other hand the spatial part of Φ_i can be expressed in terms of the Linear Combination of Atomic Orbitals (LCAO) approximation, as follows

$$\lambda_i = \sum_j c_j \chi_j \tag{7.6}$$

where χ_j are atomic orbitals.

The Hartree-Fock SCF method considers the molecular wave function to be given by a Slater determinant whose form is calculated iteratively. The energy according to the Slater determinant solution is a sum of one electron, coulomb and exchange terms[74]. The Hartree-Fock equations are obtained through the minimisation of energy, simultaneously requiring the molecular orbitals to be orthonormal.

$$\int \Phi_i \Phi_j d\tau = \delta_{ij} \tag{7.7}$$

The equation may be written in a compact and short form as in equation (7.8).

$$H^{SCF}\Phi_i(1) = E_i^{SCF}\Phi_i(1) \tag{7.8}$$

The solution has to be iterative because the Hartree-Fock operator in equation (7.8) depends upon the orbitals Φ_i, so it could not be determined until the equations are solved.

The association of the LCAO approximation with the Hartree-Fock method leads to the Roothaan equations which are much more suitable for molecular systems than the Hartree-Fock method.

As Φ_i can be expressed in terms of a linear combination of atomic orbitals χ_j.

$$\Phi_i = \sum_j a_{ij}\chi_j \tag{7.9}$$

The equation (7.8) can now be replaced by

$$H^{SCF}\sum_j a_{ij}\chi_j = E_i^{SCF}\sum_j a_{ij}\chi_j \tag{7.10}$$

If both sides of the equation (7.10) are multiplied by χ_l and integrated over all space

$$\sum_j a_{ij}\int \chi_l H^{SCF}\chi_j d\nu = E_i^{SCF}\sum_j a_{ij}\int \chi_l\chi_j d\nu \tag{7.11}$$

giving

$$\sum_j a_{ij}(H_{ij}^{SCF} - E_i^{SCF} S_{ij}) = 0 \qquad (7.11)$$

Here the problem is to find the expansion coefficients minimising the energy and demanding the functions of the basis set to be only linear independent.[75]

The secular equations in (7.11) have a non trivial solution when

$$\left| H_{ij}^{SCF} - E_i^{SCF} S_{ij} \right| = 0 \qquad (7.12)$$

This secular determinant is very similar to the secular determinant in the Hückel Molecular Orbital Method.[76] Nevertheless there is an important difference between the two procedures. The latter method sets the integrals H_{ij} and S_{ij} to zero or experimental parameters. The *ab initio* methods that have been outlined above calculate the integrals H_{ij} and S_{ij}, although by an iterative procedure as the wave function solution is supposed to be already known.

The mathematical treatment involved in Hartree-Fock method and in the LCAO-SCF method is omitted for it is beyond the scope of this work. However it is readily available in reference 7.4 or in other textbooks quoted herein. Some computer packages which perform SCF *ab initio* calculations have stored in them calculated atomic integrals to form a given basis set[74]. Thus the first step is usually the guessing of the coefficients in equation (7.11). The second step, using the guessed coefficients, is the calculation of integrals H_{ij} and S_{ij}. The third step is the resolution of the secular equations, followed by the convergence control. It may be based on the coefficients or energy values. When convergence is not attained the next cycle will start with the improved coefficients obtained from the equations solved in the previous cycle. The convergence is usually considered reached when the results from successive iterations agree within a given tolerance limit. For energy this is often 10^{-6} Hartree.

One last comment is that semi-empirical methods, as the already mentioned Hückel Method, either neglect some of the integrals contained in the secular determinant or substitute some others by parameters optimised to fit experimental

data. Obviously their answers are less accurate than those obtained for *ab initio* calculations but they are still very useful.

7.2.2 Basis Set

First the method for performing the theoretical calculations must be selected. The LCAO-SCF method was chosen to carry out the molecular orbital calculations in this work because it is adequate for this type of calculation on moderately seized organic molecules. Having selected this method, whose name implies the use of a linear combination of atomic orbitals as a basis set, the second decision is the algebraic form that those atomic orbitals must have and how many must be used.

Slater Type Orbitals (STO's)[77] whose form was suggested by the solution of the Schrödinger equation for hydrogen like atoms, are expressed by the following equation.

$$\chi_{nlm} = N_{n\xi} r^{n-1} e^{-\xi r} \gamma_{lm}(\theta,\phi) \qquad (7.13)$$

γ_{lm} - normalised spherical harmonic function

n - principal quantum number

$N_{n\xi}$ - normalisation constant

ξ - orbital exponent (dependent on the atomic number andshielding constant)

The exponents can be considered as variational parameters whose optimised values must lead to the minimisation of the total energy. STO's reproduce the electron distribution reasonably well, and they have been successfully used for diatomic molecules. However they are very time consuming in calculations. Consequently they have been replaced by Gaussian Type Orbitals (GTO's) whose algebraic form[77] is

$$\chi_{nlm} = N_{nlm} x^l \gamma^m z_n e^{-\xi r^2} \qquad (7.14)$$

These cartesian functions allow much faster calculations of polyatomic molecules because the product of two gaussian functions is still a gaussian function (multi-

centered two electron integrals are easier to calculate). However their reproduction of the atomic wave function is poorer than the representation given by STO's. This may be overcome by the use of a linear combination of GTO's[7.2]. This procedure prolongs again the time required for calculations as the number of two electron integrals to be computed increases with the fourth power of the number of basis functions[7.2]. In order to overcome this problem contracted basis set are used. This means that rather than having all the coefficients of the basis set varying independently, given coefficients are kept constant relative to one another. Each of these groups of gaussian functions are called Contracted Gaussian Type Orbitals (CGTO). A widely used procedure is the replacement of each STO by a contracted Gaussian function whose form is

$$\sum_i a_i g_i \qquad (7.15)$$

where g_i are the primitive gaussian functions and a_i are found by least squares fitting[7.8,7.9]. The STO-3G basis set is an example, where each STO is replaced by a linear combination of 3 GTO.

Other concepts must be referred to such as "minimal basis set" which is composed of one STO for each atomic orbital of each atom irrespective of the shell to which it belongs. A single STO is not the most accurate way to express an atomic orbital, so two exponential functions with different exponents may be used for a better representation. This set is designated a "double/zeta basis set".

A different type of basis set is the "split-valence basis set" for which two STO's are used for each atomic orbital of the valence shell and just one STO for each atomic orbital of the inner shell. An example is the 4-31G where each atomic orbital of the inner shell is represented by a linear combination of four Gaussian functions and each atomic orbital of the valence shell is replaced by a linear combination of three GTO's plus one GTO of different exponent.

This extended 4-31G basis set was the most commonly used in this work. It

has been found to be superior to STO-3G for energy comparisons[7.10]

More improvement can be obtained in basis sets by the addition of Gaussian polarisation functions. These functions are able to account for the distortion usually introduced in atomic orbitals when the molecule is formed. This is performed by adding a set of gaussian functions whose quantum number l is larger than the maximum l in the free atom. An example is the basis set 6-31G*. As well as using a linear combination of six GTO's for the atomic orbitals in the inner-shell, when compared with 4-31G, a new set of d-type of Gaussian functions is used for each non hydrogen atom.

7.2.3 Electron Correlation

The Hartree-Fock method deals only partially with the interactions between electrons. In a N electron system each electron is considered to move in an average potential field created by N-1 electrons.[7.5] This leads to an error in calculated energies.

Each electron has instantaneous interactions with all the other electrons in the molecule. The motion of each electron is constrained by the other electrons.[7.3] This "electron correlation" is to some extent present in the antisymmetric Hartree-Fock wave function. In other words the probability of finding electrons of the same spin in a given region of the space, simultaneously, is very small. However in order to correct the Hartree-Fock energy the total "electron correlation" must be taken into account in the Hartree-Fock wave function.

The most commonly used procedure to solve this problem is to use the "Configuration Interaction" method.

The true wave function (molecular or atomic) is built up from the contributions of different configurations rather than arising from the ground configuration only.[7.2]

The wave function becomes a linear combination of configuration functions which are Slater determinants. The coefficients of the linear combination can be determined by a variational procedure. The Slater determinants represent ground and excited configurations of the same symmetry. From the interaction of the various configurations and the application of the Variation Principle the calculated energy is lowered since the correlation energy is taken into account.

7.3 Ab Initio Calculations. Fluorotoluenes Data

No molecular orbital calculations were found in the literature for halogenotoluenes. Thus, calculations for some of these compounds were carried out using the only QCPE package available at Warwick, Gaussian 76.

In order to become familiar with the method the minimal energy for a C_{2v} geometry of protonated benzene was calculated. This benzenium ion had been studied previously[7.11] using the Gaussian 76 package. The energy was reproduced without deviation at 4-31G level. The geometry referred to had been partially optimised at STO-3G level before. This C_{2v} geometry for $C_6H_7^+$ ion is shown below.

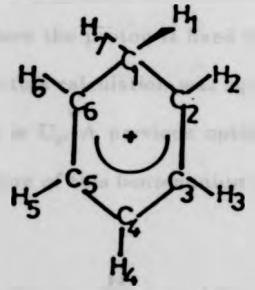

C_{2V}

The carbon atom C_1 has an almost sp^3 configuration. It was assumed that the chain $C_2-C_3-C_4-C_5-C_6$ and the hydrogens H_3, H_4, H_5 would remain constrained in the same position as in the neutral. Optimisation of the geometry by varying the other parameters led to bond length (l) and angles as follows

$<C_2C_1C_6 = 110.9$ $l(C_1H_{(1)}) = 1.106\text{Å}$
$<H_1C_1H_7 = 105.3$ $l(C_2H_{(2)}) = 1.094\text{Å}$
$<H_2C_2C_3 = 118.3$ $l(C_1C_{(2)}) = 1.472\text{Å}$

The angle $C_2C_1C_6$ changed in C_6H_6 from 120° to approximately the tetrahedral value. The closing down of the angle produced an increase in length to the C_1C_2 bond.

This structure was a starting point for the calculations performed for fluorotoluenes. The only modifications were the substitutions of 2 hydrogen atoms by a methyl group and a fluorine atom at convenient places.

Firstly energies for neutral species, *meta*, *ortho* and *para* fluorotoluenes were obtained. Secondly the energies for the correspondent protonated species were calculated. In the latter case at least six energies were determined, for each isomer considering protonation to occur at each carbon atom of the aromatic nucleus. All these energies are presented in tables 7.1, 7.2 and 7.3. The third column of these tables presents the proton affinities at all six carbons of the ring for each fluorotoluene isomer.

A single calculation was made for *para*fluorotoluene to estimate the energy of a bridged structure where the proton is fixed between two adjacent carbon atoms. The basic structure for this calculation was again a geometry proposed by Pople et al[7,11] whose symmetry is C_s. A previous optimisation at STO-3G level, had also been made. The structure of this benzenonium ion is the following

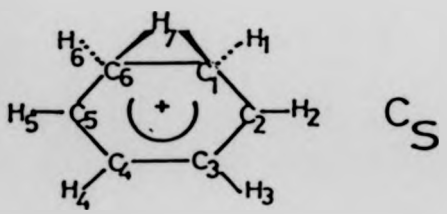

C_S

Table 7.1

*Para*fluorotoluene

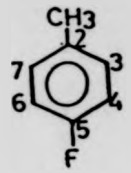

Energies and Proton Affinities
4-31G Basis

Species	−Energy Hartrees	Proton Affinities kJ mol^{-1}
Neutral	368.07112	—
Protonated[a]		
2	368.37569	800
3	368.37711	803
4	368.37865	807
5	368.33746	699
6	368.37865	807
7	368.37711	803
H / \ 3 — 4	368.33622	696

(a) The numbers define the position of the proton

Table 7.2

*Ortho*fluorotoluene

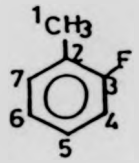

Energies and Proton Affinities
4-31G Basis

Species	−Energy Hartrees	Proton Affinities kJ mol^{-1}
Neutral	368.07169	–
Protonated[a]		
2	368.37698	802
3	368.33609	694
4	368.35666	748
5	368.36267	764
6	368.38009	810
7	368.37867	806
colinear[b]	368.26997	520.6
(c) 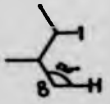	368.28169	551.4
(d) 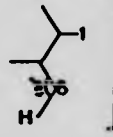	368.28139	550.6

(a) defines the position of the proton on the ring
(b), (c), (d) defines the position of the proton attached to fluorine

Table 7.3

*Meta*fluorotoluene

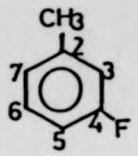

Energies and Proton Affinities
4-31G Basis

Species	−Energy Hartree	Proton Affinities kJ mol^{-1}
Neutral	368.07339	–
Protonated[a]		
2	368.36594	768
3	368.38691	823
4	368.32877	690
5	368.36905	776
6	368.36940	777
7	368.38729	824

(a) The numbers define the position of the proton

The additional hydrogen atom (H_7) has its position defined by the angles θ and γ.

$\theta = 93.9°$
$\gamma = 93.4°$

The bond length C_1-C_6 is increased by 0.05Å. The energy of the bridged structure for parafluorotoluene is given in the last row of Table 7.1.

Some calculations were carried out for orthofluorotoluene only to find out the proton affinity of this neutral when the proton is attached to the fluorine rather than to the aromatic nucleus. Three different orientations were considered for the proton. The results for these three different situations are given at the bottom of table 7.2.

Calculations on protonated chlorotoluenes were abandoned as the package imposes a maximum number of basis function smaller than those necessary for the species at the 4-31G level. Some calculations were carried out for neutrals at 4-31G and STO-3G. Calculations for chlorotoluenes with a STO-3G basis set would be possible for both species but the energies and proton affinities would not be comparable with the fluorotoluene data.

7.4 Discussion

The $C_6H_7^+$ ion has been extensively studied by theoretical means both through *ab initio* and semi-empirical calculations.[7.11,7.12]

The benzenium structure, (section 7.3), is unanimously found to be most stable in the literature. Up to now the best calculated[7.11] proton affinity (STO 4-31G basis set) overestimates the experimental value by appoximately 29 $KJmol^{-1}$.

The absolute proton affinities calculated here for fluorotoluenes using the same package and basis set as above show a similar deviation from experimental

values. The value for *ortho*fluorotoluene is 27 kJ/mol above the experimental and the shift for *meta*fluorotoluene is ca. 29 kJ/mol. However, the calculation puts the absolute proton affinity of *para*fluorotoluene at 49.6 kJ/mol above the experimental value. (Values reported in Table 7.4.) Again the para compound is exceptional in its behaviour, which must be connected with its entropic features.

Nevertheless relative values from calculations display good agreement with experiment. The order in the proton affinity scale is still the same as for the experimental values. This can be checked in Table 7.4. On the other hand for *meta* and *ortho*-fluorotoluene the differences between their proton affinities and benzene proton affinity either theoretical or experimental, are consistent within 1.5 kJ/mol. In the *para*fluorotoluene case agreement is not found. The proton affinity of *para*fluorotoluene relative to benzene, both experimental and theoretical, are apart by 20 kJ/mol.

Table 7.4

Species	Experimental PAs / kJ mol^{-1}	Theoretical PAs / kJ mol^{-1}
Benzene	759.0[a]	786.2[b]
Toluene	794.0[a]	828.1[e]
Metafluorotoluene	794.7[c]	824.0[d]
Orthofluorotoluene	782.7[c]	810.0[d]
Parafluorotoluene	757.4[c]	807.0[d]

a recommended value ref. 5.2

b ref. 7.11. STO 4-31G basis set

c values referred to toluene PA, recommended value taken from ref. 5.2.

d this work. STO 4-31G basis set

e ref 7.13. Large contracted basis set + polarisation functions 7.13 W.C.Ermler and R.S.Mulliken, *J. Am. Chem. Soc.*, (1978), **100**, 1647.

The unsatisfactory absolute results are not surprising in view of the following explanations.

Sordo et al[7.12] rethought the theoretical study of protonated benzene assum-

ing that the structure with geometry C_{2v} proposed by Pople et al[7.1] was heavily constrained. Their calculations were based on a full relaxation of the geometry which distributes distortion and obviously tension all over the molecule leading to a stabilisation of 11.9 kJ/mol. The calculations were performed by MINDO/3. New calculations[7.12] carried out at STO-3G level but using the fully optimised geometry from MINDO/3 led to energies lower by 15.5 kJ/mol than the Pople[7.11] energies obtained with the same basis. The explanation is that full optimisation and full relaxation of the geometry of these σ complexes in protonated species is fundamental.

In order to improve the absolute theoretical values, calculations at a higher level, including polarised basis sets and electron correlation would be necessary.

Corrections based on zero point vibrational energies would be indispensable. These improvements[7.14] have been available lately arising from the development of molecular orbital methods of calculation.

Pople et al[7.14] established that zero-point vibrational energy corrections usually bring down the protonation energies by factors of 21-42 kJ/ml. The overestimation found for theoretical proton affinities of fluorotoluenes nearly falls within this correction range.

An important aspect emerges from the data given in tables 7.1, 7.2 and 7.3. The sites of maximum proton affinity on fluorotoluenes calculated by ab initio methods match fairly well with the sites of protonation predicted in section 4.6.3. This comparison is shown in fig. 7.1. Ipsoprotonation in ortho and para isomers was found and this confirms previous theoretical findings.[7.15]

One can now state that the ΔS_{mix} in halogenotoluene and xylene systems will probably not exceed 3.4 $Jmol^{-1}K^{-1}$ since the maximum number of isomers for *para* and *ortho*-fluorotoluene is three and two for *meta*fluorotoluene. This brings down the previously predicted value of 7.6 $JK^{-1}mol^{-1}$

ANTICIPATED SITES FOR PROTONATION

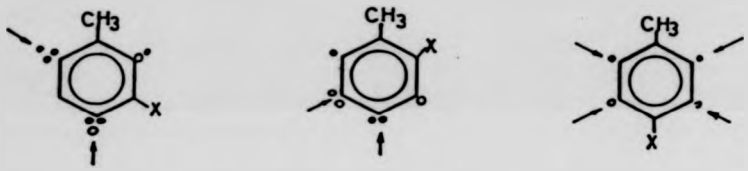

META ORTHO PARA

SITES OF MAXIMUM PROTON AFFINITY
ON FLUOROTOLUENES
AB INITIO CALCULATIONS 4-31G

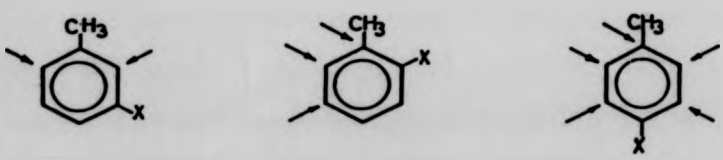

FIG. 7.1

$JK^{-1}mol^{-1}$.

In table 7.5 a relationship is summarised between the number of sites for protonation, in neighbouring carbon atoms, obtained by *ab initio* calculations and the entropies of protonation. Irrespective of the substituent, X, one can conclude that the entropy of the protonation is proportional to the number of adjacent sites for proton attachment.

Table 7.5

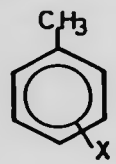	Number of Adjacent Sites for Protonation	Entropy of Protonation ($S^{\circ}/JK^{-1}mol^{-1}$)		
		X=F	X=Cl	$X=CH_3$
m	0	0	7	3
o	3	10	35	20
p	5	58	64	27

This correlation can be looked at, in a different way. Figure 7.2 displays three diagrams which are sections of the potential energy surface, for protonation, on the ring. The ordinates are in fact energy differences, obtained from theoretical proton affinities (tables 7.1, 7.2, 7.3), assuming that the maximum proton affinity for metafluorotoluene is a minimum energy, equal to zero KJ/mol. All the other coordinates are energies relative to this value. The dotted lines represent the barriers for proton migration between two adjacent carbon atoms. The actual values are not accurately known from bridged structures at 4-31G level, as will be discussed later in this chapter.

An insight into Fig. 7.2 makes clear that five carbon atoms of the ring, in parafluorotoluene, have equivalent proton affinity, within $\pm 3.5 KJmol^{-1}$; an exception is made for the carbon atom attached to fluorine. This gives rise to a sort of

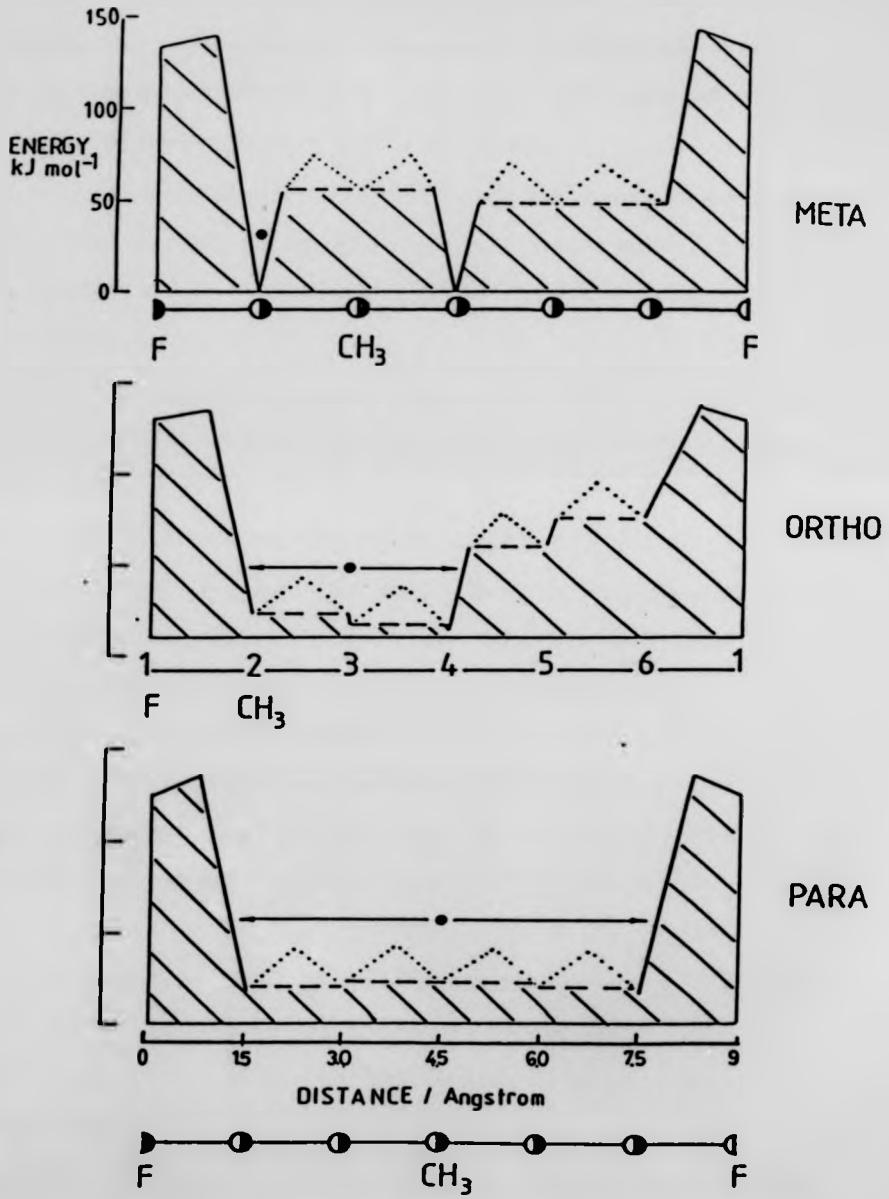

FIG.7.2. A SECTION OF THE PE SURFACE FOR $FC_6H_4CH_3$

case the proton attached to any of these positions is sitting in deeper wells compared with both previous cases. Actually meta compounds have the highest proton affinities, both experimental and theoretical and the lowest excess of entropy measured. This demonstrates the formation of strong proton bonds and makes it unlikely that the proton will move.

In the para case, where theoretical calculations determined the widest and least deep well, experimental data give the lowest proton affinity and highest excess entropy of the lot. This seems to point to a situation of maximum mobility.

The ortho compounds are in an intermediate situation. The picture drawn from the theoretical data, whereby the loosest proton (in para compounds) has the maximum number of adjacent sites to sit on and the maximum entropy of protonation agrees with the model predicted in section 1.6.6.

The degree of mobility of the proton will depend upon the temperature and the barrier height for its migration. The barrier height was calculated at 4-31G level, for *para*fluorotoluene using a bridged structure whose details were given in section 7.3. This structure was considered to be a saddle point on the potential energy surface. The benzenium ion structure is a minimum on that surface so the difference in energy between this structure and benzenonium structure will give the energy barrier to intramolecular proton transfer between two adjacent carbon atoms.

ΔE was calculated to be approximately 109.5 kJ mol $^{-1}$ for *para*fluorotoluene (table 7.1). This value compares well with 86kJmol $^{-1}$ for benzene, determined by Pople[7,11]. However it is certainly much higher than one would expect according to the earlier discussion.

Neverthless Sordo et al[7,12] calculated, by semi-empirical methods (MINDO/3), an energy barrier of 32.1 kJmol $^{-1}$, in much better agreement with

the experimental activation energy measured by Olah[7.16] (42 kJmol^{-1}) for intramolecular proton exchange in $C_6H_7^+$. Sordo[7.12] et al stated that *ab initio* methods overestimate these barriers. These methods lead to a σ complex more stable than benzene and to a benzene more stable than π complex; consequently one can only rely on electron correlation and higher level basis set to reach improved energy barriers. This was actually attained by ab initio calculations[7.17] at MP 2/6-31G/** level by which the barrier height became reduced to 33-40 kJ mol^{-1}. This new refined value is also closer to Olah's measurement in solution (38-46 kJ mol^{-1}).

For the moment one is left with the problem of not knowing exactly the energy barrier for intramolecular proton exchange between neighbouring carbon atoms in the gas phase. Although the last mentioned calculations indicate the best agreement with experimental liquid phase data it is believed that further improvement of calculations might bring down this values.

One more point deserves comment. Calculations included in table 7.2 for proton attachment on the fluorine atom prove that this structure would be more unstable than structures in which proton is attached to the ring, by a factor of 250kJ/mol. This provides further evidence for protonation on the ring, thus reinforcing the arguments in section 4.6.2.

7.5 References

7.1 R.G. Parr, "Quantum Theory of Molecular Electronic Structure", 1963, W.A. Benjamin Inc. New York.

7.2 I. N. Levine, "Quantum Chemistry", 1983, Allyn and Bacon

7.3 H.F. Schaefer, "The Electronic Structure of Atoms and Molecules", 1972. Addison-Wesley.

7.4 W.G. Richards and D.L. Cooper, "Ab Initio Molecular Orbital Calculations for Chemists", 1983, Clarendon Press.

7.5 F.L.Pilar, "Elementary Quantum Chemistry", 1968, McGraw-Hill

7.6 A. Streitwiser, "Molecular Orbital Theory for Organic Chemists", 1961, J. Wiley & Sons, New York

7.7 W.J. Hehre, R.F. Stewart and J.A. Pople, J.Chem. Phys., (1969), **51**, 2657

7.8. J.H. Foster and S.F. Boys, Rev. Mod. Phys. (1960), **32**, 303

7.9. K. O-ohata, H. Taketa and S. Huzinaga, J. Phys. Soc. Japan, (1966), **21**, 2306

7.10. W.J. Hehre, R. Ditchfield, L. Radom and J.A. Pople, J. Am. Chem. Soc. (1970), **92**, 4796

7.11 W.J. Hehre and J.A. Pople, J Am. Chem. Soc. 1972, **94**, 6901

7.12 T. Sordo, J. Bertrán, E. Canadell, J Chem. Soc. Perkin II., 1979, 1486.

7.14 J. E. del Bene, M.J. Frisch, K. Raghavachari and J. A. Pople, J. Phys. Chem. 1982, **86**, 1529

7.15 J Burdon, personal communication (Department of Chemistry, University of Birmingham)

7.16 G.A. Olah, R.H. Schlosberg, R.D. Porter, Y.K. Mo, D.P. Kelly and G.D. Mateescu, J. Am. chem. Soc., 1972, **94**, 2034

7.17 P.R. Schleyer, private communication

CHAPTER 8: GENERAL CONCLUSIONS. FUTURE WORK

8.1 General Conclusions

In this final chapter an overall survey of the data and conclusions obtained is attempted. Proton affinities determined or calculated in this work as well as values from the literature are shown in figure 8.1. The proton affinities of chlorotoluenes were excluded since values from the literature were not available. For compounds gathered in figure 8.1 the agreement between experimental values of this work and tabulated values from reference[8.1] is quite good. Important deviations are found where considerably high entropy changes were measured. This is reasonable because most of the tabulated data in reference[8.1] were obtained from measurements at one temperature. Thus the proton affinities are determined from gas phase basicities corrected by calculated entropy terms.

The agreement with theoretical values is apparently not so good. However, bearing in mind that ab initio calculations without zero point energy corrections (section 7.4) lead to proton affinities well above the experimental values by the constant shift observed in figure 8.1, the agreement seems quite satisfactory. The entropy changes measured cannot be compared with previous measurements as they are not available. In figure 8.2 all entropies of protonation relative to *meta*fluorotoluene are also displayed together.

The confirmation and evidence outlined in Chapters 5, 6 and 7 was obtained according with expectations as described there. In section 4.6.6 support for the interpretation based on mobile protons was invoked from the literature. Additional evidence was gained from work done by Beauchamp et al[8.2], in isotopic

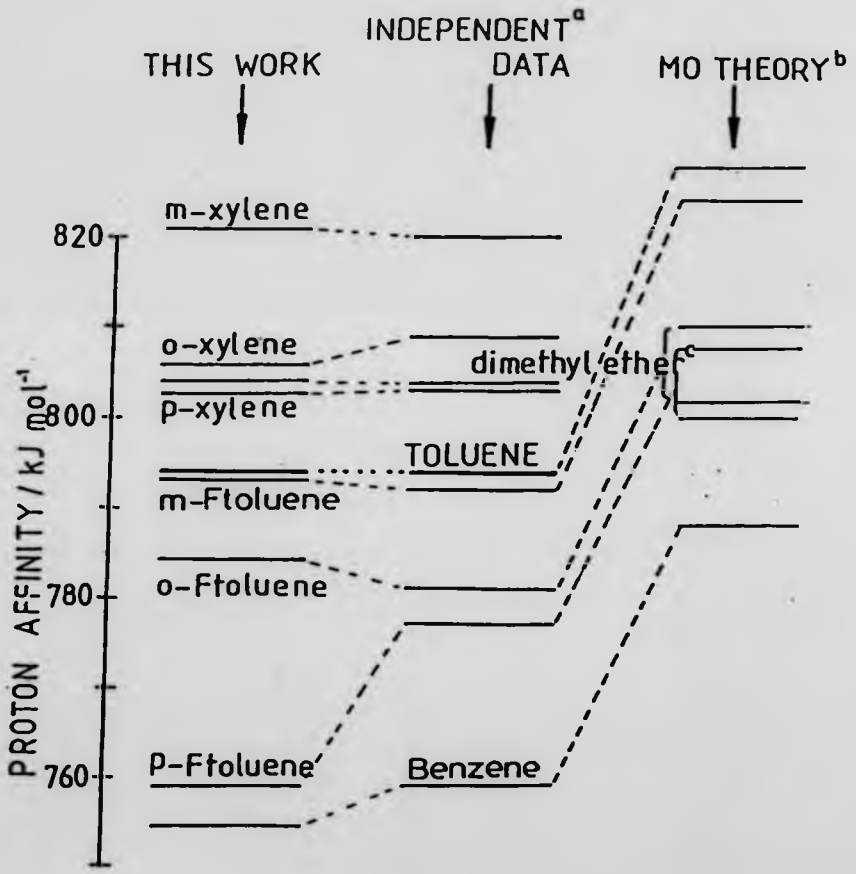

FIG.8.1. COMPARISON OF PAs FROM VARIOUS SOURCES

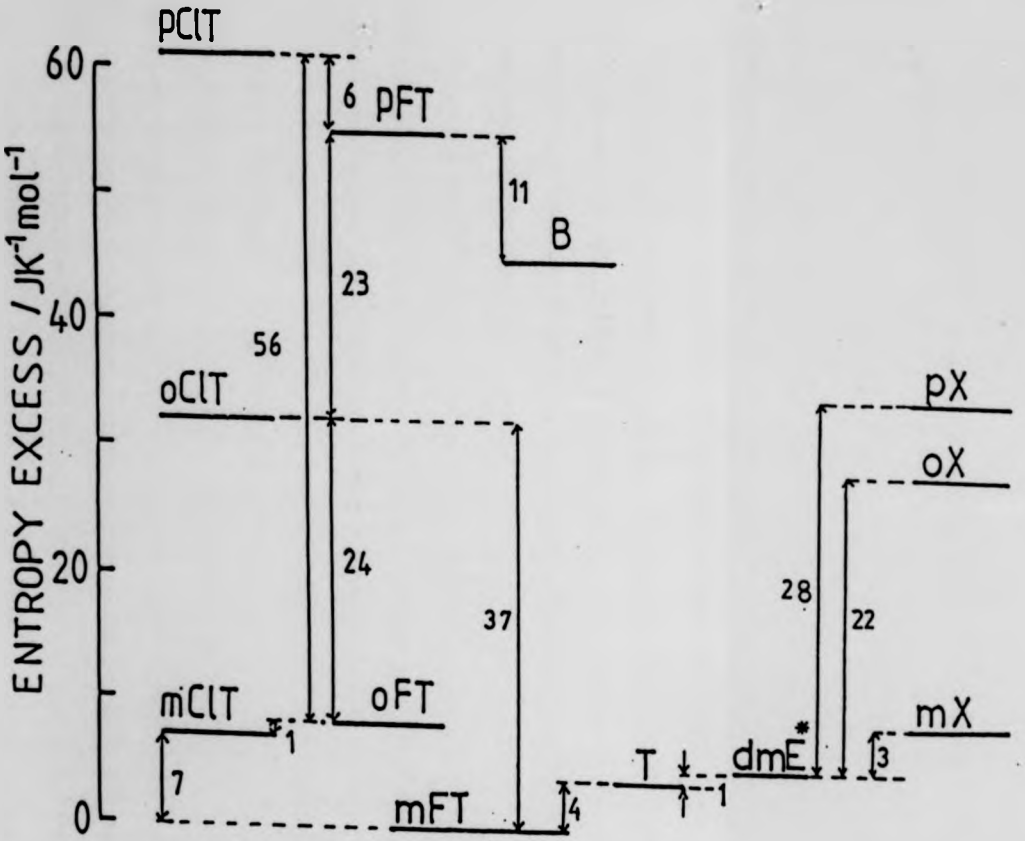

FIG.8.2. ENTROPY OF PROTONATION RELATIVE TO $1,3FC_6H_4CH_3$

exchange reactions of deuterated aromatics in gas phase. Benzene and substituted benzenes were deuterated by D_2O through the species $D_2O^{\cdot+}$ and D_3O^+ and subsequent reactions of D_2O with the deuterated aromatics trigger a sequence of deuterium-hydrogen exchange in certain cases.

$$C_6H_{7-n}D_n^{\cdot+} + D_2O \longrightarrow C_6H_{6-n}D_{n+1}^+ + HDO \qquad (8.1)$$

n = 1 - 6

$$1,m\text{-}(CH_3)_2C_6H_{5-n}D^{\cdot+} + D_20 \longrightarrow 1,m\text{-}(CH_3)_2C_6H_{4-n}D_{n+1}^+ + HDO \qquad (8.2)$$

m = 2, 3, 4 n = 1 - 4

$$C_6H_5CHO.D^{\cdot+} + D_20 \text{ —} \qquad (8.3)$$

Benzene (8.1), *para*xylene and *ortho*xylene (8.2) exchanged all the hydrogens attached to the ring by deuterium but *meta*xylene (8.2) was found to exchange just one. On the other hand benzaldehyde (8.3) did not undergo any exchange.

All these observations agree not only with the expectations expressed in the previous chapters on the grounds of the mobility of the proton, *meta*xylene, *meta*halotoluenes and benzaldehyde excepted, but also with the experimental data obtained for these compounds.

Beauchamp et al[82] arrived at the conclusion that ring protonation was a necessary but not sufficient condition for the exchange to take place. This must be extended, bearing in mind the findings of this work. A total and rapid exchange of hydrogens attached to the ring must require also the proton affinities (see section 7.4), for all positions around the ring, to be very close.

In the case of toluene no such definite interpretation can be given. The system toluene-*meta*fluorotoluene, with its small entropy change, suggests that both are probably in a similar situation where just one site is strongly favoured for protonation or two non adjacent. In *meta*fluorotoluene two non-adjacent sites are almost equally favoured so no internal translation would arise. Toluene could be envisaged as having only one site favoured, the para position to the methyl group,

which finds support in the literature[83]. An alternative suggestion would be the occurrence of more than one site for protonation, one para and two ortho to the methyl group, which may have very close proton affinities[84]. Translational entropy contribution would not be expected, as the favoured sites are alternate. The findings of Beauchamp et al[82] where toluene exchanges 5 hydrogens of the ring with deuterium, contradicts the previous expectations. Either a larger entropy change for reaction (6.3) should have been found experimentally accounting for a translational entropy contribution or a rationalisation based on a mixture 3 of isomers must be anticipated. This hypothesis would produce a $\Delta S_{mix} = R\ln(3/2) = 3.4\ Jmol^{-1}K^{-1}$ for the toluene/*meta*fluorotoluene system which agrees with the measured $\Delta S°$ (section 6.2.2.3) The latter interpretation would mean higher barriers for proton exchange around the ring for toluene than for the substituted toluenes with high S'_A studied herein. On the other hand Kuck et al[85] have found that toluenium ion does not show complete internal scrambling within 10 μs. This confirms that the complete exchange if taking place is certainly a very slow process. Toluene needs a more comprehensive study.

The theoretical work presented in Chapter 7 confirms the existence of almost equally favoured adjacent sites for protonation associated with a large entropy of protonation, nevertheless there remains the problem of the barrier height for proton migration between two carbon atoms of the ring. A summary of calculated barrier heights is presented in table 8.1. Using the transition state theory the half period of life of one proton, in each case between two carbon atoms has been calculated. Using Pople's height of the barrier[86], the period of half life would be 10^3 s in contrast with Olah's[87] value which would be 10^{-5} s for barriers of 40kJ/mol.

Table 8.1

Barrier Heights in $C_6H_7^+$

Theory		$\Delta E(kJmol^{-1})$	Reference
Ab Initio	4-31G	86	Pople (8.6)
	MP2/6−31G**	33-38	Schleyer (7.17)
Semi-Emp	MINDO/3	8-30	Köhler, Sordo (7.12)
Experimental			
Liquid Phase	NMR	~40	Olah (8.7)
Gas Phase	HPPS	< 40	This work

Earlier experiments of Nibbering et al[8.8] by ICR proved complete internal scrambling in protonated benzene. For these species it is known, from metastable studies[8.9] of unimolecular reactions, that hydrogen shifts occur within 10^{-6} s before decomposition of protonated benzene.

Kuck[8.10] studied intra-ring and inter- ring proton exchange in some aromatic compounds using chemical ionisation and deuterium labelling at 473K. MIKE analysis of unimolecular decompositions showed up randomisation of the 21 protons at the aromatic rings within 10^{-5} s. These experiments were not performed under thermal conditions.

The recollection of information on experimental and theoretical evidence points to barriers, lower than 40 $kJmol^{-1}$, in this work.

The tunnel effect is particularly important for light species such as the proton. It has been studied in proton transfer reactions in condensed phase[8.11]. This alternative rationalisation is not entirely satisfactory due to the crucial number of 40 $kJmol^{-1}$ that has been often associated with the barrier height.

According to la Vega[8.12] tunnelling has been a suitable interpretation for fast inter and intra molecular proton transfer. Symmetrical potential energy surfaces with two minima arise from similar initial and final structures. In this case fast proton exchange by tunnel effect may take place. The effect is either independent of symmetry if the barriers are well below 40 $kJmol^{-1}$ (very low and very narrow)

or strongly dependent on symmetry when barriers are higher than 40 $KJmol^{-1}$. The rotation of a methyl group is enough to disrupt the symmetry of the profile and consequently stop the effect.

Thus if barriers are $<<40$ $KJmol^{-1}$ the tunnelling could easily take place, but under these conditions, the energy available for the protonated species at the temperature of these experiments would probably be sufficient to allow the proton over the barrier. If the barriers are $>$ 40 KJ mol^{-1} the tunnel effect cannot be used to explain the proton exchange in this work. In benzene or paraxylene (B) one could justify tunnelling by the presence of symmetry in the profile of the potential energy surface for intramolecular proton transfer. However fast proton exchange would exclusively occur in paraxylene for coupled motions of the methyl groups. On the other hand in parafluorotoluene (A) the unsymmetrical profile would not allow tunnelling. This accumulates evidence for the barrier height to be lower than 40 $KJmol^{-1}$ as predicted.

(A)

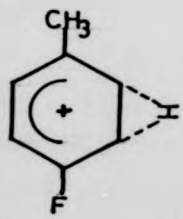

(B)

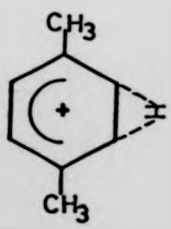

The very first questions formulated at the beginning of this project must be recalled now. The first point was raised by the difference in gas phase basicities for isomers of halotoluenes. From the experiments with temperature dependence relative proton affinities were determined and it was found that the entropy change variation was responsible for the observed gas phase basicities.

Secondly, it has been mentioned how the entropy change in Proton Transfer Reactions can bring in some information (Section 2.2.4) about the structure of the protonated species. In certain systems reported here, due to a large discrepancy found between the entropy change of the reaction and the calculated rotational

entropy and entropy of mixing, it was impossible to establish to which carbon atom the proton was attached in the ions.

Nevertheless, the information obtained from the ΔS° determinations associated with supplementary knowledge from theoretical calculations and some evidence from the literature, allows one to predict a benzenium[8.6] ion structure for the protonated species having small entropies of protonation. *Meta*fluorotoluene, *meta*chlorotoluene, *meta*xylene and probably toluene, show a tetrahedral sp^3 valence structure for the carbon atom bearing the proton. The possible carbon atoms on the ring to which proton is attached are well defined in *meta*fluorotoluene (section 7.4) and in *meta*chlorotoluene and *meta*xylene must be identical.

When the entropies of protonation are large, benzene, ortho and para substituted toluenes by halogens or a methyl group, this work indicates a dynamic structure in which the proton is not actually attached to a single carbon atom but rather roaming around the ring.

8.2 Future Work

Experiments with labelled compounds were planned. It was intended to perform experiments with one of the systems having a large entropy change, previously measured, but using perdeuterated reactants and also perdeuterated methane as a reactant gas. If internal translation was taking place the entropy change measured would account for the difference in contributions from heavy or light species. Although time and cost considerations prevented this from being done during the course of the present work, it is still worthwhile trying.

It is hoped that a higher level of ab initio calculations would reproduce more accurately the barriers for proton migration, in gas phase, in aromatic compounds which are believed to be lower than ever calculated. A face protonated structure of benzene has been suggested, by unpublished semi-empirical calculations[8.13], to

have an energy closer to a bridged structure in contrast with previous ab initio calculations[8 16]

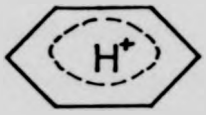

A full optimisation of the structure and higher level ab initio calculations may decrease the energy of the structure thus providing a good basis for the proposed model.

The key for the observation of the novel internal translation entropy contribution in proton transfer reactions in aromatics. is the occurrence of equally favoured adjacent sites for protonation. This was achieved in di-substituted benzenes by the two ortho-para directing substituents. Further confirmation of the effect and more light on the subject may be obtained from experiments with systems containing disubstituted benzenes carrying the same type of substituents or (meta) - (para-ortho) directing substituents. In the former case dihalobenzenes, methylanilines, halogenoanilines would be suitable and the same behaviour as for halogenotoluenes or xylenes would be expected. Meta directing substituents towards electrophilic attack are π electron withdrawing, so they tend to protonate preferentially on the substituent. Assuming that the combination of one meta directing substituent, X, with a para-ortho directing, Y, induces protonation on the ring to a considerable extent, the picture for a semi quantitative distribution of the electron density would be what is seen in figure 8.3. This trend is the reverse situation to that with two ortho-para directing substituents. The ortho and para compounds would have the highest proton affinities, and entropies of protonation close to zero. The meta substituted compound would certainly have the lowest proton affinity. Considerable entropy of protonation would arise, in this case, as 3, if not 5 (ipsoprotonation allowed) adjacent sites for protonation are probably close in energy.

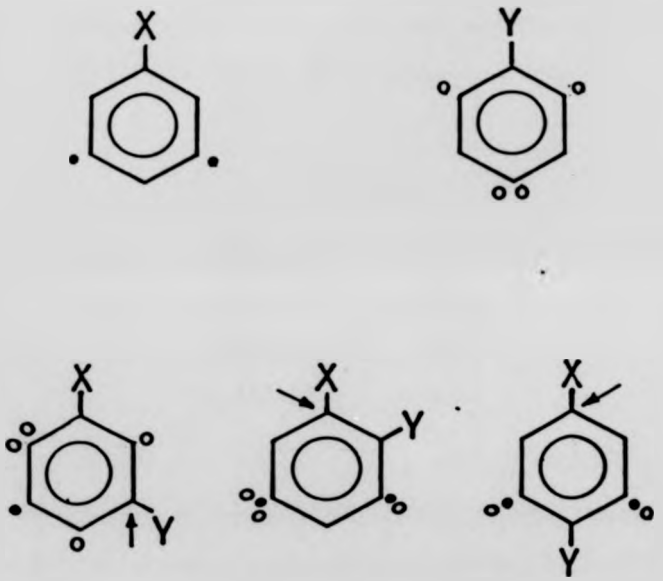

FIG. 8.3

PREDICTED SITES FOR PROTONATION

All these predictions would need support from experimental and theoretical calculations. The choice of meta directing substituents could give rise to doubts of protonation occuring exclusively on the substituent but if the trend predicted by figure 8.3 was verified the protonation would, at least partially, take place on the ring. Another difficulty to overcome is the almost certain occurrence of dimers leading to the unsuitable use of high temperatures (> 573K). Although not entirely conclusive it is worth mentioning that the proton affinity for 1,4$CH_3C_6H_4CHO$ is 852 kJ/mol. This compares with other values as shown in table 8.2

Table 8.2

Compound	PA/kJ mol^{-1}
C_6H_5-CHO	838
$C_6H_5-CH_3$	794
1,4-$CH_3C_6H_4F$	757.4

It can be argued that the high PA value for 1,4-$CH_3C_6H_4CHO$ results from protonation on substituent as for C_6H_5CHO. However if measurements carried out with temperature dependence and an adequate reference compound led to a high entropy change for the system containing 1,3-$CH_3C_6H_4CHO$, it can be said that the higher value for PA of 1,4-$CH_3C_6H_4CHO$ when compared with 1,4$CH_3C_6H_9F$ must be due to the prediction in figure 8.3, and a dynamic structure for 1,3-$CH_3C_6H_4CHO$ would be expected.

8.3 References

8.1 S.G. Lias, J. L. Liebman, R.D. Levin, J. Phys. Chem. Ref. Data, (1984), **13**, 695

8.2 B.S. Freiser, R.L. Woodin, J.L. Beauchamp, J. Am. Chem. Soc., (1975), **97**, 6893

8.3 a) J.L. Devlin, J.F. Wolf, R.W. Taft and W.J. Hehre, J. Am. Chem. Soc., (1976), **98**. 1990

b) J.F. Wolf, J. L. Devlin, D.J. De Frees, R.W. Taft and W.J. Hehre, J. Am. Chem. Soc., (1976), **98**, 5097

8.4 J. Catalán and M. Yáñez, Chem. Phys. Letters, (1979), **60**. 499

8.5 D. Kuck, J. Schneider and H.F. Grützmacher, J. Chem. Soc., Perkin Trans. II 1985, 689

8.6 W.J. Hehre and J.A. Pople, J. Am. Chem. Soc. (1972), **94**, 6901

8.7 G.A. Olah, R.H. Schlosberg, R.D. Porter, Y.K. Mo, D.P. Kelly and G.D. Mateescu, J.Am. Chem. Soc., (1972), **94**, 2034

8.8 A.P. Bruins and N. Nibbering, Org. Mass Spectrom, (1976), **11**, 950

8.9 D.H. Williams and G. Hvistendahl, J.Am. Chem. Soc. (1974), **96**, 6755

8.10 D. Kuck, Int. J. Mass Spectrom. Ion Phys., (1983), **47**, 499

8.11 E. Caldin and V. Gold, "Proton Transfer Reactions", (1975), Chapman and Hall

8.12 J. de la Vega, Acc. Chem. Res. (1982), **15**, 185

8.13 R.S. Mason, unpublished data